



# Descubrimiento de nuevos moduladores de **TRPM8** y su potencial terapéutico

**Alicia Medina Peris**

Tesis doctoral

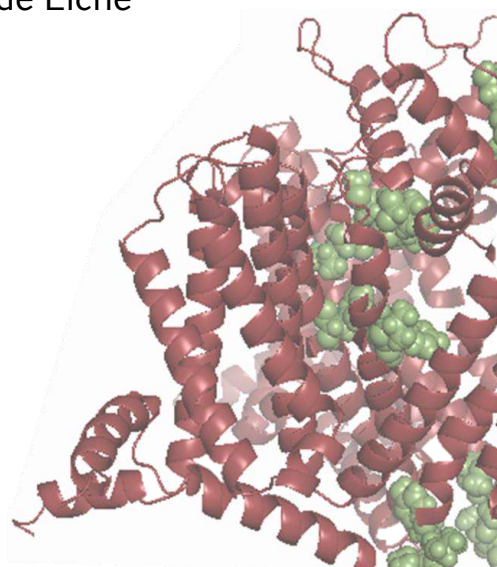
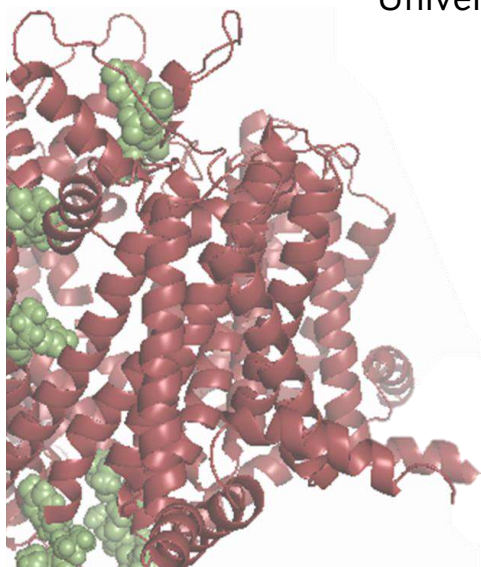
Directora de tesis: Dra. Asia Fernández Carvajal

Programa de Doctorado en Biología Molecular y Celular

Universidad Miguel Hernández de Elche

– 2022 –

**IDiBE**  
UNIVERSITAS  
Miguel Hernández





La presente Tesis Doctoral, titulada “Descubrimiento de nuevos moduladores de TRPM8 y su potencial terapéutico”, se presenta bajo la modalidad de tesis por compendio de las siguientes publicaciones recogidas en ANEXOS:

- Bonache, M. A.; Martín-Escura, C.; de la Torre Martínez, R.; Medina, A.; González-Rodríguez, S.; Francesch, A.; Cuevas, C.; Roa, A. M.; Fernández-Ballester, G.; Ferrer-Montiel, A.; Fernández-Carvajal, A.; González-Muniz, Rosario. Highly Functionalized  $\beta$ -Lactams and 2-Ketopiperazines as TRPM8 Antagonists with Antiallodynic Activity. *Scientific Reports* 2020, 10 (1), 14154. <https://doi.org/10.1038/s41598-020-70691-x> (Q1; Factor de Impacto: 4.996).
- Bonache, M. Á.; Llabrés, P. J.; Martín-Escura, C.; de la Torre-Martínez, R.; Medina-Peris, A.; Butrón, L.; Gómez-Monterrey, I.; Roa, A. M.; Fernández-Ballester, G.; Ferrer-Montiel, A.; Fernández-Carvajal, A.; González-Muñiz, R. Phenylalanine-Derived  $\beta$ -Lactam Trpm8 Modulators. Configuration Effect on the Antagonist Activity. *International Journal of Molecular Sciences* 2021, 22 (5), 1–22. <https://doi.org/10.3390/ijms22052370> (Q1; Factor de Impacto: 6.208).
- Martín-Escura, C.; Medina-Peris, A.\*; Spear, L. A.; de la Torre Martínez, R.; Olivos-Oré, L. A.; Barahona, M. V.; González-Rodríguez, S.; Fernández-Ballester, G.; Fernández-Carvajal, A.; Artalejo, A. R.; Ferrer-Montiel, A.; González-Muñiz, R.  $\beta$ -Lactam TRPM8 Antagonist RGM8-51 Displays Antinociceptive Activity in Different Animal Models. *International Journal of Molecular Sciences* 2022, 23 (5), 2692. <https://doi.org/10.3390/ijms23052692> (Q1; Factor de Impacto: 6.208).
- Iraci, N.; Ostacolo, C.; Medina-Peris, A.\*; Ciaglia, T.; Novoselov, A. M.; Altieri, A.; Cabañero, D.; Fernández-Carvajal, A.; Campiglia, P.; Gómez-Monterrey, I.; Bertamino, A.; Kurkin, A. v. In Vitro and In Vivo Pharmacological Characterization of a Novel TRPM8 Inhibitor Chemotype Identified by Small-Scale Preclinical Screening. *International Journal of Molecular Sciences* 2022, Vol. 23, Page 2070 2022, 23 (4), 2070. <https://doi.org/10.3390/IJMS23042070> (Q1; Factor de Impacto: 6.208).

---

\* Contribución como primer autor.



Otros trabajos publicados estrechamente relacionados con el objeto de interés de esta tesis no incluidos en este compendio se citan a continuación:

- Bertamino, A.; Ostacolo, C.; Medina, A.<sup>†</sup>; di Sarno, V.; Lauro, G.; Ciaglia, T.; Vestuto, V.; Pepe, G.; Basilicata, M. G.; Musella, S.; Smaldone, G.; Cristiano, C.; González-Rodríguez, S.; Fernández-Carvajal, A.; Bifulco, G.; Campiglia, P.; Gómez-Monterrey, I.; Russo, Roberto. Exploration of TRPM8 Binding Sites by  $\beta$ -Carboline-Based Antagonists and Their In Vitro Characterization and In Vivo Analgesic Activities. *Journal of Medicinal Chemistry* 2020, 63, 9672–9694. <https://doi.org/10.1021/acs.jmedchem.0c00816> (Q1-D1; Factor de Impacto: 8.039).
- Sarno, V. di; Giovannelli, P.; Medina-Peris, A.<sup>\*</sup>; Ciaglia, T.; Donato, M. di; Musella, S.; Lauro, G.; Vestuto, V.; Smaldone, G.; Matteo, F. di; Bifulco, G.; Castoria, G.; Migliaccio, A.; Fernández-Carvajal, A.; Campiglia, P.; Gómez-Monterrey, I.; Ostacolo, C.; Bertamino, A. New TRPM8 Blockers Exert Anticancer Activity over Castration-Resistant Prostate Cancer Models. *European Journal of Medicinal Chemistry* 2022, 238, 114435. <https://doi.org/10.1016/j.ejmech.2022.114435> (Q1-D1; Factor de Impacto: 7.088).

---

<sup>†</sup>Contribución como primer autor.





La **Dra. Dña. Asia Fernández Carvajal**, Catedrática de la Universidad Miguel Hernández de Elche,

**INFORMA:** Que Dña. Alicia Medina Peris ha realizado bajo mi supervisión el trabajo titulado “Descubrimiento de nuevos moduladores de TRPM8 y su potencial terapéutico.” conforme a los términos y condiciones definidos en su Plan de Investigación y de acuerdo con el Código de Buenas Prácticas de la Universidad Miguel Hernández de Elche, cumpliendo los objetivos previstos de forma satisfactoria para su defensa pública como tesis doctoral.



Y para que así conste a los efectos oportunos, se expide el presente escrito.

Fdo: Dra. Dña. Asia Fernández Carvajal

Catedrática de la Universidad Miguel Hernández de Elche

Elche, a 18 de noviembre de 2022





La **Dra. Dña. Asia Fernández Carvajal**, Coordinadora del Programa de Doctorado en Biología Molecular y Celular,

**INFORMA:** Que D./Dña. Alicia Medina Peris ha realizado bajo la supervisión de nuestro Programa de Doctorado el trabajo titulado “Descubrimiento de nuevos moduladores de TRPM8 y su potencial terapéutico.” conforme a los términos y condiciones definidos en su Plan de Investigación y de acuerdo con el Código de Buenas Prácticas de la Universidad Miguel Hernández de Elche, cumpliendo los objetivos previstos de forma satisfactoria para su defensa pública como tesis doctoral.



Y para que así conste a los efectos oportunos, se expide el presente escrito.

Fdo: Dra. Dña. Asia Fernández Carvajal

Coordinadora del Programa de Doctorado en Biología Molecular y Celular

Elche, a 18 de noviembre de 2022





La presente tesis doctoral, realizada en el Instituto de Investigación, Desarrollo e Innovación en Biotecnología Sanitaria de Elche (IDiBE), ha sido financiada por las Ayudas del Vicerrectorado de Investigación e Innovación de la Universidad Miguel Hernández de Elche para el Apoyo a la Formación de Personal Investigador.

Además, durante este periodo Dña. Alicia Medina Peris ha realizado una estancia de investigación de 3 meses en el Centro de Investigación en Biociencias y Tecnologías de la salud CBIOS – Universidade Lusófona de Lisboa, Portugal, financiada por las Ayudas del Vicerrectorado de Investigación e Innovación de la Universidad Miguel Hernández de Elche para la movilidad internacional Personal Investigador.







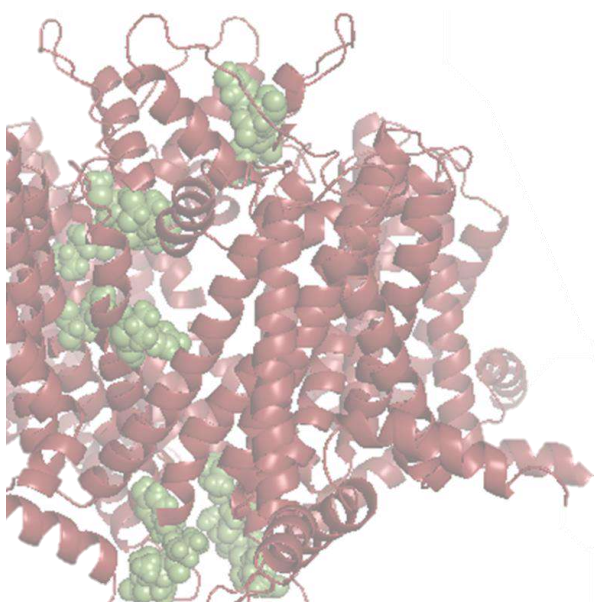
*A todos los que me han acompañado en este viaje.*

*Ciencia, compañer@s.. ¡cuánto os debo!*





## ÍNDICE





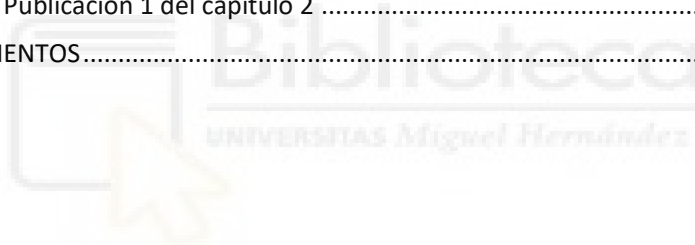
## ÍNDICE

ÍNDICE DE ABREVIATURAS.....	1
ÍNDICE DE TABLAS Y FIGURAS.....	5
RESUMEN.....	7
ABSTRACT .....	11
INTRODUCCIÓN .....	15
1. Sistema somatosensorial .....	17
1.1. Vías generales de la recepción somatosensorial.....	17
1.2. Fibras nerviosas somatosensoriales .....	18
1.3. Receptores somatosensoriales .....	19
2. Canales TRP y recepción somatosensorial.....	20
2.1. Superfamilia de canales TRP .....	21
2.1.1. Canales TRP y termorrecepción .....	23
2.1.2. Canales TRP y dolor .....	24
3. Canal iónico TRPM8 .....	26
3.1. Estructura de TRPM8 .....	27
3.3. Modulación endógena de TRPM8 .....	29
3.2. Modulación química de TRPM8 .....	30
3.2.1. Agonistas de TRPM8.....	31
3.2.2. Antagonistas de TRPM8 .....	32
3.4. Implicaciones fisiopatológicas .....	34
3.4.1. TRPM8 y dolor .....	35
3.4.2. TRPM8 y cáncer.....	36
3.4.3. TRPM8 y trastornos del sistema respiratorio .....	36
3.4.4. TRPM8 y trastornos de los sistemas digestivo y urinario .....	37
3.4.5. TRPM8 y trastornos oculares o de la piel.....	37
OBJETIVOS .....	39
MATERIALES Y MÉTODOS.....	43
1. Sistemas celulares .....	45
1.1. Cultivo de líneas celulares continuas.....	45
1.2. Transfección de <i>hTRPA1</i> .....	46
1.2.1. Amplificación del plásmido.....	46
1.2.2. Expresión de <i>hTRPA1</i> en HEK293 LTV.....	47

## Índice

1.3. Cultivo primario de neuronas GRD .....	47
2. Librería de compuestos .....	48
3. Microfluorometría de calcio .....	48
3.1. Cribados de quimiotecas .....	48
3.2. Ensayos de selectividad .....	50
3.3. Análisis de datos .....	51
3.4. Validación de los resultados - Factor Z .....	51
3.5. Determinación de la Potencia de los compuestos (IC <sub>50</sub> ) .....	52
4. Ensayos de citotoxicidad .....	53
4.1. Ensayo de viabilidad celular mediante MTT .....	53
5. Ensayos electrofisiológicos .....	54
5.1. <i>Patch clamp</i> .....	54
5.1.1. Configuración <i>voltage clamp</i> en líneas continuas .....	54
5.1.1.1. Registros en continuo a -60mV .....	54
5.1.1.2. Rampas despolarizantes de voltaje .....	55
5.1.2. Configuración <i>current clamp</i> en neuronas .....	56
5.2. Ensayos funcionales mediante matrices de microelectrodos .....	56
6. Estudios de modelado molecular .....	57
7. Ensayos <i>in vivo</i> .....	58
7.1. Modelo de alodinia al frío mediada por oxaliplatino .....	58
7.1.1. Evaluación de la alodinia al frío mediante Test de acetona .....	59
7.1.2. Administración de los compuestos .....	59
7.2. Modelo de hipersensibilidad mecánica inducida por nitroglicerina .....	60
7.2.1. Test de von Frey .....	60
7.2.2. Administración del compuesto .....	61
8. Ensayos preliminares de permeabilidad .....	61
8.1. Celdas de Franz .....	61
8.2. Recta patrón y análisis cuantitativo de las muestras mediante HPLC .....	62
RESUMEN DE LOS RESULTADOS Y DISCUSIÓN .....	65
Capítulo 1. Caracterización <i>in vitro</i> , <i>in silico</i> e <i>in vivo</i> de compuestos derivados de $\beta$ -lactamas como bloqueadores de TRPM8 .....	67
Publicación 1. <i>Highly functionalized <math>\beta</math>-lactams and 2-ketopiperazines as TRPM8 antagonists with antiallodynic activity</i> .....	68

Publicación 2. <i>Phenylalanine-Derived <math>\beta</math>-Lactam TRPM8 Modulators. Configuration Effect on the Antagonist Activity</i> .....	72
Publicación 3: <i><math>\beta</math>-Lactam TRPM8 Antagonist RGM8-51 Displays Antinociceptive Activity in Different Animal Models</i> .....	77
Capítulo 2: Búsqueda de nuevos esqueletos farmacológicos moduladores de TRPM8 .....	85
Publicación 1: <i>In Vitro and In Vivo Pharmacological Characterization of a Novel TRPM8 Inhibitor Chemotype Identified by Small-Scale Preclinical Screening</i> .....	86
CONCLUSIONES.....	93
CONCLUSIONS .....	99
BIBLIOGRAFÍA .....	107
ANEXOS.....	127
ANEXO I. Publicación 1 del capítulo 1.....	129
ANEXO II. Publicación 2 del capítulo 1.....	147
ANEXO III. Publicación 3 del capítulo 1.....	171
ANEXO IV. Publicación 1 del capítulo 2 .....	197
AGRADECIMIENTOS.....	217





## ÍNDICE DE ABREVIATURAS

ADNc	Ácido desoxirribonucleico complementario
ACN	Acetonitrilo
AITC	Alil isotiocianato
AMTB	Sal clorhidrato de N-(3-aminopropil)-2-[[[(3-metilfenil)metil]oxi]-N-(2-tienilmetil)benzamida
ASIC3	Canal catiónico sensible a la amilorida humano
ATCC	<i>American Type Culture Collection</i>
ATP	Adenosín trifosfato
BCTC	(3-cloro-piridin-2-il)-piperacina
BPS	Síndrome de vejiga dolorosa
CACO-2	Células inmortalizadas de adenocarcinoma colorrectal humano
CB2	Receptor cannabinoide de tipo 2
CGRP	Péptido relacionado con el gen de la calcitonina
CHO	Células derivadas de ovario de hámster chino
COCE-2	Carcinoma oral de células escamosas
CP	Cetopiperazina
Ct	C-terminal
DAG	Diacilglicerol
DMSO	Dimetilsulfóxido
GRD	Ganglios de la Raíz Dorsal
EC <sub>50</sub>	50% de la concentración máxima efectiva
EDTA	Ácido etilendiaminotetracético
EGTA	Ácido aminopolicarboxílico
EPOC	Enfermedad pulmonar obstructiva crónica
faTRPM8	Receptores de Potencial Transitorio de melastatina 8 de <i>Ficedula albicollis</i>
FBS	Suero bovino fetal
GT	Ganglios del nervio trigémino
GTP	Trifosfato de Guanosina

## Índice de abreviaturas

HEK293	Células embrionarias de riñón humano 293
HEPES	Ácido 4-(2-hidroxietil)piperazin-1-iletanosulfónico
HPLC	Cromatografía líquida de alta resolución
<i>h</i> TRPA1	Receptores de Potencial Transitorio de anquirina 1 de humano
<i>h</i> TRPM8	Receptores de Potencial Transitorio de melastatina 8 de humano
<i>h</i> TRPV1	Receptores de Potencial Transitorio vaniloide 1 de humano
IC <sub>50</sub>	50% de la concentración máxima inhibitoria
i.p.	Intraperitoneal
IP <sub>3</sub>	1,4,5-trifosfato de inositol
i.pl.	Intraplantar
Jss	Flujo de Estado Estacionario
LB	Luria-Bertani
LCC	Lesión crónica por constricción
LOC	Límite de cuantificación
LOD	Límite de detección
Log P <sub>ow</sub>	Coefficiente de partición n-octanol/agua
M3	Receptor muscarínico de la acetilcolina tipo M3
MEA	Matrices de microelectrodos
<i>m</i> TRPV	Receptores de Potencial Transitorio vaniloide 1 de ratón
MTT	Bromuro de 3-(4,5-dimetiltiazol-2-ilo)-2,5-difeniltetrazol
Mw	Peso molecular
Nt	N-terminal
NTG	Nitroglicerina
OAB	Síndrome de la vejiga hiperactiva
PBMC	1-feniletil-4-(benciloxi)-3-metoxibencil(2-aminoetil)carbamato
PBS	Tampón fosfato salino
PI(4,5)P <sub>2</sub>	Fosfatidilinositol 4,5-bisfosfato
Pirt	Phosphoinositide interacting regulator of TRP
PKA	Proteína quinasa A
PKC	Proteína quinasa C
PLC	Fosfolipasa C

PLA <sub>2</sub>	Fosfolipasa A <sub>2</sub>
PWT	Umbral de retirada de la pata
GPCR	Receptor acoplado a proteínas G
rTRPM8	Receptores de Potencial Transitorio de melastatina 8 de rata
S.c.	Subcutánea
SDS	Dodecilsulfato sódico
SEM	Error estándar de la media
SII	Síndrome del intestino irritable
SNC	Sistema nervioso central
SNP	Sistema nervioso periférico
THC	Tetrahidrocannabinol
THCA	Ácido tetrahidrocannabinólico
TM	Transmembrana
TRP	Receptores de Potencial Transitorio
TRPA	Receptores de Potencial Transitorio de anquirina
TRPC	Receptores de Potencial Transitorio canónicos o clásicos
TRPM	Receptores de Potencial Transitorio de melastatina
TRPML	Receptores de Potencial Transitorio de mucolipina
TRPN	Receptores de Potencial Transitorio homólogos de la proteína NOMP-C
TRPP	Receptores de Potencial Transitorio de policistina
TRPV	Receptores de Potencial Transitorio vaniloide
TRPY	Receptores de Potencial Transitorio expresado en levaduras ( <i>Yeast</i> )
VAMP7	Proteína de membrana asociada a vesículas 7
VdW	Van der Waals
VSLD	Dominio tipo sensor de voltaje
WDS	<i>Wet Dog Shake</i>



## ÍNDICE DE TABLAS Y FIGURAS

### TABLAS

<b>Tabla 1.</b> Características de las fibras nerviosas aferentes del sistema somatosensorial..	19
<b>Tabla 2.</b> Listado de los moduladores y concentraciones empleadas en los ensayos de microfluorometría de calcio en los canales <i>rTRPM8</i> y <i>hTRPM8</i> .....	49
<b>Tabla 3.</b> Listado de moduladores y concentraciones empleadas en los ensayos de selectividad en los canales <i>hTRPV1</i> y <i>hTRPA1</i> .....	50
<b>Tabla 4.</b> Preparación de los compuestos para su administración i.pl.....	60
<b>Tabla 5.</b> Estructura, configuración e $IC_{50}$ de los compuestos con mejores resultados en los ensayos de microfluorometría de calcio.....	69
<b>Tabla 6.</b> Porcentaje de actividad de los diferentes diastereoisómeros <b>13</b> , <b>14</b> , <b>15</b> y <b>16</b> para bloquear el canal <i>rTRPM8</i> .....	73
<b>Tabla 7.</b> Actividad funcional del compuesto <b>51</b> a 10 $\mu$ M en los canales TRPV1, TRPV3, TRPA1 y ASIC3 mediante ensayos de microfluorometría de $Ca^{2+}$ .....	78
<b>Tabla 8.</b> Resumen de los resultados de permeabilidad del compuesto <b>79</b> .....	84
<b>Tabla 9.</b> $IC_{50}$ s y eficacias de los compuestos seleccionados como más potentes y eficaces en los ensayos de microfluorometría de calcio.....	88

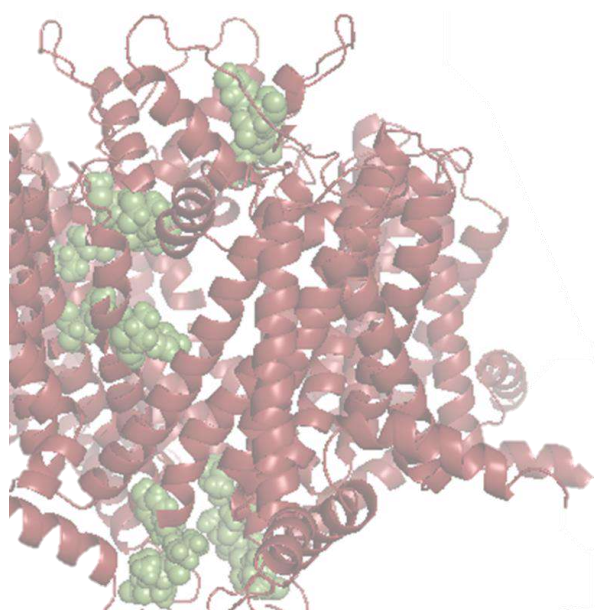
### FIGURAS

<b>Figura 1.</b> Vista anterior de las vías generales de recepción somatosensorial: la vía lemniscal y la vía espinotalámica .....	18
<b>Figura 2.</b> Transducción y transmisión somatosensorial .....	21
<b>Figura 3.</b> Árbol filogenético de los canales TRP .....	22
<b>Figura 4.</b> Rango de temperaturas de activación de los termoTRPs en mamíferos y su clasificación en temperaturas inocuas y nocivas. ....	24
<b>Figura 5.</b> Canales TRP en el dolor nociceptivo, inflamatorio y neuropático .....	26
<b>Figura 6.</b> Estructura del canal TRPM8 .....	28
<b>Figura 7.</b> Esquema simplificado de los diferentes estados de los canales TRPM8 .....	30
<b>Figura 8.</b> Funciones fisiológicas de TRPM8 .....	34
<b>Figura 9.</b> Ensayo de microfluorometría de calcio.....	50
<b>Figura 10.</b> Heterociclos derivados de aminoácidos con potencial bloqueador de TRPM8. 68	
<b>Figura 11.</b> Los compuestos <b>24a</b> y <b>29a</b> bloquearon las respuestas de <i>rTRPM8</i> a mentol 100 $\mu$ M en células HEK293- <i>rTRPM8</i> .....	70
<b>Figura 12.</b> Sitios de unión principales del compuesto <b>24a</b> a TRPM8 .....	71
<b>Figura 13.</b> El compuesto <b>24a</b> disminuye la hipersensibilidad al frío inducida por oxaliplatino .....	72
<b>Figura 14.</b> Conjugado de aminoácidos inicial para la obtención de la $\beta$ -lactama descrita en la publicación 2 .....	73
<b>Figura 15.</b> Los compuestos <b>14</b> y <b>16</b> bloquearon las respuestas de <i>rTRPM8</i> a mentol 100 $\mu$ M en células HEK293- <i>rTRPM8</i> .....	74

<b>Figura 16.</b> Los compuestos <b>14</b> y <b>16</b> no alteraron el potencial de membrana de las neuronas GRD.....	75
<b>Figura 17.</b> Los compuestos <b>14</b> y <b>16</b> no alteraron la actividad neuronal en neuronas GRD .	76
<b>Figura 18.</b> Estructura de la $\beta$ -lactama descrita en la tercera publicación.....	77
<b>Figura 19.</b> El compuesto <b>51</b> bloqueó la actividad de <i>rTRPM8</i> mediada mentol 100 $\mu$ M en células HEK293- <i>rTRPM8</i> .....	78
<b>Figura 20.</b> El compuesto <b>51</b> no alteró el potencial de membrana de las neuronas GRD....	79
<b>Figura 21.</b> Interacciones principales de la $\beta$ -lactama <b>51</b> con <i>rTRPM8</i> .....	80
<b>Figura 22.</b> El compuesto <b>51</b> disminuye la hipersensibilidad al frío inducida por oxaliplatino hasta 1 hora después de su administración .....	81
<b>Figura 23.</b> El compuesto <b>51</b> reduce la hipersensibilidad mecánica inducida por NTG de manera dependiente del sexo.....	82
<b>Figura 24.</b> Perfil de permeabilidad del compuesto <b>79</b> .....	84
<b>Figura 25.</b> Confirmación de la actividad de los compuestos <b>1-21</b> mediante técnicas de microfluorimetría de calcio .....	87
<b>Figura 26.</b> Estructuras de los compuestos más activos y eficaces como bloqueadores de TRPM8 en ensayos de microfluorimetría.....	87
<b>Figura 27.</b> Curva dosis-respuesta para el compuesto <b>13</b> y el <b>19</b> en las que se muestra la activación de <i>hTRPV1</i> en la línea celular HEK293- <i>hTRPV1</i> .....	88
<b>Figura 28.</b> Los compuestos <b>14</b> y <b>15</b> bloquearon las corrientes de <i>rTRPM8</i> mediadas por mentol 100 $\mu$ M en células HEK293- <i>rTRPM8</i> .....	89
<b>Figura 29.</b> La administración i.pl. del compuesto <b>14</b> disminuyó la alodinia al frío inducida por oxaliplatino.....	90



## RESUMEN





## RESUMEN

Los Receptores de Potencial Transitorio o TRPs constituyen una de las familias de canales iónicos más importantes en la transducción somatosensorial. Algunos miembros de esta familia se relacionan con los procesos de termorrecepción y nocicepción. En este contexto, el canal TRPM8 destaca por ser el principal sensor fisiológico de temperaturas frías, por su amplia ubicuidad en el organismo y por su participación en numerosos procesos fisiopatológicos que incluyen dolor, inflamación y cáncer. Todas estas razones convierten a TRPM8 en una diana terapéutica a explorar en el tratamiento de estas condiciones y nos llevan a la búsqueda de nuevos moduladores potentes y selectivos del canal, dividiendo el trabajo realizado en dos capítulos según la procedencia de los compuestos.

En el capítulo 1 nos centramos en la caracterización *in vitro*, *in silico* e *in vivo* de compuestos derivados de  $\beta$ -lactamas. Se realizaron varios cribados de alto rendimiento de una amplia serie de derivados  $\beta$ -lactámicos empleando técnicas de microfluorimetría de calcio en la línea celular estable HEK293-*r*TRPM8. Destacaron cinco compuestos (**24a**, **29a**, **14**, **16** y **51**) como potentes bloqueadores de TRPM8 que se caracterizaron posteriormente mediante técnicas electrofisiológicas, obteniéndose  $IC_{50}$ s comprendidas entre 0,05 y 1,56  $\mu$ M. Todos los compuestos mostraron selectividad hacia el canal. Por otra parte, debido a la implicación de TRPM8 en algunos cánceres, también se demostró la actividad antitumoral de algunas de las  $\beta$ -lactamas (**24a** y **29a**). Los resultados de modelado molecular demostraron sitios de unión distintos a los ya descritos para otros antagonistas de TRPM8. Por último, en los ensayos *in vivo* las  $\beta$ -lactamas **24a** y **51** redujeron la alodinia al frío en un modelo de neuropatía periférica inducida por oxaliplatino. Además, la  $\beta$ -lactama **51** también atenuó la hipersensibilidad mecánica y al frío en un modelo de dolor neuropático de lesión crónica por constricción (LCC) y mitigó la hipersensibilidad mecánica en un modelo de migraña inducida por nitroglicerina. Adicionalmente, se muestran algunos resultados preliminares de permeabilidad cutánea de estas  $\beta$ -lactamas.

Por otra parte, en el Capítulo 2 nos centramos en la búsqueda de nuevos esqueletos farmacofóricos capaces de modular TRPM8 mediante el cribado virtual de la biblioteca molecular EDASA Scientific. De este cribado se eligieron 21 compuestos por presentar

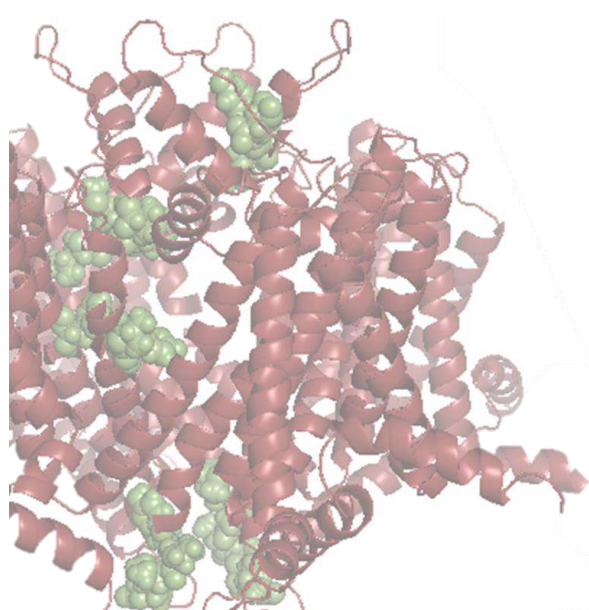
## Resumen

las mejores energías de unión con la proteína diana. Los resultados se validaron *in vitro* mediante técnicas de microfluorometría de calcio en la línea celular citada previamente, clasificándose seis de ellos como potentes bloqueadores del canal. De estos seis compuestos, destacaron el **14** y **15** por presentar los mejores resultados de potencia, eficacia y selectividad; y el **13** y **19**, por presentar carácter agonista frente al canal *hTRPV1*, convirtiéndose en moduladores de doble acción. Los resultados de actividad y potencia de los compuestos **14** y **15** se corroboraron mediante técnicas electrofisiológicas obteniéndose IC<sub>50</sub>s de 1,25 y 2,95 µM, respectivamente. De la misma manera que las β-lactamas, los estudios de modelado molecular revelaron sitios de unión a TRPM8 distintos a los descritos para otros antagonistas de TRPM8. Por último, el compuesto **14** también disminuyó la alodinia al frío en un modelo de ratón de neuropatía periférica inducida por oxaliplatino.

Para finalizar, en este trabajo se han identificado y caracterizado nuevos quimiotipos relevantes en el bloqueo de TRPM8. Estas estructuras constituyen importantes puntos de partida hacia futuras modificaciones con el fin de optimizar sus características farmacológicas y obtener un mayor conocimiento del canal y de las estructuras que discriminan la selectividad frente a los diversos canales TRP.



## **ABSTRACT**





## ABSTRACT

The Transient Receptor Potential channels or TRPs constitute one of the most important families of ion channels in the somatosensory transduction. Some members of this family are related with thermoreception and nociception processes. In this context, the TRPM8 channel stands out for being the main physiological receptor of cold temperatures, being widely distributed through the mammal's body and taking part in many physiopathological processes including pain, inflammation and cancer. These reasons turn TRPM8 into a therapeutic target to explore in the treatment of several conditions and lead us to the search of new potent and selective channel modulators, dividing our work in two different chapters depending on the origin of the compounds.

Chapter 1 focuses on the *in vitro*, *in silico* and *in vivo* characterization of a series of  $\beta$ -lactam derivatives. First, a large number of  $\beta$ -lactams underwent a high throughput screening through calcium microfluorometry techniques using the HEK293-rTRPM8 stable cell line. Five compounds (**24a**, **29a**, **14**, **16** and **51**) were identified as the most potent TRPM8 blockers. The mentioned  $\beta$ -lactams were further characterised using electrophysiological techniques, obtaining  $IC_{50}$ s between 0.05 y 1.56  $\mu$ M. All five compounds also exhibited selectivity towards TRPM8. Furthermore, due to the implication of TRPM8 in some cancers, the antitumoral activity of some  $\beta$ -lactams (**24a** y **29a**) was studied providing promising results. Molecular modelling studies revealed new TRPM8 binding sites different to the ones described for other TRPM8 antagonists. Last, in *in vivo* assays, the  $\beta$ -lactams **24a** and **51** decreased the cold allodynia in an oxaliplatin-induced peripheral neuropathy model.  $\beta$ -lactam **51** also reduced the mechanical and cold hypersensitivity in a neuropathic pain model induced by chronic constriction injury (LCC) and alleviated the mechanical hypersensitivity in a nitroglycerin induced migraine model. In addition, some preliminary cutaneous permeability results obtained for these compounds are summarised in this chapter.

On the other hand, Chapter 2 focuses on the search of new chemical scaffolds able to modulate TRPM8 through virtual screening of the EDASA scientific molecular library. The 21 molecules exhibiting the best TRPM8 interaction energies were selected from this screening. These results were validated *in vitro* using calcium microfluorometry

## Abstract

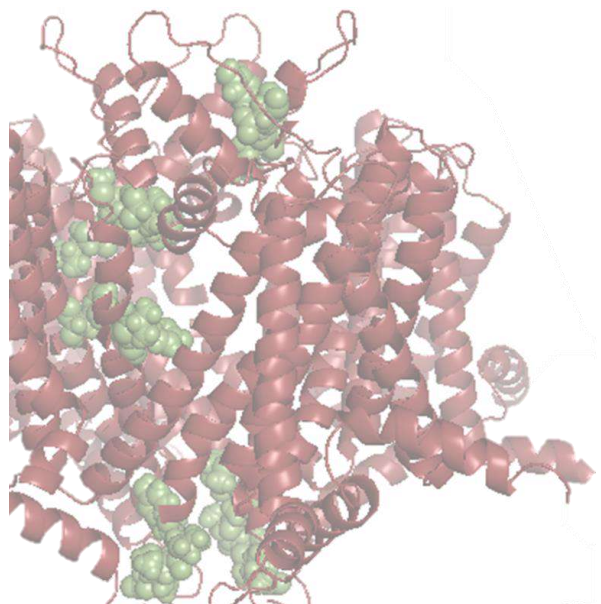
techniques in the cell line mentioned above. Six out of these 21 compounds were identified as potent TRPM8 blockers standing out the compounds **14** and **15**, exhibiting the best potency, efficacy, and selectivity results; and compounds **13** and **19**, displaying agonist activity towards the *h*TRPV1 channel and becoming dual activity modulators. The activity and potency results of compounds **14** and **15** were confirmed by electrophysiological techniques obtaining IC<sub>50</sub>s equal to 1.25 y 2.95 μM respectively. Regarding the molecular modelling results, the main binding sites identified for the compounds are different to the ones described for other TRPM8 blockers. Finally, compound **14** also decreased cold allodynia in a mice model of oxaliplatin-induced peripheral neuropathy.

In conclusion, new relevant chemotypes in the TRPM8 blockade have been identified and characterised in this work. These structures constitute a starting point towards future modifications to optimise their pharmacological characteristics and to obtain a better understanding of the channel and the structures' selectivity towards different TRP channels.





## INTRODUCCIÓN





## INTRODUCCIÓN

### 1. Sistema somatosensorial

El sistema somatosensorial es la parte del sistema nervioso que nos permite relacionarnos con el entorno e interactuar con él. Este sistema tiene dos componentes principales con rutas distintas en la transmisión de estímulos: un subsistema para la detección de estímulos mecánicos que nos brinda información sobre el tacto y la posición, y un subsistema para la detección de estímulos térmicos y dolorosos<sup>1,2</sup>. La recepción somatosensorial en ambos subsistemas consta de 4 etapas principales como se muestra en la Figura 1. Consiste en una fase inicial de recepción y transducción de los estímulos a señales eléctricas; una fase de transmisión del impulso nervioso hasta el sistema nervioso central (SNC); una tercera fase de modulación del estímulo que incluye los cambios que se producen en el SNC; y, por último, la fase de percepción del estímulo en la cual la información llega al cerebro y se interpreta<sup>3</sup>.

#### 1.1. Vías generales de la recepción somatosensorial

Existen dos vías generales del sistema somatosensorial: la vía espinotalámica, para el subsistema que percibe estímulos térmicos y dolorosos, y la vía lemniscal, para el subsistema que detecta estímulos mecánicos (Figura 1). Ambas vías se componen de 3 tipos de neuronas: las neuronas de primer orden, de segundo orden y de tercer orden. Las neuronas de primer orden son células pseudounipolares con un extremo distal en la periferia que inerva los receptores somatosensoriales, un cuerpo celular en los ganglios de la raíz dorsal (GRD) o del nervio trigémino (GNT), y un extremo proximal que participa en la sinapsis con la neurona de segundo orden. Dependiendo de la vía somatosensorial, esta sinápsis se produce en distintas áreas del SNC. En la vía espinotalámica, la sinapsis tiene lugar en las astas dorsales de la medula espinal para las sensaciones del cuerpo y en el bulbo raquídeo para las sensaciones del rostro. Mientras que en la vía lemniscal, la sinapsis siempre tiene lugar en las columnas dorsales del bulbo raquídeo. Los axones ascendentes de estas neuronas decusan hacia el lado opuesto hasta llegar al núcleo ventral posterior del tálamo donde tiene lugar la sinapsis con la neurona de tercer orden. Esta última neurona es la que conducirá el estímulo hasta el área somatosensorial primaria de la corteza cerebral, donde se procesará la información<sup>1,2,4</sup>.

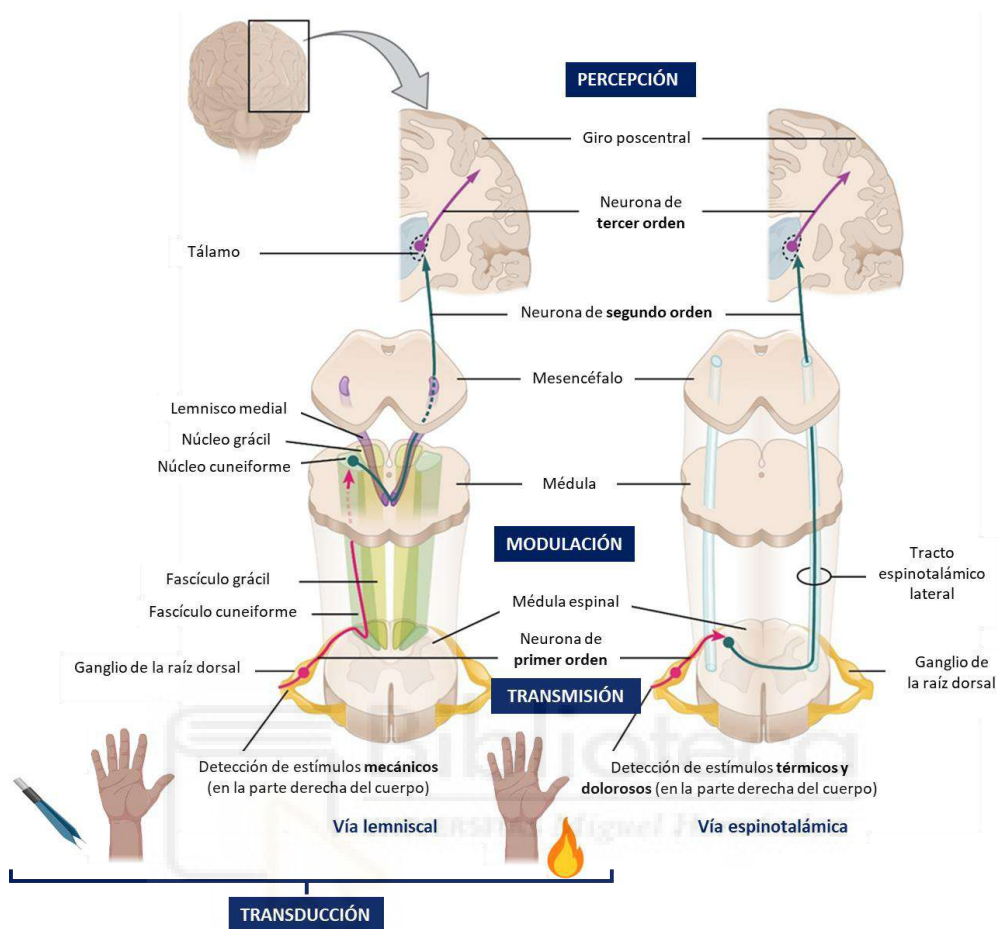


**Figura 1.** Vista anterior de las vías generales de recepción somatosensorial: la vía lemniscal (o vía de la columna dorsal) y la vía espinotalámica. Se muestran las neuronas de primer, segundo y tercer orden que componen las distintas vías somatosensoriales y las 4 etapas comunes en el proceso de recepción somatosensorial: transducción, transmisión, modulación y percepción. Editada de Betts 2013<sup>4</sup>.

## 1.2. Fibras nerviosas somatosensoriales

Las fibras nerviosas somatosensoriales constituyen los axones periféricos de las neuronas de primer orden y son las encargadas de transmitir el estímulo desde los receptores somatosensoriales hasta el SNC. Estas fibras nerviosas pueden clasificarse en fibras tipo A ( $A\alpha$ ,  $A\beta$  y  $A\delta$ ) y tipo C según su anatomía y su función (Tabla 1)<sup>5-7</sup>:

- Las fibras tipo  $A\alpha$  son las de mayor diámetro y grado de mielinización, por lo tanto, son las más rápidas. Su principal función es la propiocepción.
- Las fibras tipo  $A\beta$  tienen un menor diámetro y un menor grado de mielinización que las anteriores. Son las responsables de la transmisión del tacto y de la presión.

- Las fibras tipo A $\delta$  son todavía menores en diámetro, grado de mielinización y velocidad de transmisión. Participan en la transmisión de las sensaciones de dolor, temperatura y tacto.
- Las fibras tipo C son las más pequeñas y las únicas que carecen de mielina, siendo por lo tanto, las más lentas en la transmisión de estímulos. Su función es también la transmisión de las sensaciones de dolor, temperatura y picor <sup>5,6</sup>.

**Tabla 1.** Características de las fibras nerviosas aferentes del sistema somatosensorial <sup>7</sup>.

Fibras nerviosas	Estímulo somatosensorial	Diámetro de las fibras nerviosas	Mielina	Velocidad de conducción del estímulo nervioso
A $\alpha$	Propiorrecepción	12-22 $\mu$ m	Sí	70-120 m/s
A $\beta$	Tacto y presión	5-12 $\mu$ m	Sí	30-70 m/s
A $\delta$	Dolor, temperatura y tacto.	1-5 $\mu$ m	Sí	5-30 m/s
C	Dolor, temperatura y picor.	0,1-1,3 $\mu$ m	No	0.6-2 m/s

### 1.3. Receptores somatosensoriales

Los receptores somatosensoriales son las terminaciones nerviosas especializadas que inervan la piel, los músculos, las articulaciones y las vísceras, capaces de captar estímulos internos o externos y generar un impulso nervioso <sup>8</sup>. Estos receptores se clasifican en tres grandes grupos según el tipo de estímulo que perciben <sup>2</sup>:

- a) Mecanorreceptores. Esta familia de receptores puede dividirse en dos grupos: los mecanorreceptores especializados en recibir información táctil y los mecanorreceptores especializados en la propiocepción. Los primeros se encuentran principalmente en la piel y detectan estímulos mecánicos como el tacto, tensión, vibración o presión <sup>2,9</sup>. Mientras que los propioceptores, se encuentran en las articulaciones y aportan información sobre la posición y el movimiento del cuerpo. Todos ellos presentan cierto grado de encapsulación y se denominan mecanorreceptores de bajo umbral, ya que estimulaciones débiles pueden desencadenar potenciales de acción <sup>2,10</sup>.
- b) Termorreceptores. Los termorreceptores son terminaciones nerviosas libres que reconocen la temperatura cutánea. Existen receptores para el frío, que responden a

un amplio intervalo de temperaturas entre 10 y 35°C, y receptores para el calor, que se activan a temperaturas de entre 30°C y 43°C <sup>11</sup>.

c) Nociceptores. Los nociceptores reaccionan ante estímulos nocivos capaces de causar daño tisular. Estos también están formados por terminaciones nerviosas cutáneas libres que, a diferencia de las anteriores, poseen un alto umbral de estimulación. Según el tipo de estímulo que son capaces de identificar se pueden clasificar en:

- Nociceptores Térmicos. Se activan cuando los estímulos térmicos son superiores a 45°C o inferiores a 5°C.
- Nociceptores Mecánicos. Se activan cuando el tejido se somete a un estímulo mecánico intenso.
- Nociceptores Polimodales. Se activan por estímulos de alta intensidad de varios tipos (mecánicos, químicos o térmicos) <sup>1,12</sup>.
- Nociceptores Silenciosos. Estos nociceptores no se activan tras estímulos nocivos directos, sino que son sensibilizados por mediadores inflamatorios producidos tras un estímulo dañino <sup>13</sup>.

## 2. Canales TRP y recepción somatosensorial

A nivel molecular, los receptores somatosensoriales poseen en sus terminales una gran variedad de receptores proteicos específicos y canales iónicos que se encargan de reconocer y transducir los estímulos mecánicos, térmicos y nociceptivos a potenciales de acción (Figura 2) <sup>14</sup>. Una de las familias de canales iónicos más importantes en la transducción de las distintas modalidades somatosensoriales en mamíferos es la familia de Receptores de Potencial Transitorio o TRP (Transient Receptor Potencial) <sup>15</sup>.

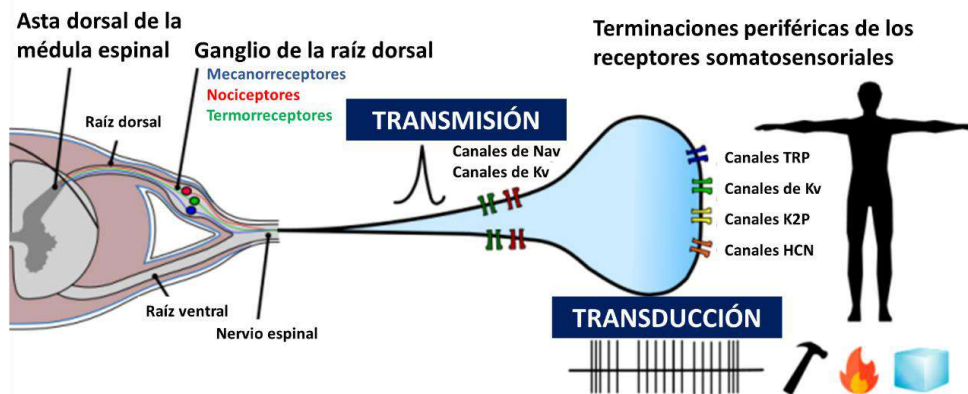


**Figura 2.** Transducción y transmisión somatosensorial. Los receptores sensoriales poseen una gran diversidad de canales iónicos encargados de la transducción de los distintos estímulos en potenciales de acción. Estos potenciales de acción se transmiten hasta el SNC mediante las neuronas sensoriales periféricas, cuyos somas se encuentran en los GRD. Editada de Arcas-Santos 2019 <sup>16</sup>.

## 2.1. Superfamilia de canales TRP

Los Receptores de Potencial Transitorio o TRP constituyen una gran superfamilia de canales catiónicos que median el flujo de  $\text{Na}^+$  y  $\text{Ca}^{2+}$  a través de la membrana plasmática <sup>17</sup>. Hace más de medio siglo, Consens y Manning descubrieron una mutación de *Drosophila melanogaster* la cual mostraba una respuesta o potencial transitorio, en vez de sostenido, a la luz constante <sup>18,19</sup>. Este fenotipo adoptó el término, por primera vez utilizado, de receptor de potencial transitorio o TRP. Sin embargo, su etiología genética no se identificó hasta casi dos décadas más tarde por Montell y Rubin <sup>18,20</sup>.

En la actualidad, se han descubierto más de 100 genes TRP en una gran variedad de organismos multicelulares que constituyen una superfamilia de 30 canales iónicos <sup>15,18</sup>. Estos 30 canales se clasifican en 8 subfamilias según la homología de sus secuencias (Figura 3): canónica o clásica (TRPC), vaniloide (TRPV), melastatina (TRPM), policistina (TRPP), mucolipina (TRPML), anquirina (TRPA) y por último, las subfamilias *no-mecanoreceptor potencial C* (TRPN) presente en invertebrados <sup>15,18</sup> y en el pez cebra, y *yeast* (TRPY) expresado en levaduras <sup>15</sup>.

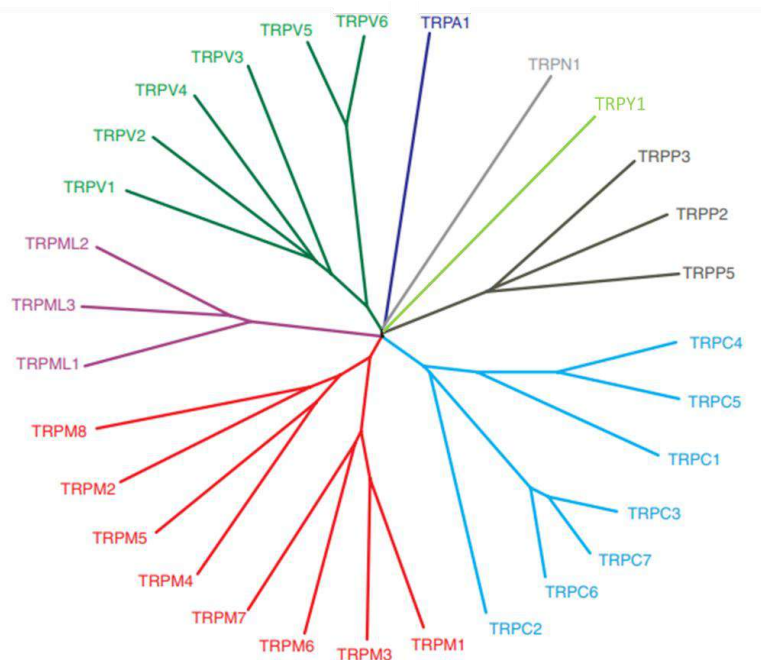


**Figura 3.** Árbol filogenético de los canales TRP. La familia de canales TRP se divide en siete subfamilias según la homología de sus secuencias. Editado de Nilius 2011 <sup>18</sup>.

A pesar de las diferencias en las secuencias de las distintas subfamilias de canales TRP, todos poseen una misma estructura general. Se componen de 6 segmentos transmembrana (TM1 a TM6) de los cuales dos de ellos (TM5 y TM6) forman el poro <sup>17,21</sup>. Esta región del poro es la más conservada entre las diferentes subfamilias, indicando la importancia de los aminoácidos que la componen en la formación y apertura del canal <sup>17,22</sup>. Para que el canal sea funcional, se requiere el ensamblaje de cuatro subunidades formando homo o heterotetrameros <sup>17</sup>. En cuanto a las regiones amino (NH<sub>2</sub>) y carboxilo (COOH) terminales, ambas son intracelulares y contienen sitios de regulación mediante proteínas quinasas, chaperonas y proteínas de anclaje, estando involucrados en la regulación, función y ensamblaje del canal <sup>17,18,21</sup>.

Esta gran familia de canales se encuentra ampliamente distribuida en los diferentes tejidos de los seres vivos, encargándose de numerosas funciones fisiológicas que abarcan desde la recepción sensorial y somatosensorial <sup>23</sup>, hasta funciones homeostáticas y motoras <sup>18</sup>. Así pues, cambios en la expresión, la función y la regulación de estos canales se ha visto implicada en numerosas condiciones o patologías, entre ellas distintos tipos de dolor <sup>23</sup>, cáncer <sup>24</sup> y enfermedades genéticas <sup>18</sup>.

### 2.1.1. Canales TRP y termorrecepción

Dentro de la familia de canales TRP, destacan tres superfamilias por su implicación en la termosensación: las superfamilias TRPV, TRPM y TRPA, recibiendo el nombre de termoTRPs. Estos canales detectan un amplio rango de temperaturas frías y calientes, inocuas y dolorosas (Figura 4) <sup>15,25</sup>.

La familia TRPV se compone de 6 miembros (TRPV1-TRPV6), siendo los 4 primeros (TRPV1-TRPV4) los que responden a estímulos térmicos. El canal más estudiado de esta familia es el TRPV1, el cual se activa por temperaturas nocivas superiores a 37°C-43°C según la especie. Este canal es el receptor natural de la capsaicina, principio activo responsable de la sensación de picor del chili <sup>25,26</sup>. El canal TRPV2 responde a un rango de temperaturas nocivas superiores a 52°C <sup>27</sup>, mientras que los otros dos, TRPV3 <sup>28</sup> y TRPV4<sup>29</sup>, responden a temperaturas calientes inocuas (25°C-37°C).

Por otra parte, la subfamilia TRPM también juega un papel crucial en la termorrecepción. Esta subfamilia consta de 8 miembros (TRPM1-TRPM8) de los cuales 3 se han relacionado con la termorrecepción de temperaturas tanto frías como calientes. En esta familia destaca el canal TRPM8 por ser el principal sensor fisiológico de temperaturas frías <sup>30</sup>, activándose por temperaturas tanto inocuas como dolorosas por debajo de 30°C según la especie <sup>25</sup>. Por otra parte, los canales TRPM2 <sup>31,32</sup> y TRPM3 <sup>31</sup> están implicados en la sensación de temperaturas inocuas y dolorosas respectivamente.

Otra subfamilia termoTRP es la TRPA, compuesta por un único miembro, el canal TRPA1. Este canal reacciona a temperaturas dolorosas por debajo de 17°C <sup>15</sup>. Por último, algunos autores como Hoffstaetter <sup>25</sup> incluyen a la subfamilia TRPC dentro de los canales termoTRP. Esta familia está compuesta por siete miembros (TRPC1-TRPC7), de los cuales solo el TRPC5 está involucrado en la recepción de temperaturas inocuas (25°C-35°C) <sup>25</sup>.

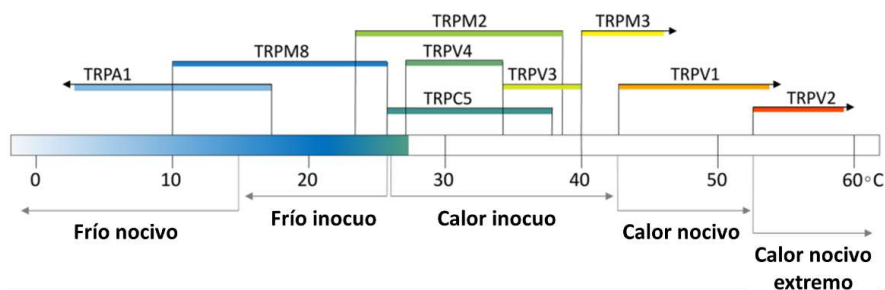


**Figura 4.** Rango de temperaturas de activación de los termoTRPs en mamíferos y su clasificación en temperaturas inocuas y nocivas. Editada de Hoffstaetter 2018<sup>25</sup>.

### 2.1.2. Canales TRP y dolor

Algunos miembros de la familia TRP se han localizado en los nociceptores dónde actúan como transductores de varios estímulos térmicos, químicos y mecánicos de alto umbral, viéndose implicados en la percepción de dolor (Figura 5)<sup>33</sup>. Este término se define como “una experiencia sensorial y emocional desagradable asociada, o que parece asociada, a una lesión tisular real o potencial”<sup>34</sup>. El dolor puede catalogarse atendiendo a diversos parámetros<sup>8,35</sup>. Para relacionarlo con la implicación de los canales TRP, lo clasificaremos según su origen en dolor nociceptivo, inflamatorio y neuropático<sup>36</sup>.

El dolor nociceptivo se debe a la activación de los nociceptores tras un estímulo dañino de alta intensidad. Este tipo de dolor juega un papel importante en el sistema de protección del organismo, ya que identifica agentes nocivos y activa mecanismos protectores para limitar el daño en el tejido<sup>33</sup>. En este tipo de dolor cobran principal importancia los canales TRPV1 y TRPA1, ya que ambos pueden activarse por una gran variedad de estímulos dolorosos (Figura 5A)<sup>33</sup>. Algunos ejemplos serían moléculas como la capsaicina, toxinas de araña<sup>37</sup>, metabolitos del ácido araquidónico<sup>38</sup>, pHs bajos<sup>39</sup> y temperaturas altas (> 43°C)<sup>25</sup> para el canal TRPV1; e ingredientes picantes como el AITC y el cinamaldehído<sup>40</sup>, agentes nocivos como la nicotina<sup>41</sup> y el isoflurano<sup>42</sup>, y temperaturas bajas (< 18°C)<sup>33</sup> para el canal TRPA1. Además de estos dos canales, también se han relacionado con el dolor nociceptivo los canales TRPV2-TRPV4 y TRPM8, aunque su función exacta no está descrita en profundidad<sup>33</sup>. Esto se debe a que los canales TRPV2<sup>15</sup> y TRPM8<sup>31</sup> están involucrados en la recepción de estímulos dolorosos calientes y fríos, respectivamente; el TRPV4 en la recepción de estímulos

mecánicos dañinos; y este último junto al TRPV3, en la recepción de estímulos químicos nocivos<sup>33</sup>.

Por otra parte, el dolor inflamatorio se debe a la sensibilización de las rutas nociceptivas producida por numerosos mediadores inflamatorios y productos del estrés oxidativo. Esta sensibilización de los nociceptores involucra principalmente a los canales TRP, concretamente al TRPV1, TRPV2, TRPV4, TRPA1 y TRPM8 (Figura 5B). Los metabolitos originados por los tejidos inflamatorios pueden activar directamente a estos canales o pueden sensibilizarlos mediante 3 mecanismos: aumentando la expresión de dichos canales en las neuronas sensoriales, aumentando el número de canales funcionales en la membrana plasmática e impidiendo la inhibición de los canales mediada por fosfatidilinositol 4,5-bisfosfato (PI(4,5)P<sub>2</sub>)<sup>33</sup>.

Por último, el dolor neuropático se origina tras estímulos directos en el SNC o lesiones en el sistema nervioso periférico (SNP) y se considera patológico, ya que no actúa como mecanismo de protección<sup>33,43</sup>. Este dolor neuropático se presenta en neuropatías de diverso origen en las que pueden cursar con la diabetes, tras el tratamiento con agentes quimioterapéuticos o tras infecciones herpéticas. Estas lesiones en el sistema nervioso dan lugar a cambios en la expresión de los canales TRP en las neuronas sensoriales. Dichos cambios llevan a alteraciones en el procesamiento de los estímulos en el SNC<sup>33</sup>. Los canales TRP que participan en este tipo de dolor son principalmente el TRPV1, TRPA1 y TRPM8. En las neuronas sensoriales dañadas se observa una disminución de la expresión de dichos canales, mientras que en las neuronas colindantes se observa un aumento de su expresión y de la excitabilidad neuronal. Esto podría deberse a la liberación o no reabsorción de determinados neurotransmisores y factores de crecimiento por parte de las neuronas dañadas (Figura 5C)<sup>33,44,45</sup>. Existen numerosos modelos animales de dolor neuropático en los que se describe un incremento en la expresión de estos canales TRP que se correlaciona con los comportamientos típicos de dolor. Además, tanto el bloqueo farmacológico como la ablación génica de dichos canales reducen dichas conductas dolorosas<sup>33,44-51</sup>. Por último, también se ha relacionado con este tipo de dolor el canal TRPV4<sup>52</sup>, y recientemente el TRPM2<sup>53</sup>, mediando la hipersensibilidad mecánica.

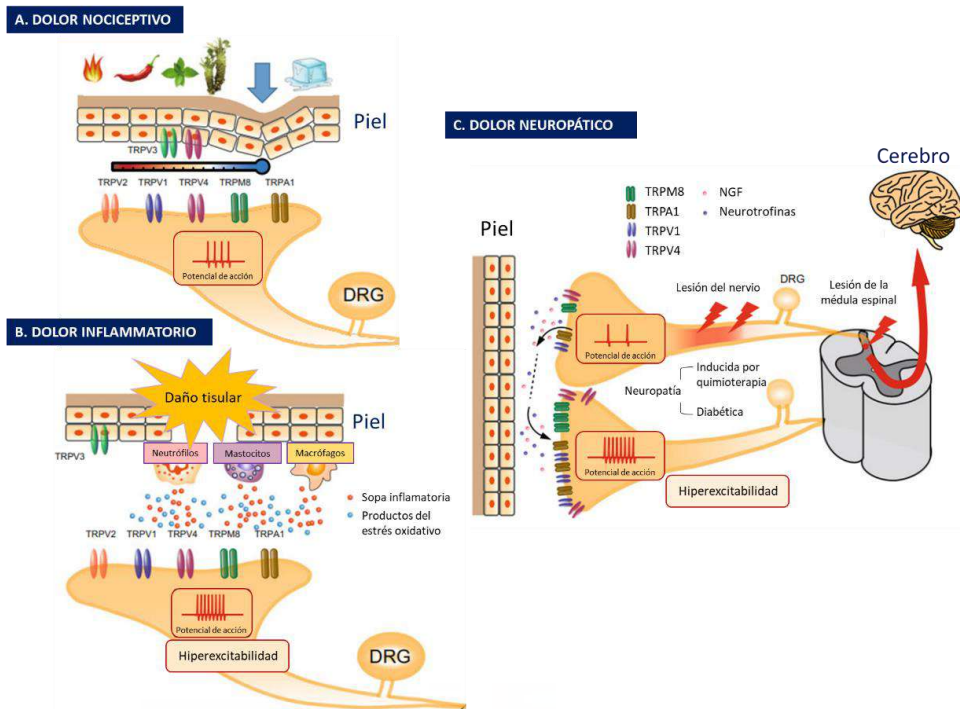


**Figura 5.** Canales TRP en el dolor nociceptivo (A), inflamatorio (B) y neuropático (C). A) En el dolor nociceptivo, estímulos dolorosos como el frío, el calor, la presión, etc. activan directamente a los canales TRP en las neuronas sensoriales. B) En el dolor inflamatorio, la sopa inflamatoria y productos del estrés oxidativo activan o sensibilizan los canales TRP en las neuronas sensoriales. C) En el dolor neuropático, los canales TRP se ven disminuidos en las fibras de las neuronas sensoriales dañadas y sobreexpresados en las fibras colindantes. Esto se debe a un aumento de neurotransmisores y factores de crecimiento producido por las neuronas dañadas. Editada de Dai 2016 <sup>33</sup>.

### 3. Canal iónico TRPM8

El miembro 8 de los Receptores de Potencial Transitorio de Melastatina es un canal catiónico no selectivo permeable a calcio que presenta mecanismos polimodales de apertura y que pertenece a la familia de canales termoTRPs <sup>54,55</sup>. Este canal se ha identificado como el sensor fisiológico de temperaturas frías, activándose por un rango de temperaturas tanto inocuas como dolorosas (10-28°C) <sup>56,57</sup>, agentes refrescantes naturales como el mentol y sintéticos como la icilina <sup>58</sup>, cambios en la osmolaridad <sup>59</sup> y cambios en el voltaje <sup>60,61</sup>.

El gen que codifica TRPM8 se identificó y clonó por primera vez a partir de una librería de ADNc de próstata <sup>62</sup>. Posteriormente, este canal se detectó también en otros tejidos como en las fibras aferentes C y Aδ de las neuronas sensoriales de las GRDs y de los GNTs <sup>56,63</sup> que inervan tejidos sensibles al frío como la piel, el epitelio de la boca, los

dientes, la lengua, y la córnea<sup>63,64</sup>. Otros tejidos en los que encontramos este canal son el tejido broncopulmonar, la vejiga y el tracto urogenital<sup>65</sup>. Su amplia ubicuidad y sus diversas funciones fisiológicas relacionan al canal con un gran número de patologías como el dolor, la inflamación, la migraña, el cáncer y trastornos genitourinarios y digestivos entre otros<sup>30,56</sup>. Así pues, la regulación de la expresión o de la actividad de este canal puede ser una nueva oportunidad de intervención terapéutica en estas condiciones fisiopatológicas.

### 3.1. Estructura de TRPM8.

Recientemente se ha resuelto la estructura completa de TRPM8 mediante criomicroscopía electrónica a partir del ave *Ficedula albicollis* (*fa*TRPM8) por el grupo de Seok-Yong Lee. Esta estructura comparte un 83% de homología con la secuencia del canal TRPM8 humano<sup>66</sup>. Este canal posee una estructura similar a los demás miembros de la superfamilia TRP. Es un homotetrámero formado por cuatro subunidades idénticas de 1104 aminoácidos cada una y con un peso molecular de aproximadamente 128KDa (Figura 6)<sup>67-69</sup>. Cada monómero está compuesto por 6 segmentos helicoidales transmembrana (TM1-TM6) con un dominio tipo sensor de voltaje (VSLD), formado por los segmentos TM1 a TM4, y un poro, formado por los segmentos TM5 y TM6. La región del poro presenta una región hidrofóbica conservada con un residuo de aspartato responsable de la selectividad de los iones y la función del canal<sup>65,70,71</sup>. En esta región también encontramos dos residuos de cisteína esenciales para la funcionalidad del canal y un sitio de glicosilación importante para la expresión del canal en la membrana plasmática<sup>68</sup>.

En cuanto a los dominios terminales, tanto el dominio N-terminal (Nt) como el C-terminal (Ct) se encuentran en la región citoplasmática y constan de 733 y 124 residuos, respectivamente<sup>71</sup>. El dominio Nt comprende cuatro regiones de homología de melastatina, propias de la familia TRPM, que podrían estar relacionadas con procesos de localización celular<sup>72</sup>; y el dominio pre-S1, involucrado en la activación alostérica del canal. Respecto al dominio Ct, este contiene la región TRP entre los residuos 990-1025 que se relaciona con la regulación de la apertura del canal frente a (PI(4,5)P<sub>2</sub>) y a otros

## Introducción

agonistas <sup>73</sup>, y el dominio *coiled-coil*, el cual posee un papel crítico en la tetramerización del canal <sup>68,72</sup>.

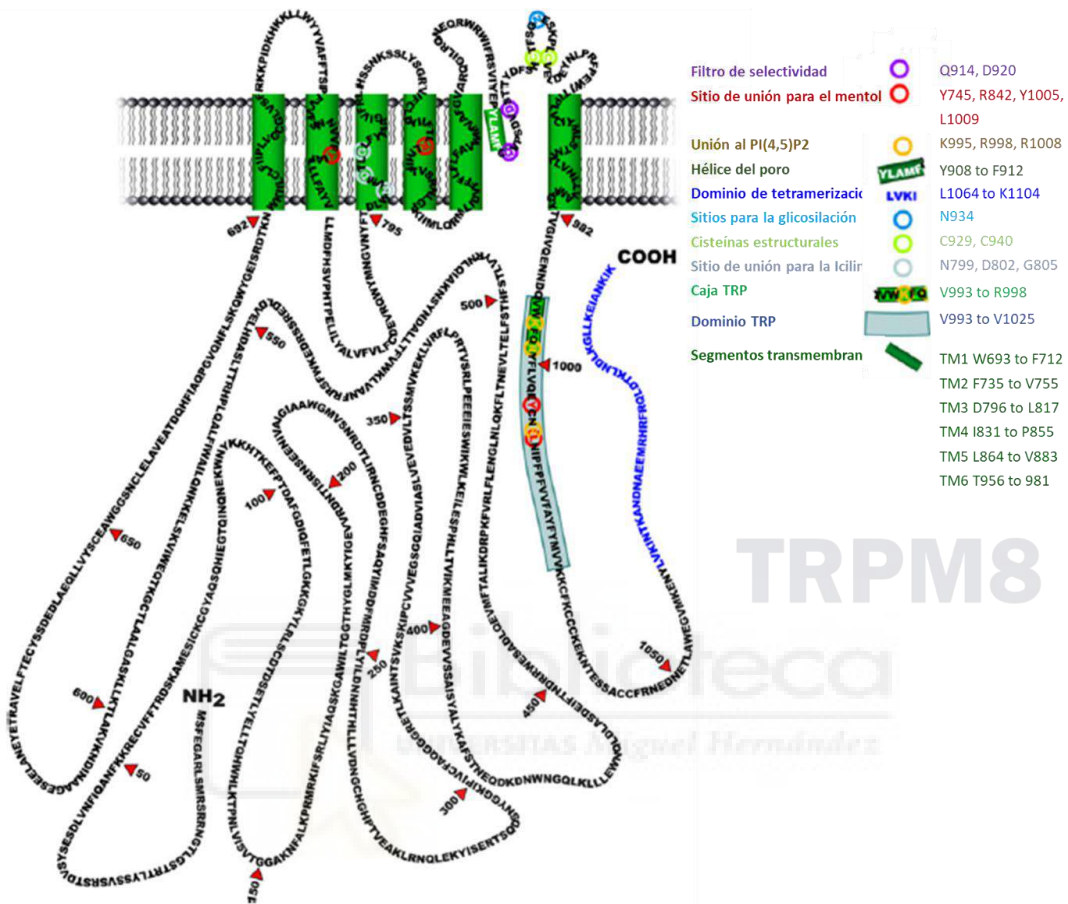


Figura 6. Cada subunidad del canal TRPM8 consta de 6 segmentos transmembrana (TM1-TM6) y dos dominios terminales intracelulares. El dominio transmembrana consta de un módulo sensor de voltaje (TM1-TM4), que contienen los sitios de unión para el mentol e icilina, y un módulo que forma el poro (TM5-TM6), que contiene sitios para la glicosilación, la hélice del poro, el filtro de selectividad y los dos residuos de cisteína. En cuanto a los extremos terminales intracelulares, posee un módulo Nt y un módulo Ct en el que se encuentra la caja TRP, el dominio TRP, los aminoácidos implicados en la modulación del canal por PI(4,5)P<sub>2</sub> y un dominio de tetramerización. Editada de La Torre 2007 <sup>74</sup>.

Respecto a los aminoácidos importantes en la modulación del canal, estos se han identificado mediante estudios de mutagénesis <sup>66</sup>. Estos estudios demostraron la relevancia de residuos aromáticos para la activación del canal por mentol: la Tyr745 <sup>75</sup> en TM2, la Arg842 <sup>76</sup> en TM3, y la Tyr1005 y Leu1009 <sup>75</sup> en el dominio TRP. Mutaciones como Tyr745Ala, Tyr745Phe <sup>75,77</sup>, Tyr1005Ala, Tyr1005Phe, Leu1009Arg <sup>75</sup> y Arg842Ala <sup>76</sup> produjeron insensibilidad o una menor respuesta al mentol. También se han identificados otros aminoácidos importantes en la modulación del canal por otras moléculas. Para la icilina son de gran importancia los residuos Asn799, Asp802, y Gly805,

todos situados entre las regiones TM2-TM3 <sup>66,77</sup> mientras que para el PI(4,5)P<sub>2</sub> los residuos que juegan un papel importante son: Lys995, Arg998 y Arg1008, los cuales se encuentran en el dominio TRP <sup>78</sup>.

### 3.3. Modulación endógena de TRPM8

El canal TRPM8 posee diversos mecanismos de modulación endógena que incluyen la actuación de fosfolípidos de membrana destacando el PI(4,5)P<sub>2</sub> <sup>79</sup>, lisofosfolípidos, ácidos grasos poliinsaturados y diversas modificaciones postraduccionales <sup>56</sup>.

El PI(4,5)P<sub>2</sub> corresponde al 1% de los lípidos presentes en la membrana plasmática. Este fosfolípido es capaz de modular positivamente 20 de los 28 canales que constituyen la familia TRP, incluyendo el canal TRPM8 <sup>80</sup>. Se sabe que PI(4,5)P<sub>2</sub> modula tanto la activación como la desensibilización del canal <sup>79</sup>, siendo imprescindible para la activación de TRPM8 mediante frío y mentol <sup>81</sup>. Este lípido se hidroliza mediante la fosfolipasa C (PLC) dando lugar a los dos segundos mensajeros clásicos, el 1,4,5-trifosfato de inositol (IP<sub>3</sub>) y el diacilglicerol (DAG). Ambos componentes actúan sinérgicamente para activar la proteína quinasa C (PKC), la cual puede fosforilar TRPM8 dando lugar a una reducción de su actividad <sup>82,83</sup>. Además de la PKC, la actividad de otras proteínas quinasas como la PKA también parece inhibir la actividad de TRPM8 <sup>82,84</sup>.

La regulación de TRPM8 mediante fosfoinosítidos también puede estar mediada por Pirt (Regulador de TRP que interactúa con fosfoinosítidos). Pirt es una proteína transmembrana que actúa de manera sinérgica con PI(4,5)P<sub>2</sub> aumentando la sensibilidad de TRPM8 al mentol y a las temperaturas frías <sup>85,86</sup>. Otros mecanismos de regulación de TRPM8 mediados por lípidos incluyen a la fosfolipasa A<sub>2</sub> (PLA<sub>2</sub>) <sup>56</sup>. La PLA<sub>2</sub> es una enzima que cataliza la hidrólisis de fosfolípidos de membrana dando lugar a lisofosfolípidos, entre otros ácidos grasos poliinsaturados. Estos lisofosfolípidos actúan como agonistas endógenos de TRPM8 activándolo a temperaturas fisiológicas <sup>87</sup>.

Otra proteína involucrada en la modulación del canal es la proteína G <sup>82,88</sup>. Cuando esta proteína se activa por un receptor acoplado a proteínas G (GPCR) puede inhibir el canal de manera directa mediante su subunidad G $\alpha$  <sup>88</sup> o de manera indirecta tras activar la PLC <sup>82</sup>.

## Introducción

Por último, otros mecanismos estudiados en la modulación del canal, incluyen las isoformas cortas de TRPM8, las cuales se originan durante la transcripción del canal y forman tetrámeros no funcionales <sup>89</sup>; la proteína de membrana asociada a vesículas 7 (VAMP7), las cuales participan en la incorporación funcional de TRPM8 a la membrana plasmática <sup>90</sup>; y diferentes hormonas como la testosterona, la cual no solo activa el canal de manera directa sino que también puede regular la expresión del gen <sup>91</sup>.

### 3.2. Modulación química de TRPM8

Debido a la implicación de TRPM8 en diferentes patologías, este se ha convertido en una diana terapéutica a explorar. En los últimos años, han sido muchas las empresas farmacéuticas y biotecnológicas que se han interesado por el desarrollo de moduladores del canal, lo que ha llevado a la identificación de numerosas y diversas familias de moduladores de TRPM8 <sup>92</sup>. Para entender el por qué la búsqueda de moduladores no se limita a agonistas o antagonistas para tratar una misma condición como por ejemplo el dolor, es necesario saber que el canal TRPM8 se desensibiliza tras exposiciones prolongadas a agonistas. Esta desensibilización se debe a la hidrólisis del lípido de membrana PI(4,5)P<sub>2</sub> necesario para su activación (Figura 7). Así pues, tanto el empleo de agonistas como de antagonistas del canal puede llevar a un estado cerrado de este evitando el paso de iones <sup>93</sup>.

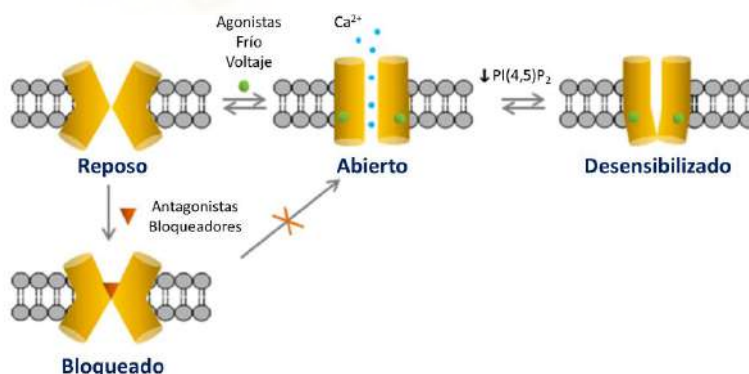


*Figura 7. Esquema simplificado de los diferentes estados de los canales TRPM8 (reposo, abierto, desensibilizado y bloqueado). Editada de Jesús 2016 <sup>56</sup>.*

### 3.2.1. Agonistas de TRPM8

El agonista más conocido del canal TRPM8 es el mentol, un alcohol terpénico secundario que se encuentra en la menta <sup>94</sup>. El mentol ha participado en más de 200 estudios clínicos a distintas concentraciones (3,5-40%) para fines cosméticos, alimentarios o médicos <sup>71</sup>. A pesar del gran número de estudios realizados, solo algunos han generado resultados positivos, como es el caso de la administración de mentol tópico para tratar algunos tipos de dolor <sup>92</sup>; o de mentol oral en el tratamiento de la presión arterial y otros cambios metabólicos en pacientes prehipertensos e hipertensos leves <sup>95</sup>. Otras moléculas en fase clínica son el derivado del mentol mentoxipropanodiol, efectivo en el tratamiento del picor que cursa con las dermatitis atópicas <sup>96</sup>; moléculas como el criosim-1 y criosim-3, efectivos en el tratamiento tópico del dolor <sup>97</sup> y de la sequedad ocular <sup>98</sup> respectivamente; y el compuesto AVX-012 de Avizorex Pharma, también efectivo en el tratamiento de la sequedad ocular. Este último sigue en desarrollo clínico tras concluir con éxito los ensayos clínicos de Fase I y IIa <sup>92</sup>.

Además de los compuestos citados, son muchas las moléculas naturales o sintéticas identificadas como activadoras de TRPM8. En la naturaleza, además del mentol, y con actividad similar, encontramos el borneol. Este se extrae de plantas medicinales como la *Blumea balsamifera* la cual se ha utilizado durante años en la medicina tradicional china para tratar diferentes condiciones oculares <sup>99</sup> y como analgésico tópico <sup>100</sup>. Su actividad en ambas condiciones se debe principalmente a su capacidad para activar TRPM8 <sup>99,100</sup>. Otros compuestos presentes en la naturaleza capaces de activar el canal serían el linalool, geraniol, eucaliptol, hidroxilcitronelal y alcanfor <sup>101</sup>.

En cuanto a los activadores sintéticos de TRPM8, su principal objetivo es evitar los inconvenientes que presentan los agonistas naturales, como serían la irritación o el gusto amargo, y mejorar sus propiedades farmacológicas, consiguiendo un inicio más rápido y una duración más larga de su efecto <sup>71</sup>. Para ello, parte de la investigación se ha centrado en el estudio de derivados del mentol, siendo un ejemplo de estos derivados los compuestos WS, entre los cuales destaca el WS-12 por ser el agonista de TRPM8 más potente identificado hasta el momento <sup>102</sup>. Otros compuestos relacionados

químicamente con el mentol y eficaces en la activación de TRPM8 son el Frescolat MGA, Frescolat ML, PMD 38, Coolact P y *Cooling agent 10*<sup>94,103</sup>.

Por otra parte, también existen agonistas sintéticos del canal que difieren químicamente del mentol, el ejemplo más conocido es la icilina (AG-3-5). La icilina se considera un agente superrefrigerante siendo más potente que el mentol y poseyendo un mecanismo de acción diferente a este<sup>104,105</sup>. Ejemplos de otros agonistas sintéticos de TRPM8 identificados recientemente por farmacéuticas y grupos de investigación se resumen en revisiones como la de Izquierdo<sup>71</sup> o la de González-Muñiz<sup>65</sup>. Entre los resultados más relevantes cabe destacar las patentes de Procter and Gamble, en las que modificaciones del mentol llevaron a compuestos muy potentes propuestos para patologías metabólicas, para el síndrome del intestino irritable (SII) y para el tratamiento del dolor<sup>106</sup>; y la serie de 1-diisopropil-fosfinoil-alcanos de E.T. Wei indicados para tratar múltiples condiciones como los síntomas de ojo seco<sup>107</sup>, dolor sensorial<sup>108</sup>, enfermedades del tracto gastrointestinal bajo<sup>109</sup> y la incomodidad respiratoria<sup>110</sup>. Por último, nombrar la existencia de medicamentos en el mercado, con diferentes indicaciones terapéuticas, que han demostrado activar TRPM8. Estos serían el fármaco antihelmíntico praziquantel<sup>111</sup> y el inmunosupresor tacrólimus<sup>112</sup>.

### 3.2.2. Antagonistas de TRPM8

De la misma manera que sucede para los agonistas de TRPM8, los antagonistas del canal que han llegado a ensayos clínicos son muy escasos. Entre ellos encontramos el compuesto PF-05105679 de Pfizer, el AMG-333 de AMGEN y la Cannabidivarina. El primero de ellos, demostró inhibir el dolor en la prueba de inmersión en agua fría (*cold pressor test*), pero se retiró en la fase I tras producir efectos adversos relacionados la sensación de calor en la boca y en las extremidades que impedían su progreso<sup>113</sup>. El compuesto AMG-333, mostró resultados positivos para la profilaxis de la migraña, sin embargo, también se retiró en la Fase I debido a efectos adversos severos que comprendían sensación de calor, parestesias, disestesias y disgeusias<sup>114</sup>. El último de ellos, la Cannabidivarina, aunque posee un efecto antagonista para TRPM8, se está estudiando en el tratamiento del trastorno del espectro autista por sus efectos en los

receptores cannabinoides. Esta es la única molécula que sigue en fase II de ensayos clínicos <sup>115</sup>.

A pesar del bajo éxito de los bloqueadores de TRPM8 que han llegado a fases clínicas, son muchas las moléculas halladas hasta el momento <sup>65,71</sup>. Recientemente se han identificado algunos compuestos naturales capaces de bloquear TRPM8. Entre ellos encontramos la sesamina, extraída del sésamo, la cual además de ser inocua, selectiva y potente frente a TRPM8, demostró suprimir la proliferación celular en diversas líneas celulares tumorales de próstata <sup>116</sup>; los flavonoides como la crisina, la escutellareína o la hispidulina <sup>117</sup>; los cannabinoides como el Tetrahidrocannabinol (THC), el ácido tetrahidrocannabinólico (THCA), el cannabigerol y cannabidiol <sup>115</sup>; y algunos moduladores del canal TRPV1 como la capsaicina, la resiniferatoxina <sup>118</sup> y la capsacepina <sup>101</sup>. De origen sintético, también encontramos antagonistas de TRPV1 con la capacidad de bloquear TRPM8 como serían el BCTC, el tio-BCTC <sup>101</sup> y el bloqueador de la entrada de calcio SKF-96365 <sup>119</sup>.

Otras moléculas sintéticas con un papel importante en la inhibición de TRPM8 incluyen el AMTB por ser el primer bloqueador del canal caracterizado <sup>120</sup>. Este demostró selectividad hacia otros TRP, pero no hacia otros canales como los de Na<sup>+</sup> dependientes de voltaje <sup>121</sup>. Y el PBMC por ser de los primeros bloqueadores potentes y selectivos caracterizados de TRPM8 <sup>122</sup>. Por otra parte, también existen moléculas en el mercado capaces de bloquear este canal, estos compuestos son los antifúngicos clotrimazol <sup>123</sup> y econazol <sup>124</sup>.

Por último, algunas de las moléculas prometedoras en el bloqueo de TRPM8 identificadas en los últimos años son el KPR-5714 de Kissei Pharmaceutical Co. <sup>125</sup> y el RQ-00434739 de Aizawa en RaQualia Pharma <sup>126</sup>. El primero, consiguió aumentar el volumen y el intervalo de micción en ratas en varios modelos de vejiga hiperactiva (OAB) <sup>125</sup>. Respecto al RQ-00434739, además de inhibir completamente el *wet dog shake* (WDS) inducido por icilina en ratas y ser efectivo en modelos de alodinia al frío mediada por oxaliplatino en ratas y monos, mejoró la condición de OAB en ratas, con la ventaja de no alterar su temperatura corporal. La alteración de la temperatura corporal es un efecto adverso común producido por los antagonistas de TRPM8, así pues, este hecho

convierte a RQ-00434739 en una interesante opción terapéutica en el tratamiento de esta condición <sup>126</sup>.

### 3.4. Implicaciones fisiopatológicas

El canal TRPM8 destaca por su función en la percepción de temperaturas frías. Sin embargo, su amplia distribución en el organismo lo relaciona con numerosos procesos tanto fisiológicos como patológicos (Figura 8) <sup>30</sup>. Entre ellos, destacan los procesos de termorregulación y termogénesis <sup>127</sup>; la regulación de las respuestas autonómicas del sistema respiratorio ante el frío <sup>128</sup>; la modulación de la respuesta inmunitaria <sup>129</sup>; la regulación del lagrimeo <sup>130</sup>; la contracción y la función mecanosensorial en la vejiga <sup>131–133</sup>; la regulación de la proliferación o apoptosis celular en la próstata <sup>134</sup>; y la reducción de la pigmentación en la piel <sup>135</sup>. Dada esta amplia distribución del canal y su participación en procesos vitales, cualquier alteración en la función o expresión puede dar lugar a procesos patológicos entre los que destacan el dolor, el cáncer y algunos trastornos de los sistemas respiratorio, digestivo, urinario y de la piel <sup>30</sup>.

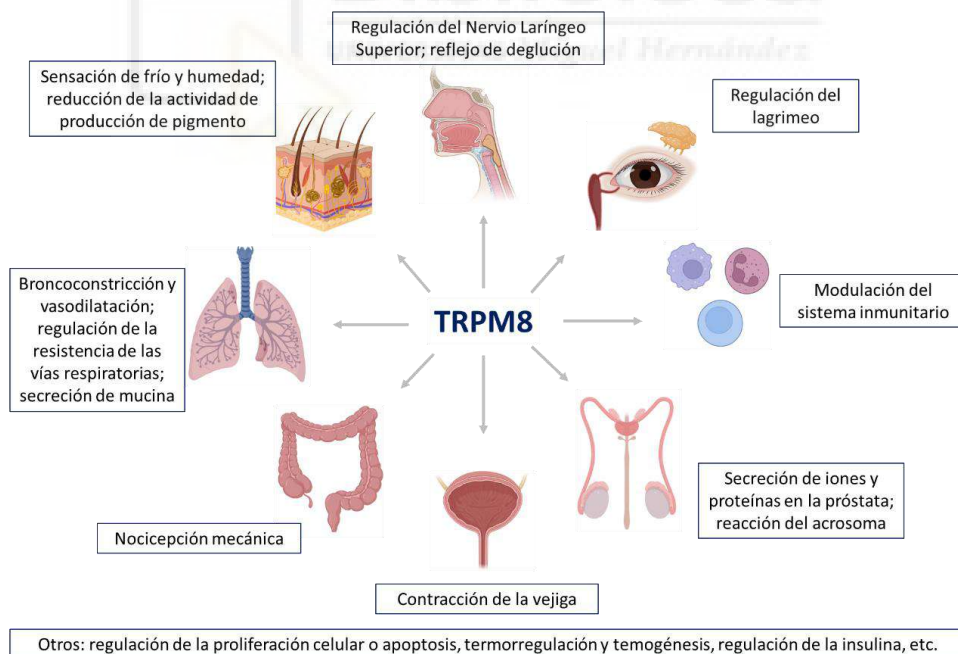


Figura 8. Funciones fisiológicas de TRPM8. Imagen editada de Liu 2020 <sup>30</sup>.

### 3.4.1. TRPM8 y dolor

Como se ha visto previamente, algunos canales TRP están estrechamente involucrados en la nocicepción, entre ellos el canal TRPM8<sup>33</sup>. Este canal cobra especial importancia en la hipersensibilidad (alodinia y/o hiperalgesia) al frío que cursa con algunos tipos de dolor neuropático<sup>48,49</sup>. Existen numerosos estudios en modelos animales, como el modelo de dolor neuropático inducido por el oxaliplatino<sup>51</sup> o el originado por lesión crónica por constricción (LCC)<sup>50</sup>, en los cuales se observa un aumento de la expresión de TRPM8 que se correlaciona con las respuestas hiperalgésicas<sup>47-50</sup>. También existe evidencia científica de que el bloqueo farmacológico<sup>49,51</sup> o la disminución en la expresión de TRPM8<sup>50</sup> disminuye las conductas dolorosas en dichos modelos. Además, cabe destacar que en estudios clínicos de pacientes con cáncer tratados con oxaliplatino, dichos pacientes presentan una mayor sensibilidad al mentol, sugiriendo una sobreexpresión del canal o una potenciación de su actividad<sup>136</sup>.

Atendiendo a otros tipos de dolor, el canal TRPM8 también se ha relacionado con la hipersensibilidad al frío que cursa con el dolor inflamatorio, como demuestran algunos modelos animales de inflamación inducida por el adyuvante completo de Freund<sup>122</sup>. Y también con el dolor nociceptivo, ya que la activación de TRPM8 ha demostrado disminuir las respuestas nocifensivas frente a estímulos dolorosos agudos como el calor, la capsaicina, la acroleína o el ácido acético. Estos efectos analgésicos no se observaron en ratones tratados con un bloqueador del canal ni en ratones carentes del gen TRPM8, confirmándose así la participación del canal en la actividad analgésica<sup>137</sup>.

Por último, existe evidencia científica de la implicación de TRPM8 en migraña<sup>138</sup>. Se ha identificado una variante del gen TRPM8 que otorga una mayor susceptibilidad a la migraña común y que podría tener un papel importante en la alodinia cutánea presente en la mayoría de los pacientes con migraña<sup>139</sup>. Otros estudios también demuestran que la activación de TRPM8 en condiciones normales puede causar dolores de cabeza como ocurre, por ejemplo, al comer helado o estar expuesto a temperaturas frías<sup>140</sup>. Sin embargo, su activación en condiciones patológicas demuestra tener un efecto analgésico como ocurre tras la aplicación de mentol<sup>141</sup>.

### 3.4.2. TRPM8 y cáncer

Cambios en la expresión de TRPM8 también se asocian a múltiples tipos de cáncer, a su desarrollo y a su metástasis. Este hecho le añade valor como diana terapéutica, convirtiéndolo en un marcador tumoral tanto de diagnóstico como de evolución<sup>30,142</sup>. Entre estos cánceres destaca el cáncer de próstata por ser el primer tejido en el que se identificó TRPM8. En esta condición se observa un aumento de la expresión del ARNm de TRPM8 que se correlaciona con la agresividad del cáncer<sup>62,143,144</sup>. Otros cánceres que implican al canal y en los que un aumento de su expresión se correlaciona con estadios más avanzados y un peor pronóstico son: el cáncer de mama<sup>62,121</sup>, el cáncer de páncreas<sup>145</sup>, el cáncer de estómago<sup>146</sup>, el cáncer colorrectal<sup>62</sup>, el carcinoma cutáneo de células escamosas<sup>147</sup>, el osteosarcoma<sup>148</sup> y el glioblastoma<sup>149</sup>. Por último, existen otros cánceres como el carcinoma oral de células escamosas (COCE) y el melanoma, en los que no es tan importante su sobreexpresión, sino su función. En el primer caso, COCE, la activación del canal se relaciona con la migración e invasión de las células tumorales, y su bloqueo con el efecto opuesto<sup>150</sup>. Mientras que en el caso del melanoma, contrariamente a los casos anteriores, tanto la activación como el bloqueo de TRPM8 se asocian a una disrupción del balance de  $Ca^{2+}$  en el citosol de las células que puede dar lugar a la muerte celular y, por lo tanto, a la inhibición de la proliferación del melanoma<sup>151</sup>.

### 3.4.3. TRPM8 y trastornos del sistema respiratorio

En el sistema respiratorio, el aumento de la expresión de TRPM8 en las células epiteliales de los bronquios se correlaciona con la enfermedad pulmonar obstructiva crónica (EPOC) y con la hipertensión pulmonar ligada al EPOC<sup>30,152</sup>. Este canal también se asocia con la exacerbación de los síntomas y la excesiva producción de moco en respuesta al aire frío que ocurre en las enfermedades inflamatorias crónicas de las vías respiratorias, como la citada anteriormente o el asma<sup>128</sup>. En el caso del asma, esta hiperreactividad al frío se asocia con un polimorfismo del canal<sup>153</sup>.

#### 3.4.4. TRPM8 y trastornos de los sistemas digestivo y urinario

El canal TRPM8 se ha visto sobreexpresado en diversas patologías del sistema digestivo y del sistema urinario <sup>155,156</sup>. Dentro de los trastornos del sistema digestivo, el canal TRPM8 se encuentra sobreexpresado en el síndrome del Intestino Irritable (SII) <sup>155</sup>. Esta condición también se ha relacionado con un polimorfismo del canal <sup>154</sup>.

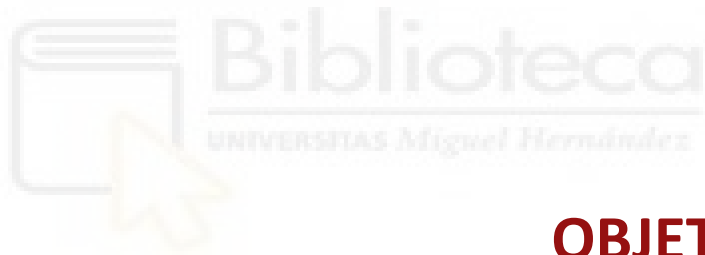
Por otro lado, en lo referente a los trastornos del sistema urinario, el canal TRPM8 se ha visto sobreexpresado en el urotelio y/o en las neuronas sensoriales de la vejiga en el síndrome de la vejiga dolorosa o cistitis intersticial (BPS) <sup>156</sup>, en el síndrome de la vejiga hiperactiva (OAB) <sup>120</sup> y en trastornos de la vejiga hipersensible <sup>131</sup>. También se ha observado la participación del canal en la respuesta de la vejiga al enfriamiento induciendo la micción <sup>30,131</sup>. Todos estos datos sugieren que el bloqueo de TRPM8 reduciría los síntomas de BPS y del resto de condiciones citadas previamente <sup>94</sup>.

#### 3.4.5. TRPM8 y trastornos oculares o de la piel.

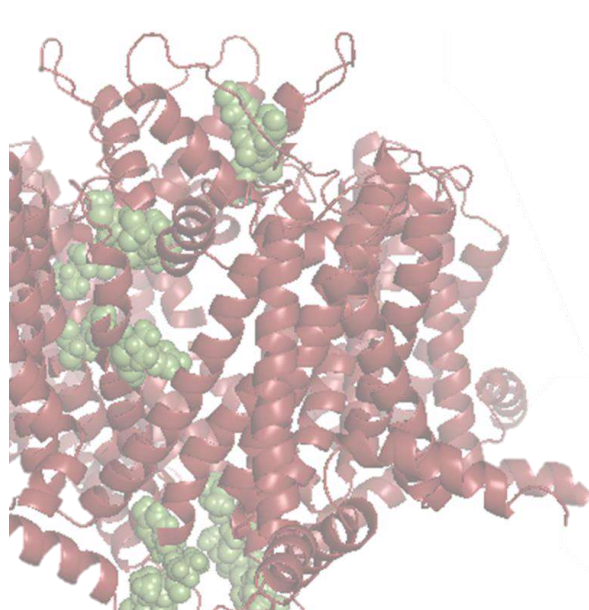
El canal TRPM8 está involucrado en el síndrome del ojo seco, observándose una reducción en la secreción lagrimal en ratones *knock-out* <sup>130</sup>. Esto se debe a la participación del canal en la detección de la evaporación inducida por temperatura y en el cambio de osmolaridad en la superficie de la cornea <sup>158</sup>. Por lo tanto, la activación de TRPM8 podría resultar beneficiosa en el síndrome del ojo seco aumentando el lagrimeo y mejorando de esta manera la sequedad ocular <sup>99,158</sup>.

Por último, el canal TRPM8 también se ha relacionado con el prurito agudo y crónico, ya que su activación por temperaturas frías y moléculas refrescantes provoca una mejoría de los síntomas como demuestra el estudio de Palkar <sup>159</sup> en un modelo *in vivo* de picor inducido por histamina, sal de difosfato de cloroquina y compuesto liberador de histamina 48/80 en ratón.





## **OBJETIVOS**





## OBJETIVOS

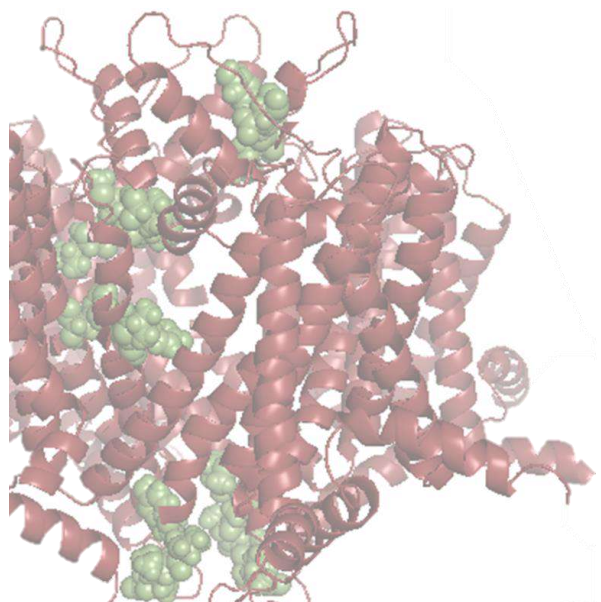
Teniendo en cuenta el potencial terapéutico del canal TRPM8 y la falta de compuestos moduladores potentes y selectivos de dicho canal en fases clínicas, este trabajo se propone identificar y caracterizar nuevos moduladores de TRPM8 mediante ensayos *in vitro*, *in silico* e *in vivo*. Para ello, se llevarán a cabo los siguientes objetivos específicos:

- Identificar nuevos moduladores del canal TRPM8 mediante técnicas de cribado de alto rendimiento y realizar estudios de potencia y selectividad.
- Profundizar en la caracterización de los mejores candidatos mediante técnicas electrofisiológicas y evaluar las propiedades farmacológicas en sistemas celulares más complejos.
- Analizar la citotoxicidad de los compuestos mediante el ensayo de viabilidad celular MTT.
- Realizar estudios de modelado molecular de interacción proteína ligando para conocer el sitio de unión al receptor y la relación estructura actividad de los compuestos.
- Estudiar la actividad de los compuestos más eficaces en modelos *in vivo* de dolor neuropático.
- Llevar a cabo estudios preliminares de la permeabilidad de los compuestos en membranas artificiales para evaluar su aplicación tópica.





## **MATERIALES Y MÉTODOS**





## MATERIALES Y MÉTODOS

### 1. Sistemas celulares

#### 1.1. Cultivo de líneas celulares continuas

Para poder llevar a cabo los diferentes experimentos se utilizaron distintas líneas celulares. Para los cribados de moléculas y los ensayos de potencia se emplearon las células embrionarias de riñón humano HEK293-*rTRPM8* y HEK293-*hTRPM8* las cuales expresan de manera estable el canal TRPM8 de rata (*rTRPM8*) y de humano (*hTRPM8*) respectivamente. Por otro lado, para los ensayos de selectividad se emplearon las líneas celulares HEK293-*hTRPV1*, que expresa de manera estable el canal TRPV1 humano (*hTRPV1*), y la línea HEK293-LTV transfectada con el canal TRPA1 humano (*hTRPA1*). Por último, para los ensayos de viabilidad celular se empleó la línea celular HEK293.

Los medios de cultivo empleados para las distintas líneas celulares fueron los siguientes:

- Para la línea HEK293-*rTRPM8* se empleó el medio de cultivo Dulbecco's Modified Eagle Medium (DMEM) (1X) GlutaMAX (Gibco, Paisley, GB, Europa) suplementado con suero bovino fetal (FBS) (Gibco, Paisley, GB, Europa) al 10%, solución Pen Strep (penicilina 10 000 unidades/mL; estreptomicina 10 000 µg/mL) (Gibco, Grand Island, NE, EE.UU.) al 1% y 50 mg/mL del antibiótico de selección geneticina (Gibco, Paisley, GB, Europa) al 1,5%.
- Para las líneas HEK293 y HEK293-LTV se empleó el mismo medio de cultivo y la misma suplementación que para la línea HEK293-*rTRPM8* sin el antibiótico de selección (geneticina). Además, a la línea HEK293-LTV se le añadió una solución de Minimum Essential Medium Non-essential Amino Acids (MEM NEAA) 100X al 0,1% (MEM NEAA) (Gibco, Paisley, GB, Europa).
- Para la línea HEK293-*hTRPV1* se empleó el medio Dulbecco's Modified Eagle Medium F-12 Nutrient Mixture (DMEM/F-12) 1:1 1X (Gibco, Paisley, GB, Europa) suplementado con FBS al 10%, Pen Strep al 1%, MEM NEAA 100X al 1% y geneticina al 1,5%.
- Por último, para la línea HEK293-*hTRPM8* se empleó el medio Eagle's Minimum Essential Medium (EMEM) (ATCC, Manassas, VA, EE.UU.) suplementado con FBS al

10%, Pen Strep al 1%, geneticina al 1,5%, L-glutamina 200 mM 100X (Gibco, Paisley, GB, Europa) al 1% y 2,5 mg/mL de glucosa (Sigma-Aldrich, Madrid, ES, UE).

Todas las líneas celulares se cultivaron en monocapa en un incubador (ThermoScientific modelo 371, EE.UU.) en condiciones controladas de temperatura (37°C), humedad y CO<sub>2</sub> (5%). El cultivo celular se llevó a cabo en frascos de 25 cm<sup>2</sup> los cuales se tripsinizaban con 0.25% Trypsin-EDTA 1X (Gibco, Paisley, GB, Europa) cuando llegaban a una confluencia del ~90% para sembrar *flasks* de mantenimiento y placas para los distintos experimentos. Se realizaron cambios de medio a los cultivos cada 2-3 días. Todo el proceso de manipulación celular se llevó a cabo en una cabina de flujo laminar Faster Bio48 (Faster, Ferrara, IT, UE). Las células (*stock*) se almacenaron en criotubos en nitrógeno líquido (~196°C) que contenían medio de congelación (50% medio de la línea celular, 40% FBS y 10% dimetilsulfóxido (DMSO) (PanReac AppliChem ITV Reagents, Barcelona, ES, UE).

### 1.2. Transfección de *hTRPA1*

#### 1.2.1. Amplificación del plásmido

El plásmido de *hTRPA1* (pCAGGSN2/Ires/GFP\_*hTRPA1*) se obtuvo del laboratorio de investigación sobre canales iónicos en la Universidad Católica de Leuven, Bélgica. El proceso de transformación bacteriana y de amplificación del plásmido se llevó a cabo en bacterias *Esterichia coli* C41. Para la transformación bacteriana se añadieron 1,7 µL de una disolución 1:10 de β-mercaptoetanol (Sigma Aldrich, Steinhein, DE, UE) en agua estéril por cada 100 µL de suspensión de bacterias. La mezcla se agitó y dejó en hielo durante 10 minutos, agitando de nuevo en intervalos de 2 minutos. Posteriormente, se cogieron 90 µL de la suspensión de bacterias (con el β-mercaptoetanol) y se les añadió 100 ng de plásmido. La solución se dejó en hielo durante 30 minutos. Tras este periodo de tiempo, se procedió al choque térmico. Para ello, se colocó la solución de bacterias con el plásmido en un baño a 42°C durante 45 segundos y rápidamente se metió en hielo durante exactamente 2 minutos. Este aumento repentino de la temperatura produce una diferencia de presión entre el exterior y el interior de la célula que induce a la formación de poros a través de los cuales se puede introducir DNA plasmídico<sup>160</sup>. Tras

este periodo de tiempo se añadieron 900  $\mu\text{L}$  de medio Luria-Bertani (LB) (MP Biomedicals, Salon, OH, EE.UU.) autoclavado y se incubó todo durante 1 hora a 37°C. Posteriormente se sembraron 200  $\mu\text{L}$  de la suspensión de bacterias de en una placa Petri con medio LB solido que contenía el antibiótico de resistencia ampicilina (Sigma Aldrich) a 100  $\mu\text{g}/\text{mL}$  y se dejó durante 24h en una estufa a 37°C para la recuperación de las bacterias. Tras aproximadamente 24 horas se recogió una colonia aislada y se dejó crecer en 50 mL de medio LB con el antibiótico de resistencia durante 1 día en agitación a 37°C. Todo el proceso se llevó a cabo en condiciones de asepsia bajo la llama de un mechero Bunsen. La purificación del plásmido se llevó a cabo con el kit de *EZNA Plasmid DNA Mini Kit* (Omega Biotek, Norcross, GA, EE.UU.) según las instrucciones del fabricante. El plásmido purificado se cuantificó usando el espectofotómetro NanoDrop™ (Thermo Scientific) teniendo en cuenta que las ratios 260/280 nm y 260/230 nm se encontraran entre 1,8 y 2,0 respectivamente. Valores por debajo de 1,8 y 2,0 indicarían posibles contaminaciones proteicas o por compuestos fenólicos del kit.

### 1.2.2. Expresión de hTRPA1 en HEK293 LTV

Para la transfección de las células HEK293-LTV con hTRPA1 se empleó el kit Lipofectamina 3 000 (Invitrogen, CA, EE.UU.) según las instrucciones del fabricante. La transfección de las células se llevó a cabo en flasks de T25  $\text{cm}^2$  en los que la confluencia de las células era del  $\sim 60\%$  y la cantidad de DNA añadida por flask fue de 15  $\mu\text{g}$ . 48 horas tras la transfección, las células se tripsinizaron y sembraron en placas de 96 pocillos como se detalla posteriormente en los experimentos de microfluorescencia de calcio.

### 1.3. Cultivo primario de neuronas GRD

Las neuronas se extrajeron de los GRDs de ratas Wistar neonatales (3-7 días de edad). Tras la extracción de los ganglios se digirieron con colagenasa (tipo IA) al 0,25% (w/v) (Sigma-Aldrich, Madrid, ES, UE) en un medio DMEM (1X) GlutaMAX con Pen Strep al 1%. La colagenasa se dejó actuar durante 1 hora en un incubador a 37 °C con condiciones de humedad controladas y un 5% de  $\text{CO}_2$ . Tras la digestión enzimática se realizó una disgregación mecánica con una pipeta. Posteriormente, se filtró la suspensión celular empleando un filtro con un diámetro de poro de 100  $\mu\text{M}$  y se lavó

con el medio de cultivo anterior suplementado con FBS al 10%. Las células se sembraron en gota y se dejaron en el incubador 1 hora. Tras este periodo de tiempo se añadieron 500µL por pocillo de medio de cultivo suplementado con factor de crecimiento nervioso de ratón 2,5S (Promega, ES, EU) a una concentración de 50 ng/ml y con arabinósido de citosina a 1,25 µg/ml. Todos los experimentos se realizaron uno o dos días tras la siembra.

### **2. Librería de compuestos**

Todos los compuestos testados en los experimentos provienen de los laboratorios de la Doctora Rosario González Muñiz Instituto de Química Médica (IQM-CSIC) en Madrid y de la Doctora Isabel Gómez Monterrey en el departamento de farmacología de la Universidad de Nápoles. Dichos compuestos fueron disueltos en DMSO a una concentración de 50mM (stocks). Las concentraciones finales deseadas se prepararon en distintas soluciones según la técnica a emplear. En los experimentos de microfluorimetría de calcio se empleó Hanks Balanced Salts Solution (HBSS) 1X; en los ensayos electrofisiológicos, solución extracelular (detallada en el apartado 5.1.1.); y en los ensayos *in vivo*, agua para inyección.

### **3. Microfluorimetría de calcio**

#### **3.1. Cribados de quimiotecas**

Los ensayos de fluorescencia se llevaron a cabo en los equipos PolarStar Omega y FluoStar Omega (ambos de BMG LABTECH, Offenberg, DE, UE). Para ello, las células se sembraron en monocapa en placas negras de 96 pocillos con el fondo transparente (Costar, Kennebunk, ME, EEUU) tratadas previamente con una solución de poli-L-lisina (Sigma-Aldrich, Madrid, ES, UE) al 0,01% en tampón fosfato salino (PBS). Para los cribados y los estudios de potencia se emplearon las líneas celulares HEK293-*rTRPM8* y HEK293-*hTRPM8*, las cuales se sembraron a una concentración de 30 000 y 50 000 células por pocillo (100 µL), respectivamente, 3 o 4 días antes del experimento.

El día del experimento, el medio se sustituyó por sonda Fluo-4 disuelta en tampón HBSS y suplementada con 7,7 mg de probenecid en 100 µL de DMSO (*Fluo-4*

*NW Calcium Assay Kit*, Invitrogen, OR, EEUU). La sonda Fluo-4 es una sonda fluorescente que se une al calcio. Esta se activa por las esterasas cuando entra en el interior celular. Cuando los canales TRP se activan dejan pasar iones de calcio al interior celular. Estos iones se unirán a la sonda provocando un incremento en la señal de fluorescencia <sup>161</sup>. Tras la adición de la sonda, las placas se incubaron en la oscuridad durante una hora. Los primeros 30 minutos se mantuvo a 37°C en el incubador y la siguiente media hora a 30°C en el equipo que se realizó el experimento (PolarStar o FluoStar Omega). La fluorescencia se midió usando una longitud de onda de excitación de 485 nm y de emisión de 520 nm. Las medidas se realizaron durante 20 ciclos de tiempo (cada ciclo equivale a 96 segundos, 1 segundo por pocillo) a una temperatura constante de 30°C. Los 3 primeros ciclos muestran la fluorescencia basal, después del ciclo 3 se añaden manualmente los compuestos a 3 concentraciones (50, 5 y 0,5  $\mu\text{M}$ ), el vehículo (DMSO) y el antagonista de referencia (1  $\mu\text{M}$ ) (Tabla 2) empleando una pipeta multicanal (Rainin E4 XLS 0,5-10  $\mu\text{l}$ ). Posteriormente, en el ciclo 10 se añade automáticamente el agonista de referencia en todos los pocillos (10  $\mu\text{l}$ ) (Tabla 2). Todas las condiciones se ensayan por triplicado ( $n=3$ ) en 3 experimentos diferentes ( $N=3$ ). En la Figura 9 se muestra un ejemplo representativo de las distintas condiciones de un experimento de microfluorometría de calcio.

**Tabla 2.** Listado de las concentraciones de agonistas y antagonistas empleadas en los ensayos de microfluorometría de calcio en los canales *rTRPM8* y *hTRPM8*. Todos los compuestos se obtienen de Sigma-Aldrich.

Línea celular	Agonista de referencia	[ $\mu\text{M}$ ]	Agonista de referencia	[ $\mu\text{M}$ ]
HEK293- <i>rTRPM8</i>	Mentol	100	AMTB	10
HEK293- <i>hTRPM8</i>	Mentol	100	AMTB	5

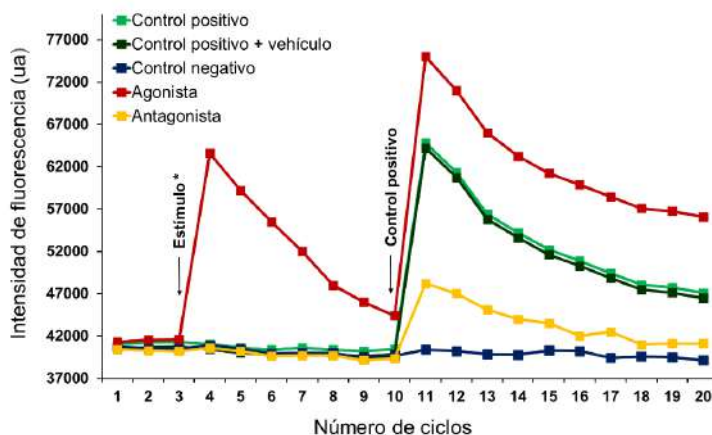


**Figura 9.** Representación de la intensidad de fluorescencia en las distintas condiciones de un ensayo de microfluorometría de calcio (controles, vehículo y compuestos) para el estudio de los moduladores de canales TRP. Todos los estímulos (vehículo, control negativo, agonistas y antagonistas) se añaden en el ciclo 3 excepto en el control positivo que, como en el resto de pocillos, se añadirá automáticamente en el ciclo 10.

### 3.2. Ensayos de selectividad

Para la determinación de la selectividad de los compuestos hacia otros canales TRP se realizaron los mismos experimentos en las líneas celulares HEK293-*hTRV1* y HEK293 LTV transfectadas con el plásmido *hTRPA1*. Las células HEK293-*hTRV1* se sembraron a una densidad de 40 000 células por pocillo de 3 a 4 días antes del experimento, mientras que las células HEK LTV transfectadas con el plásmido *hTRPA1* se sembraron a una densidad celular de 90 000 células por pocillo un día antes del experimento. El día del ensayo se procede de la misma manera que en el apartado anterior (metodología 3.1.), sustituyendo los agonistas y antagonistas empleados por aquellos propios del canal sobre el que vayamos a testar los compuestos (Tabla 3).

**Tabla 3.** Listado de agonistas y antagonistas y de las concentraciones empleadas en los ensayos de selectividad en los canales *hTRPV1* y *hTRPA1*. Todos los compuestos se obtienen de Sigma-Aldrich excepto el RR que se obtiene de Research Biochemical Inc (Natick, MA, EE.UU.).

Canal/Línea celular	Agonista	Concentración	Antagonista	Concentración
HEK293- <i>hTRPV1</i>	Capsaicina	10 $\mu$ M	Rojo de Rutenio	1 $\mu$ M
HEK293 LTV- <i>hTRPA1</i>	AITC	250 $\mu$ M	Rojo de Rutenio	20 $\mu$ M

### 3.3. Análisis de datos

El análisis de datos se llevó a cabo con una plantilla elaborada con el programa informático Excel. La modulación de los canales TRP se calculó en función de si los compuestos presentan actividad agonista o antagonista para los distintos canales. Cuando los compuestos son agonistas, se compara el aumento de la fluorescencia tras la aplicación de los compuestos en el ciclo 3 con el incremento de la fluorescencia producido por el control positivo (mentol, capsaicina o AITC) en el ciclo 11 (Ecuación 1). Por otra parte, cuando son antagonistas, se compara el aumento de fluorescencia producida por el agonista de referencia en presencia de los compuestos en el ciclo 11, con el aumento de fluorescencia producida por el control positivo en el ciclo 11 (Ecuación 2) <sup>161</sup>.

$$\% \text{ Activación} = \left( \frac{F_{\text{ciclo4}} - F_{\text{ciclo3}}}{FC_{\text{ciclo11}} - FC_{\text{ciclo10}}} \right) * 100 \quad (1)$$

$$\% \text{ Inhibición} = \left( 1 - \frac{F_{\text{ciclo11}} - F_{\text{ciclo10}}}{FC_{\text{ciclo11}} - FC_{\text{ciclo10}}} \right) * 100 \quad (2)$$

Donde **F** es la fluorescencia de los pocillos “compuesto” (ciclo 3, antes de añadir los compuestos; ciclo 4, tras añadir los compuestos; ciclo 10, antes de añadir el control positivo en presencia de compuesto; y ciclo 11, tras añadir el control positivo en presencia de compuesto) y **FC** es la fluorescencia de los pocillos “control positivo” (ciclo 10, antes de añadir el control positivo, y ciclo 11, tras añadir el control positivo).

### 3.4. Validación de los resultados - Factor Z

Para validar los resultados y determinar su fiabilidad se emplea un parámetro estadístico llamado factor Z. Este es una medida del tamaño del efecto estadístico propuesto para este tipo de ensayos <sup>162</sup>. Se calculó mediante la Ecuación 3 y solo se tuvieron en cuenta los ensayos con un factor Z mayor o igual a 0,5 <sup>161</sup>.

$$Factor\ Z = 1 - \frac{3 * (SD_{max} + SD_{min})}{Media_{max} - Media_{min}} \quad (3)$$

Donde **Media<sub>max</sub>** equivale a la media de la fluorescencia máxima en presencia del agonista; **SD<sub>max</sub>** es la desviación estándar de la fluorescencia máxima en presencia del agonista; **Media<sub>min</sub>** es la media de la fluorescencia máxima en presencia del agonista y del antagonista; y **SD<sub>min</sub>** es la desviación estándar de la fluorescencia máxima en presencia del agonista y del antagonista.

### 3.5. Determinación de la Potencia de los compuestos (IC<sub>50</sub>)

La determinación de la potencia de los compuestos se llevó a cabo empleando la técnica previamente descrita (microfluorometría de calcio) incrementando el número de concentraciones a las que se probaron los compuestos. Estos ensayos se realizaron en las líneas celulares HEK293-rTRPM8 y HEK293-hTRPM8. Los resultados obtenidos se analizaron como se describe en el apartado 3.3. Una vez calculado el porcentaje de inhibición de todas las concentraciones de los compuestos se procedió al cálculo de la IC<sub>50</sub>. Para ello se representó la respuesta normalizada (%) frente al logaritmo de la concentración de los compuestos (μM) y se realizó el ajuste a la ecuación de Hill (Ecuación 4) empleando el programa estadístico GraphPad Prism 6.0. Todos los datos de IC<sub>50</sub> se expresaron como la media ± el error estándar de la media (SEM) o el intervalo de confianza. Cada condición se analizó por triplicado (n=3) en 3 experimentos diferentes (N = 3).

$$y = Bottom + \frac{(Top - Bottom)}{1 + 10^{(X - LogIC50)}} \quad (4)$$

Donde **y** equivale al porcentaje de la respuesta normalizada, **x** equivale al logaritmo de la concentración del compuesto y **Top** y **Bottom** equivalen a la actividad máxima y mínima de TRPM8, respectivamente, tras la aplicación de los compuestos (mismas unidades que y). La ecuación posee una pendiente de Hill estándar = -1.

#### 4. Ensayos de citotoxicidad

##### 4.1. Ensayo de viabilidad celular mediante MTT

La viabilidad celular se estableció mediante un ensayo colorimétrico empleando Bromuro de 3-(4,5-dimetiltiazol-2-ilo)-2,5-difeniltetrazol (MTT) (Sigma-Aldrich, GB, Europa). La enzima succinato-deshidrogenasa es una enzima mitocondrial capaz de convertir el MTT en formazán, un compuesto de color azul cuya intensidad será proporcional a la cantidad de células vivas <sup>163</sup>.

La línea celular empleada para estos ensayos fue la HEK293. Estas células se sembraron a una densidad de 20 000 células por pocillo (100  $\mu$ L) en placas de 96 pocillos, pretratadas con una solución de poli-L-lisina 0,01% en PBS, y se incubaron a 37°C en condiciones de humedad y CO<sub>2</sub> controladas durante 3 días para permitir su adherencia. El tercer día se añadieron los compuestos a las concentraciones deseadas, el vehículo (DMSO), el control de muerte celular y el control de supervivencia. Para el control de muerte celular se empleó una solución de PBS con dodecilsulfato sódico (SDS) al 0,1% y tritón al 1% (m/v) (ambos de Sigma-Aldrich, Madrid, ES, UE), mientras que para el control de supervivencia no se añadió nada a los pocillos. Tras la adición de los compuestos, las células se incubaron durante 1 día más. Transcurridas 24 horas, se añadieron 5  $\mu$ L de MTT (5 mg/mL en PBS) en cada pocillo. Tras la adición del MTT, las células se volvieron a incubar durante 4 horas a 37°C para permitir la formación de los cristales de formazán. Posteriormente, se retiró el sobrenadante de cada pocillo y se sustituyó por 150  $\mu$ L de DMSO puro. El DMSO se dejó en agitación a temperatura ambiente durante 10 minutos para que los cristales de formazán se disolvieran. Por último, se procedió a la lectura de la densidad óptica de cada pocillo mediante el lector PolarStar Omega. La lectura se realizó a una longitud de onda de 570 nm. El porcentaje de viabilidad celular se obtuvo siguiendo la Ecuación 5 para cada pocillo. Los compuestos se ensayaron por triplicado (n=3) en 3 experimentos independientes (N=3).

$$\% Viabilidad = \frac{DO \text{ células tratadas}}{DO \text{ células control}} \cdot 100 \quad (5)$$

Donde **DO** equivale a densidad óptica.

### 5. Ensayos electrofisiológicos

#### 5.1. Patch clamp

Los experimentos de *patch clamp* se llevaron a cabo en dos modalidades distintas de *whole-cell patch clamp* con dos tipos celulares distintos. Para estudiar la potencia de los compuestos, los ensayos se llevaron a cabo en la línea celular HEK293-rTRPM8 usando la configuración *voltage clamp*, mientras que para estudiar cómo los compuestos afectaban al potencial de membrana en reposo se realizaron en neuronas GRD mediante la configuración *current clamp*. En ambos casos, las micropipetas se prepararon a partir de capilares de borosilicato (Warner Instruments Novato, CA, EE.UU.) estirados con un estirador horizontal de micropipetas P-97 (Sutter Instruments, Novato, CA, EE.UU.) para conseguir una resistencia de entre 2 y 8 M $\Omega$ . La frecuencia de muestreo fue de 10 kHz (Amplificador EPC10; PatchMaster 2.53 software; HEKA; Electronics, Lambrecht, DE, UE).

##### 5.1.1. Configuración *voltage clamp* en líneas estables

Para los experimentos de *voltage clamp* se emplearon células HEK293-rTRPM8 sembradas a una densidad de 15 000-20 000 células por pocillo (500  $\mu$ L) en placas de 24 pocillos (Corning Incorporated, Kennebunk, ME, EE.UU.) 24 o 48 horas antes del experimento. Estas placas contenían cristales de 12mm de diámetro pretratadas con una solución de poli-L-lisina. La solución intracelular empleada en los experimentos contenía (en mM): 150 NaCl, 5 EGTA, 3 MgCl<sub>2</sub> and 10 HEPES ajustada a un pH de 7,2 con KOH; y la solución extracelular empleada contenía (en mM): 150 NaCl; 6 CsCl; 1,5 CaCl<sub>2</sub>; 1 MgCl<sub>2</sub>; 10 D-glucosa y 10 HEPES, ajustada a un pH de 7,4 con NaOH. Todos los registros se llevaron a cabo a temperatura ambiente (entre 22 y 24°C). Mediante esta configuración se llevan a cabo dos tipos de registros, registros en continuo a un voltaje fijo y rampas despolarizantes de voltaje.

##### 5.1.1.1. Registros en continuo a -60mV

En estos registros se fija el voltaje a -60mV y se registran las corrientes generadas por diversos estímulos. En condiciones control se aplicaron dos pulsos de mentol a 100

$\mu\text{M}$  (definidos como p1 y p2) con un espacio temporal de 90 segundos con el fin de tener en cuenta la desensibilización del canal TRPM8. Para probar los compuestos, estos se aplicaron a diferentes concentraciones (0,01-10  $\mu\text{M}$ ) 30 segundos antes y durante el segundo pulso de mentol. Los resultados se expresaron como porcentaje de activación de TRPM8 tras la adición de los compuestos. Este porcentaje se calculó normalizando la relación p2/p1 de las condiciones testadas con la relación p2/p1 del control. Tanto el mentol como los compuestos a ensayar se aplicaron directamente en la célula a investigar mediante una perfusión por gravedad.

El análisis de los datos se llevó a cabo mediante GraphPad Prism 6.0. Para realizar comparaciones múltiples se empleó el análisis estadístico *Ordinary One-Way ANOVA* seguido por el test *post hoc* Bonferroni, mientras que para identificar *outliers* se empleó el método ROUT (Q=10%). Para la obtención de la curva de regresión no lineal y la  $\text{IC}_{50}$  se representó el porcentaje de la actividad del canal frente al logaritmo de la concentración del compuesto y se hizo el ajuste a la ecuación de Hill (Ecuación 6) con la restricción de la actividad máxima del canal al 100% (Top = 100) cuando la concentración de compuesto es cero. Se empleó un valor estándar para la pendiente de Hill igual a -1. Todos los datos se expresan como la media  $\pm$  el error estándar de la media (SEM).

$$y = \text{Bottom} + \frac{(\text{Top} - \text{Bottom})}{(1 + 10^{((\text{LogIC}_{50} - X) * \text{HillSlope}))}} \quad (6)$$

Donde **y** equivale al porcentaje de activación de TRPM8; **x** equivale al logaritmo de la concentración del compuesto; **Top** y **Bottom** equivalen a la actividad máxima y mínima de TRPM8 tras la aplicación de los compuestos (mismas unidades que y), respectivamente; por último, *Hillslope* equivale a la pendiente de Hill.

#### 5.1.1.2. Rampas despolarizantes de voltaje

Para las rampas de intensidad-voltaje (IV) se empleó un protocolo de voltajes de -120 mV a 120 mV en 300 milisegundos y se registró la corriente celular a los diferentes voltajes. Se anotó también la capacitancia celular para calcular la densidad de corriente (J, pA/pF) y representarla gráficamente frente a los diferentes voltajes (cada 20 mV). Los resultados se expresaron como la media  $\pm$  SEM.

### 5.1.2. Configuración *current clamp* en neuronas

Para los experimentos de *current clamp* se emplearon neuronas extraídas de GRDs sembradas en gota en placas de 24 pocillos con cristales de 12mm de diámetro pretratados con poli-L-lisina y laminina (Sigma-Aldrich, Madrid, ES, UE) a concentraciones de 8,3  $\mu\text{g}/\text{mL}$  y 5  $\mu\text{g}/\text{mL}$ , respectivamente. Se sembraron 24 cristales por rata neonata. La solución intracelular empleada contenía (en mM): 4 NaCl; 126 K gluconato; 0,02  $\text{CaCl}_2$ ; 1  $\text{MgSO}_4$ ; 5 HEPES; 15 glucosa; 3 ATP; 0,1 GTP y 5 EGTA ajustada a un pH de 7,2 con KOH; Y la solución extracelular contenía (en mM): 140 NaCl, 4 KCl, 2  $\text{CaCl}_2$ , 2  $\text{MgCl}_2$ , 10 HEPES, 5 glucosa y 20 manitol ajustada a un pH de 7,4 con NaOH.

En los experimentos de *current clamp* se midió el potencial (voltaje) de la membrana celular sin aplicar corriente y se estudió el cambio en dicho potencial tras la adición de los compuestos a 10  $\mu\text{M}$ . El cambio del potencial de membrana se calculó restando el potencial de membrana tras la adición del compuesto al potencial de reposo de la célula. Los datos se analizaron usando el GraphPad 6.0, para realizar comparaciones múltiples se empleó el análisis estadístico *Ordinary One-Way ANOVA* seguido por el test *post hoc* Bonferroni y para identificar *outliers* se empleó el método ROUT (Q=10%).

### 5.2. Ensayos funcionales mediante matrices de microelectrodos

Los ensayos funcionales mediante matrices microelectrodo (MEA) se llevaron a cabo en neuronas GRD. Estas se sembraron en gota en placas de MEA tratadas con poli-L-lisina y laminina a concentraciones de 8,3  $\mu\text{g}/\text{ml}$  y 5  $\mu\text{g}/\text{ml}$  respectivamente. Se sembraron 5 placas por rata neonatal.

Las medidas de la actividad neuronal se llevaron a cabo mediante la aplicación de dos pulsos cortos de 15 segundos (p1 y p2) del estímulo control, KCl 40 mM, usando un sistema de perfusión continua (2 ml/min). Entre cada estímulo las células se lavaron con solución externa durante 10 min. Para evaluar el efecto del compuesto, estos se aplicaron durante 1 minuto antes del segundo pulso de KCl y durante este segundo

pulso. Todas las mediciones se realizaron a  $\sim 34,5$  °C con un controlador de temperatura en la perfusión.

Para el análisis de datos se empleó un clasificador de picos MC\_RACK con una frecuencia de muestreo de 25 kHz. Se consideró potencial de acción aquella actividad eléctrica neuronal cuya amplitud era 5 veces mayor que la desviación estándar de la señal basal. La actividad de los electrodos se registró durante 30 segundos mientras se aplicaban los estímulos. Los electrodos que no mostraron actividad eléctrica en el primer pulso se desecharon. Posteriormente, se hizo el promedio del número de potenciales de acción registrados en cada pulso y durante la aplicación del compuesto. Para el cálculo de la actividad del compuesto se estudió la relación del promedio de los picos  $p_2/p_1$  y se normalizó al control. No se analizó el efecto del compuesto cuando se aplicó por sí solo, ya que no produjo ningún potencial de acción.

## 6. Estudios de modelado molecular

Para los estudios de acoplamiento molecular se empleó un modelo de *r*TRPM8 creado por el profesor Gregorio Fernández Ballester a partir de la estructura de TRPM8 de *fa*TRPM8 resuelta por microscopía crioelectrónica (PDBs ID: 6BPQ). En el modelo se añadieron los bucles que faltan en la estructura de *fa*TRPM8 y se eliminaron los extremos N y C terminal <sup>164</sup>.

Para el estudio de las interacciones de los compuestos con el canal *r*TRPM8 se realizó un acoplamiento molecular global con AutoDock 4 <sup>165</sup> implementado en Yasara. En estos estudios se lanzó el compuesto con un total de 800 intentos de acoplamiento. Los ligandos se agruparon alrededor de los posibles sitios de unión. Posteriormente, el programa realizó una optimización simulada del alineamiento de cada complejo para llevarlos al mínimo de energía estable más cercano utilizando el campo de fuerza AMBER03 <sup>91</sup>. El comando de pH de Yasara se fijó en 7,0 para garantizar que las moléculas conservaran su dependencia del pH de los órdenes de enlace y patrones de protonación. Los resultados del acoplamiento molecular se analizaron con un script de Python que identificó los residuos que interaccionan con el ligando con mayor frecuencia <sup>166</sup>. El script proporcionó la frecuencia de interacción y la media  $\pm$  SD de la energía de

interacción de cada ligando. El complejo con mejor energía de enlace de cada grupo se almacenó, analizó y usó para conocer el sitio de unión de los compuestos más probable. La visualización y edición de las moléculas también se hizo con Yasara, mientras que las figuras se dibujaron con Pymol 1.8 (Schrödinger, LLC).

### **7. Ensayos *in vivo***

Todos los procedimientos experimentales se aprobaron por los Comités de Cuidado y Uso de Animales de la Universidad Miguel Hernández y del gobierno regional, y se llevaron a cabo de acuerdo con los principios éticos de la Asociación Internacional para el Estudio del Dolor para la evaluación del dolor en animales conscientes <sup>167</sup>, la Directiva 2010/63/UE del Parlamento Europeo y del Consejo <sup>168</sup> y el Real Decreto 53/2013 <sup>169</sup>. Los animales se mantuvieron en condiciones ambientales controladas: temperatura  $21 \pm 1^\circ\text{C}$  y humedad relativa de  $55 \pm 15\%$  en un ciclo de luz/oscuridad cada 12 horas. Los animales tenían libre acceso a alimento y a agua excepto durante la habituación o las medidas experimentales. En todo momento se procuró minimizar el número de animales utilizados y el dolor y el estrés que estos experimentaron.

#### **7.1. Modelo de alodinia al frío mediada por oxaliplatino**

Para el Modelo de dolor neuropático mediado por oxaliplatino se emplearon ratones C57BL6 de entre 5 y 15 semanas (20-30 g) (Harlan, NL, UE). Los ratones se dividieron en dos grupos, grupo oxaliplatino y grupo control. El dolor neuropático se indujo al grupo oxaliplatino tras administrar por vía intraperitoneal (i.p.) o subcutánea (s.c.) 6 mg/kg de oxaliplatino (Tocris, Bristol, GB, Europa) durante tres días alternos. El oxaliplatino se disolvió en agua para inyección (Braun, Melsungen, DE, UE) con dextrosa o manitol al 5%. Esta solución se preparó cada día justo antes de su administración. Al grupo control se le suministró la misma solución de agua para inyección con dextrosa o manitol al 5% también durante tres días alternos. La alodinia al frío se evaluó mediante el test de acetona antes del tratamiento con oxaliplatino o vehículo y 3 días después de su última administración.

### 7.1.1. Evaluación de la alodinia al frío mediante Test de acetona

La sensibilidad térmica generada en el modelo de alodinia al frío mediada por oxaliplatino se evaluó utilizando el test de acetona. Para medir la sensibilidad a la acetona, los ratones se colocaron en cajas individuales de metacrilato sobre una rejilla de metal que permitía aplicar la acetona. La gota de acetona (20  $\mu$ l) se aplicó sobre la superficie plantar media de la pata trasera derecha y se contabilizó el número de respuestas de tipo nociceptivo que consistían en lamer, atender, arrastrar o levantar la pata; o la duración de estas. Las respuestas se midieron durante un periodo de tiempo determinado con un cronómetro digital. Para cada medición, se aplicó acetona dos o tres veces (en intervalos superiores a 3 minutos) y se calculó la media. El test de acetona se realizó entre los 15 minutos y las 3 horas posteriores a la administración del compuesto según la duración del efecto. Los ratones se manipularon y se habituaron al experimentador y al lugar de experimentación (rejilla) durante la semana anterior a los experimentos. El día de los experimentos, los ratones se colocaron entre 30 minutos y una hora antes en la rejilla para su aclimatación. El comportamiento animal se analizó con un test ANOVA de medidas repetidas seguido de una prueba *post hoc* Tukey utilizando el GraphPad Prism 6.0. Se consideraron estadísticamente significativos valores de p inferiores a 0,05.

### 7.1.2. Administración de los compuestos

Los ratones tratados con oxaliplatino y los ratones control se dividieron a la vez en 2 grupos: el grupo que recibía el compuesto a testar y el grupo que recibía el vehículo de dicho compuesto. Los compuestos a testar se prepararon según la Tabla 4 y se administraron de manera intraplantar (i.pl.) en un volumen de 25  $\mu$ L. El stock de los compuestos se preparó en DMSO (la cantidad de DMSO administrada siempre fue inferior al 5%).

**Tabla 4.** Preparación de los compuestos para su administración i.pl.. Se indica la concentración del compuesto en la solución inyectable y el volumen y la cantidad de los compuestos administrados.

Compuesto	Preparación del compuesto para inyección	Concentración del compuesto en la solución inyectable.	Volumen administrado i.pl.	Cantidad de compuesto administrada
<b>14</b>	solución salina para inyección + cremophor EL® (MA, EE.UU.) al 2,5 %	400 y 1 200 µg/mL	25 µL	10 y 30 µg
<b>24a</b>	solución salina para inyección	40 y 120 µg/ml	25 µL	1 y 3 µg
<b>51</b>	solución salina para inyección	4 y 40 µg/ml	25 µL	0.1 y 1 µg

### 7.2. Modelo de hipersensibilidad mecánica inducida por nitroglicerina

Para el modelo de hipersensibilidad mecánica inducida por nitroglicerina (NTG) se emplearon ratones C57BL6 machos y hembras ( $\approx 25$  g) (Envigo, Blackthorn, GB, Europa). El modelo se generó administrando vía i.p. una solución de NTG (Nitro Pohl) diluida en solución salina a 10 mg/kg 2 horas antes de las mediciones. El grupo control recibió solamente inyecciones de solución salina. La hipersensibilidad mecánica se midió mediante el test de von Frey.

#### 7.2.1. Test de von Frey

Los valores del umbral mecánico se obtuvieron mediante los filamentos de von Frey (Stoelting, Wood Dale, IL, EE. UU.). Estas medidas se realizaron antes de la aplicación del compuesto y a diferentes intervalos de tiempo tras la inyección del compuesto (a los 15, 30, 60 y 120 minutos en los ratones macho y a los 30, 60, 120 y 180 minutos en los ratones hembra). Para los experimentos los ratones se colocaron en una rejilla de alambre 20 minutos antes de empezar las medidas. Los filamentos de von Frey se aplicaron en la superficie plantar de las patas traseras siguiéndose el método *up and down* de Dixon<sup>170</sup>. En este método, una respuesta positiva (levantar, sacudir o lamer la pata) lleva a la aplicación del filamento posterior más delgado, mientras que una respuesta negativa (sin respuesta) lleva a la aplicación del filamento posterior más grueso. Los filamentos empleados fueron 2,44; 2,83; 3,22; 3,61; 4,08 y 4,56. Se partió

del filamento 3,61 y se tomaron 6 medidas en cada animal en una pata aleatoria (izquierda o derecha). El umbral de respuesta del 50 % se calculó mediante la siguiente ecuación (Ecuación 7):

$$\text{Umbral del 50 \% (g)} = \frac{(10^{(Xf+Kd)})}{10\ 000} \quad (7)$$

Donde **Xf** es el valor del último filamento de von Frey aplicado; **K** es un factor de corrección basado en el patrón de respuestas (obtenido de la Tabla de calibración de Dixon); y **d** es la distancia media en unidades logarítmicas entre estímulos (0,4 en este caso).

Se calculó el umbral de von Frey para cada animal y se representó la media  $\pm$  SEM. El análisis de datos se realizó utilizando GraphPad 6.0 para realizar comparaciones múltiples se empleó el análisis estadístico *two-way* ANOVA seguido de la prueba *post hoc* de Bonferroni.

### 7.2.2. Administración del compuesto

El compuesto a testar (**51**) se preparó en DMSO y se diluyó en solución salina para inyecciones. Este fue administrado vía i.p. a 10 mg/kg y 30 mg/kg 2 horas después de la administración de NTG.

## 8. Ensayos preliminares de permeabilidad

Todos los ensayos de permeabilidad se llevaron a cabo durante la estancia de investigación en el Centro de Investigación en Biociencias y Tecnologías de la Salud (CBIOS) de la Universidad Lusófona en Lisboa, Portugal.

### 8.1. Celdas de Franz

Los ensayos de permeabilidad se llevaron a cabo utilizando celdas de Franz de vidrio con un volumen receptor de  $\sim$ 4 mL y con un área de difusión de 0,95 cm<sup>2</sup>. La membrana que se empleó en los experimentos para simular la epidermis fue la membrana de silicona Liveo™ 7-4107 (Dupont, Delaware, EE.UU.).

Las celdas de Franz se dividen en un compartimento dador y un compartimento receptor separados por una membrana. En cada compartimento dador ( $n=4$ ) se depositaron 300  $\mu\text{L}$  de la solución de los compuestos a testar (1 mg/mL) en etanol:agua (50:50). En el compartimento receptor se depositaron  $\sim 4$  mL (se anotó el volumen exacto) de etanol:agua (50:50) como medio receptor. El compartimento receptor se mantuvo en agitación constante (150 rpm) en un baño termostático a 37°C. Todos los experimentos de difusión se llevaron a cabo en condiciones oclusivas sellando el compartimento dador con un cubreobjetos.

En lo referente a la toma de muestras, se recogieron 400  $\mu\text{L}$  del compartimento receptor a los diferentes intervalos de tiempo designados (2h, 4h, 6h, 8h, 10h and 24h). Tras el muestreo se reemplazaron rápidamente los 400  $\mu\text{L}$  extraídos por nueva solución receptora (etanol:agua) atemperada previamente. Las muestras se almacenaron a -20°C hasta el día del análisis mediante cromatografía líquida de alta eficacia (HPLC).

### **8.2. Recta patrón y análisis cuantitativo de las muestras mediante HPLC**

El análisis de las muestras se llevó a cabo mediante un equipo de HPLC (1200 Infinity Agilent Technologies) equipado con un horno de columna y un detector de diodos G1315D, 1260 DAD VL. Los solventes empleados fueron el Acetonitrilo (ACN) (Fisher Chemical, Leicester, GB, Europa) y agua acidulada con ácido trifluoroacético (Sigma, Deisenhofen, DE, UE) al 0,3% v/v.

Los experimentos se llevaron a cabo en una columna de fase reversa Eclipse XBD-C18 (4,6 x 250 mm, 5 Micron) con un volumen de inyección de 20  $\mu\text{L}$  y un gradiente compuesto por el eluyente A (ACN) y eluyente C (agua acidulada) en las siguientes proporciones: 0 min, 5% A, 95% B; 5 min, 95% A, 5% B; 7 min, 95% A, 5% B; 9 min, 5% A, 95% B; 15 min, 5% A, 95% B. El flujo fue de 1 mL/min y la temperatura de los experimentos 25°C. El tiempo de análisis fue de 15 minutos, incluyendo la estabilización de la columna. La longitud de onda seleccionada fue de 220 nm, ya que mostraba áreas de detección mayores. El procesamiento de datos se llevó a cabo con Agilent OpenLAB CDS ChemStation Workstation.

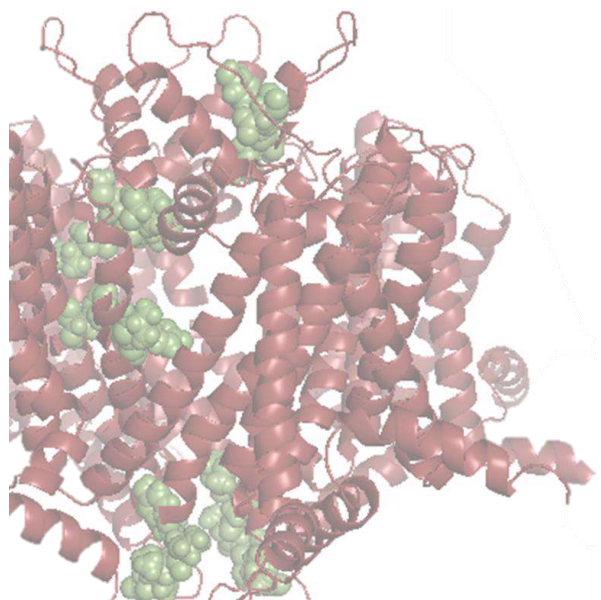
Los estándares se prepararon en metanol mientras que las muestras estaban disueltas en etanol:agua 50:50. Se analizaron los estándares mediante HPLC y se representó el área (mAU\*s) frente a la concentración analizada (mg/ml) obteniéndose la recta de calibración. Además de la recta de calibración, se calcularon los coeficientes de correlación el límite de cuantificación (LOC) y el límite de detección (LOD). Para la cuantificación de las muestras se empleó la recta de calibración de cada compuesto, y sabiendo el área de las muestras se calculó su concentración (mg/ml) a cada intervalo de tiempo. Posteriormente se calculó la acumulación del compuesto ( $\mu\text{g}/\text{cm}^2$ ) y se representó frente al tiempo obteniendo una línea de regresión para cada celda de Franz cuya pendiente equivalió al flujo de difusión de los compuestos ( $\mu\text{g}/\text{cm}^2/\text{h}$ ).







## **RESUMEN DE LOS RESULTADOS Y DISCUSIÓN**





## RESUMEN DE LOS RESULTADOS Y DISCUSIÓN

### Capítulo 1. Caracterización *in vitro*, *in silico* e *in vivo* de compuestos derivados de $\beta$ -lactamas como bloqueadores de TRPM8

Nuestro grupo de investigación lleva años colaborando con el grupo de la Dra. Rosario Gómez Muñiz del Instituto de Química Médica de Madrid en la búsqueda de moduladores de los canales TRP. Ambos grupos realizaron una campaña de cribado de diversos compuestos derivados de  $\beta,\gamma$ -diamino ésteres en diferentes canales TRP (TRPA1, TRPV1 y TRPM8). Estos derivados poseen un gran número de enlaces rotables que les permiten adoptar varias conformaciones y adaptarse así a los diferentes canales TRP, siendo poco selectivos hacia un canal en concreto. Esta hipótesis junto con el estudio de otras estructuras químicas llevó a la introducción de un núcleo de  $\beta$ -lactama en las estructuras de los derivados de  $\beta,\gamma$ -diamino ésteres <sup>171</sup>.

Las  $\beta$ -lactamas surgen con el descubrimiento de la Penicilina en 1928 <sup>172</sup>, aunque su estructura no se describió hasta 20 años más tarde <sup>171</sup>. Estas  $\beta$ -lactamas constituyen el grupo de antibióticos más usado en el mundo <sup>172</sup>. Su mecanismo de acción consiste en inhibir la última etapa de la síntesis de la pared celular bacteriana <sup>173</sup>. Sin embargo, en la actualidad también poseen otras indicaciones terapéuticas. Un ejemplo disponible en el mercado es el fármaco Ezetimibe, el cual actúa como un inhibidor de la absorción del colesterol <sup>174</sup>. Estas estructuras también se están estudiando para el tratamiento de otras condiciones como las patologías neurodegenerativas <sup>175,176</sup>, el cáncer <sup>177</sup> y la hiperalgesia y/o alodinia al frío que cursa con algunos tipos de dolor neuropático <sup>178</sup>.

Entre las múltiples ventajas del anillo  $\beta$ -lactámico en la síntesis de distintas moléculas <sup>171</sup> cabe destacar la rigidez que aporta a las estructuras peptídicas mediante su ciclación <sup>179</sup>, convirtiéndolas en estructuras estables. Esta estabilidad puede llevar a una mayor potencia y selectividad de los compuestos, acotando posibles interacciones con otras proteínas. De este modo, para continuar con la búsqueda de moduladores más específicos, se preparó una serie de  $\beta$ -lactamas derivadas de conjugados de los aminoácidos fenilalanina (Phe) y ácido aspártico (Asp) o de Phe y ácido glutámico (Glu), en la cual se identificaron 2 compuestos (compuestos **1** y **2** de la Figura 10A) como bloqueadores potentes y selectivos de TRPM8 <sup>180</sup>. Estos dos compuestos se convirtieron

en los primeros miembros de una nueva clase de moduladores de canales TRP basados en un esqueleto  $\beta$ -lactámico. A partir del descubrimiento de esta nueva clase de moduladores de TRPM8 se ha continuado con la búsqueda de modificaciones estructurales para mejorar las propiedades farmacológicas y conseguir la aplicación terapéutica de estos compuestos en el dolor y el cáncer, como veremos en las publicaciones que forman parte de esta tesis.

**Publicación 1. Highly functionalized  $\beta$ -lactams and 2-ketopiperazines as TRPM8 antagonists with antiallodynic activity**

En la publicación citada previamente, de La Torre-Martínez <sup>180</sup>, se identificaron los compuestos **1** y **2** (Figura 10 A) como bloqueadores potentes y selectivos de TRPM8. En dichos estudios se observó que el derivado corto de Asp era más potente que el derivado largo de Glu y que los 3 grupos bencilos y el grupo hidrofóbico tert-butylloxycarbonyl eran importantes para su actividad. Así pues, en esta publicación, se propuso buscar derivados  $\beta$ -lactámicos más cortos con cuatro sustituyentes hidrofóbicos que pudieran mejorar la actividad farmacológica de los compuestos previos. Para ello, se prepararon una serie de conjugados de Z-fenilalaninol con derivados de aminoácidos y se ciclaron dando lugar a 16 compuestos heterocíclicos con núcleos de  $\beta$ -lactama o de 2-cetopiperazina (CP) (Figura 10 B).

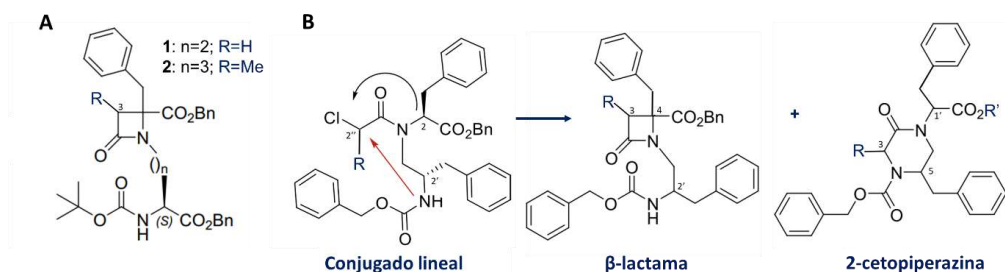


**Figura 10.** Heterociclos derivados de aminoácidos con potencial bloqueador de TRPM8. A) Derivados  $\beta$ -lactámicos identificados en trabajos anteriores (**1** y **2**) <sup>180</sup>. B) Ciclación del conjugado lineal de Z-fenilalaninol dando lugar a derivados heterocíclicos con núcleos de  $\beta$ -lactama y de 2-cetopiperazina. Se muestran las fórmulas generales de las moléculas que conforman este trabajo.

En un primer lugar, se realizaron cribados de las moléculas sintetizadas mediante microfluorimetría de calcio en células HEK293-rTRPM8. Estos estudios demostraron la actividad bloqueadora de todos los compuestos sintetizados y permitieron determinar las configuraciones más interesantes para cada una de las estructuras principales

( $\beta$ -lactamas o CPs). Para las  $\beta$ -lactamas se observó una mayor actividad antagonista en la configuración 2'R mientras que en las CP destacan las configuraciones 5R, 1'R. Cabe destacar que todas las CP y parte de las  $\beta$ -lactamas se ensayaron como mezclas de diastereoisómeros, por lo que las relaciones estructura-actividad no se pudieron definir con precisión. También se corroboró la importancia del fenilo en la posición 4 como habían demostrado los estudios anteriores<sup>180</sup>. Posteriormente, se amplió el número de concentraciones a las que se probaron los compuestos permitiéndonos calcular las curvas dosis-respuesta y los valores de IC<sub>50</sub>, obteniéndose los mejores resultados para la  $\beta$ -lactama **29a** y la CP **30ab**, con IC<sub>50</sub>s de 0,4 ± 1,5 y 0,2 ± 1,6  $\mu$ M respectivamente (Tabla 5). Sin embargo, se continuaron los ensayos solo con las  $\beta$ -lactamas **24a** y **29a** por ser los compuestos enantiopuros con mejor actividad. Por otra parte, se realizaron estudios de selectividad mediante las mismas técnicas frente al canal TRPV1 en células HEK293-*hTRPV1*. Ninguno de los derivados mostró actividad agonista ni antagonista en este canal, indicando selectividad hacia TRPM8.

**Tabla 5.** Estructura, configuración e IC<sub>50</sub> de los compuestos con mejores resultados en los ensayos de microfluorometría de calcio.

Compuesto	R	R'	Configuración	IC <sub>50</sub> ± SEM ( $\mu$ M)
$\beta$ -lactama <b>24a</b>	Me	-	3S,4S,2'S	2,4 ± 1,2
$\beta$ -lactama <b>29a</b>	Me	-	3S,4S,2'R	0,4 ± 1,5
CP <b>30ab</b>	Me	Bn	3R,5R,1'S/3R,5R,1'R	0,2 ± 1,6

Posteriormente, se confirmó la actividad de los compuestos enantiopuros más potentes (**24a** y **29a**) mediante experimentos de *patch clamp* configuración *whole-cell* en la misma línea celular. Ambos compuestos fueron capaces de bloquear de manera dosis dependiente las corrientes de *rTRPM8* producidas por mentol 100  $\mu$ M a un voltaje fijo de -60 mV (Figura 11 B y D). Los valores de IC<sub>50</sub> obtenidos mediante técnicas electrofisiológicas confirmaron los resultados previos. Se obtuvo una IC<sub>50</sub> de 1,4 ± 1,1  $\mu$ M para el compuesto **24a** y de 0,8 ± 1,1  $\mu$ M para el compuesto **29a**. También se estudió la densidad de corriente del canal tras su estimulación con 100  $\mu$ M de mentol en presencia y ausencia de los compuestos. Se observó que ambos compuestos a 10  $\mu$ M disminuían las corrientes mediadas por mentol (Figura 11 A y C).

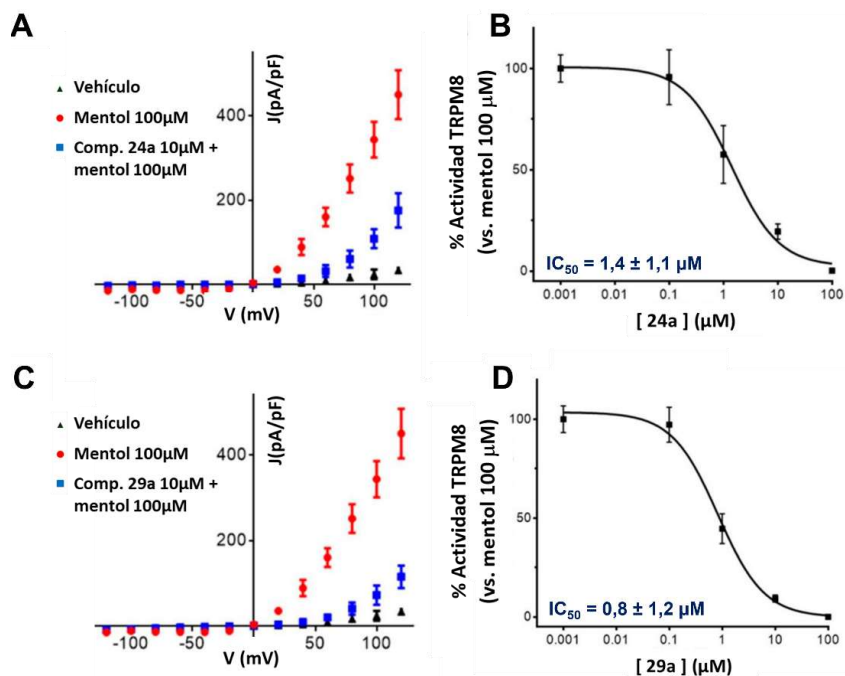


**Figura 11.** Los compuestos **24a** y **29a** bloquearon las respuestas de rTRPM8 a mentol 100 μM en células HEK293-rTRPM8. A) y C) Densidad de corriente de rTRPM8 a los diferentes voltajes (rampas de -120 a +120mV) en condiciones basales (vehículo), en presencia de estímulo (mentol 100 μM) y en presencia de estímulo más el bloqueador **24a** (A) y **29a** (C) a 10 μM. La corriente se expresa como pA/pF (para permitir la comparación entre células de diferentes tamaños). B) y D) Curvas dosis-respuesta e  $IC_{50}$  del bloqueo de la corriente de rTRPM8 mediada por mentol 100 μM tras la adición de diferentes concentraciones de los compuestos **24a** (B) y **29a** (D) a un voltaje fijo de -60mV. Todos los resultados se expresan como media ± SEM.

Por otra parte, dada la participación y/o sobreexpresión del canal TRPM8 en diferentes tumores malignos (próstata, mama, colon, piel, etc.)<sup>30</sup>, se quiso estudiar el efecto de las β-lactamas **24a** y **29a** a 10 μM en 60 líneas celulares tumorales mediante un screening llevado a cabo en el Instituto Nacional de Cáncer de EE.UU.. En todas las líneas celulares se observó un efecto citotóxico no selectivo, obteniéndose los mejores resultados para las líneas celulares de leucemia, melanoma, cáncer de pulmón, colon, ovario, riñón y próstata. También se llevaron estudios de citotoxicidad en colaboración con la empresa PharmaMar en cuatro líneas celulares humanas de cáncer de pulmón, colon, mama y páncreas; y los resultados se compararon con los del agente quimioterapéutico doxorrubicina. El compuesto **24a** mostró mejor actividad citotóxica que el compuesto **29a** en las líneas celulares de cáncer de pulmón, colon y páncreas; presentando potencia micromolar. Cabe destacar que los resultados no se correlacionan con la potencia de los compuestos para bloquear TRPM8 y que ninguno de ellos fue más potente que el control doxorrubicina. Este hecho, junto con la escasez de datos que existen

en la expresión de TRPM8 en las distintas líneas celulares tumorales, no nos permite asegurar que la actividad antitumoral de estos compuestos se deba únicamente al bloqueo de TRPM8, pudiendo poseer mecanismos de acción independientes de este canal. Por otra parte, también estudiamos la citotoxicidad de los derivados  $\beta$ -lactámicos mediante ensayos de viabilidad celular (MTT) en la línea celular no tumoral HEK293. Ninguno de los compuestos mostró citotoxicidad ni a concentraciones elevadas de 500  $\mu$ M.

Tras los estudios *in vitro*, se investigaron posibles sitios de unión de ambas familias de compuestos al canal *r*TRPM8 mediante ensayos de modelado molecular. Se continuó con el estudio de las  $\beta$ -lactamas **24a** (Figura 12) y **29a**, y se eligió la CP **13a** como ejemplo de este segundo grupo. Se observó que los 3 compuestos interactúan con TRPM8 en la zona del poro (>80% de las soluciones) mostrando dos soluciones principales. Este sitio de unión mayoritario se encuentra en la mitad de la región TM, principalmente entre los dominios TM5 y TM6 (dominios TM de las regiones S5 y S6) de una subunidad del canal con los dominios TM5 y TM6 (o el segmento que los conecta) de una subunidad adyacente. El segundo sitio de unión, sitio 2, corresponde a la boca citosólica del poro en las hélices que conectan los dominios TM6 y la región TRP de las 4 subunidades que forman el canal. En ambos sitios de unión se observan principalmente interacciones hidrofóbicas, apilamientos  $\pi$ - $\pi$  y puentes de hidrógeno. En el manuscrito se describen con mayor detalle las interacciones con los diferentes aminoácidos de la proteína (Anexo I, páginas 5-8). Ninguno de los sitios de unión coincide con los identificados para otros antagonistas del canal descritos en bibliografía como el AMTB o el TC-I<sup>181</sup>, haciéndolos una clase única de antagonistas de TRPM8.

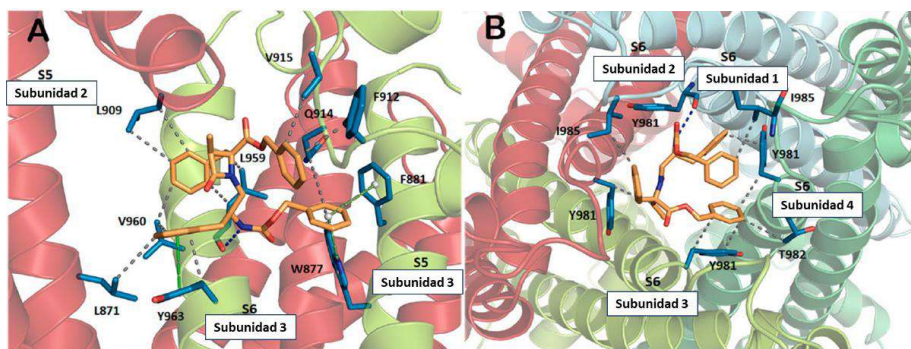


**Figura 12.** Sitios de unión principales para el compuesto **24a**. A) Sitio 1. B) Sitio 2. El compuesto **24a** está en naranja. Mientras que las cadenas laterales de TRPM8 que interactúan con el compuesto están en azul. Los heteroátomos se indican en rojo (O) y en azul oscuro (N).

Por último, se realizaron estudios in vivo de la  $\beta$ -lactama **24a** en un modelo de neuropatía periférica inducida por quimioterapia (NPIC), concretamente inducida por oxaliplatino. Varios agentes quimioterapéuticos en primera línea clínica inducen NPIC, empeorando la adhesión al tratamiento y la calidad de vida del paciente. En las NPIC ocasionadas por oxaliplatino, se desarrolla una hipersensibilidad al frío que se correlaciona con un aumento de la expresión de los canales TRPM8 y que disminuye tras la administración de un antagonista del canal<sup>47,48,136,182</sup>. Así pues, en estos estudios se indujo una NPIC tras administrar oxaliplatino 6mg/kg durante tres días alternos. El octavo día se midió la alodinia al frío mediante el test de acetona, contabilizándose el tiempo de lamido en respuesta a una gota de acetona. Los resultados demostraron que 1  $\mu$ g del compuesto **24a** administrado vía intraplantar (i.pl.) disminuye de manera significativa el tiempo de lamido 15 minutos tras su administración. Se observa una duración del efecto de hasta 2 horas, mostrando su actividad máxima a los 30 y 60 minutos (Figura 13 A). Cuando se aumentó la dosis del compuesto a 3  $\mu$ g, se alcanzó con anterioridad la actividad máxima y se alargó su duración. Comenzando a los 15 minutos tras su administración y prolongándose hasta los 60 minutos. Sin embargo, no se observó efecto a las 2 horas (Figura 13 B).

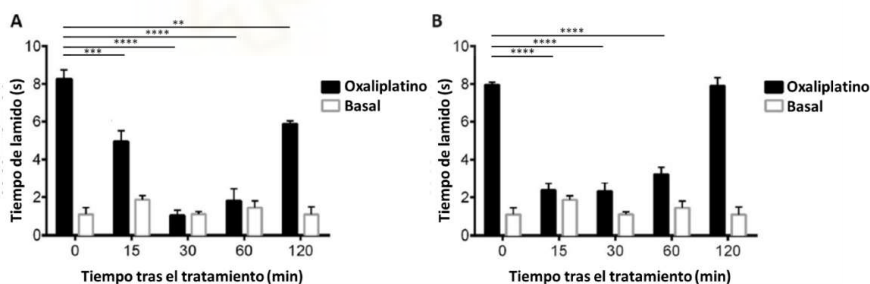


**Figura 13.** El compuesto **24a** disminuye la hipersensibilidad al frío inducida por oxaliplatino a 1  $\mu$ g (A) y 3  $\mu$ g (B) vía i.pl. Se realizó el test de acetona a los animales tratados con oxaliplatino y con vehículo antes y después de la aplicación del compuesto. Los datos se dan como la media  $\pm$  SEM (n=5). \*\*P <0,05; \*\*\*P <0,001; \*\*\*\*P <0,0001.

## **Publicación 2. Phenylalanine-Derived $\beta$ -Lactam TRPM8 Modulators. Configuration Effect on the Antagonist Activity**

En el trabajo anterior se empezó a intuir el posible efecto de la configuración de los centros estereogénicos sobre la actividad de las  $\beta$ -lactamas. Este hecho nos llevó a estudiar más exhaustivamente el efecto de la configuración espacial de las  $\beta$ -lactamas en su actividad frente a TRPM8 dando lugar a este trabajo. Por razones de eficiencia de

síntesis, se substituyó el grupo protector de aminas Z del precursor de las  $\beta$ -lactamas empleado en el trabajo anterior por dos grupos bencilo dando lugar a la  $\beta$ -lactama 4-bencil-1-[(3'-fenil-2'-dibencilamino)prop-1'-il]-4-benciloxicarbonil-3-metil-2 oxoazetidina. Esta substitución evitó que el nitrógeno ciclara con el carbono 2'' dando lugar a la CP (Figuras 10 y 14). Así pues, en este trabajo se prepararon y caracterizaron mediante ensayos de microfluorometría de calcio, *patch clamp* y modelado molecular los compuestos **13**, **14**, **15** y **16**, cuatro posibles derivados diastereoisoméricos de la  $\beta$ -lactama previamente citada, cuyas configuraciones se muestran en la Tabla 6.

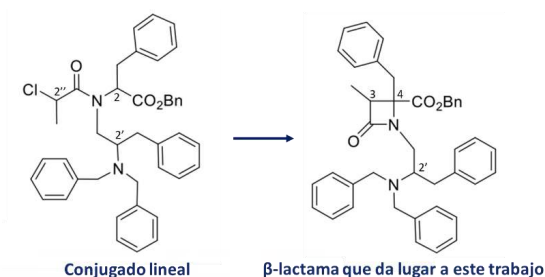


Figura 14. Conjugado de aminoácidos inicial para la obtención de la  $\beta$ -lactama descrita en la publicación actual.

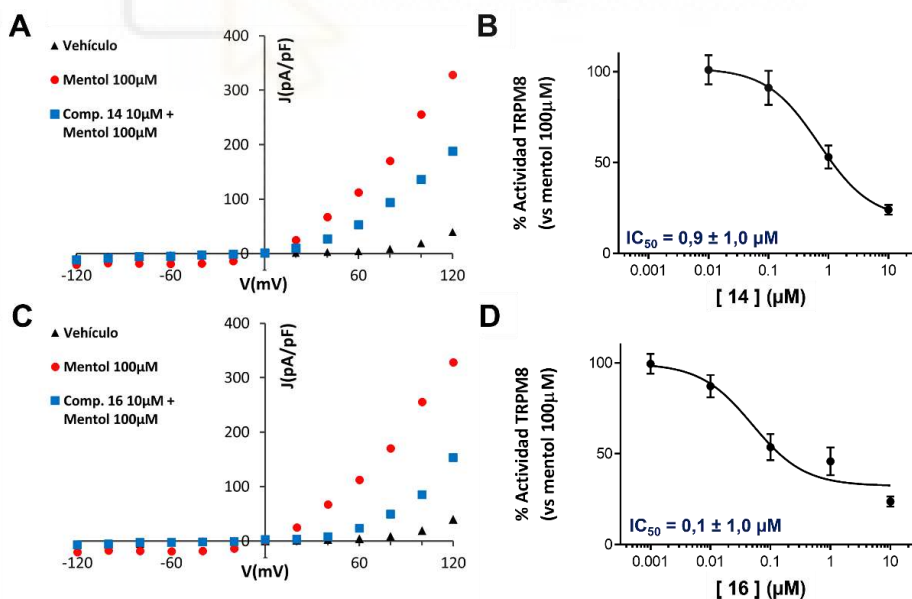
Los cuatro compuestos diastereoisómeros fueron capaces de bloquear en mayor o menor grado la entrada de calcio mediada por la activación de *r*TRPM8 con mentol 100  $\mu$ M en ensayos de microflorigrafía de calcio, mostrando una potencia más elevada que el antagonista de referencia AMTB (Tabla 6). El estereoisómero más potente resultó ser el **16**, con una configuración R para todos sus estereocentros. Posteriormente le siguieron el compuesto **14**, confirmando la importancia de la configuración R en el carbono 2'; el compuesto **15**, con una configuración 3R,4R,2'S; y, por último, el compuesto **13**, con una configuración S para sus tres estereocentros. Esta configuración S reduce la potencia del compuesto unas 10 veces. La eficacia y potencia de los compuestos se indica en la Tabla 6.

Tabla 6. Porcentaje de bloqueo de *r*TRPM8 (en presencia de mentol 100  $\mu$ M) mediado por los diastereoisómeros **13**, **14**, **15** y **16** a 5 y 50  $\mu$ M en ensayos de microfluorometría de calcio. Se indica también la configuración de los compuestos y sus  $IC_{50}$ s. Todos los resultados se expresan como media  $\pm$  SEM.

Compuesto	Configuración	% Bloqueo de TRPM8 a 5 $\mu$ M	% Bloqueo de TRPM8 a 50 $\mu$ M	Potencia $IC_{50}$ ( $\mu$ M)
<b>13</b>	3S,4S,2'S	57,7 $\pm$ 7,2	86,1 $\pm$ 5,0	3,1 $\pm$ 1,1
<b>14</b>	3S,4S,2'R	78,9 $\pm$ 1,2	87,7 $\pm$ 3,1	0,3 $\pm$ 1,0
<b>15</b>	3R,4R,2'S	71,1 $\pm$ 4,3	90,3 $\pm$ 2,8	0,7 $\pm$ 1,1
<b>16</b>	3R,4R,2'R	87,3 $\pm$ 8,1	98,5 $\pm$ 3,2	0,02 $\pm$ 1,1
AMTB <sup>164</sup>				7,3 $\pm$ 1,5

Para comprobar si los compuestos presentaban actividad hacia otros canales TRP se realizaron estudios de selectividad mediante las mismas técnicas en los canales *hTRPV1* y *hTRPA1* en las líneas celulares HEK293-*hTRPV1* y HEK293-LTV-*hTRPA1* respectivamente. Ninguna de las cuatro configuraciones mostró actividad agonista ni antagonista hacia estos canales TRP. Así pues, a diferencia de la mayoría de los antagonistas de TRPM8 descritos hasta la fecha <sup>180</sup>, los compuestos revelaron una importante selectividad frente a otros miembros TRP.

Adicionalmente, se corroboró la actividad antagonista de los compuestos más potentes (**14** y **16**) mediante técnicas electrofisiológicas (*whole-cell patch clamp*). Se comprobó que los dos compuestos a diferentes concentraciones bloquearon las respuestas de *rTRPM8* a 100  $\mu\text{M}$  de mentol a un voltaje fijo de -60 mV, obteniéndose unos valores  $\text{IC}_{50}$  de  $0,9 \pm 1,0 \mu\text{M}$  (**14**) y  $0,1 \pm 1,0 \mu\text{M}$  (**16**) (Figura 15 B y D). Hasta el momento, podemos decir que el compuesto 16 es el más potente identificado dentro de esta serie de  $\beta$ -lactamas. También se estudió la densidad de corriente del canal mediante rampas de voltaje y se observó que ambos compuestos inhibían las corrientes mediadas por mentol a 100  $\mu\text{M}$  (Figura 15 A y C).



**Figura 15.** Los compuestos **14** y **16** bloquearon las respuestas de *rTRPM8* a mentol 100  $\mu\text{M}$  en células HEK293-*rTRPM8*. A) y C) Registros representativos de rampas de voltaje (-120 a +120mV) en condiciones basales (vehículo), en presencia de estímulo (mentol 100  $\mu\text{M}$ ) y en presencia de estímulo más los bloqueadores **14** (A) y **16** (C) a 10  $\mu\text{M}$ . La corriente se expresa como pA/pF. B) y D) Curvas dosis-respuesta e  $\text{IC}_{50}$  del bloqueo de la corriente de *rTRPM8* mediada por mentol 100  $\mu\text{M}$  en presencia de varias concentraciones de compuesto **14** (B) y **16** (D) a un voltaje fijo de -60mV. Los resultados se dan como media  $\pm$  SEM.

Tras conocer la actividad bloqueadora de TRPM8, se quiso estudiar si los compuestos interactuaban con otros canales iónicos alterando el potencial de membrana celular en reposo. Para ello, se emplearon sistemas celulares más complejos, como son las neuronas GRD de rata, y la configuración *current clamp*, aplicando los compuestos (o vehículo) como único estímulo. Ninguno de los dos compuestos alteró el potencial de membrana a 10  $\mu\text{M}$  (Figura 16).

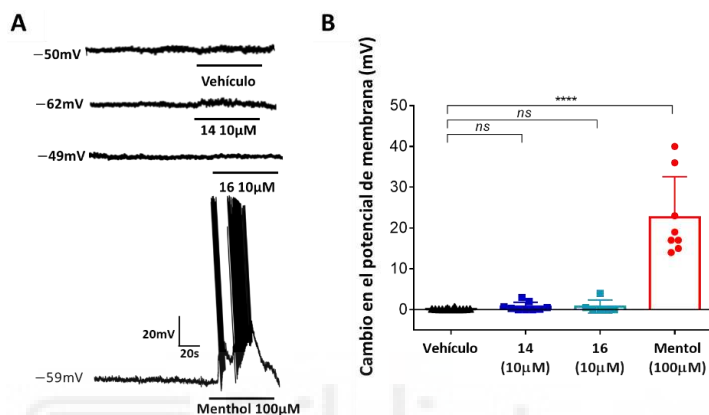


**Figura 16.** Los compuestos **14** y **16** no alteraron el potencial de membrana de las neuronas GRD. A) Registros representativos del cambio de potencial de la membrana de las neuronas en presencia de vehículo, de los compuestos **14** y **16** a 10  $\mu\text{M}$ , y de mentol a 100  $\mu\text{M}$ . B) Representación gráfica del cambio en el potencial de membrana de las neuronas tras la aplicación del vehículo, de los compuestos **14** y **16** a 10  $\mu\text{M}$  y de mentol a 100  $\mu\text{M}$ . Los resultados se muestran como media  $\pm$  SEM.

Para profundizar con el estudio de los compuestos sobre la excitabilidad neuronal, se emplearon matrices de multielectrodos (MEA). En este caso se registraron los potenciales de acción generados por una red neuronal tras la aplicación de los compuestos **14** y **16**. Se observó que ninguno de los compuestos inducía potenciales de acción ni inhibía aquellos producidos por el control positivo (KCl 40 mM) (Figura 17). Estos resultados indican que los derivados  $\beta$ -lactámicos **14** y **16** no afectan a los canales de sodio ni de potasio dependientes de voltaje, descartando un posible efecto anestésico y corroborando la selectividad de los compuestos hacia TRPM8.

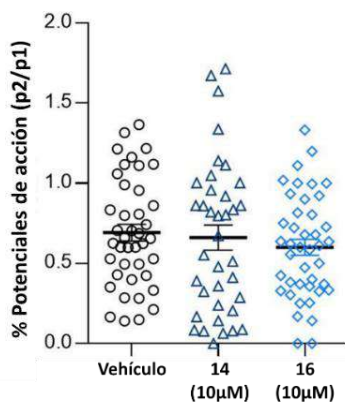


**Figura 17.** Los compuestos **14** y **16** no alteraron la actividad neuronal en neuronas GRD. Se representa la frecuencia de potenciales de acción entre dos pulsos de potasio 40mM en presencia y ausencia de los compuestos **14** y **16** a 10  $\mu$ M. Los resultados se dan como media  $\pm$  SEM.

Por último, se estudió como la configuración espacial afecta a la interacción proteína ligando mediante ensayos de modelado molecular. El hecho de que todos los isómeros descritos en esta publicación bloqueen *r*TRPM8 sugiere que la unión de dichos compuestos ocurre en un área lo suficientemente grande para acomodar a las diferentes configuraciones tridimensionales de los sustituyentes hidrofóbicos. Los resultados mostraron que los cuatro diastereoisómeros se unen a la zona del poro preferencial o exclusivamente. Dos de las cuatro soluciones mayoritarias coinciden con las de la anterior publicación (subsitio 1: parte media del poro, entre los dominios TM5 Y TM6 de una subunidad del canal con el dominio TM6 de una subunidad adyacente. Subsitio 2: parte interna del poro, entre las hélices que conectan TM6 y TRP). El subsitio 3 está ubicado en la parte superior del poro e involucra residuos en los dominios TM3 y TM4 de una subunidad y el dominio TM6 de una subunidad adyacente. Por último, el subsitio 4 se sitúa en la parte externa del poro en las dos hélices alfa que conectan las subunidades TM5 y TM6 de 3 subunidades contiguas. En todos los casos, la mayoría de las conexiones entre el canal y las  $\beta$ -lactamas son interacciones de Van de Waals (VdW) y apilamientos  $\pi$ - $\pi$ . Dichas interacciones se describen en mayor profundidad en el manuscrito (Anexo II, páginas 9-11). Estos estudios indican una vez más un modo diferente de interacción de los derivados  $\beta$ -lactámicos con respecto a otros antagonistas de TRPM8 descritos en la bibliografía<sup>181</sup>, haciéndolos una clase única de antagonistas de TRPM8.

**Publicación 3:  *$\beta$ -Lactam TRPM8 Antagonist RGM8-51 Displays Antinociceptive Activity in Different Animal Models***

Además de las  $\beta$ -lactamas descritas en las publicaciones anteriores, se llevaron a cabo estudios con otros derivados de la misma serie, destacando el compuesto **51** (Figura 18) por su alta eficacia. Así pues, en esta publicación se lleva a cabo una evaluación más exhaustiva tanto *in vitro* como *in vivo* de la  $\beta$ -lactama **51**. Se realizaron ensayos de actividad, potencia y selectividad mediante diversas técnicas seguidos de estudios en tres modelos animales de dolor: el modelo de NPIC concretamente mediada por oxaliplatino, visto anteriormente; un modelo de hiperestesia inducida por NTG; y un modelo de LCC del nervio ciático.

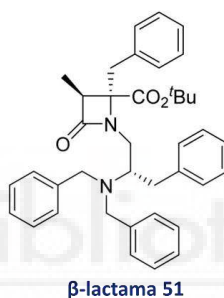
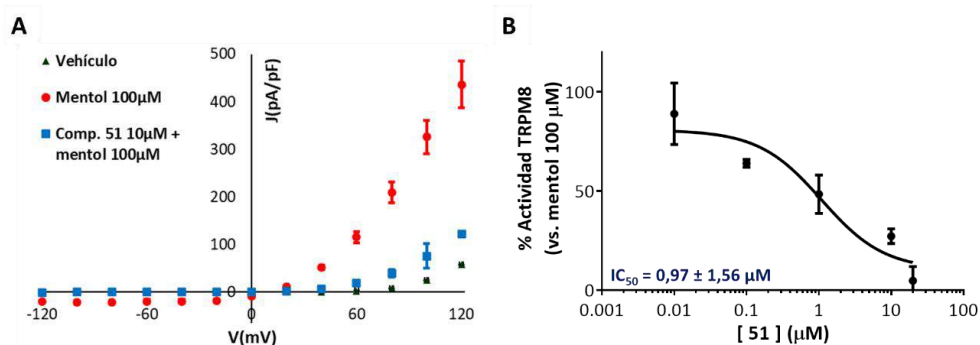


Figura 18.  $\beta$ -lactama descrita en esta tercera publicación.

Los estudios de actividad *in vitro* se realizaron nuevamente mediante técnicas de microfluorometría de calcio en células HEK293-*rTRPM8*, y por primera vez, en HEK293-*hTRPM8* expresando el canal TRPM8 humano. En ambos casos, el compuesto bloqueaba de manera dosis dependiente la entrada de calcio producida por mentol 100 $\mu$ M. Para ambas isoformas se obtuvieron valores de IC<sub>50</sub> de rango micromolar siendo 1,06  $\pm$  1,21  $\mu$ M para *rTRPM8* y 1,74  $\pm$  1,19  $\mu$ M para *hTRPM8*. Estos resultados se confirmaron posteriormente mediante *whole-cell patch clamp* en el canal *rTRPM8*. En este caso, se observó que el compuesto bloqueaba de manera dosis-dependiente las corrientes celulares mediadas por mentol a 100 $\mu$ M a un voltaje fijo de -60mV, obteniéndose una IC<sub>50</sub> de 0,97  $\pm$  1,56  $\mu$ M (Figura 19 B). También se estudiaron las corrientes celulares mediante rampas de voltajes (desde -120 a +120mV), observándose una disminución de las corrientes producidas por mentol 100  $\mu$ M cuando se aplicó el compuesto **51** a 10  $\mu$ M (Figura 19 A).



**Figura 19.** El compuesto **51** bloquea la actividad de *rTRPM8* mediada mentol 100  $\mu\text{M}$  en células HEK293-*rTRPM8*. A) Rampas despolarizantes de voltaje (-120 a +120mV) en condiciones basales (vehículo), en presencia de estímulo (mentol 100  $\mu\text{M}$ ) y en presencia de estímulo más el bloqueador **51** a 10  $\mu\text{M}$ . La corriente se expresa en J(pA/pF). B) Curva dosis-respuesta e  $\text{IC}_{50}$  del bloqueo de la corriente de *rTRPM8* mediada por mentol 100  $\mu\text{M}$  en presencia de varias concentraciones de compuesto **51** a un voltaje fijo de -60mV. Cada punto es la media  $\pm$  SEM.

Para descubrir la selectividad del compuesto **51** hacia el canal TRPM8, se midió su actividad en otros canales pertenecientes a la familia TRP y en el canal iónico sensible al ácido ASIC3 (Tabla 7). El compuesto mostró cierta capacidad para activar y bloquear el canal *hTRPV1* a 10  $\mu\text{M}$ , una concentración entre 10 y 6 veces mayor que la  $\text{IC}_{50}$  para *rTRPM8* o *hTRPM8* respectivamente. En cuanto al resto de canales, el compuesto no mostró actividad agonista ni antagonista para *hTRPA1* ni actividad antagonista para *hTRPV3* y ASIC3. También se midió la capacidad de unión del compuesto **51** a otros receptores relacionados con el dolor como son el péptido relacionado con el gen de la calcitonina (CGRPR), el receptor cannabinoide de tipo 2 (CB2) y el receptor muscarínico tipo M3 (M3) en la línea celular derivada de ovario de hámster chino (CHO) transfectada con estos receptores. A 10 $\mu\text{M}$ , el compuesto tampoco mostró afinidad significativa por los receptores mencionados, reforzando así su selectividad para el canal TRPM8.

**Tabla 7.** Actividad funcional del compuesto **51** a 10  $\mu\text{M}$  en los canales TRPV1, TRPV3, TRPA1 y ASIC3 mediante ensayos de microfluorometría de  $\text{Ca}^{2+}$ . Los datos se dan como media  $\pm$  SEM.

<i>hTRPV1</i> ago. (%)	<i>hTRPV1</i> antago. (%)	<i>hTRPV3</i> antago. (%)	<i>hTRPA1</i> ago. (%)	<i>hTRPA1</i> antago. (%)	ASIC3 antago. (%)
31,3 $\pm$ 3,6	19,4 $\pm$ 1,7	-6,3 $\pm$ 5,9	0,4 $\pm$ 0,3	4,3 $\pm$ 1,1	6,0 $\pm$ 0,9

El compuesto **51** también se caracterizó en cultivos celulares primarios de neuronas GRD mediante técnicas electrofisiológicas de *whole-cell patch clamp*. De acuerdo con los experimentos realizados en las líneas celulares continuas, se observó que el compuesto **51** a 1  $\mu\text{M}$  era capaz de bloquear al 65,01  $\pm$  4,67% las corrientes

mediadas por mentol 100  $\mu\text{M}$ . A esta concentración, también se observó que no tuvo efecto en las corrientes de  $\text{Na}^+$  y  $\text{K}^+$  mediadas por voltaje tras aplicar un pulso de despolarización a +10 mV. Por último, también se comprobó si el compuesto alteraba el potencial de reposo de las neuronas a concentraciones mayores. Para ello, se empleó el modo de registro *current clamp* sin inyectar corriente (Figura 20). Los resultados demostraron que el compuesto **51** a 10  $\mu\text{M}$  no altera el potencial de membrana de las neuronas GRD.

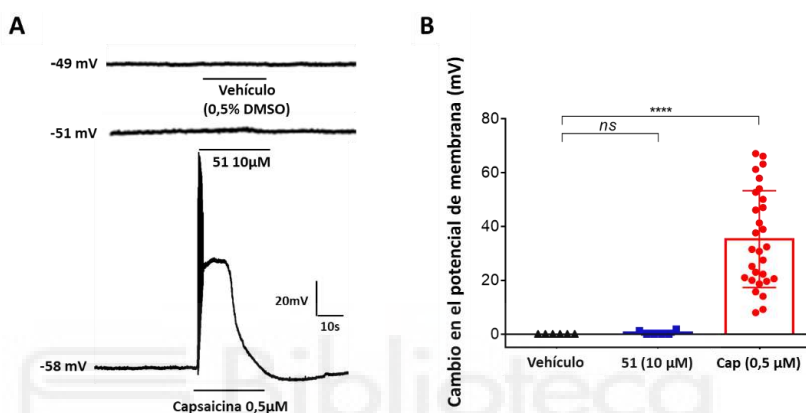


**Figura 20.** El compuesto **51** no alteró el potencial de membrana de las neuronas GRD. A) Registros representativos del cambio de potencial de la membrana de las neuronas en presencia de vehículo, compuesto **51** a 10  $\mu\text{M}$  y capsaicina a 0,5  $\mu\text{M}$ . B) Representación gráfica del cambio en el potencial de membrana de las neuronas tras la aplicación del vehículo, el compuesto **51** a 10  $\mu\text{M}$  y la capsaicina a 0,5  $\mu\text{M}$ .

Para la  $\beta$ -lactama **51** se realizaron estudios adicionales de farmacocinética que fueron subcontratados a Eurofins-CEREP. La  $\beta$ -lactama demostró buena solubilidad en condiciones gástricas (pH < 5,5) pero no pudo permear las monocapas de células inmortalizadas de adenocarcinoma colorrectal humano (CACO-2) indicando que la administración oral no sería adecuada para experimentos *in vivo*. Tampoco mostró buena estabilidad en microsomas hepáticos humanos ( $t_{1/2}$  = 11 min) ni buen aclaramiento intrínseco metabólico (Clint = 614 L/min/mg), además de mostrar una alta unión a proteínas séricas (99-100%). Sin embargo, como veremos a continuación, el compuesto **51** demostró poseer efecto en ensayos *in vivo* tras su administración *i.p.* e *i.pl.*.

Antes de continuar con los ensayos *in vivo*, se estudió la interacción del compuesto **51** con *rTRPM8* mediante modelado molecular. Para esta  $\beta$ -lactama se volvieron a encontrar cuatro soluciones principales coincidentes con las publicaciones

previas (Figura 21) <sup>164,183</sup>. En el sitio 1 (58% de las soluciones), el compuesto se une a la proteína mediante 3 apilamientos  $\pi$ - $\pi$ . Dos de ellos involucran el anillo aromático del grupo 4-Bn del compuesto **51** con los residuos Trp877 y Phe881 de TRPM8. El tercer apilamiento  $\pi$ - $\pi$  se origina entre el grupo N-Bn y la Phe963. Además de estas tres interacciones, la unión **51**-proteína está estabilizada por numerosos enlaces de VdW. Por otra parte, en el sitio 2, la interacción está mediada por una red de interacciones VdW que involucran a todos los sustituyentes de la  $\beta$ -lactama. Estos estudios indican una vez más un modo diferente de interacción de los derivados  $\beta$ -lactámicos con respecto a otros antagonistas de TRPM8 descritos <sup>181</sup>, haciéndolos una clase única de antagonistas de TRPM8.

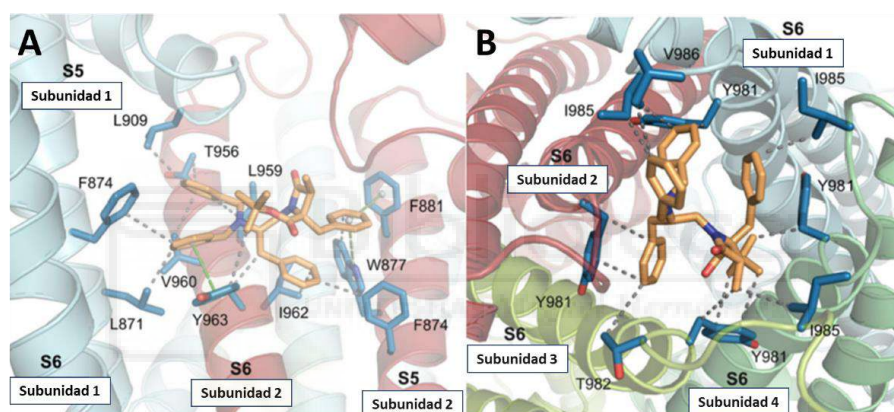


**Figura 21.** Interacciones principales de la  $\beta$ -lactama **51** con rTRPM8. A) Subsio 1. B) Subsio 2. El compuesto **51** se encuentra en naranja con los heteroátomos en rojo (O) y en azul (N). Los aminoácidos de TRPM8 que interactúan con el compuesto se encuentran en azul. Las interacciones VdW se indican mediante líneas punteadas grises, mientras que los apilamientos  $\pi$ - $\pi$  se indican mediante líneas verdes discontinuas.

Por último, el compuesto se probó en tres modelos *in vivo* de dolor, un modelo de NPIC mediada por oxaliplatino, un modelo de hipersensibilidad mecánica inducida por NTG y un modelo de LCC del nervio ciático. En el primer modelo se indujo un NPIC inducida por oxaliplatino (6 mg/kg) en ratones. El oxaliplatino se administró vía subcutánea (s.c.) y se realizó la prueba de acetona como se explica previamente (publicación 1) <sup>164</sup>. 1  $\mu$ g de compuesto administrado vía i.pl. atenuó las respuestas al frío a los 15 minutos posteriores a su administración, manteniendo un efecto significativo hasta los 60 minutos. El compuesto continuó mostrando actividad a dosis inferiores de 0,1  $\mu$ g, aunque en este caso la duración del efecto significativo fue más corto (30

minutos). Comparado el compuesto **51** con la  $\beta$ -lactama **24a** de la publicación 1<sup>164</sup>, este mostró el mismo efecto antialodínico al frío a dosis más bajas (Figura 22).

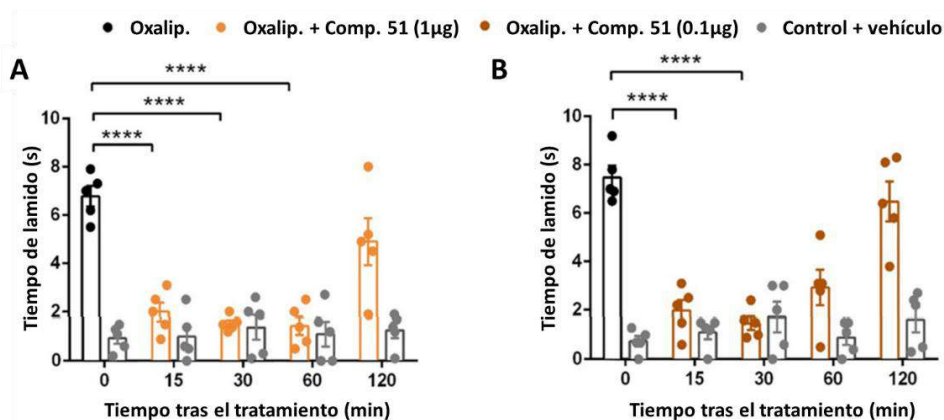


**Figura 22.** El compuesto **51** disminuye la hipersensibilidad al frío inducida por oxaliplatino hasta 1 hora después de su administración (prueba de la gota de acetona). Se administraron  $1\mu\text{g}$  (A) o  $0,1\mu\text{g}$  (B) de compuesto **51** a los ratones tratados con oxaliplatino y con vehículo, y se realizó el test de acetona a los 15, 30, 60 y 120 minutos. Los datos se dan como la media  $\pm$  SEM ( $n = 5$ ) (\*\*\*\*  $p < 0,0001$ ).

El segundo modelo de hipersensibilidad mecánica es un modelo de migraña crónica en ratón inducida por la administración intermitente de NTG. La migraña es un dolor de cabeza severo que constituye una de las enfermedades más frecuentes en el mundo, afectando a un 14% de la población y mayoritariamente a mujeres. Recientemente, se ha demostrado que el canal TRPM8 está relacionado con el desarrollo de la migraña<sup>138</sup>. Así pues, tras la actividad in vivo del compuesto **51** en el modelo de NIPC, nos propusimos probarlo en este modelo de migraña. Para el experimento se emplearon ratones macho y ratones hembra para investigar simultáneamente un posible dimorfismo sexual. La hipersensibilidad mecánica se midió con la prueba de von Frey. Tanto en ratones macho (Figura 23 A) como en hembra (Figura 23 B) la administración de NTG disminuyó la tolerancia a la estimulación mecánica. En el caso de los ratones macho, el compuesto **51** fue capaz de aumentar esta tolerancia mecánica de manera significativa a 30 mg/kg i.p. 60 minutos después de la administración. Por otra parte, en el caso de los ratones hembra, el compuesto redujo significativamente la hiperestesia mecánica tanto a 10 como a 30 mg/kg i.p. 30 minutos tras su administración. En hembras, el efecto no solo comenzó antes que en machos, sino que duró más tiempo (hasta las 2 horas) (Figura 23). Este comportamiento

diferencial podría deberse a la testosterona, principal hormona sexual masculina, ya que por ser un activador de TRPM8 podría estar contrarrestando el efecto de la  $\beta$ -lactama<sup>91</sup>.

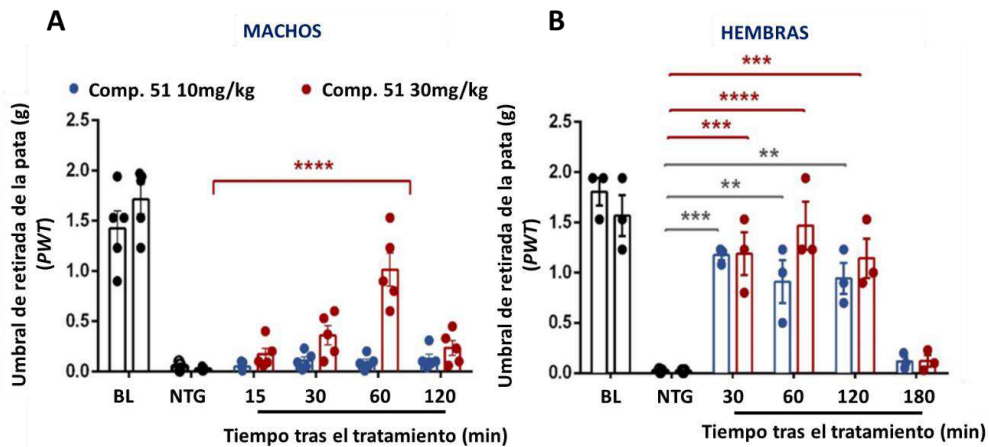
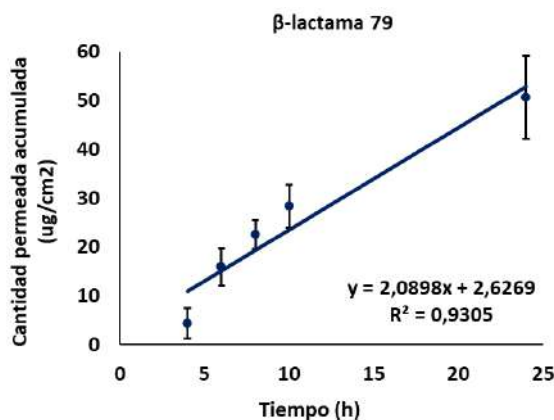


Figura 23. El compuesto 51 reduce la hipersensibilidad mecánica inducida por NTG de manera dependiente del sexo. Se representa el umbral de retirada de la pata (PWT) en ratones macho (A) y en ratones hembra (B) en condiciones basales, tras el tratamiento con NTG y tras la administración del bloqueador 51 a 10 y 30 mg/kg. Se representa la evolución temporal del efecto del compuesto 51. Todos los datos se dan como media  $\pm$  SEM (n = 3-5) (\*\* p < 0,05; \*\*\* p < 0,001; \*\*\*\* p < 0,0001) (BL = Basal).

Por último, en colaboración con el departamento del Dr. Antonio R. Artalejo en la universidad Complutense de Madrid, también se estudió el efecto del compuesto 51 en un modelo de LCC del nervio ciático. En este segundo modelo se evaluó la sensibilidad al frío mediante el test de acetona, la sensibilidad al calor mediante de la prueba de Hargreaves y la sensibilidad mecánica mediante la prueba de von Frey automatizada. El efecto del compuesto se evaluó antes y después de la cirugía LCC. Se observó que la administración i.p. del compuesto 51 (10 y 30 mg/kg) redujo de manera dosis dependiente la hipersensibilidad al frío, la hipersensibilidad al calor y la hipersensibilidad mecánica. Sin embargo, la administración local (i.pl.) de 10  $\mu$ g de compuesto solo pudo reducir la hipersensibilidad al frío y la hipersensibilidad mecánica sin influir en la respuesta de los ratones al calor. Este hecho podría indicar que el efecto del compuesto se debe a la regulación de la temperatura corporal más que a la sensación de calor. Cabe añadir que, en los estudios previos a la cirugía, el compuesto 51 no tuvo ningún efecto sobre la percepción del frío, del calor o sobre la retirada de la pata. Estos resultados sugieren que el compuesto 51 posee un efecto antinociceptivo multisensorial (estímulos fríos, calientes y mecánicos) sin afectar a la percepción sensorial normal.

Tras la obtención de estos resultados, se decidió realizar estudios complementarios de permeabilidad cutánea con algunas de las  $\beta$ -lactamas, incluida la **51**, para evaluar su administración tópica. Todos estos estudios se realizaron durante la estancia de investigación en el Cbios-Universidade Lusófona de Lisboa, Portugal. Para ello, se emplearon las celdas de Franz y una membrana de silicona Liveo™ simulando la epidermis. Se estudió la permeabilidad de 300  $\mu$ l de compuesto a 1 mg/ml (300  $\mu$ g) en etanol:agua (50:50). Las muestras se recogieron en intervalos de 2 horas hasta las 10 horas y el día posterior (24 h), y se analizaron mediante HPLC. Todos los experimentos se realizaron por cuatuplicado. En la actualidad, solamente se han obtenido resultados preliminares para el compuesto **79**, el cual se diferencia del **51** por poseer una amida de isobutilo sustituyendo al ester de terbutilo del compuesto **51**. Aunque el compuesto **79** presente características que indiquen una baja permeabilidad cutánea<sup>184</sup> como son un elevado peso molecular (Mw) de 588.8 Da y un alto coeficiente de partición n-octanol/agua (Log P<sub>ow</sub>) de 5.44, este se detectó en el compartimento receptor a las 4 horas tras su administración. Tras 24 horas, un 15,6% de la dosis inicial de compuesto **79** había permeado la membrana de silicona con un flujo de estado estacionario (J<sub>ss</sub>) de  $2,09 \pm 0,57 \mu\text{g}/\text{cm}^2 \cdot \text{h}$  (Figura 24, Tabla 8). Por este motivo, para garantizar la inocuidad de la administración tópica del compuesto, se debe continuar con los estudios de permeabilidad, ya que los ensayos preliminares no son suficientes para establecer el porcentaje real de absorción cutánea ni la seguridad del compuesto<sup>185</sup>. Para ello, se deberían de elaborar una formulación cosmética adecuada y llevar a cabo de nuevo los estudios de permeabilidad en piel humana o piel porcina siguiendo la Guía para testar la absorción dérmica *in vitro* de compuestos químicos OECD n<sup>o</sup>428<sup>186</sup> y los criterios básicos de dichos experimentos SCCP/0970/06<sup>187</sup> como se hizo con la  $\beta$ -lactamas **52** en trabajos previos<sup>184</sup>. Dicha  $\beta$ -lactama (**52**) sí resultó segura para la administración tópica<sup>178</sup>.



**Figura 24.** Perfil de permeabilidad del compuesto 79. Se representa la cantidad acumulada de compuesto difundida por unidad de área frente al tiempo. La pendiente de la ecuación de la recta representa el  $J_{ss}$ . Los resultados se expresan como la media  $\pm$  SD de  $n=4$ .

**Tabla 8.** Resumen de los resultados de permeabilidad del compuesto 79. Se recopilan los valores obtenidos en las cuatro celdas de Franz y su promedio  $\pm$  SD.

Celda de Franz (n)	$J_{ss}$ ( $\mu\text{g}/\text{cm}^2 \cdot \text{h}$ )	Cantidad Acumulada a las 24h ( $\mu\text{g}$ ).	% de compuesto difundido a las 24h (dosis inicial 300 $\mu\text{g}$ )
1	2,82	52,22	17,41
2	2,25	51,03	17,01
3	1,71	42,84	14,28
4	1,58	40,54	13,51
<b>Promedio</b>	<b>2,09 <math>\pm</math> 0,57</b>	<b>46,66 <math>\pm</math> 5,83</b>	<b>15,55 <math>\pm</math> 1,95</b>

En resumen, todos los compuestos seleccionados para su caracterización farmacológica demostraron ser potentes y selectivos para TRPM8. Además, pese a no presentar una buena farmacocinética, el compuesto **51** mostró una actividad significativa en 3 modelos *in vivo* de dolor. Todos estos resultados, indican que los dos sistemas heterocíclicos derivados de fenilalaninol-Phe, especialmente los derivados  $\beta$ -lactámicos, constituyen un nuevo quimiotipo de bloqueadores de TRPM8 como punto de partida para futuras modificaciones hacia compuestos con mejores perfiles farmacológicos. Así pues, nuestros laboratorios continúan con los estudios de dichos derivados  $\beta$ -lactámicos tanto para incrementar el conocimiento sobre el canal TRPM8 como para mejorar sus características farmacológicas, pensando en futuras aplicaciones terapéuticas tanto en el campo del dolor como en el del cáncer. Paralelamente, se siguen llevando a cabo los ensayos de permeabilidad para estudiar la administración tópica de dichas  $\beta$ -lactamas.

**Capítulo 2: Búsqueda de nuevos esqueletos farmacológicos moduladores de TRPM8**

Desde hace varios años, nuestro grupo de investigación colabora con la Doctora Isabel Gómez Monterrey de la Universidad de Nápoles, Italia, en el desarrollo de nuevas estructuras capaces de modular el canal TRPM8 <sup>188-191</sup>. Hasta el momento se han identificado diversas estructuras capaces de modular dicho canal. Entre ellas destacan las triptaminas N-sustituidas <sup>55,188</sup>, concretamente la triptamina **31a** [(5R,11aS)-5-(4-chlorophenyl)-2-(4-fluorobenzyl)-5,6,11,11a-tetrahydro-1H-imidazo[1',5':1,6] pyrido[3,4-b] indole-1,3(2H)-dione], la cual se ha identificado como un potente antagonista del canal ( $IC_{50} = 4,1 \pm 1,2$  nM), selectivo, metabólicamente estable y con actividad en diversos modelos animales como son el modelo de *WDS* inducido por icilina, el modelo de alodinia al frío inducida por oxaliplatino y la hiperalgesia térmica inducida por LCC. Constituyendo este núcleo de triptamina un farmacóforo a estudiar en el diseño de potentes moduladores de TRPM8 <sup>55</sup>.

Recientemente, debido a la implicación de TRPM8 en varios cánceres, entre ellos el cáncer de próstata <sup>142</sup>, se ha estudiado la actividad antitumoral de compuestos mejorados. En estos compuestos se ha sustituido el núcleo de triptamina por diferentes aminoácidos, mostrando mejores perfiles de potencia y selectividad hacia TRPM8, además de capacidad para reducir la proliferación, migración e invasividad de las células tumorales en diversos modelos de cáncer de próstata <sup>191</sup>.

Por último, existe una tercera publicación, incluida como índice de calidad de esta tesis (Anexo IV), en la que se emplean métodos computacionales para identificar nuevos quimiotipos capaces de modular TRPM8 <sup>190</sup>. Para ello, se lleva a cabo un cribado virtual basado en estructuras que permite estudiar la interacción de un alto número de compuestos con la proteína diana <sup>77,192</sup>. Este screening virtual constituye una de las técnicas más prometedoras *in silico* para la identificación y el diseño de nuevas moléculas. Además de considerarse una herramienta efectiva, permite ahorrar tiempo y costes en el proceso de identificación de compuestos <sup>192</sup>, aunque es necesario tener en cuenta que este tipo de ensayos necesitan de la validación *in vitro* de los resultados obtenidos como veremos a continuación <sup>77</sup>.

**Publicación 1: *In Vitro and In Vivo Pharmacological Characterization of a Novel TRPM8 Inhibitor Chemotype Identified by Small-Scale Preclinical Screening***

En este trabajo se realizó un cribado virtual de la biblioteca molecular EDASA Scientific, disponible comercialmente, frente al canal *hTRPM8* con el fin de encontrar nuevas estructuras químicas capaces de bloquear su actividad. Posteriormente, los resultados se validaron mediante ensayos de microfluorometría de calcio y se continuó con la caracterización de los compuestos más potentes mediante técnicas electrofisiológicas. También se estudió la interacción de los compuestos más interesantes con *hTRPM8* mediante técnicas de modelado molecular con el fin de identificar las características estructurales responsables de su potencia. Por último, el compuesto con mejores propiedades farmacológicas se estudió en ensayos *in vivo* de alodinia al frío, revelando su eficacia e idoneidad para un posterior desarrollo.

El screening virtual de la quimioteca EDASA Scientific (2543 compuestos) se llevó a cabo en dos modelos de *hTRPM8* contruidos a partir de las estructuras de *Parus major* interaccionando con dos bloqueadores de TRPM8: AMTB y TC-I 2014. Ambos modelos están disponibles en Protein Data Bank (PDBs ID: 6O6R y 6O72 respectivamente). Toda la biblioteca se lanzó hacia las dos estructuras mediante un protocolo que consta de dos etapas de acoplamiento proteína-ligando, usando Glide SP y Glide XP. Se seleccionaron los 21 compuestos con mejores energías de interacción.

Posteriormente, se validaron los resultados de los 21 compuestos mediante ensayos de microfluorometría de calcio en las células HEK293-*rTRPM8*. En primer lugar, se probaron los compuestos a 3 concentraciones (50, 5 y 0,5 $\mu$ M) y se estudió el % de actividad del canal mediado por mentol 100  $\mu$ M en presencia de los compuestos (Figura 25).

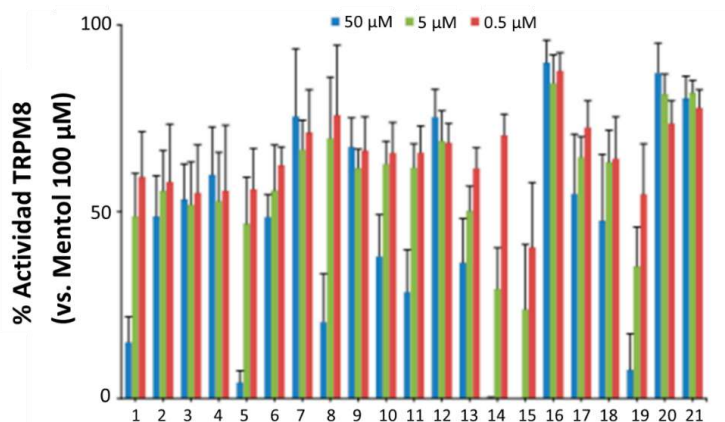


**Figura 25.** Porcentaje de actividad del canal rTRPM8 tras la administración de mentol 100  $\mu\text{M}$  en presencia de los compuestos 1-21 a 3 concentraciones (50, 5 y 0,05  $\mu\text{M}$ ) en la línea celular HEK293-rTRPM8 mediante ensayos de microfluorometría de calcio. Los resultados están normalizados frente al efecto del agonista de referencia (mentol a 100  $\mu\text{M}$ ) y se expresan como la media  $\pm$  SEM ( $N=3$ ,  $n=3$ ).

De los 21 compuestos, destacaron los compuestos **1**, **5**, **13-15** y **19** por demostrar un mayor porcentaje de bloqueo de TRPM8 en presencia de mentol 100  $\mu\text{M}$ . Se estudiaron un mayor número de concentraciones de los compuestos mencionados para estudiar su potencia y calcular su  $\text{IC}_{50}$  (Tabla 9). Los compuestos **14** y **15**, cuyas estructuras se muestran en la Figura 26, se identificaron como los más potentes, presentando unas  $\text{IC}_{50}$ s de  $0,25 \pm 0,15$  y  $0,22 \pm 0,10$   $\mu\text{M}$ , valores 30 veces inferiores a los del antagonista de referencia AMTB ( $7,15 \pm 1,24$ )<sup>188</sup>. Ambos compuestos, además de ser los más potentes, resultaron ser los más eficaces bloqueando el 100% de la actividad del canal a 50  $\mu\text{M}$ .

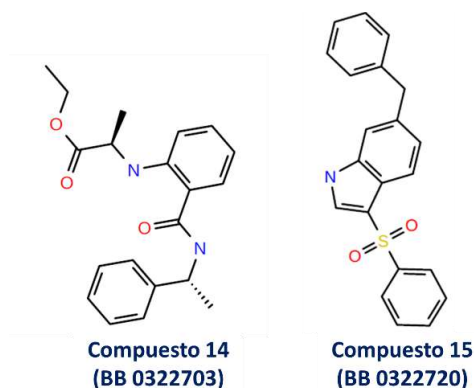


**Figura 26.** Estructuras de los compuestos más activos y eficaces bloqueando el canal TRPM8 en ensayos de microfluorometría de calcio. Entre paréntesis están los códigos originales de la librería EDASA Scientific.

## Resumen de los resultados y discusión. Capítulo 2.

**Tabla 9.**  $IC_{50}$ s y eficacias de los compuestos seleccionados como más potentes en los ensayos de microfluorometría de calcio ( $N = 3$ ,  $n = 3$ ).

Compuesto	$IC_{50}$ $\mu$ M (media $\pm$ SD)	Eficacia a 50 $\mu$ M*
<b>1 (BB 0220221)</b>	10,21 $\pm$ 1,31	85 %
<b>5 (BB 0304240)</b>	11,10 $\pm$ 1,32	90 %
<b>13 (BB 0310244)</b>	1,01 $\pm$ 0,51	90 %
<b>14 (BB 0322703)</b>	0,25 $\pm$ 0,15	100 %
<b>15 (BB 0322720)</b>	0,22 $\pm$ 0,10	100 %
<b>19 (BB 0310198)</b>	5,52 $\pm$ 1,45	90 %
AMTB <sup>188</sup>	7,15 $\pm$ 1,24	100 %

\*Expresado como porcentaje de inhibición de la actividad del mentol 100  $\mu$ M.

Como se explica en el capítulo anterior, uno de los principales problemas que presentan los bloqueadores de TRPM8 es su interacción con otros canales TRP<sup>122,188</sup>. Así pues, se estudió la selectividad de estos 6 compuestos frente al canal *hTRPV1* en la línea celular HEK293-*hTRPV1*, empleando las mismas técnicas. Solamente los compuestos **13** y **19** mostraron actividad agonista frente a *hTRPV1*, obteniéndose unos valores de  $EC_{50}$  entre 1,34 y 1,68  $\mu$ M (Figura 27). El estudio de estos compuestos sería interesante para la identificación de las estructuras que discriminan la selectividad hacia los distintos canales TRP.

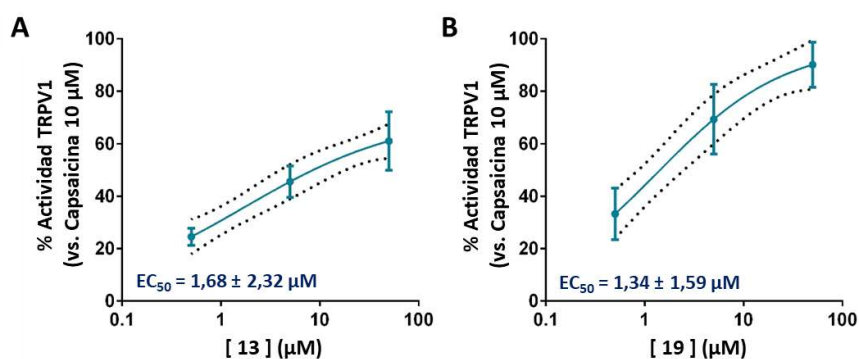


**Figura 27.** Curvas dosis-respuesta para los compuestos **13** (A) y **19** (B) en las que se muestra la activación de *hTRPV1* en la línea celular HEK293-*hTRPV1*. La respuesta se expresa como porcentaje de activación de TRPV1 normalizado al efecto del agonista de referencia, capsaicina a 10  $\mu$ M. Se representa la media  $\pm$  SEM. La línea discontinua muestra los intervalos de confianza del 95%.

Posteriormente, con el fin de tener una mejor caracterización funcional de los compuestos **14** y **15**, se estudiaron mediante técnicas electrofisiológicas de *whole-cell patch clamp* en el canal *rTRPM8*. A voltajes constantes de -60mV, ambos compuestos

bloquearon las corrientes de *r*TRPM8 mediadas por mentol 100 $\mu$ M a distintas concentraciones (0,1; 1; 5 y 10  $\mu$ M), obteniéndose una curva dosis-respuesta para cada compuesto (Figura 28 B y C) y unos valores de  $IC_{50}$  de  $1,25 \pm 0,26\mu$ M para el compuesto **14** y de  $2,95 \pm 1,83\mu$ M para el compuesto **15**. Los resultados corroboraron una mayor potencia para el compuesto **14**. También se empleó un protocolo de rampas de voltaje (-120 a +120mV) mediante el que se observó que ambos compuestos a 10 $\mu$ M bloqueaban todas las corrientes mediadas TRPM8 en presencia de mentol 100 $\mu$ M (Figura 28 A y C).

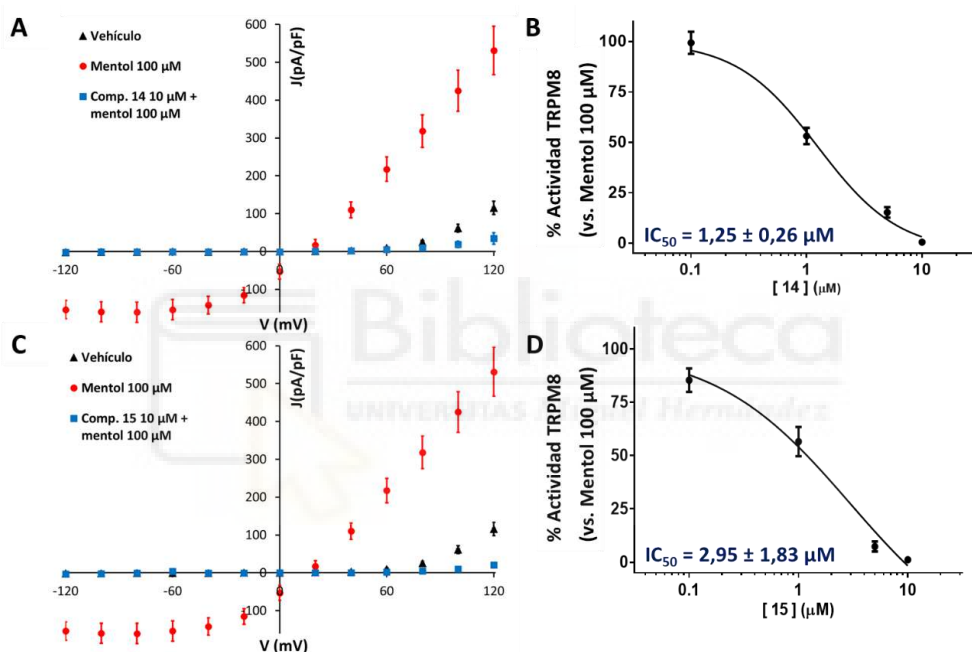


**Figura 28.** Los compuestos **14** y **15** bloquearon las corrientes de *r*TRPM8 mediadas por mentol 100 $\mu$ M en células HEK293-*r*TRPM8. A) y C) Densidad de corriente de TRPM8 a los diferentes voltajes (rampas de -120 a +120mV) en condiciones basales, en presencia de estímulo (mentol 100  $\mu$ M) y en presencia de estímulo más los bloqueadores **14** (A) y **15** (C) a 10  $\mu$ M. La corriente se expresa como pA/pF. B) y D) Curvas dosis-respuesta e  $IC_{50}$ s del bloqueo de la corriente de *r*TRPM8 mediada por mentol 100  $\mu$ M en presencia de los compuestos **14** (B) y **15** (D) a diferentes concentraciones (0,1; 1; 5 y 10 $\mu$ M). Cada punto es la media  $\pm$  SEM.

Tras los estudios funcionales se quiso estudiar con más detalle la interacción ligando-proteína de los compuestos **14** y **15** en *h*TRPM8. Se observó que ambos compuestos interaccionaban de manera similar. Ambos se dirigieron al dominio VSLD, rodeados por los dominios TM1-TM4 y los residuos TRP, y alejados del sitio de unión del AMTB y del TC-I 2014<sup>181</sup>. El compuesto **14** interaccionó de manera estable con los residuos Val742, Tyr745, Ile846, Tyr1005 Y Phe1013 en la región VSLD. El oxígeno del

grupo éster interaccionó mediante un enlace de hidrógeno con el residuo Tyr745, mientras que el grupo fenilo interaccionó mediante apilamiento  $\pi$ - $\pi$  con el residuo Tyr1005. Por otra parte, el compuesto **15** interaccionó de manera estable con los aminoácidos Phe735, Phe738, Arg842, His845, Leu1001 en la parte inferior de la región VSLD, por encima de la caja TRP. Su grupo bencilo interaccionó mediante apilamiento  $\pi$ - $\pi$  con el grupo aromático del aminoácido Phe735; el anillo indol interaccionó mediante enlaces de hidrógeno con el nitrógeno de la Leu1001 y mediante apilamiento  $\pi$ - $\pi$  con el aminoácido Phe738; y por último, el grupo bencenosulfonilo interaccionó mediante enlaces de hidrógeno con los aminoácidos His845 y Arg842. Existen muchas otras interacciones menores que se muestran en el manuscrito (Anexo IV, páginas 4-6).

El compuesto **14**, tras mostrar los mejores perfiles de potencia, eficacia y selectividad, se seleccionó para estudiar su efecto en un modelo animal de alodinia al frío. Como se ha descrito en varias ocasiones a lo largo de la tesis, los antagonistas de TRPM8 son capaces de contrarrestar el dolor neuropático inducido por algunos agentes quimioterapéuticos como el oxaliplatino<sup>51</sup>. Así pues, se emplea el modelo animal de dolor neuropático inducido por oxaliplatino explicado en la publicación 1 del capítulo 1. Para estudiar la alodinia al frío se empleó de nuevo el test de acetona y se contabilizaron el número de respuestas dolorosas. Como demuestra la Figura 29, la administración i.pl. de 30  $\mu$ g del compuesto **14** llevó a una disminución de la alodinia al frío mediada por oxaliplatino que se mantuvo durante al menos 1 hora. Los resultados obtenidos para 10  $\mu$ g de compuesto también muestran una tendencia a disminuir la alodinia al frío respecto al grupo control. Sin embargo, no se observaron diferencias significativas.

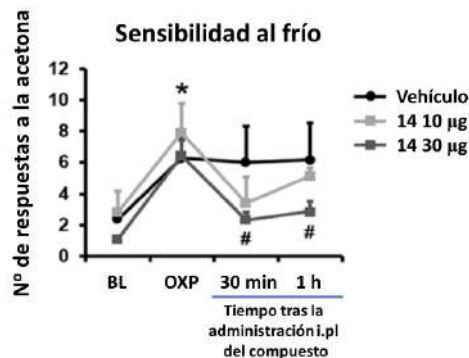


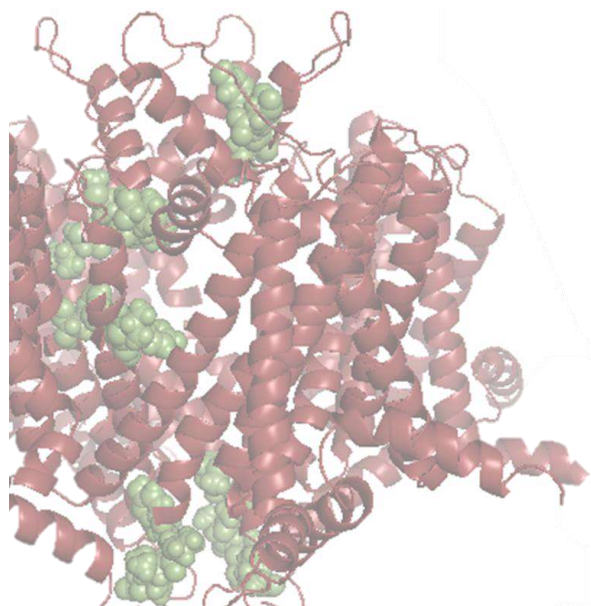
Figura 29. La administración i.pl. del compuesto **14** disminuyó la alodinia al frío inducida por oxaliplatino en el test de acetona. Tras inducir la alodinia al frío mediante el tratamiento con oxaliplatino, se administraron vía i.pl. 10 o 30  $\mu$ g del compuesto. Se representa la evolución temporal del efecto del compuesto a ambas concentraciones. Los datos se dan como media  $\pm$  SEM. \*  $p < 0,05$  oxaliplatino frente al valor inicial. #  $p < 0,05$  oxaliplatino frente a 30  $\mu$ g del compuesto **14**.

En resumen, en este trabajo se demuestra como el empleo de técnicas de cribado *in silico* constituye una primera aproximación muy adecuada para identificar compuestos bloqueadores del canal TRPM8. Los resultados obtenidos mediante estas técnicas se validaron mediante ensayos funcionales obteniéndose 6 compuestos bloqueadores del canal, de los cuales dos poseen doble actividad tras activar al canal TRPV1. De esos 6 compuestos se seleccionaron los compuestos **14** y **15** por ser los más potentes y efectivos. Los resultados obtenidos para ambos compuestos se confirmaron mediante técnicas electrofisiológicas. También se quiso estudiar la interacción de los compuestos con el canal humano, resultando ser distintos a los antagonistas identificados hasta la fecha (AMTB y TC-I 2014). Por último, el compuesto **14** demostró su eficacia en un modelo animal de alodinia al frío inducido por oxaliplatino, indicando su idoneidad para seguir con un posterior desarrollo del compuesto. Cabe destacar que este compuesto es una mezcla diastereoisómera de (R)-etilo 2-((2-(((S)-1-feniletil)carbamoil)fenil)amino)propanoato y (R)-etilo 2-((2-(((R)-1-feniletil) carbamoil) fenil) amino) propanoato, siendo la configuración S el eutómero, ya que la configuración R no obtuvo una buena puntuación en el *screening* inicial. Un estudio más exhaustivo de este quimiotipo y de ambos enantiómeros podría ayudar al descubrimiento de derivados más potentes. En lo referente al compuesto **15**, aunque no se hayan realizado estudios *in vivo*, los resultados de potencia, efectividad y selectividad obtenidos *in vitro*, lo convierten en otro quimiotipo interesante a investigar en la modulación de TRPM8. Por otro lado, respecto a los compuestos de doble acción **13** y **19**, capaces de inhibir TRPM8 y activar TRPV1, podrían ser útiles en el estudio de las estructuras que discriminan la selectividad de los distintos canales TRP. Además, sería interesante estudiar este tipo de compuestos de doble acción con fines terapéuticos en procesos patológicos que impliquen a ambos canales como el dolor y el cáncer.





## **CONCLUSIONES**





## CONCLUSIONES

En lo referente al **Capítulo 1, Caracterización *in vitro*, *in silico* e *in vivo* de compuestos derivados de  $\beta$ -lactamas como bloqueadores de TRPM8**, concluimos que:

- Los derivados  $\beta$ -lactámicos **24a**, **29a**, **13**, **14**, **15**, **16** y **51** demostraron una potente actividad antagonista y selectividad hacia el canal TRPM8 en ensayos de microfluorometría de calcio, presentando IC<sub>50</sub>s en el rango micromolar.
- Los compuestos **24a**, **29a**, **14**, **16** y **51** bloquearon las corrientes de TRPM8 mediadas por mentol en ensayos electrofisiológicos de *patch clamp*, corroborándose su potencia en el rango micromolar.
- La configuración R de todos los estereocentros (3R,4R,2'R) de los derivados  $\beta$ -lactámicos mostró mejores resultados de actividad que la configuración S.
- Los derivados  $\beta$ -lactámicos **14**, **16** y **51** no alteraron el potencial de membrana en reposo de neuronas GRD ni afectaron a la excitabilidad neuronal a concentraciones 10 veces superiores a su concentración eficaz.
- Las  $\beta$ -lactamas **24a** y **29a** también mostraron actividad antitumoral no selectiva en diferentes líneas celulares tumorales. Ambas  $\beta$ -lactamas resultaron inocuas en ensayos de viabilidad celular (MTT) en la línea HEK293.
- Los estudios de modelado molecular propusieron dos sitios de unión en la zona del poro. Ambas regiones halladas resultaron distintas a los sitios de unión descritos para otros antagonistas de TRPM8.
- Las  $\beta$ -lactamas **24a** y **51** mostraron ser efectivas en ensayos *in vivo*. Ambas  $\beta$ -lactamas disminuyeron la alodinia al frío inducida por oxaliplatino. La  $\beta$ -lactama **51** también atenuó la hipersensibilidad mecánica y al frío en el modelo de dolor neuropático mediado por LCC y mitigó, de manera dependiente del sexo, la hipersensibilidad mecánica inducida por NTG en un modelo de migraña.
- Los ensayos preliminares de permeabilidad con la  $\beta$ -lactama **79** demostraron una permeabilidad del 15,6% a través de membranas artificiales a las 24 horas tras su administración. Sin embargo, son necesarios estudios adicionales en piel para concluir la seguridad de su administración tópica.

## Conclusiones

Todas estas conclusiones, convierten al anillo de lactama 1,3,4,4-tetrasustituido en una valiosa estructura central en la búsqueda de nuevos bloqueadores de TRPM8. El estudio de la mejora farmacológica de este tipo de compuestos continúa en nuestros laboratorios con la finalidad de obtener un producto neurocosmético para el alivio de la alodinia al frío que cursa con diversas neuropatías periféricas.



En lo referente al **Capítulo 2, Búsqueda de nuevos esqueletos farmacofóricos moduladores de TRPM8 mediante cribados virtuales y su posterior caracterización *in vitro*, *in silico* e *in vivo***, concluimos que:

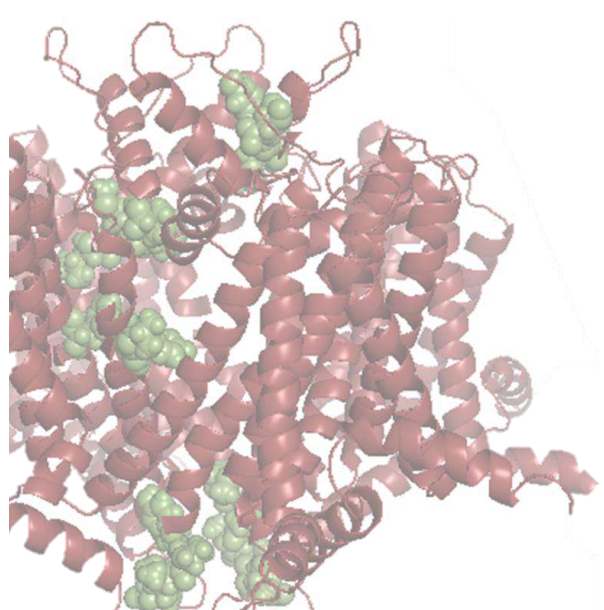
- Los compuestos **1, 5, 13, 14, 15** y **19** mostraron los mejores resultados en el bloqueo de *r*TRPM8 en ensayos de microfluorometría de calcio, destacando los compuestos **14** y **15** por ser los más potentes y eficaces.
- Los compuestos **1, 5, 14** y **15** no demostraron actividad hacia el canal *h*TRPV1 presentando selectividad hacia TRPM8. Sin embargo, los compuestos **13** y **19** sí activaron *h*TRPV1 convirtiéndose en moduladores de doble acción.
- Tanto el compuesto **14** como el **15** bloquearon las corrientes de *r*TRPM8 mediadas por mentol corroborándose los valores de IC<sub>50</sub> en el rango micromolar.
- Ambos compuestos interaccionaron con *h*TRPM8 en el dominio VSLD, entre las regiones TM1-TM4 y los residuos TRP, constituyendo sitios de unión diferentes a otros antagonistas de TRPM8 descritos.
- El compuesto **14** mostró actividad en ensayos *in vivo* disminuyendo la alodinia al frío mediada por oxaliplatino hasta 1 hora después de su administración.

Tanto los compuestos **14** y **15**, por su potencia y efectividad hacia TRPM8, como los compuestos **13** y **19**, por su actividad dual, constituyen nuevos quimiotipos a explorar en la modulación del canal. Los cuatro compuestos constituyen una base hacia el estudio del funcionamiento de TRPM8 y las estructuras que discriminan la selectividad frente a los diferentes canales TRP.





## **CONCLUSIONS**





## CONCLUSIONS

Regarding the **Chapter 1, *In vitro, in silico* and *in vivo* characterization of  $\beta$ -lactam derivatives as TRPM8 blockers**, it can be concluded that:

- $\beta$ -lactam derivatives **24a, 29a, 13, 14, 15, 16** and **51** behaved as potent and selective TRPM8 antagonist in calcium microfluorometry experiments, exhibiting  $IC_{50}$ s in the micromolar range.
- Compounds **24a, 29a, 14, 16** and **51** were able to block menthol evoked TRPM8 currents in electrophysiological patch clamp experiments, confirming the micromolar  $IC_{50}$  values.
- The R configuration of all compounds' stereocenters (3R,4R,2'R) exhibited better activity results than the S configuration.
- $\beta$ -lactam derivatives **14, 16** and **51** did not affect the GRDs' resting membrane potential or the neuronal excitability at concentrations 10 times higher than their effective concentration.
- Compounds **24a** and **29a** also displayed non-selective antitumoral activity in different tumoral cell lines. Both  $\beta$ -lactams demonstrated to be innocuous in cell viability assays (MTT) in the HEK293 cell line.
- Molecular modelling results proposed two main binding sites near the pore zone. Both regions are different to the ones identified for other TRPM8 blockers described.
- $\beta$ -lactams **24a** and **51** showed good results in *in vivo* assays. Both  $\beta$ -lactams diminished the cold allodynia in a model of NPIC induced by oxaliplatin.  $\beta$ -lactam **51** also reduced the mechanical and cold hypersensitivity in a neuropathic pain model induced by LCC and alleviated the mechanical hypersensitivity in a nitroglycerin induced migraine model in a sex-dependent manner.
- Preliminary permeability tests concerning  $\beta$ -lactam **79** indicated a permeability of 15.6% across artificial membranes 24 hours after administration. However, additional skin studies are required to conclude the safety of its topical administration.

All these conclusions, turn the 1,3,4,4-tetrasubstituted lactam scaffold in a valuable structure in the search for new TRPM8 blockers. Therefore, our laboratories

## Conclusions

keep studying the pharmacological improvement of these molecules with the aim of obtaining neuro-cosmetics for the alleviation of cold allodynia that appears in several peripheral neuropathies.



On the other hand, regarding **Chapter 2, Searching for new pharmacophoric scaffolds able to modulate TRPM8 through virtual screenings and their subsequent *in vitro*, *in silico* and *in vivo* characterisation**, it can be concluded that:

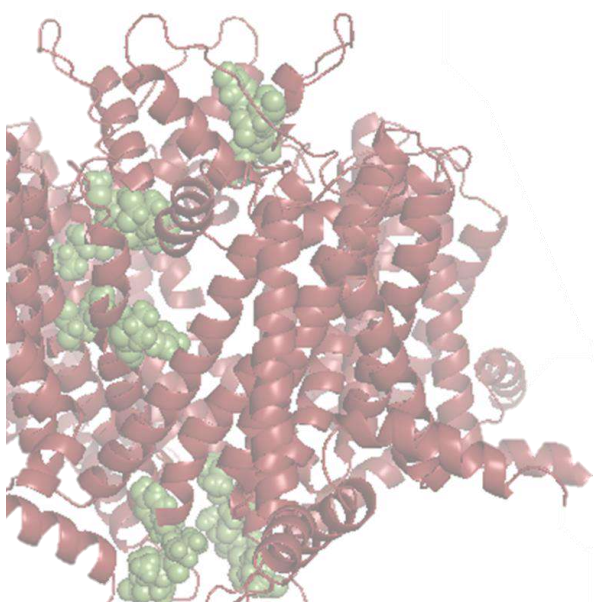
- Compounds **1**, **5**, **13**, **14**, **15** and **19** exhibited the best *r*TRPM8 blocking results using calcium microfluorometry techniques, highlighting compounds **14** and **15** as the most potent and effective.
- Compounds **1**, **5**, **14** and **15** did not display activity towards the *h*TRPV1 channel behaving as selective TRPM8 blockers. However, compounds **13** and **19** did activate *h*TRPV1 becoming dual action modulators.
- Both compounds **14** and **15** blocked *r*TRPM8 menthol-evoked currents confirming the micromolar IC<sub>50</sub> values.
- Molecular modelling studies demonstrated that compounds **14** and **15** interact with *h*TRPM8 in the VSLD domain surrounded by TM1-TM4 and TRP residues, differing from the binding sites of other described TRPM8 antagonists.
- Compound **14** also demonstrated activity *in vivo* by decreasing the cold allodynia in a model of NPIC induced by oxaliplatin even 1 hour after its administration.

Compounds **14** and **15** constitute new interesting chemotypes in the modulation of the channel due to its potency and efficacy towards TRPM8; as well as compounds **13** and **19** due to its dual activity. All four represent a baseline towards the study of the TRPM8 functionality and the structures that discriminate the selectivity towards the members of the TRP family.





## **BIBLIOGRAFÍA**





## BIBLIOGRAFÍA

- (1) Purves, D.; Augustine, G. J.; David, F. Dolor. In *Neurociencia*; Médica Panamericana: Madrid, Buenos Aires, 2008; pp 227–248.
- (2) Purves, D.; Augustine, G. J.; Fitzpatrick, D. El Sistema Somatosensitivo. In *Neurociencia*; Médica Panamericana: Madrid, Buenos Aires, 2008; pp 205–225.
- (3) The Anatomy and Physiology of Pain. In *Pain and Disability: Clinical, Behavioral, and Public Policy Perspectives*; Osterweis, M., Kleinmann, A., Mechanic, D., Eds.; The National Academies: Washington D. C., 1987; pp 123–145.
- (4) Betts, J. G.; Young, K. A.; Wise, J. A.; Johnson, E.; Poe, B.; Kruse, D.; Korol, O.; Johnson, J. E.; Womble, M.; Desaix, P. The Somatic Nervous System. In *Anatomy and Physiology*; OpenStax: Huston, 2013.
- (5) Glatte, P.; Buchmann, S. J.; Hijazi, M. M.; Illigens, B. M.-W.; Siepmann, T. Architecture of the Cutaneous Autonomic Nervous System. *Front Neurol* **2019**, *10* (970). <https://doi.org/10.3389/fneur.2019.00970>.
- (6) Julius, D.; Basbaum, A. I. Molecular Mechanisms of Nociception. *Nature* **2001**, *413* (6852), 203–210. <https://doi.org/10.1038/35093019>.
- (7) Manzano, G. M.; Giuliano, L. M. P.; Nóbrega, J. A. M. A Brief Historical Note on the Classification of Nerve Fibers. *Arq Neuropsiquiatr* **2008**, *66* (1), 117–119. <https://doi.org/10.1590/S0004-282X2008000100033>.
- (8) Pabón-Henao, T.; Pineda-Saavedra, L.-F.; Cañas-Mejía, O.-D. Pathophysiology, Assessment and Management of Acute Pain in Pediatrics. *Salutem Scientia Spiritus* **2015**, *2* (1), 2463–1426.
- (9) Moriwaki, K.; Yuge, O. Topographical Features of Cutaneous Tactile Hypoesthetic and Hyperesthetic Abnormalities in Chronic Pain. *Pain* **1999**, *81* (1–2), 1–6. [https://doi.org/10.1016/S0304-3959\(98\)00257-7](https://doi.org/10.1016/S0304-3959(98)00257-7).
- (10) Bullich, S. J. Mecanorreceptores y Sensibilidad Propioceptiva de La Rodilla. *Biomecánica* **1996**, *4* (6), 42–50.
- (11) Waldman, S. D. Functional Anatomy of the Thermoreceptors. In *Pain Review*; Elsevier, 2017.
- (12) Serra-Catafau, J. Fisiopatología Del Dolor Neuropático. In *Tratado de dolor neuropático*; Editorial Médica Panamericana S.A., 2007.
- (13) Prato, V.; Taberner, F. J.; Hockley, J. R. F.; Callejo, G.; Arcourt, A.; Tazir, B.; Hammer, L.; Schad, P.; Heppenstall, P. A.; Smith, E. S.; Lechner, S. G. Functional and Molecular Characterization of Mechanoinsensitive “Silent” Nociceptors. *Cell Rep* **2017**, *21* (11), 3102–3115. <https://doi.org/10.1016/J.CELREP.2017.11.066>.

## Bibliografía

- (14) Romera, E.; Perena, M.; Perena, M. Neurophysiology of Pain. *Rev Soc Esp Dolor* **2000**, *11*, 11–17.
- (15) Ferrer-Montiel, A. Los Canales de Comunicación Sensorial TRPs Como Dianas Farmacológicas. **2011**, *54* (3), 290–294.
- (16) Arcas-Santos, J. M. The Cold-Activated TRPM8 Channel: Agonism by Macrolide Immunosuppressants and Modulation by Gq Protein-Coupled Receptors Signaling Pathways (Tesis Doctoral), Universidad Miguel Hernández-CSIC, 2019.
- (17) Song, M. Y.; Yuan, J. X. Introduction to TRP Channels: Structure, Function, and Regulation. *Adv Exp Med Biol* **2010**, *661*, 99–108. [https://doi.org/10.1007/978-1-60761-500-2\\_6](https://doi.org/10.1007/978-1-60761-500-2_6).
- (18) Nilius, B.; Owsianik, G. The Transient Receptor Potential Family of Ion Channels. *Genome Biology* **2011**, *12* (3), 1–11. <https://doi.org/10.1186/GB-2011-12-3-218>.
- (19) Cosens, D. J.; Manning, A. Abnormal Electroretinogram from a *Drosophila* Mutant. *Nature* **1969**, *224*, 285–287. <https://doi.org/10.1038/224285a0>.
- (20) Montell, C.; Rubin, G. M. Molecular Characterization of the *Drosophila* Trp Locus: A Putative Integral Membrane Protein Required for Phototransduction. *Neuron* **1989**, *2* (4), 1313–1323. [https://doi.org/10.1016/0896-6273\(89\)90069-X](https://doi.org/10.1016/0896-6273(89)90069-X).
- (21) Zheng, J. Molecular Mechanism of TRP Channels. *Compr Physiol* **2013**, *3* (1), 221–242. <https://doi.org/10.1002/CPHY.C120001>.
- (22) Nilius, B.; Talavera, K.; Owsianik, G.; Prenen, J.; Droogmans, G.; Voets, T. Gating of TRP Channels: A Voltage Connection? *J Physiol* **2005**, *567* (Pt 1), 35. <https://doi.org/10.1113/JPHYSIOL.2005.088377>.
- (23) Mickle, A. D.; Shepherd, A. J.; Mohapatra, D. P.; Edu, A. D. M. S.; Szallasi, A.; Huang, S. M. Nociceptive TRP Channels: Sensory Detectors and Transducers in Multiple Pain Pathologies. *Pharmaceuticals* **2016**, *9* (4), 72. <https://doi.org/10.3390/PH9040072>.
- (24) Prevarskaya, N.; Zhang, L.; Barritt, G. TRP Channels in Cancer. *Biochim Biophys Acta Mol Basis Dis* **2007**, *1772* (8), 937–946. <https://doi.org/10.1016/j.bbadis.2007.05.006>.
- (25) Hoffstaetter, L. J.; Bagriantsev, S. N.; Gracheva, E. O. TRPs et al.: A Molecular Toolkit for Thermosensory Adaptations. *European Journal of Physiology* **2017**, *470*, 745–759. <https://doi.org/10.1007/s00424-018-2120-5>.

- (26) Talavera, K.; Nilius, B.; Voets, T. Neuronal TRP Channels: Thermometers, Pathfinders and Life-Savers. *Trends Neurosci* **2008**, *31* (6), 287–295. <https://doi.org/10.1016/J.TINS.2008.03.002>.
- (27) Caterina, M. J.; Rosen, T. A.; Tominaga, M.; Brake, A. J.; Julius, D. A Capsaicin-Receptor Homologue with a High Threshold for Noxious Heat. *Nature* **1999**, *398* (6726), 436–441. <https://doi.org/10.1038/18906>.
- (28) Xu, H.; Ramsey, I. S.; Kotecha, S. A.; Moran, M. M.; Chong, J. A.; Lawson, D.; Ge, P.; Lilly, J.; Silos-Santiago, I.; Xie, Y.; DiStefano, P. S.; Curtis, R.; Clapham, D. E. TRPV3 Is a Calcium-Permeable Temperature-Sensitive Cation Channel. *Nature* **2002**, *418* (6894), 181–186. <https://doi.org/10.1038/NATURE00882>.
- (29) Watanabe, H.; Vriens, J.; Suh, S. H.; Benham, C. D.; Droogmans, G.; Nilius, B. Heat-Evoked Activation of TRPV4 Channels in a HEK293 Cell Expression System and in Native Mouse Aorta Endothelial Cells\*. *Journal of Biological Chemistry* **2002**, *277*, 47044–47051. <https://doi.org/10.1074/jbc.M208277200>.
- (30) Liu, Y.; Mikrani, R.; He, Y.; Faran Ashraf Baig, M. M.; Abbas, M.; Naveed, M.; Tang, M.; Zhang, Q.; Li, C.; Zhou, X. TRPM8 Channels: A Review of Distribution and Clinical Role. *Eur J Pharmacol* **2020**, *882*, 173312. <https://doi.org/10.1016/j.ejphar.2020.173312>.
- (31) Vriens, J.; Owsianik, G.; Hofmann, T.; Philipp, S. E.; Stab, J.; Chen, X.; Benoit, M.; Xue, F.; Janssens, A.; Kerselaers, S.; Oberwinkler, J.; Vennekens, R.; Gudermann, T.; Nilius, B.; Voets, T. TRPM3 Is a Nociceptor Channel Involved in the Detection of Noxious Heat. *Neuron* **2011**, *70* (3), 482–494. <https://doi.org/10.1016/J.NEURON.2011.02.051>.
- (32) Tan, C. H.; McNaughton, P. A. The TRPM2 Ion Channel Is Required for Sensitivity to Warmth. *Nature* **2016**, *536* (7617), 460–463. <https://doi.org/10.1038/NATURE19074>.
- (33) Dai, Y. TRPs and Pain. *Semin Immunopathol* **2016**, *38* (3), 277–291. <https://doi.org/10.1007/S00281-015-0526-0>.
- (34) International Association for the Study of Pain. *Terminology - Pain*. <https://www.iasp-pain.org/resources/terminology/#pain> (acceso el 2022-04-25).
- (35) del Arco, J. Fisiopatología, Clasificación y Tratamiento Farmacológico. *Farmacia comunitaria* **2015**, *29* (1), 36–43.
- (36) Woolf, C. J. What Is This Thing Called Pain? *J Clin Invest* **2010**, *120* (11), 3742.
- (37) Siemens, J.; Zhou, S.; Piskorowski, R.; Nikai, T.; Lumpkin, E. A.; Basbaum, A. I.; King, D.; Julius, D. Spider Toxins Activate the Capsaicin Receptor to Produce Inflammatory Pain. *Nature* **2006**, *444* (7116), 208–212. <https://doi.org/10.1038/nature05285>.

- (38) Huang, S. M.; Bisogno, T.; Trevisani, M.; Al-Hayani, A.; de Petrocellis, L.; Fezza, F.; Tognetto, M.; Petros, T. J.; Krey, J. F.; Chu, C. J.; Miller, J. D.; Davies, S. N.; Geppetti, P.; Walker, J. M.; di Marzo, V. An Endogenous Capsaicin-like Substance with High Potency at Recombinant and Native Vanilloid VR1 Receptors. *Proc Natl Acad Sci U S A* **2002**, *99* (12), 8400–8405. <https://doi.org/10.1073/PNAS.122196999>.
- (39) Tominaga, M.; Caterina, M. J.; Malmberg, A. B.; Rosen, T. A.; Gilbert, H.; Skinner, K.; Raumann, B. E.; Basbaum, A. I.; Julius, D. The Cloned Capsaicin Receptor Integrates Multiple Pain-Producing Stimuli. *Neuron* **1998**, *21* (3), 531–543. [https://doi.org/10.1016/S0896-6273\(00\)80564-4](https://doi.org/10.1016/S0896-6273(00)80564-4).
- (40) Bandell, M.; Story, G. M.; Hwang, S. W.; Viswanath, V.; Eid, S. R.; Petrus, M. J.; Earley, T. J.; Patapoutian, A. Noxious Cold Ion Channel TRPA1 Is Activated by Pungent Compounds and Bradykinin. *Neuron* **2004**, *41* (6), 849–857. [https://doi.org/10.1016/S0896-6273\(04\)00150-3](https://doi.org/10.1016/S0896-6273(04)00150-3).
- (41) Talavera, K.; Gees, M.; Karashima, Y.; Meseguer, V. M.; Vanoirbeek, J. A. J.; Damann, N.; Everaerts, W.; Benoit, M.; Janssens, A.; Vennekens, R.; Viana, F.; Nemery, B.; Nilius, B.; Voets, T. Nicotine Activates the Chemosensory Cation Channel TRPA1. *Nature Neuroscience* **2009**, *12* (10), 1293–1299. <https://doi.org/10.1038/nn.2379>.
- (42) Matta, J. A.; Cornett, P. M.; Miyares, R. L.; Abe, K.; Sahibzada, N.; Ahern, G. P. General Anesthetics Activate a Nociceptive Ion Channel to Enhance Pain and Inflammation. *Proc Natl Acad Sci U S A* **2008**, *105* (25), 8784–8789. <https://doi.org/10.1073/PNAS.0711038105>.
- (43) del Arco, J. Curso Básico Sobre Dolor. Tema 1. Fisiopatología, Clasificación y Tratamiento Farmacológico. *Farmacia profesional* **2015**, *29* (1), 36–43.
- (44) Hudson, L. J.; Bevan, S.; Wotherspoon, G.; Gentry, C.; Fox, A.; Winter, J. VR1 Protein Expression Increases in Undamaged GRD Neurons after Partial Nerve Injury. *European Journal of Neuroscience* **2001**, *13* (11), 2105–2114. <https://doi.org/10.1046/J.0953-816X.2001.01591.X>.
- (45) Obata, K.; Katsura, H.; Mizushima, T.; Yamanaka, H.; Kobayashi, K.; Dai, Y.; Fukuoka, T.; Tokunaga, A.; Tominaga, M.; Noguchi, K. TRPA1 Induced in Sensory Neurons Contributes to Cold Hyperalgesia after Inflammation and Nerve Injury. *J Clin Invest* **2005**, *115* (9), 2393–2401. <https://doi.org/10.1172/JCI25437>.
- (46) Tatsumi, E.; Katsura, H.; Kobayashi, K.; Yamanaka, H.; Tsuzuki, K.; Noguchi, K.; Sakagami, M. Changes in Transient Receptor Potential Channels in the Rat Geniculate Ganglion after Chorda Tympani Nerve Injury. *Neuroreport* **2015**, *26* (14), 856–861. <https://doi.org/10.1097/WNR.0000000000000436>.
- (47) Yamamoto, S.; Egashira, N.; Tsuda, M.; Masuda, S. Riluzole Prevents Oxaliplatin-Induced Cold Allodynia via Inhibition of Overexpression of Transient Receptor

- Potential Melastatin 8 in Rats. *J Pharmacol Sci* **2018**, *138* (3), 214–217. <https://doi.org/10.1016/J.JPHS.2018.10.006>.
- (48) Descoeur, J.; Pereira, V.; Pizzoccaro, A.; Francois, A.; Ling, B.; Maffre, V.; Couette, B.; Busserolles, J.; Courteix, C.; Noel, J.; Lazdunski, M.; Eschalier, A.; Authier, N.; Bourinet, E. Oxaliplatin-Induced Cold Hypersensitivity Is Due to Remodelling of Ion Channel Expression in Nociceptors. *EMBO Mol Med* **2011**, *3* (5), 266–278. <https://doi.org/10.1002/emmm.201100134>.
- (49) Xing, H.; Chen, M.; Ling, J.; Tan, W.; Gu, J. G. TRPM8 Mechanism of Cold Allodynia after Chronic Nerve Injury. *The Journal of neuroscience* **2007**, *27* (50), 13680–13690. <https://doi.org/10.1523/JNEUROSCI.2203-07.2007>.
- (50) Su, L.; Wang, C.; Yu, Y. hao; Ren, Y. ying; Xie, K. liang; Wang, G. lin. Role of TRPM8 in Dorsal Root Ganglion in Nerve Injury-Induced Chronic Pain. *BMC Neurosci* **2011**, *12* (1), 1–15. <https://doi.org/10.1186/1471-2202-12-120/FIGURES/6>.
- (51) Aierken, A.; Xie, Y.-K.; Dong, W.; Apaer, A.; Lin, J.-J.; Zhao, Z.; Yang, S.; Xu, Z.-Z.; Yang, F.; Aierken, A.; Apaer, A.; Yang, F.; Xie, Y.-K.; Lin, J.-J.; Xu, Z.-Z.; Dong, W.; Zhao, Z.; Yang, S. Rational Design of a Modality-Specific Inhibitor of TRPM8 Channel against Oxaliplatin-Induced Cold Allodynia. **2021**. <https://doi.org/10.1002/advs.202101717>.
- (52) Alessandri-Haber, N.; Dina, O. A.; Yeh, J. J.; Parada, C. A.; Reichling, D. B.; Levine, J. D. Transient Receptor Potential Vanilloid 4 Is Essential in Chemotherapy-Induced Neuropathic Pain in the Rat. *The Journal of Neuroscience* **2004**, *24* (18), 4444. <https://doi.org/10.1523/JNEUROSCI.0242-04.2004>.
- (53) So, K.; Haraguchi, K.; Asakura, K.; Isami, K.; Sakimoto, S.; Shirakawa, H.; Mori, Y.; Nakagawa, T.; Kaneko, S. Involvement of TRPM2 in a Wide Range of Inflammatory and Neuropathic Pain Mouse Models. *J Pharmacol Sci* **2015**, *127* (3), 237–243. <https://doi.org/10.1016/J.JPHS.2014.10.003>.
- (54) Vay, L.; Gu, C.; McNaughton, P. The Thermo-TRP Ion Channel Family: Properties and Therapeutic Implications. *Br J Pharmacol* **2012**, *165* (4), 787–801. <https://doi.org/10.1111/J.1476-5381.2011.01601.X>.
- (55) Bertamino, A.; Ostacolo, C.; Medina, A.; di Sarno, V.; Lauro, G.; Ciaglia, T.; Vestuto, V.; Pepe, G.; Basilicata, M. G.; Musella, S.; Smaldone, G.; Cristiano, C.; Gonzalez-Rodriguez, S.; Fernandez-Carvajal, A.; Bifulco, G.; Campiglia, P.; Gomez-Monterrey, I.; Russo, R. Exploration of TRPM8 Binding Sites by  $\beta$ -Carboline-Based Antagonists and Their in Vitro Characterization and in Vivo Analgesic Activities. *J Med Chem* **2020**, *63* (17), 9672–9694. <https://doi.org/10.1021/acs.jmedchem.0c00816>.
- (56) Jesús, M.; Pérez De Vega, J.; Gómez-Monterrey, I.; Ferrer-Montiel, A.; Gonzalez-Muñiz, R. Transient Receptor Potential Melastatin 8 Channel (TRPM8)

- Modulation: Cool Entryway for Treating Pain and Cancer. **2016**.  
<https://doi.org/10.1021/acs.jmedchem.6b00305>.
- (57) Babes, A.; Cristian Ciobanu, A.; Neacsu, C.; Babes, R.-M. TRPM8, a Sensor for Mild Cooling in Mammalian Sensory Nerve Endings. *Curr Pharm Biotechnol* **2010**, *12* (1), 78–88. <https://doi.org/10.2174/138920111793937835>.
- (58) Kühn, F. J. P.; Kühn, C.; Lückhoff, A. Inhibition of TRPM8 by Icilin Distinct from Desensitization Induced by Menthol and Menthol Derivatives. *J Biol Chem* **2009**, *284* (7), 4102–4111. <https://doi.org/10.1074/JBC.M806651200>.
- (59) Quallo, T.; Vastani, N.; Horridge, E.; Gentry, C.; Parra, A.; Moss, S.; Viana, F.; Belmonte, C.; Andersson, D. A.; Bevan, S. TRPM8 Is a Neuronal Osmosensor That Regulates Eye Blinking in Mice. *Nat Commun* **2015**, *6* (7150). <https://doi.org/10.1038/ncoms8150>.
- (60) Fernández, J. A.; Skryma, R.; Bidaux, G.; Magleby, K. L.; Scholfeld, C. N.; McGeown, J. G.; Prevarskaya, N.; Zholos, A. V. Voltage- and Cold-Dependent Gating of Single TRPM8 Ion Channels. *J Gen Physiol* **2011**, *137* (2), 173. <https://doi.org/10.1085/JGP.201010498>.
- (61) Raddatz, N.; Castillo, J. P.; Gonzalez, C.; Alvarez, O.; Latorre, R. Temperature and Voltage Coupling to Channel Opening in Transient Receptor Potential Melastatin 8 (TRPM8). *J Biol Chem* **2014**, *289* (51), 35438. <https://doi.org/10.1074/JBC.M114.612713>.
- (62) Tsavaler, L.; Shapero, M. H.; Morkowski, S.; Laus, R. Trp-P8, a Novel Prostate-Specific Gene, Is up-Regulated in Prostate Cancer and Other Malignancies and Shares High Homology with Transient Receptor Potential Calcium Channel Proteins. *Cancer Res* **2001**, *61* (9), 3760–3769.
- (63) Dhaka, A.; Earley, T. J.; Watson, J.; Patapoutian, A. Visualizing Cold Spots: TRPM8-Expressing Sensory Neurons and Their Projections. *Journal of Neuroscience* **2008**, *28* (3), 566–575. <https://doi.org/10.1523/JNEUROSCI.3976-07.2008>.
- (64) Yajima, T.; Sato, T.; Hosokawa, H.; Kondo, T.; Saito, M.; Shimauchi, H.; Ichikawa, H. Distribution of Transient Receptor Potential Melastatin-8-Containing Nerve Fibers in Rat Oral and Craniofacial Structures. *Ann Anat* **2015**, *201*, 1–5. <https://doi.org/10.1016/J.AANAT.2015.04.003>.
- (65) Gonzalez-Muñiz, R.; Bonache, M. A.; Martin-Escura, C.; Gomez-Monterrey, I. Recent Progress in TRPM8 Modulation: An Update. *Int J Mol Sci* **2019**, *20* (11), 2618.
- (66) Yin, Y.; Wu, M.; Zubcevic, L.; Borschel, W. F.; Lander, G. C.; Lee, S. Structure of the Cold- and Menthol-Sensing Ion Channel. **2017**, 4325 (December), 1–11.

- (67) Dragoni, I.; Guida, E.; McIntyre, P. The Cold and Menthol Receptor TRPM8 Contains a Functionally Important Double Cysteine Motif. *J Biol Chem* **2006**, *281* (49), 37353–37360. <https://doi.org/10.1074/JBC.M607227200>.
- (68) Tsuruda, P. R.; Julius, D.; Minor, D. L.; Jr. Coiled Coils Direct Assembly of a Cold-Activated TRP Channel. *Neuron* **2006**, *51* (2), 201. <https://doi.org/10.1016/J.NEURON.2006.06.023>.
- (69) Phelps, C. B.; Gaudet, R. The Role of the N Terminus and Transmembrane Domain of TRPM8 in Channel Localization and Tetramerization \*. *Journal of Biological Chemistry* **2007**, *282* (50), 36474–36480. <https://doi.org/10.1074/JBC.M707205200>.
- (70) Bidaux, G.; Sgobba, M.; Lemonnier, L.; Borowiec, A.-S.; Noyer, L.; Jovanovic, S.; Zholos, A. v.; Haider, S. Functional and Modeling Studies of the Transmembrane Region of the TRPM8 Channel. *Biophys J* **2015**, *109* (9), 1840–1851. <https://doi.org/10.1016/J.BPJ.2015.09.027>.
- (71) Izquierdo, C.; Martín-Martínez, M.; Gómez-Monterrey, I.; González-Muñiz, R. TRPM8 Channels: Advances in Structural Studies and Pharmacological Modulation. *Int J Mol Sci* **2021**, *22* (16). <https://doi.org/10.3390/IJMS22168502>.
- (72) Erler, I.; Al-Ansary, D. M. M.; Wissenbach, U.; Wagner, T. F. J.; Flockerzi, V.; Niemeyer, B. A. Trafficking and Assembly of the Cold-Sensitive TRPM8 Channel \*. *Journal of Biological Chemistry* **2006**, *281* (50), 38396–38404. <https://doi.org/10.1074/JBC.M607756200>.
- (73) Zheng, W.; Cai, R.; Hofmann, L.; Nesin, V.; Hu, Q.; Long, W.; Fatehi, M.; Liu, X.; Hussein, S.; Kong, T.; Li, J.; Light, P. E.; Tang, J.; Flockerzi, V.; Tsiokas, L.; Chen, X.-Z. Direct Binding between Pre-S1 and TRP-like Domains in TRPP Channels Mediates Gating and Functional Regulation by PIP2. *Cell Rep* **2018**, *22* (6), 1560. <https://doi.org/10.1016/J.CELREP.2018.01.042>.
- (74) Latorre, R.; Brauchi, S.; Orta, G.; Zaelzer, C.; Vargas, G. ThermoTRP Channels as Modular Proteins with Allosteric Gating. *Cell Calcium* **2007**, *42* (4–5), 427–438. <https://doi.org/10.1016/J.CECA.2007.04.004>.
- (75) Bandell, M.; Dubin, A. E.; Petrus, M. J.; Orth, A.; Mathur, J.; Sun, W. H.; Patapoutian, A. High-Throughput Random Mutagenesis Screen Reveals TRPM8 Residues Specifically Required for Activation by Menthol. *Nat Neurosci* **2006**, *9* (4), 493–500. <https://doi.org/10.1038/nn1665>.
- (76) Voets, T.; Owsianik, G.; Janssens, A.; Talavera, K.; Nilius, B. TRPM8 Voltage Sensor Mutants Reveal a Mechanism for Integrating Thermal and Chemical Stimuli. *Nat Chem Biol* **2007**, *3* (3), 174–182. <https://doi.org/10.1038/NCHEMBO862>.
- (77) Beccari, A. R.; Gemei, M.; Monte, M. I.; Menegatti, N.; Fanton, M.; Pedretti, A.; Bovolenta, S.; Nucci, C.; Molteni, A.; Rossignoli, A.; Brandolini, L.; Taddei, A.; Za, L.; Liberati, C.; Vistoli, G. Novel Selective, Potent Naphthyl TRPM8 Antagonists

- Identified through a Combined Ligand-and Structure-Based Virtual Screening Approach. *Sci Rep* **2017**, 7 (1), 1–15. <https://doi.org/10.1038/s41598-017-11194-0>.
- (78) Rohács, T.; Lopes, C. M. B.; Michailidis, I.; Logothetis, D. E. PI(4,5)P2 Regulates the Activation and Desensitization of TRPM8 Channels through the TRP Domain. *Nature Neuroscience* **2005**, 8:5 **2005**, 8 (5), 626–634. <https://doi.org/10.1038/nn1451>.
- (79) Rohács, T.; Lopes, C. M. B.; Michailidis, I.; Diomedes, & Logothetis, E. PI(4,5)P 2 Regulates the Activation and Desensitization of TRPM8 Channels through the TRP Domain. *Nat Neurosci* **2005**, 8 (5). <https://doi.org/10.1038/nn1451>.
- (80) Rohacs, T. Phosphoinositide Regulation of TRP Channels. *Handb Exp Pharmacol* **2014**, 223, 1143. [https://doi.org/10.1007/978-3-319-05161-1\\_18](https://doi.org/10.1007/978-3-319-05161-1_18).
- (81) Zakharian, E.; Thyagarajan, B.; French, R. J.; Pavlov, E.; Rohacs, T. Inorganic Polyphosphate Modulates TRPM8 Channels. *PLoS One* **2009**, 4 (4), e5404. <https://doi.org/10.1371/JOURNAL.PONE.0005404>.
- (82) Iftinca, M.; Altier, C. The Cool Things to Know about TRPM8! *Channels (Austin)* **2020**, 14 (1), 413–420. <https://doi.org/10.1080/19336950.2020.1841419>.
- (83) Sarria, I.; Gu, J. Menthol Response and Adaptation in Nociceptive-Like and Nonnociceptive-Like Neurons: Role of Protein Kinases: <https://doi.org/10.1186/1744-8069-6-47> **2010**, 6. <https://doi.org/10.1186/1744-8069-6-47>.
- (84) Mckemy, D. D. The Molecular and Cellular Basis of Cold Sensation. *ACS Chem. Neurosci* **2013**, 4, 247. <https://doi.org/10.1021/cn300193h>.
- (85) Tang, M.; Wu, G.; Dong, X.; Tang, Z. Phosphoinositide Interacting Regulator of TRP (Pirt) Enhances TRPM8 Channel Activity in Vitro via Increasing Channel Conductance. *Acta Pharmacologica Sinica* **2015**, 37 (1), 98–104. <https://doi.org/10.1038/aps.2015.110>.
- (86) Tang, Z.; Kim, A.; Masuch, T.; Park, K.; Weng, H.; Wetzal, C.; Dong, X. Pirt Functions as an Endogenous Regulator of TRPM8. *Nat Commun* **2013**, 4, 2179. <https://doi.org/10.1038/NCOMMS3179>.
- (87) Andersson, D. A.; Nash, M.; Bevan, S. Modulation of the Cold-Activated Channel TRPM8 by Lysophospholipids and Polyunsaturated Fatty Acids. *Journal of Neuroscience* **2007**, 27 (12), 3347–3355. <https://doi.org/10.1523/JNEUROSCI.4846-06.2007>.
- (88) Zhang, X.; Mak, S.; Li, L.; Parra, A.; Denlinger, B.; Belmonte, C.; McNaughton, P. A. Direct Inhibition of the Cold-Activated TRPM8 Ion Channel by Gaq. *Nat Cell Biol* **2012**, 14 (8), 851. <https://doi.org/10.1038/NCB2529>.

- (89) Fernández, J. A.; Skryma, R.; Bidaux, G.; Magleby, K. L.; Scholfield, C. N.; McGeown, J. G.; Prevarskaya, N.; Zholos, A. V. Short Isoforms of the Cold Receptor TRPM8 Inhibit Channel Gating by Mimicking Heat Action Rather than Chemical Inhibitors. *Journal of Biological Chemistry* **2012**, *287* (5), 2963–2970. <https://doi.org/10.1074/JBC.M111.272823>.
- (90) Ghosh, D.; Pinto, S.; Danglot, L.; Vandewauw, I.; Segal, A.; Van Ranst, N.; Benoit, M.; Janssens, A.; Vennekens, R.; Vanden Berghe, P.; Galli, T.; Vriens, J.; Voets, T. VAMP7 Regulates Constitutive Membrane Incorporation of the Cold-Activated Channel TRPM8. *Nature Communications* **2015**, *7*:1 **2016**, *7* (1), 1–15. <https://doi.org/10.1038/ncomms10489>.
- (91) Asuthkar, S.; Demirkhanyan, L.; Sun, X.; Elustondo, P. A.; Krishnan, V.; Baskaran, P.; Velpula, K. K.; Thyagarajan, B.; Pavlov, E. v.; Zakharian, E. The TRPM8 Protein Is a Testosterone Receptor: II. Functional Evidence for an Ionotropic Effect of Testosterone on TRPM8. *Journal of Biological Chemistry* **2015**, *290* (5), 2670. <https://doi.org/10.1074/JBC.M114.610873>.
- (92) Fernández-Carvajal, A.; González-Muñiz, R.; Fernández-Ballester, G.; Ferrer-Montiel, A. Investigational Drugs in Early Phase Clinical Trials Targeting Thermotransient Receptor Potential (ThermoTRP) Channels. *Expert Opinion on Investigational Drugs*. Taylor and Francis Ltd. November 1, 2020, pp 1209–1222. <https://doi.org/10.1080/13543784.2020.1825680>.
- (93) Gordon-Shaag, A.; Zagotta, W. N.; Gordon, S. E. Channels Mechanism of Ca<sup>2+</sup>-Dependent Desensitization in TRP Channels. **2008**. <https://doi.org/10.4161/chan.2.2.6026>.
- (94) Knowlton, W. M.; Mckemy, D. D. TRPM8: From Cold to Cancer, Peppermint to Pain. *Curr Pharm Biotechnol* **2011**, *12*, 68–77.
- (95) Sun, J.; Yang, T.; Wang, P.; Ma, S.; Zhu, Z.; Pu, Y.; Li, L.; Zhao, Y.; Xiong, S.; Liu, D.; Zhu, Z. Activation of Cold-Sensing Transient Receptor Potential Melastatin Subtype 8 Antagonizes Vasoconstriction and Hypertension through Attenuating RhoA/Rho Kinase Pathway. *Hypertension* **2014**, *63* (6), 1354–1363. <https://doi.org/10.1161/HYPERTENSIONAHA.113.02573>.
- (96) Misery, L.; Santerre, A.; Batardière, A.; Hornez, N.; Nedelec, A. S.; le Caër, F.; Bourgeois, P.; Huet, F.; Neufang, G. Real-Life Study of Anti-Itching Effects of a Cream Containing Menthoxypropanediol, a TRPM8 Agonist, in Atopic Dermatitis Patients. *Journal of the European Academy of Dermatology and Venereology* **2019**, *33* (2), e67–e69. <https://doi.org/10.1111/JDV.15199>.
- (97) Jung, M. J.; Kim, J. C.; Wei, E. T.; Selescu, T.; Chung, B. Y.; Park, C. W.; Kim, H. O. A Randomized, Vehicle-Controlled Clinical Trial of a Synthetic TRPM8 Agonist (Cryosim-1) Gel for Itch. *J Am Acad Dermatol* **2021**, *84* (3), 869–871. <https://doi.org/10.1016/J.JAAD.2020.10.065>.

## Bibliografía

- (98) Yoon, H. J.; Kim, J.; Yang, J. M.; Wei, E. T.; Kim, S. J.; Yoon, K. C. Topical TRPM8 Agonist for Relieving Neuropathic Ocular Pain in Patients with Dry Eye: A Pilot Study. *J Clin Med* **2021**, *10* (2), 1–7. <https://doi.org/10.3390/JCM10020250>.
- (99) Chen, G. L.; Lei, M.; Zhou, L. P.; Zeng, B.; Zou, F. Borneol Is a TRPM8 Agonist That Increases Ocular Surface Wetness. *PLoS One* **2016**, *11* (7). <https://doi.org/10.1371/JOURNAL.PONE.0158868>.
- (100) Wang, S.; Zhang, D.; Hu, J.; Jia, Q.; Xu, W.; Su, D.; Song, H.; Xu, Z.; Cui, J.; Zhou, M.; Yang, J.; Xiao, J. A Clinical and Mechanistic Study of Topical Borneol-induced Analgesia. *EMBO Mol Med* **2017**, *9* (6), 802. <https://doi.org/10.15252/EMMM.201607300>.
- (101) Behrendt, H. J.; Germann, T.; Gillen, C.; Hatt, H.; Jostock, R. Characterization of the Mouse Cold-Menthol Receptor TRPM8 and Vanilloid Receptor Type-1 VR1 Using a Fluorometric Imaging Plate Reader (FLIPR) Assay. *Br J Pharmacol* **2004**, *141* (4), 737. <https://doi.org/10.1038/SJ.BJP.0705652>.
- (102) Bödding, M.; Wissenbach, U.; Flockerzi, V. Characterisation of TRPM8 as a Pharmacophore Receptor. *Cell Calcium* **2007**, *42* (6), 618–628. <https://doi.org/10.1016/J.CECA.2007.03.005>.
- (103) Proudfoot, C. J.; Garry, E. M.; Cottrell, D. F.; Rosie, R.; Anderson, H.; Robertson, D. C.; Fleetwood-Walker, S. M.; Mitchell, R. Analgesia Mediated by the TRPM8 Cold Receptor in Chronic Neuropathic Pain. *Current Biology* **2006**, *16* (16), 1591–1605. <https://doi.org/10.1016/j.cub.2006.07.061>.
- (104) Yin, Y.; Le, S. C.; Hsu, A. L.; Borgnia, M. J.; Yang, H.; Lee, S. Y. Structural Basis of Cooling Agent and Lipid Sensing by the Cold-Activated TRPM8 Channel. *Science* **2019**, *363* (6430). <https://doi.org/10.1126/SCIENCE.AAV9334>.
- (105) Chuang, H. H.; Neuhausser, W. M.; Julius, D. The Super-Cooling Agent Icilin Reveals a Mechanism of Coincidence Detection by a Temperature-Sensitive TRP Channel. *Neuron* **2004**, *43* (6), 859–869. <https://doi.org/10.1016/J.NEURON.2004.08.038>.
- (106) Bunke, G. M.; Frederick, H. A.; Haight, J. C.; Wos, J. A.; Yelm, K. E. Preparation of Aromatic, Adamantyl, and Highly Branched Aliphatic Compounds, Including Esters and Amides, Useful as Coolants in Oral and Skin Compositions. US20190330141, October 31, 2019.
- (107) Yang, J. M.; Li, F.; Liu, Q.; Rüedi, M.; Wei, E.; Lentsman, M.; Lee, H. S.; Choi, W.; Kim, S. J.; Yoon, K. C. A Novel TRPM8 Agonist Relieves Dry Eye Discomfort. *BMC Ophthalmol* **2017**, *17* (101). <https://doi.org/10.1186/S12886-017-0495-2>.
- (108) Wei, E. T. Di-Isopropyl-Phosphinoyl-Alkanes as Topical Agents for the Treatment of Sensory Discomfort. WO2015059432, April 30, 2015.

- (109) Wei, E. T. Dialkyl-Phosphinoyl-Alkane (DAPA) Compounds and Compositions for Treatment of Lower Gastrointestinal Tract Disorders. US20170189428, July 6, 2017.
- (110) Wei, E. T. Method to Reduce Face Mask and Respirator Discomfort. US20200289533, September 17, 2020.
- (111) Babes, R.-M.; Selescu, T.; Domocos, D.; Babes, A. The Anthelmintic Drug Praziquantel Is a Selective Agonist of the Sensory Transient Receptor Potential Melastatin Type 8 Channel. *Toxicol Appl Pharmacol* **2017**, *336*, 55–65. <https://doi.org/10.1016/J.TAAP.2017.10.012>.
- (112) Arcas, J. M.; González, A.; Gers-Barlag, K.; González-González, O.; Bech, F.; Demirkhanyan, L.; Zakharian, E.; Belmonte, C.; Gomis, A.; Félix Viana, X. The Immunosuppressant Macrolide Tacrolimus Activates Cold-Sensing TRPM8 Channels. **2019**. <https://doi.org/10.1523/JNEUROSCI.1726-18.2018>.
- (113) Andrews, M. D.; Forselles, K. af; Beaumont, K.; Galan, S. R. G.; Glossop, P. A.; Grenie, M.; Jessiman, A.; Kenyon, A. S.; Lunn, G.; Maw, G.; Owen, R. M.; Pryde, D. C.; Roberts, D.; Tran, T. D. Discovery of a Selective TRPM8 Antagonist with Clinical in Cold-Related Pain. *ACS Med Chem Lett* **2015**, *6* (4), 419. <https://doi.org/10.1021/ML500479V>.
- (114) Horne, D. B.; Biswas, K.; Brown, J.; Bartberger, M. D.; Clarine, J.; Davis, C. D.; Gore, V. K.; Harried, S.; Horner, M.; Kaller, M. R.; Lehto, S. G.; Liu, Q.; Ma, V. v.; Monenschein, H.; Nguyen, T. T.; Yuan, C. C.; Youngblood, B. D.; Zhang, M.; Zhong, W.; Allen, J. R.; Chen, J. J.; Gavva, N. R. Discovery of TRPM8 Antagonist (S)-6-(((3-Fluoro-4-(Trifluoromethoxy)Phenyl)(3-Fluoropyridin-2-Yl)methyl)Carbamoyl)Nicotinic Acid (AMG 333), a Clinical Candidate for the Treatment of Migraine. *J Med Chem* **2018**, *61* (18), 8186–8201. <https://doi.org/10.1021/acs.jmedchem.8b00518>.
- (115) de Petrocellis, L.; Ligresti, A.; Moriello, A. S.; Allarà, M.; Bisogno, T.; Petrosino, S.; Stott, C. G.; di Marzo, V. Effects of Cannabinoids and Cannabinoid-Enriched Cannabis Extracts on TRP Channels and Endocannabinoid Metabolic Enzymes. *Br J Pharmacol* **2011**, *163* (7), 1479. <https://doi.org/10.1111/J.1476-5381.2010.01166.X>.
- (116) Sui, Y.; Li, S.; Zhao, Y.; Liu, Q.; Qiao, Y.; Feng, L.; Li, S. Identification of a Natural Compound, Sesamin, as a Novel TRPM8 Antagonist with Inhibitory Effects on Prostate Adenocarcinoma. *Fitoterapia* **2020**, *145*. <https://doi.org/10.1016/J.FITOTE.2020.104631>.
- (117) Sanechika, S.; Shimobori, C.; Ohbuchi, K. Identification of Herbal Components as TRPA1 Agonists and TRPM8 Antagonists. *J Nat Med* **2021**, *75* (3), 717–725. <https://doi.org/10.1007/S11418-021-01515-Z>.

- (118) De Petrocellis, L.; Starowicz, K.; Moriello, A. S.; Vivese, M.; Orlando, P.; Di Marzo, V. Regulation of Transient Receptor Potential Channels of Melastatin Type 8 (TRPM8): Effect of CAMP, Cannabinoid CB1 Receptors and Endovanilloids. *Exp Cell Res* **2007**, *313* (9), 1911–1920. <https://doi.org/10.1016/j.yexcr.2007.01.008>.
- (119) Merritt, J. E.; Armstrong, W. P.; Benham, C. D.; Hallam, T. J.; Jacob, R.; Jaxa-Chamiec, A.; Leigh, B. K.; Mccarthy, S. A.; Moores, K. E.; Rink, T. J. SK&F 96365, a Novel Inhibitor of Receptor-Mediated Calcium Entry. *Biochem. J* **1990**, *271*, 515–522.
- (120) Lashinger, E. S. R.; Steiginga, M. S.; Hieble, J. P.; Leon, L. A.; Gardner, S. D.; Nagilla, R.; Davenport, E. A.; Hoffman, B. E.; Laping, N. J.; Su, X. AMTB, a TRPM8 Channel Blocker: Evidence in Rats for Activity in Overactive Bladder and Painful Bladder Syndrome. *Am J Physiol Renal Physiol* **2008**, *295*, 803–810. <https://doi.org/10.1152/ajprenal.90269.2008>.-The.
- (121) Yapa, K. T. D. S.; Deuis, J.; Peters, A. A.; Kenny, P. A.; Roberts-Thomson, S. J.; Vetter, I.; Monteith, G. R. Assessment of the TRPM8 Inhibitor AMTB in Breast Cancer Cells and Its Identification as an Inhibitor of Voltage Gated Sodium Channels. *Life Sci* **2018**, *198*, 128–135. <https://doi.org/10.1016/J.LFS.2018.02.030>.
- (122) Knowlton, W. M.; Daniels, R. L.; Palkar, R.; McCoy, D. D.; McKemy, D. D. Pharmacological Blockade of TRPM8 Ion Channels Alters Cold and Cold Pain Responses in Mice. *PLoS One* **2011**, *6* (9). <https://doi.org/10.1371/journal.pone.0025894>.
- (123) Meseguer, V.; Karashima, Y.; Talavera, K.; D'Hoedt, D.; Donovan-Rodríguez, T.; Viana, F.; Nilius, B.; Voets, T. Transient Receptor Potential Channels in Sensory Neurons Are Targets of the Antimycotic Agent Clotrimazole. *Journal of Neuroscience* **2008**, *28* (3), 576–586. <https://doi.org/10.1523/JNEUROSCI.4772-07.2008>.
- (124) Mälkiä, A.; Madrid, R.; Meseguer, V.; de La Peña, E.; Valero, M.; Belmonte, C.; Viana, F. Bidirectional Shifts of TRPM8 Channel Gating by Temperature and Chemical Agents Modulate the Cold Sensitivity of Mammalian Thermoreceptors. *J Physiol* **2007**, *581* (Pt 1), 155. <https://doi.org/10.1113/JPHYSIOL.2006.123059>.
- (125) Nakanishi, O.; Fujimori, Y.; Aizawa, N.; Hayashi, T.; Matsuzawa, A.; Kobayashi, J. I.; Hirasawa, H.; Mutai, Y.; Tanada, F.; Igawa, Y. KPR-5714, a Novel Transient Receptor Potential Melastatin 8 Antagonist, Improves Overactive Bladder via Inhibition of Bladder Afferent Hyperactivity in Rats. *J Pharmacol Exp Ther* **2020**, *373* (2), 239–247. <https://doi.org/10.1124/JPET.119.263616>.
- (126) Aizawa, N.; Ohshiro, H.; Watanabe, S.; Kume, H.; Homma, Y.; Igawa, Y. RQ-00434739, a Novel TRPM8 Antagonist, Inhibits Prostaglandin E2-Induced Hyperactivity of the Primary Bladder Afferent Nerves in Rats. *Life Sci* **2019**, *218*, 89–95. <https://doi.org/10.1016/J.LFS.2018.12.031>.

- (127) Masamoto, Y.; Kawabata, F.; Fushiki, T. Intragastric Administration of TRPV1, TRPV3, TRPM8, and TRPA1 Agonists Modulates Autonomic Thermoregulation in Different Manners in Mice. *Biosci Biotechnol Biochem* **2009**, *73* (5), 1021–1027. <https://doi.org/10.1271/BBB.80796>.
- (128) Li, M.; Li, Q.; Gang, Y. G.; Kolosov, V.; Perelman, J. M.; Zhou, X. D. Cold Temperature Induces Mucin Hypersecretion from Normal Human Bronchial Epithelial Cells in Vitro through a Transient Receptor Potential Melastatin 8 (TRPM8)-Mediated Mechanism. *J Allergy Clin Immunol* **2011**, *128* (3). <https://doi.org/10.1016/J.JACI.2011.04.032>.
- (129) Kume, H.; Tsukimoto, M. TRPM8 Channel Inhibitor AMTB Suppresses Murine T-Cell Activation Induced by T-Cell Receptor Stimulation, Concanavalin A, or External Antigen Re-Stimulation. *Biochem Biophys Res Commun* **2019**, *509* (4), 918–924. <https://doi.org/10.1016/J.BBRC.2019.01.004>.
- (130) Parra, A.; Madrid, R.; Echevarria, D.; del Olmo, S.; Morenilla-Palao, C.; Acosta, M. C.; Gallar, J.; Dhaka, A.; Viana, F.; Belmonte, C. Ocular Surface Wetness Is Regulated by TRPM8-Dependent Cold Thermoreceptors of the Cornea. *Nat Med* **2010**, *16* (12), 1396–1399. <https://doi.org/10.1038/nm.2264>.
- (131) Vahabi, B.; Parsons, B. A.; Doran, O.; Rhodes, A.; Dean, S.; Drake Marcus J. TRPM8 Agonists Modulate Contraction of the Pig Urinary Bladder. *Can J Physiol Pharmacol* **2013**, *91* (7), 503–509. <https://doi.org/10.1139/CJPP-2012-0406>.
- (132) Ito, H.; Aizawa, N.; Sugiyama, R.; Watanabe, S.; Takahashi, N.; Tajimi, M.; Fukuhara, H.; Homma, Y.; Kubota, Y.; Andersson, K. E.; Igawa, Y. Functional Role of the Transient Receptor Potential Melastatin 8 (TRPM8) Ion Channel in the Urinary Bladder Assessed by Conscious Cystometry and Ex Vivo Measurements of Single-Unit Mechanosensitive Bladder Afferent Activities in the Rat. *BJU Int* **2016**, *117* (3), 484–494. <https://doi.org/10.1111/bju.13225>.
- (133) Sidaway, P. Urinary Incontinence: TRPM8 Influences Bladder Filling. *Nat Rev Urol* **2015**, *12* (9), 476. <https://doi.org/10.1038/NRUROL.2015.194>.
- (134) Zhang, L.; Barritt, G. J. Evidence That TRPM8 Is an Androgen-Dependent Ca<sup>2+</sup> Channel Required for the Survival of Prostate Cancer Cells. *Cancer Res* **2004**, *64* (22), 8365–8373. <https://doi.org/10.1158/0008-5472.CAN-04-2146>.
- (135) Guo, H.; Carlson, J. A.; Slominski, A. Role of TRPM in Melanocytes and Melanoma. *Exp Dermatol* **2012**, *21* (9), 650–654. <https://doi.org/10.1111/J.1600-0625.2012.01565.X>.
- (136) Kono, T.; Satomi, M.; Suno, M.; Kimura, N.; Yamazaki, H.; urukawa, H.; Matsubara, K. Oxaliplatin-Induced Neurotoxicity Involves TRPM8 in the Mechanism of Acute Hypersensitivity to Cold Sensation. *Brain Behav* **2012**, *2* (1), 68–73. <https://doi.org/10.1002/BRB3.34>.

## Bibliografia

- (137) Liu, B.; Fan, L.; Balakrishna, S.; Sui, A.; Morris, J. B.; Jordt, S.-E. TRPM8 Is the Principal Mediator of Menthol-Induced Analgesia of Acute and Inflammatory Pain. *Pain* **2013**, *154* (10), 2169–2177. <https://doi.org/10.1016/J.PAIN.2013.06.043>.
- (138) Benemei, S.; Dussor, G. TRP Channels and Migraine: Recent Developments and New Therapeutic Opportunities. *Pharmaceuticals* **2019**, *12* (54). <https://doi.org/10.3390/ph12020054>.
- (139) De Vries, B.; Anttila, V.; Freilinger, T.; Wessman, M.; Kaunisto, M. A.; Kallela, M.; Artto, V.; Vijfhuizen, L. S.; Göbel, H.; Dichgans, M.; Kubisch, C.; Ferrari, M. D.; Palotie, A.; Terwindt, G. M.; Van Den Maagdenberg, A. M. J. M. Systematic Re-Evaluation of Genes from Candidate Gene Association Studies in Migraine Using a Large Genome-Wide Association Data Set. *Cephalalgia* **2016**, *36* (7), 604–614. <https://doi.org/10.1177/0333102414566820>.
- (140) Prince, P. B.; Rapoport, A. M.; Sheftell, F. D.; Tepper, S. J.; Bigal, M. E. The Effect of Weather on Headache. *Headache* **2004**, *44* (6), 596–602. <https://doi.org/10.1111/J.1526-4610.2004.446008.X/FORMAT/PDF>.
- (141) Borhani-Haghighi, A.; Motazedian, S.; Rezaii, R.; Mohammadi, F.; Salarian, L.; Pourmokhtari, M.; Khodaei, S.; Vossoughi, M.; Miri, R. Cutaneous Application of Menthol 10% Solution as an Abortive Treatment of Migraine without Aura: A Randomised, Double-Blind, Placebo-Controlled, Crossed-over Study. *Int J Clin Pract* **2010**, *64* (4), 451–456. <https://doi.org/10.1111/J.1742-1241.2009.02215.X/FORMAT/PDF>.
- (142) Liu, Z.; Wu, H.; Wei, Z.; Wang, X.; Shen, P.; Wang, S.; Wang, A.; Chen, W.; Lu, Y. TRPM8: A Potential Target for Cancer Treatment. *J Cancer Res Clin Oncol* **2016**, *142* (9), 1871–1881. <https://doi.org/10.1007/S00432-015-2112-1>.
- (143) Noyer, L.; Grolez, G. P.; Prevarskaya, N.; Gkika, D.; Lemonnier, L. TRPM8 and Prostate: A Cold Case? *Pflugers Arch* **2018**, *470* (10), 1419–1429. <https://doi.org/10.1007/S00424-018-2169-1>.
- (144) De Souza, M. F.; Kuasne, H.; Barros-Filho, M. D. C.; Cilião, H. L.; Marchi, F. A.; Fuganti, P. E.; Rogatto, S. R.; Cólus, I. M. D. S. Circulating mRNA Signature as a Marker for High-Risk Prostate Cancer. *Carcinogenesis* **2020**, *41* (2), 139–145. <https://doi.org/10.1093/CARCIN/BGZ129>.
- (145) Du, J.; Zheng, X.; Chen, Y.; Huang, Z.; Cai, S.; Jiao, H.; Zhu, Z.; Hu, B. Elevated Transient Receptor Potential Melastatin 8 (TRPM8) Expression Is Correlated with Poor Prognosis in Pancreatic Cancer. *Med Sci Monit* **2018**, *24*, 3720. <https://doi.org/10.12659/MSM.909968>.
- (146) Xu, Q.; Kong, N.; Zhang, J.; Bai, N.; Bi, J.; Li, W. Expression of Transient Receptor Potential Cation Channel Subfamily M Member 8 in Gastric Cancer and Its Clinical

- Significance. *Exp Ther Med* **2021**, *21* (4), 377. <https://doi.org/10.3892/ETM.2021.9808>.
- (147) Oh, S. T.; Yang, K. J.; Kim, Y. H.; Bae, J. M.; Park, H. J.; Kim, J. W.; Park, Y. M. Increased Immunoreactivity for TRPM8 in Cutaneous Squamous Cell Carcinoma. *J Cutan Pathol* **2018**, *45* (12), 970–972. <https://doi.org/10.1111/CUP.13358>.
- (148) Wang, Y.; Yang, Z.; Meng, Z.; Cao, H.; Zhu, G.; Liu, T.; Wang, X. Knockdown of TRPM8 Suppresses Cancer Malignancy and Enhances Epirubicin-Induced Apoptosis in Human Osteosarcoma Cells. *Int J Biol Sci* **2014**, *10* (1), 90. <https://doi.org/10.7150/IJBS.7738>.
- (149) Klumpp, D.; Frank, S. C.; Klumpp, L.; Sezgin, E. C.; Eckert, M.; Edalat, L.; Bastmeyer, M.; Zips, D.; Ruth, P.; Huber, S. M. TRPM8 Is Required for Survival and Radioresistance of Glioblastoma Cells. *Oncotarget* **2017**, *8* (56), 95896–95913. <https://doi.org/10.18632/ONCOTARGET.21436>.
- (150) Okamoto, Y.; Ohkubo, T.; Ikebe, T.; Yamazaki, J. Blockade of TRPM8 Activity Reduces the Invasion Potential of Oral Squamous Carcinoma Cell Lines. *Int J Oncol* **2012**, *40* (5), 1431–1440. <https://doi.org/10.3892/IJO.2012.1340>.
- (151) Kijpornyongpan, T.; Sereemasun, A.; Chanchao, C. Dose-Dependent Cytotoxic Effects of Menthol on Human Malignant Melanoma A-375 Cells: Correlation with TRPM8 Transcript Expression. *Asian Pacific Journal of Cancer Prevention* **2014**, *15* (4), 1551–1556. <https://doi.org/10.7314/APJCP.2014.15.4.1551>.
- (152) Xiong, M.; Wang, J.; Guo, M.; Zhou, Q.; Lu, W. International Journal of COPD Dovepress TRPM8 Genetic Variations Associated with COPD Risk in the Chinese Han Population. *International Journal of COPD* **2016**, 11–2563. <https://doi.org/10.2147/COPD.S109026>.
- (153) Naumov, D. E.; Kotova, O. O.; Gassan, D. A.; Sugaylo, I. Y.; Afanas'eva, E. Y.; Sheludko, E. G.; Perelman, J. M. Effect of TRPM8 and TRPA1 Polymorphisms on COPD Predisposition and Lung Function in COPD Patients. *J Pers Med* **2021**, *11* (2), 1–11. <https://doi.org/10.3390/JPM11020108>.
- (154) Henstrom, M., Hadizadeh, F., Beyder, A., Bonfiglio, F., Zheng, T., Assadi, G., Rafter, J., Bujanda, L., Agreus, L., Andreasson, A., Dlugosz, A., Lindberg, G., Schmidt, P.T., Karling, P., Ohlsson, B., Talley, N.J., Simren, M., Walter, S., Wouters, M., Farr, M. TRPM8 Polymorphisms Associated with Increased Risk of IBS-C and IBS-M. *Gut* **2017**, *66*, 1725–1727. <https://doi.org/10.1136/gutjnl-2016-313346>.
- (155) Ramachandran, R.; Hyun, E.; Zhao, L.; Lapointe, T. K.; Chapman, K.; Hirota, C. L.; Ghosh, S.; McKemy, D. D.; Vergnolle, N.; Beck, P. L.; Altier, C.; Hollenberg, M. D. TRPM8 Activation Attenuates Inflammatory Responses in Mouse Models of Colitis. *Proc Natl Acad Sci U S A* **2013**, *110* (18), 7476–7481. <https://doi.org/10.1073/PNAS.1217431110>.

- (156) Wu, L.; Zhang, J.; Zhou, F.; Zhang, P. Increased Transient Receptor Potential Melastatin 8 Expression in the Development of Bladder Pain in Patients With Interstitial Cystitis/Bladder Pain Syndrome. *Urology* **2020**, *146*, 301.e1-301.e6. <https://doi.org/10.1016/J.UROLOGY.2020.09.037>.
- (157) Aizawa, N.; Fujimori, Y.; Kobayashi, J.-I.; Nakanishi, O.; Hirasawa, H.; Kume, H.; Homma, Y.; Igawa, Y. KPR-2579, a Novel TRPM8 Antagonist, Inhibits Acetic Acid-Induced Bladder Afferent Hyperactivity in Rats. *NeuroUrol Urodyn* **2018**, *37* (5), 1633–1640. <https://doi.org/10.1002/NAU.23532>.
- (158) Yang, J. M.; Wei, E. T.; Kim, S. J.; Yoon, K. C. TRPM8 Channels and Dry Eye. *Pharmaceuticals* **2018**, *11* (4), 125. <https://doi.org/10.3390/PH11040125>.
- (159) Palkar, R.; Ongun, S.; Catich, E.; Li, N.; Borad, N.; Sarkisian, A.; McKemy, D. D. Cooling Relief of Acute and Chronic Itch Requires TRPM8 Channels and Neurons. *Journal of Investigative Dermatology* **2018**, *138* (6), 1391–1399. <https://doi.org/10.1016/j.jid.2017.12.025>.
- (160) *Bacterial Transformation Using Heat Shock and Competent Cells | Basic Methods in Cellular and Molecular Biology | JoVE*. <https://www.jove.com/es/v/5059/bacterial-transformation-the-heat-shock-method?language=Spanish> (acceso el 2022-05-16).
- (161) Cordero-Sánchez, C.; Mudarra-Fraguas, I.; Fernández-Carvajal, A. Fluorescence-Based Functional Assays for Ca<sup>2+</sup>-Permeable ThermoTRP Channels. In *TRP Channels: Methods and Protocols. Methods in molecular biology*; Ferrer-Montiel, A., Hucho, T., Eds.; Humana Press: New York, NY, 2019; pp 99–110.
- (162) Zhang, J. H.; Chung, T. D. Y.; Oldenburg, K. R. A Simple Statistical Parameter for Use in Evaluation and Validation of High Throughput Screening Assays. *J Biomol Screen* **1999**, *4* (2), 67–73. <https://doi.org/10.1177/108705719900400206>.
- (163) Herráez, A. *Ensayo de viabilidad celular (actividad metabólica) por reducción del compuesto MTT*. <https://biomodel.uah.es/tecnicas/cel/MTT.htm> (acceso el 2022-05-16).
- (164) Bonache, M. A.; Martín-Escura, C.; de la Torre Martínez, R.; Medina, A.; González-Rodríguez, S.; Francesch, A.; Cuevas, C.; Roa, A. M.; Fernández-Ballester, G.; Ferrer-Montiel, A.; Fernández-Carvajal, A.; González-Muniz, Rosario. Highly Functionalized  $\beta$ -Lactams and 2-Ketopiperazines as TRPM8 Antagonists with Antiallodynic Activity. *Sci Rep* **2020**, *10* (1), 14154. <https://doi.org/10.1038/s41598-020-70691-x>.
- (165) Morris, G. M.; Ruth, H.; Lindstrom, W.; Sanner, M. F.; Belew, R. K.; Goodsell, D. S.; Olson, A. J. AutoDock4 and AutoDockTools4: Automated Docking with Selective Receptor Flexibility. *J Comput Chem* **2009**, *30* (16), 2785–2791. <https://doi.org/10.1002/JCC.21256>.

- (166) Nikolaeva-Koleva, M. Desing and Functional Validation of Pain Modulators: Crosstalk between TRAAK and TRPV1 (Tesis Doctoral), Universidad Miguel Hernández de Elche, 2021.
- (167) Zimmermann, M. Ethical Considerations in Relation to Pain in Animal Experimentation. **1986**, *554*, 221–233.
- (168) *Directiva 2010/63/UE Del Parlamento Europeo y Del Consejo, de 22 de Septiembre de 2010, Relativa a La Protección de Los Animales Utilizados Para Fines Científicos*; Diario Oficial de la Unión Europea, 2010; pp 33–79.
- (169) *Real Decreto 53/2013, de 1 de Febrero, Por El Que Se Establecen Las Normas Básicas Aplicables Para La Protección de Los Animales Utilizados En Experimentación y Otros Fines Científicos, Incluyendo La Docencia*; Boletín Oficial del Estado, 2013; pp 11370–11421.
- (170) Dixon, W. J. Efficient Analysis of Experimental Observations. *Annu Rev Pharmacol Toxicol* **1980**, *20*, 441–462.
- (171) Pérez-Faginas, P. Azetidinas y  $\beta$ -Lactamas Derivadas de Aminoácido: Síntesis y Descubrimiento de Nuevos Compuestos Bioactivos (Tesis Doctoral), Universidad Autónoma de Madrid, 2010.
- (172) Rothstein, J. D.; Patel, S.; Regan, M. R.; Haenggeli, C.; Huang, Y. H.; Bergles, D. E.; Jin, L.; Hoberg, M. D.; Vidensky, S.; Chung, D. S.; Toan, S. V.; Bruijn, L. I.; Su, Z.; Gupta, P.; Fisher, P. B. B-Lactam Antibiotics Offer Neuroprotection by Increasing Glutamate Transporter Expression. *Nature* **2005**, *433*, 73–77.
- (173) von Nussbaum, F.; Brands, M.; Hinzen, B.; Weigand, S.; Häbich, D. Antibacterial Natural Products in Medicinal Chemistry - Exodus or Revival? *Angewandte Chemie - International Edition* **2006**, *45* (31), 5072–5129. <https://doi.org/10.1002/ANIE.200600350>.
- (174) Kvaernø, L.; Werder, M.; Hauser, H.; Carreira, E. M. Synthesis and in Vitro Evaluation of Inhibitors of Intestinal Cholesterol Absorption. *J Med Chem* **2005**, *48*, 6035–6053. <https://doi.org/10.1021/jm050422p>.
- (175) Miller, T. M.; Cleveland, D. W. Treating Neurodegenerative Diseases with Antibiotics. *Science (1979)* **2005**, *307*, 361–362.
- (176) Kumari, S.; Deshmukh, R.  $\beta$ -Lactam Antibiotics to Tame down Molecular Pathways of Alzheimer's Disease. *Eur J Pharmacol* **2021**, *895* (173877). <https://doi.org/10.1016/J.EJPBAR.2021.173877>.
- (177) Fu, D. J.; Zhang, Y. F.; Chang, A. Q.; Li, J.  $\beta$ -Lactams as Promising Anticancer Agents: Molecular Hybrids, Structure Activity Relationships and Potential Targets. *Eur J Med Chem* **2020**, *201* (112510). <https://doi.org/10.1016/J.EJMECH.2020.112510>.

## Bibliografía

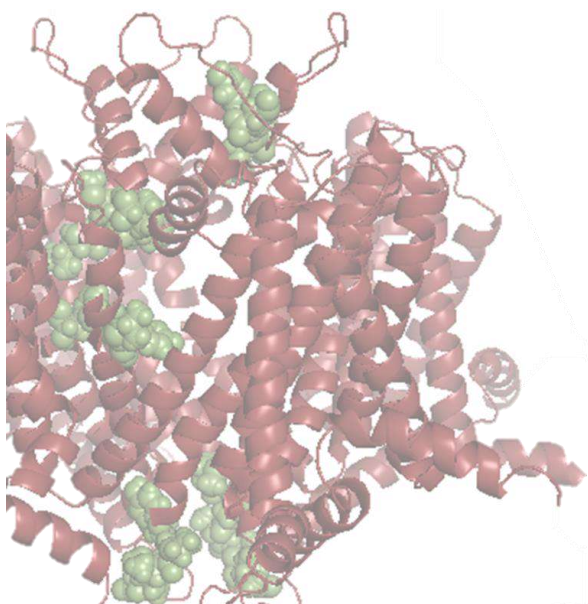
- (178) Martín-Escura, C. Desarrollo Preclínico de Antagonistas de Canales TRPM8 Para El Tratamiento de La Alodinia Asociada a Quimioterapia Antitumoral (Tesis Doctoral), Universidad de Alcalá, 2021.
- (179) Palomo, C.; Aizpurua, J. M.; Benito, A.; Galarza, R.; Khamrai, U. K.; Vazquez, J.; de Pascual-Teresa, B.; Nieto, P. M.; Linden, A. A-Alkyl- $\alpha$ -Amino- $\beta$ -Lactam Peptides: Design, Synthesis, and Conformational Features. *Angewandte Chemie - International Edition* **1998**, *38* (20), 3056–3058.
- (180) de La Torre-Martínez, R.; Angeles Bonache, M.; Llabrés-Campaner, P. J.; Balsera, B.; Fernández-Carvajal, A.; Fernández-Ballester, G.; Ferrer-Montiel, A.; Jesús Pérez De Vega, M.; González-Muñiz, R. Synthesis, High-Throughput Screening and Pharmacological Characterization of  $\beta$ -Lactam Derivatives as TRPM8 Antagonists. *Sci Rep* **2017**, *7* (10766). <https://doi.org/10.1038/s41598-017-10913-x>.
- (181) Diver, M. M.; Cheng, Y.; Julius David. Structural Insights into TRPM8 Inhibition and Desensitization. *Science* **2019**, *365* (6460), 1434–1440. <https://doi.org/10.1126/SCIENCE.AAX6672>.
- (182) Bertamino, A.; Iraci, N.; Ostacolo, C.; Ambrosino, P.; Musella, S.; di Sarno, V.; Ciaglia, T.; Pepe, G.; Sala, M.; Soldovieri, M. V.; Mosca, I.; Gonzalez-Rodriguez, S.; Fernandez-Carvajal, A.; Ferrer-Montiel, A.; Novellino, E.; Tagliatela, M.; Campiglia, P.; Gomez-Monterrey, I. Identification of a Potent Tryptophan-Based TRPM8 Antagonist with in Vivo Analgesic Activity. *J Med Chem* **2018**, *61* (14), 6140–6152. <https://doi.org/10.1021/acs.jmedchem.8b00545>.
- (183) Bonache, M. Á.; Llabrés, P. J.; Martín-Escura, C.; de la Torre-Martínez, R.; Medina-Peris, A.; Butrón, L.; Gómez-Monterrey, I.; Roa, A. M.; Fernández-Ballester, G.; Ferrer-Montiel, A.; Fernández-Carvajal, A.; González-Muñiz, R. Phenylalanine-Derived  $\beta$ -Lactam Trpm8 Modulators. Configuration Effect on the Antagonist Activity. *Int J Mol Sci* **2021**, *22* (5), 1–22. <https://doi.org/10.3390/ijms22052370>.
- (184) Scientific Committee on Consumer Safety. *The SCCS Notes of Guidance for Testing of Cosmetic Ingredients and Their Safety Evaluation-11th Revision-SCCS/1602/18*; European Commission, 2018.
- (185) The Organisation for Economic Co-operation and Development (OECD). *Guidance Notes on Dermal Absorption. Series on Testing and Assessment 156. (Draft Second Edition)*; 2019.
- (186) The Organisation for Economic Co-operation and Development. *OECD Guideline for the Testing of Chemicals. Skin Absorption in Vitro Method 428.*; 2004.
- (187) Scientific Committee on Consumer Safety. *Opinion on Basic Criteria for the in Vitro Assessment of Dermal Absorption of Cosmetic Ingredients - SCCS/0970/06*; European Commission, 2006; pp 1–12.
- (188) Bertamino, A.; Ostacolo, C.; Ambrosino, P.; Musella, S.; di Sarno, V.; Ciaglia, T.; Soldovieri, M. v.; Iraci, N.; Fernandez Carvajal, A.; de la Torre-Martinez, R.; Ferrer-

- Montiel, A.; Gonzalez-Muñiz, R.; Novellino, E.; Tagliatela, M.; Campiglia, P.; Gomez-Monterrey, I. Tryptamine-Based Derivatives as Transient Receptor Potential Melastatin Type 8 (TRPM8) Channel Modulators. *J Med Chem* **2016**, *59* (5), 2179–2191. <https://doi.org/10.1021/ACS.JMEDCHEM.5B01914>.
- (189) Bertamino, A.; Ostacolo, C.; Medina, A.; di Sarno, V.; Lauro, G.; Ciaglia, T.; Vestuto, V.; Pepe, G.; Basilicata, M. G.; Musella, S.; Smaldone, G.; Cristiano, C.; Gonzalez-Rodriguez, S.; Fernandez-Carvajal, A.; Bifulco, G.; Campiglia, P.; Gomez-Monterrey, I.; Russo, Roberto. Exploration of TRPM8 Binding Sites by  $\beta$ -Carboline-Based Antagonists and Their In Vitro Characterization and In Vivo Analgesic Activities. *J Med Chem* **2020**, *63*, 9672–9694. <https://doi.org/10.1021/acs.jmedchem.0c00816>.
- (190) Iraci, N.; Ostacolo, C.; Medina-Peris, A.; Ciaglia, T.; Novoselov, A. M.; Altieri, A.; Cabañero, D.; Fernandez-Carvajal, A.; Campiglia, P.; Gomez-Monterrey, I.; Bertamino, A.; Kurkin, A. v. In Vitro and In Vivo Pharmacological Characterization of a Novel TRPM8 Inhibitor Chemotype Identified by Small-Scale Preclinical Screening. *International Journal of Molecular Sciences* **2022**, *Vol. 23*, Page 2070 **2022**, *23* (4), 2070. <https://doi.org/10.3390/IJMS23042070>.
- (191) Sarno, V. di; Giovannelli, P.; Medina-Peris, A.; Ciaglia, T.; Donato, M. di; Musella, S.; Lauro, G.; Vestuto, V.; Smaldone, G.; Matteo, F. di; Bifulco, G.; Castoria, G.; Migliaccio, A.; Fernandez-Carvajal, A.; Campiglia, P.; Gomez-Monterrey, I.; Ostacolo, C.; Bertamino, A. New TRPM8 Blockers Exert Anticancer Activity over Castration-Resistant Prostate Cancer Models. *Eur J Med Chem* **2022**, *238*, 114435. <https://doi.org/10.1016/j.ejmech.2022.114435>.
- (192) Maia, E. H. B.; Assis, L. C.; de Oliveira, T. A.; da Silva, A. M.; Taranto, A. G. Structure-Based Virtual Screening: From Classical to Artificial Intelligence. *Front Chem* **2020**, *8*, 343. <https://doi.org/10.3389/FCHEM.2020.00343>.





## **ANEXOS**





**ANEXO I. Publicación 1 del capítulo 1*****Highly Functionalized 6-Lactams and 2-Ketopiperazines as TRPM8 Antagonists with Antiallodynic Activity.***

M.Ángeles Bonache<sup>1</sup>, Cristina Martín-Escura<sup>1,4</sup>, Roberto de la Torre Martínez<sup>2</sup>, Alicia Medina<sup>2</sup>, Sara González-Rodríguez<sup>2</sup>, Andrés Francesch<sup>3</sup>, Carmen Cuevas<sup>3</sup>, Ana María Roa<sup>4</sup>, Gregorio Fernández-Ballester<sup>2</sup>, Antonio Ferrer-Montiel<sup>2</sup>, Asia Fernández-Carvajal<sup>2</sup> y Rosario González-Muñiz<sup>1</sup>.

<sup>1</sup>Instituto de Química Médica (IQM-CSIC), Juan de la Cierva 3, 28006 Madrid, España.

<sup>2</sup>IDiBE, Universidad Miguel Hernández, Avda. de la Universidad s/n, 03202 Elche, España.

<sup>3</sup>PharmaMar S.A, Avda. de los Reyes 1, 28770 Colmenar Viejo, España.

<sup>4</sup>Alodia Farmacéutica SL, Santiago Grisolia 2, Tres Cantos, 28760 Madrid, España.

Scientific Reports 2020, 10 (1), 14154

<https://doi.org/10.1038/s41598-020-70691-x>

(Q1; Factor de Impacto: 4.996)





OPEN

# Highly functionalized $\beta$ -lactams and 2-ketopiperazines as TRPM8 antagonists with antiallodynic activity

M.Ángeles Bonache<sup>1</sup>, Cristina Martín-Escura<sup>1,4</sup>, Roberto de la Torre Martínez<sup>2</sup>, Alicia Medina<sup>2</sup>, Sara González-Rodríguez<sup>2</sup>, Andrés Francesch<sup>3</sup>, Carmen Cuevas<sup>3</sup>, Ana María Roa<sup>4</sup>, Gregorio Fernández-Ballester<sup>2</sup>, Antonio Ferrer-Montiel<sup>2</sup>, Asia Fernández-Carvajal<sup>2</sup>✉ & Rosario González-Muñiz<sup>1</sup>✉

The cool sensor transient receptor potential melastatin channel 8 (TRPM8) is highly expressed in trigeminal and dorsal root ganglia, playing a key role in cold hypersensitivity associated to different peripheral neuropathies. Moreover, these channels are aberrantly expressed in different cancers, and seem to participate in tumor progression, survival and invasion. Accordingly, the search for potent and selective TRPM8 modulators attracted great interest in recent years. We describe new heterocyclic TRPM8 antagonist chemotypes derived from *N*-chloroalkyl phenylalaninol-Phe conjugates. The cyclization of these conjugates afforded highly substituted  $\beta$ -lactams and/or 2-ketopiperazine (KP) derivatives, with regioselectivity depending on the *N*-chloroalkyl group and the configuration. These derivatives behave as TRPM8 antagonists in the  $\text{Ca}^{2+}$  microfluorometry assay, and confirmed electrophysiologically for the best enantiopure  $\beta$ -lactams 24a and 29a ( $\text{IC}_{50}$  1.4 and 0.8  $\mu\text{M}$ ). Two putative binding sites by the pore zone, different from those found for typical agonists and antagonists, were identified by in silico studies for both  $\beta$ -lactams and KPs.  $\beta$ -Lactams 24a and 29a display antitumor activity in different human tumor cell lines (micromolar potencies, A549, HT29, PSN1), but correlation with TRPM8 expression could not be established. Additionally, compound 24a significantly reduced cold allodynia in a mice model of oxaliplatin-induced peripheral neuropathy.

The transient receptor potential melastatin 8 (TRPM8) receptor is a multimodal channel, activated by cold and cooling compounds, such as menthol and icilin, but also by membrane depolarization and changes in extracellular osmolarity<sup>1</sup>. In the periphery, these channels are highly expressed in the afferent A $\delta$  and C fibers of sensory neurons, where they have been implicated in the perception and transduction of pain. Thus, cumulative evidence is signaling TRPM8 channels as pivotal players in cold hypersensitivity, especially that provoked by cancer chemotherapy<sup>2–4</sup>. Acute and chronic oxaliplatin-induced cold hypersensitivity has been reproduced in rats and correlated with TRPM8 expression and function<sup>5,6</sup>. Similarly, it is known that TRPM8 channels are implicated in inflammatory pain and migraine<sup>7</sup>. The thesis that migraine locus lies in the peripheral nervous system<sup>8</sup>, and the identification of TRPM8 as a candidate susceptibility gene for migraine<sup>9,10</sup>, points to the modulation of TRPM8 channels as a plausible mechanism for the treatment of this pathology<sup>11</sup>.

TRPM8 channels are also expressed in prostate, pancreas, and vascular, bronchopulmonary and urogenital tissues<sup>12–16</sup>. There are also numerous experimental evidences demonstrating that TRPM8 channels play important roles in tumor development and progression, including prostate, pancreas, breast, lung, colon, bladder and melanoma malignancies, among others<sup>12,17</sup>. In many cases, the aberrant expression of TRPM8 channels is correlated to tumor growth, progression and invasion capacity, at least in initial stages<sup>18–21</sup>, while sometimes TRPM8 channels are downregulated in final phases of the disease, and their activation seems to have a protective role<sup>22</sup>.

<sup>1</sup>Instituto de Química Médica (IQM-CSIC), Juan de la Cierva 3, 28006 Madrid, Spain. <sup>2</sup>DiBE, Universidad Miguel Hernández, Avda. de la Universidad s/n, 03202 Elche, Spain. <sup>3</sup>PharmaMar S.A, Avda. de los Reyes 1, 28770 Colmenar Viejo, Spain. <sup>4</sup>Alodia Farmacéutica SL, Santiago Grisolia 2, Tres Cantos, 28760 Madrid, Spain. ✉email: asia.fernandez@umh.es; iqmg313@iqm.csic.es

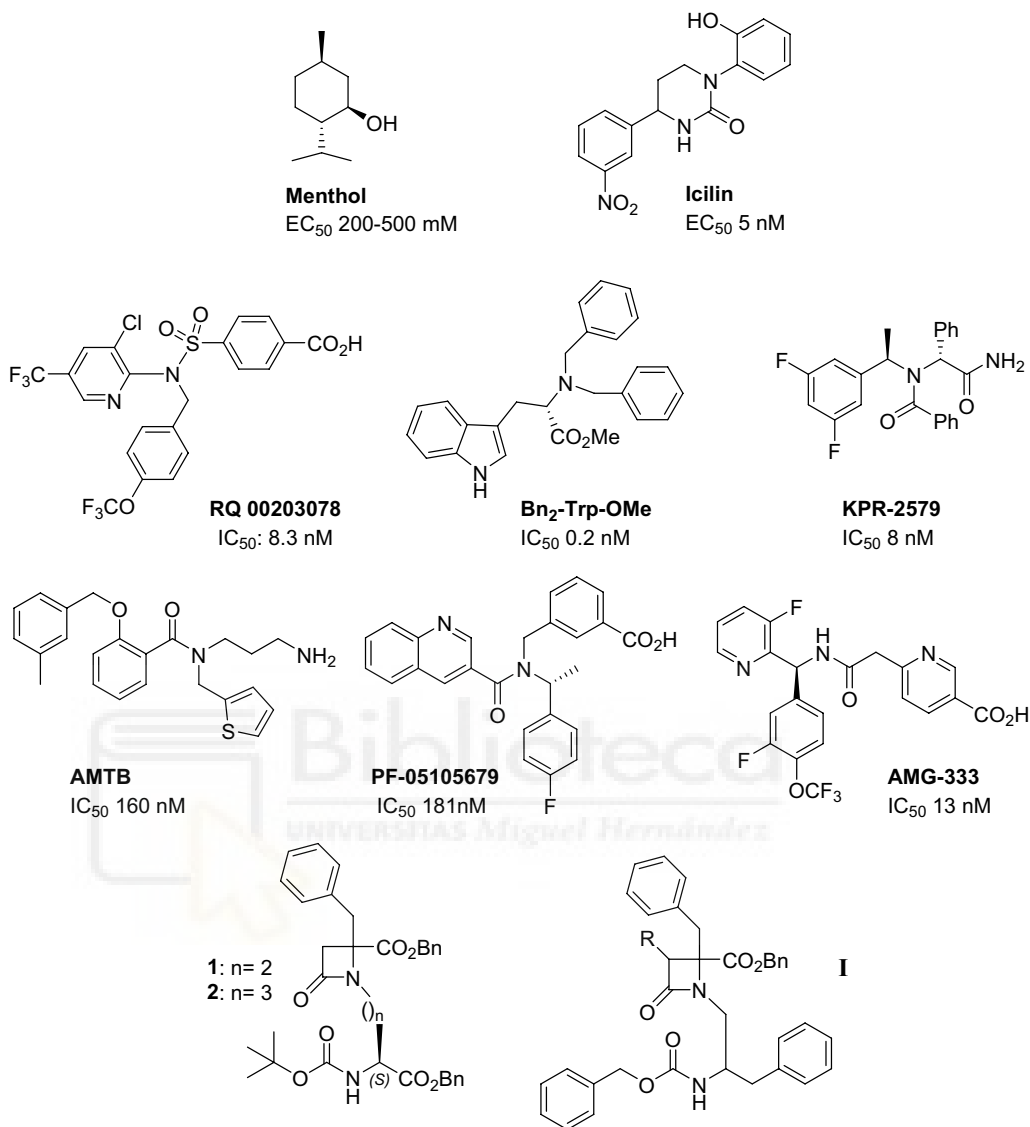


**Figure 1.** Representative TRPM8 modulators,  $\beta$ -lactams TRPM8 antagonists and general formula for phenylalaninol-derived analogues (**I**, this paper).

It is also described that TRPM8 is expressed in the central nervous system, thus opening new opportunities to study and understand its potential role within the brain<sup>23</sup>.

Cryo-electron microscopy has demonstrated that the TRPM8 channel is a tetrameric protein, with 6TM helical segments (S1-S6) and intracellular N- and C-terminal domains, with the pore delimited by a region situated between S5 and S6 helices<sup>24</sup>. The structure of TRPM8 in complex with some agonist compounds is disclosed, indicating a cavity for agonists delimited by S1, S4 and the TRP domain<sup>25</sup>. This highly adaptable pocket, delineated by the lower part of the S1-S4 transmembrane and the TRP domain, has also been described as the main cleft to bind AMTB and CT-I antagonists<sup>26</sup>.

Because of the physiological and therapeutic significance of TRPM8 channels, many efforts have been devoted to the search for selective modulators, both agonists and antagonists<sup>27-29</sup>. Among the agonists, we can find menthol, diverse menthol derivatives, icilin, tertiary amides and different natural products<sup>29-31</sup>. As for the antagonists, most important chemotypes encompass different heterocyclic systems, including monocyclic central cores, like thiazole and  $\beta$ -lactam, and bicyclic structures, as benzothiofene, benzimidazole, and isoquinoline, among others<sup>27,29,32</sup>. Also different acyclic central scaffolds (amide, sulfonamide, urea, glycine, tryptophan), decorated with aromatic and heterocyclic rings are reported as TRPM8 antagonists (Fig. 1)<sup>33-35</sup>. Among the latter, AMG-333 and PF-05105679 reached phase I clinical trials for the oral treatment of cold induced pain and migraine,

respectively<sup>33,36</sup>, but both studies were discontinued due to adverse secondary effects, including non-tolerated hot sensations. Therefore, there is still a need for TRPM8 antagonists with improved properties.

In this context, we have recently described a series of compounds derived from Phe and Asp/Glu amino acid conjugates and having a monocyclic  $\beta$ -lactam central core, which were able to potently and selectively inhibit the activation of TRPM8 by menthol, cool and voltage<sup>37</sup>. Among this series, the shorter Asp derivative **1** ( $n = 2$ , Fig. 1) was more potent than the longer Glu analogue **2** ( $n = 3$ , Fig. 1), while all the three benzyl and the Boc hydrophobic moieties are important for activity<sup>37</sup>.

Looking for shorter  $\beta$ -lactam derivatives, bearing four hydrophobic substituents, in this manuscript we describe the preparation of conjugates of *Z*-phenylalaninol with amino acid derivatives and their cyclization to heterocyclic compounds having a  $\beta$ -lactam or a 2-ketopiperazine central scaffold. Both series of compounds behave as TRPM8 antagonists and, among them, selected  $\beta$ -lactam derivatives display antitumor activity, and antiallodynic properties in a model of chemotherapy-induced cold allodynia.

## Results

**Design.** The preparation of a shorter analogue of compounds **1** and **2** was initially projected starting from Boc-Ser-OBn ( $n = 1$ ). However, all attempts to condense this Ser derivative with Ns-Phe-OBn, were unsuccessful due to the formation of the corresponding dehydroalanine analogue, as described in related reactions<sup>38</sup>. As the structure of TRPM8 channel was unknown at the moment of conceiving this work, we hypothesized that compounds of general formula **I** (Fig. 1), which maintain the  $\beta$ -lactam ring, its substitution at position 4, but change the Asp- or Glu-derived *N*-substituent by phenylalaninol-derived moieties, could constitute a new chemotype for TRPM8 modulation. Although the changes are not bioisosteric, compounds **I** preserve two hydrophobic substituents on the *N*-appendage, which were demonstrated to be important for the activity of **1** and **2**.

**Chemistry.** As previously described for Phe-Asp conjugates<sup>37</sup>, the preparation of chloroacetyl derivatives **10** and **11** started by a Mitsunobu reaction between Ns-L-Phe-OBn (**3**) and the corresponding *Z*-phenylalaninol derivative (**4** or **5**) to give compounds **6** and **7** (Scheme 1). Then, the removal of the nosyl group afforded NH derivatives **8** and **9** that, finally, were reacted with chloroacetyl chloride to give key intermediates **10** and **11** (Scheme 1). The cyclization of these L-Phe-phenylalaninol conjugates in the presence of phosphazene bulky bases (BTPP, BEMP) led almost exclusively to the 2-ketopiperazine (KP) derivatives **13** and **15** (Scheme 1, Table 1), resulting from the cyclization through the NH group of the phenylalaninol-derived moiety. Under these conditions, formation of less than 3% of the expected  $\beta$ -lactams was observed in the HPLC chromatograms of the crude reaction mixtures. The ratio of  $\beta$ -lactams **12** and **14** increased slightly when the smaller Cs<sub>2</sub>CO<sub>3</sub> base was employed in the cyclization, allowing their isolation in 8 and 11% yield, respectively (Table 1). The chloroacetyl phenylalaninol-D-Phe-OMe-derived conjugate **19**, despite bearing a smaller methyl ester that could favor the four-membered ring formation, exclusively led to the KP derivative **20** (Scheme 1, Table 1), independently of the base used. The benzyl ester analogue **21** was prepared by transesterification of **20**, in order to compare its activity with those of diastereoisomers **13** and **15**.

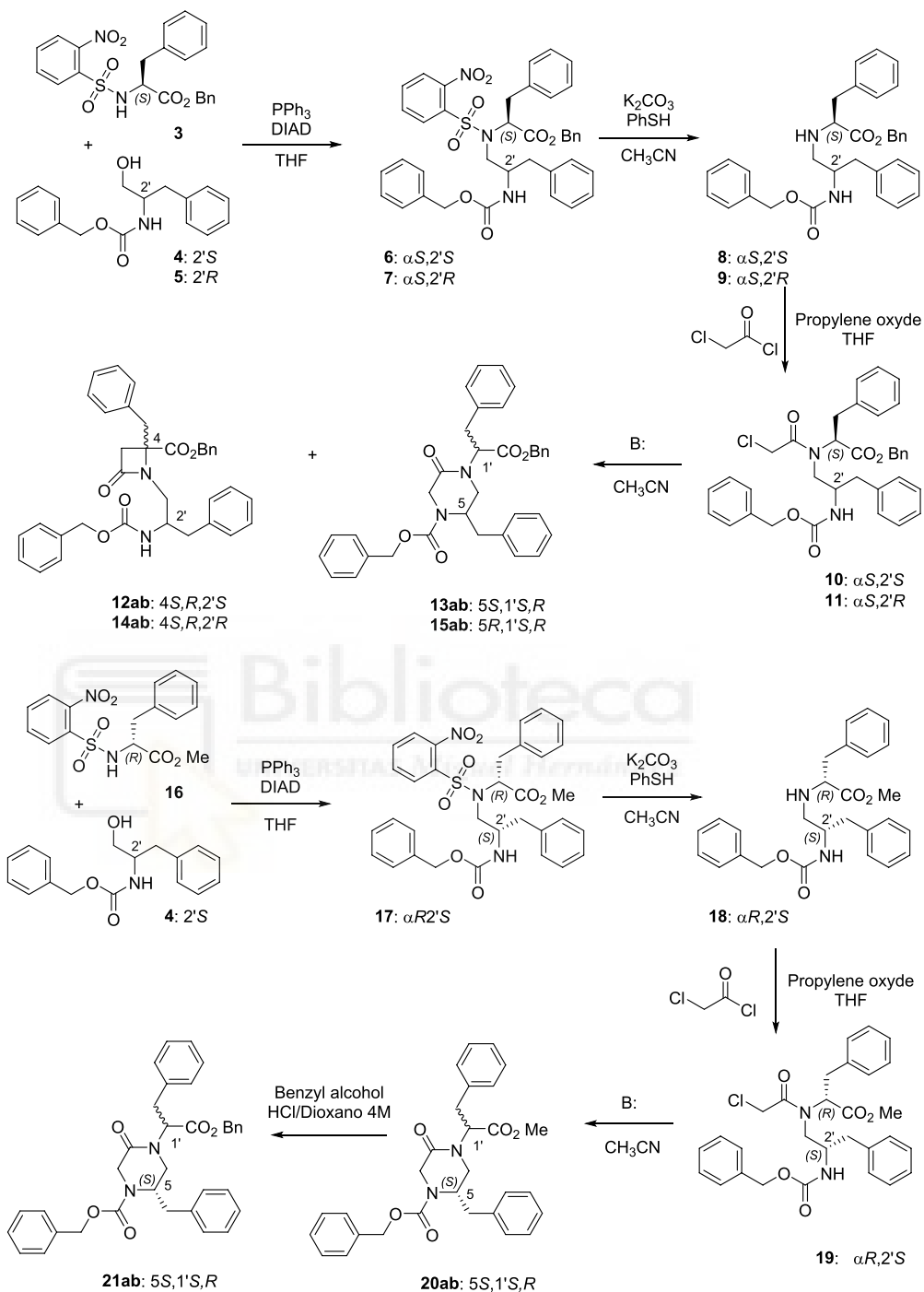
All these KP derivatives were obtained as mixtures of two diastereoisomers at C1' in variable proportions (Table 1). The configuration was indirectly assigned by the preparation of Ala dipeptide derivatives from **13ab** (see supplementary information for details), and applying the known rule of differential HPLC retention times and chemical shifts of the Ala CH<sub>3</sub> group between homochiral and heterochiral dipeptide derivatives<sup>39,40</sup>.

$\beta$ -Lactam derivatives **12** and **14** were also formed as mixtures of two diastereoisomers at C4. Considering that the memory of chirality favors the formation of 4*S* isomers when starting from L-Phe<sup>39,41,42</sup>, the configuration of the major diastereoisomer was assigned as 4*S*.

To attempt to obtain  $\beta$ -lactams as single isomers, we prepare enantiopure 2-chloropropanoyl *Z*-phenylalaninol-Phe-OBn conjugates **22**, **23**, **27** and **28** (Scheme 2). For this, conjugates **8** and **9** were reacted with 2*S*- or 2*R*-chloropropionic acid in the presence of trichloroacetonitrile and triphenylphosphine. We have previously demonstrated that related 2-chloropropanoyl derivatives afforded pure  $\beta$ -lactams, with the stereochemistry at C3, C4 dictated by the configuration of the chloropropionic moiety<sup>43</sup>. In good agreement with our precedents, cyclization of the all *S* isomer **22** with BTPP led almost exclusively to the formation of the 3*S*,4*S*,2'*S*  $\beta$ -lactam **24a** (Table 2), along with less than 11% of the corresponding KP (not isolated). Again, the percentage of conversion to the four-membered ring was higher when Cs<sub>2</sub>CO<sub>3</sub> was used as base (Table 2). Similarly, the basic treatment of the 2'*R*,2''*S*-chloropropanoyl derivative **27** with BTPP afforded enantiopure 3*S*,4*S*,2'*R* 2-azetidinone **29a**. However, in this case, the indicated  $\beta$ -lactam was obtained along with about 50% of the corresponding KP **30ab** (a:b, 81:18). Cyclization of **27** with Cs<sub>2</sub>CO<sub>3</sub> afforded a mixture of  $\beta$ -lactam and KP in the same ratio (48:52), but in this case the 2-azetidinone derivative was obtained as a mixture of two diastereoisomers (**29ab**, 73:27, see SI for a possible explanation). The KP derivative **26ab** was the main reaction product (>85%) during the treatment of the 2'*S*,2''*R*-chloropropanoyl precursor **23**, and the minor  $\beta$ -lactam was also obtained as a diastereomeric mixture (**25ab**, Table 2). Contrastingly, the 2-azetidinone derivative **31ab** was the main product (>70%) after the cyclization of the 2'*R*,2''*R*-chloropropanoyl precursor **28**. Therefore, the configuration of the linear precursor influenced both the regioselectivity ( $\beta$ -lactam versus KP) and the stereoselectivity in the formation of  $\beta$ -lactam derivatives.

A similar reactivity was observed during the cyclization of Ala derivatives (Supplementary Scheme S1). Accordingly, treatment with BTPP of the chloroacetyl derivative **36** afforded exclusively the 6-membered KP **38ab** (a:b, 86:14, Table 1), while chloropropanoyl analogue **37** led to a 42:58 mixture of the 2-azetidinone derivative **39a** (single isomer, 3*S*,4*S*,2'*R*, Table 2) and the KP **40ab** (a:b, 58:42).

**TRPM8 in vitro activity.** The ability to inhibit menthol-induced Ca<sup>2+</sup> intracellular influx into the cytosol on HEK293 cells heterologously expressing the rat TRPM8 channel was measured and compared to that of AMTB,



**Scheme 1.** Preparation of chloroacetyl phenylalaninol-Phe conjugates and cyclization reactions.

Starting Compd	Base	Time (h)	$\beta$ -L/KP ratio (HPLC)		$\beta$ -Lactam# Yield (%)	Configuration (Isomer ratio)	KP # Yield (%)	Configuration (isomer ratio)
10	BTPP	5	3:97	NI	–	–	13ab (77)	5S,1'S/5S,1'R (80:20)
	BEMP	3	2:98	NI	–	–	NI	5S,1'S/5S,1'R (93:7)
	Cs <sub>2</sub> CO <sub>3</sub>	3	11:89	12ab (8.5)	4S,2'S/4R,2'S (83:17)	–	13ab (68)	5S,1'S/5S,1'R (95:5)
11	BTPP	5	2:98	NI	–	–	15ab (77)	5R,1'S/5R,1'R (81:19)
	BEMP	6	2:98	NI	–	–	NI	5R,1'S/5R,1'R (80:20)
	Cs <sub>2</sub> CO <sub>3</sub>	6	27:73	14ab (11)	4S,2'R/4R,2'R (88:12)	–	15ab (69)	5R,1'S/5R,1'R (90:10)
19	BTPP	5	0:100	–	–	–	NI	5S,1'S/5S,1'R (40:60)
	Cs <sub>2</sub> CO <sub>3</sub>	6	0:100	–	–	–	20ab (60)	5S,1'S/5S,1'R (4:96)
20ab	–	–	–	–	–	–	21ab (55)	5S,1'S/5S,1'R (10:90)
36	BTPP	5	0:100	–	–	–	38ab (81)	5R,1'S/5R,1'R (86:14)

**Table 1.** Results of the cyclization reaction of chloroacetyl phenylalaninol-Phe conjugates. NI not isolated.

a well-known TRPM8 antagonist. The results obtained for  $\beta$ -lactam and KP derivatives are depicted in Table 3. Representative recordings of fluorescence obtained in microfluorometry experiments for selected compounds are in Supplementary Fig. S3. No agonist activity was observed for these compounds in the absence of menthol.

As shown in Table 3, slightly better antagonist activity was observed for  $\beta$ -lactam with an *N*-2'*R*-appendage (compare 2'*R*-derivatives 14ab, 29a and 31ab to 2'*S*-analogues 12ab, 24a and 25ab, respectively). However, in the case of diastereoisomeric mixtures (ab), the exact contribution to the activity of each individual isomer cannot be assessed. As previously described for the first generation of  $\beta$ -lactam TRPM8 antagonists<sup>37</sup>, the phenyl group at position 4 is important for Ca<sup>2+</sup> entrance inhibition, since the 4-CH<sub>3</sub> derivative 39a was one order of magnitude less active than the 4-Bn analogue 29a.

All KP derivatives were assayed as mixtures of two diastereoisomers, therefore the structure–activity relationships should be considered as tendencies, not as absolute statements. As for the  $\beta$ -lactam derivatives, the configuration of the stereocenter coming from the phenylalaninol moiety seems to dictate the antagonist activity, with 5*R*-KPs more potent than 5*S*-isomers (compare 15ab to 13ab) (Table 3). The 1'-configuration appears also to play a role for the inhibition of menthol-induced TRPM8 activation, with a preference for the 1'*R*- (21ab, 10:90) over the 1'*S*-isomer (13ab, 80:20). The OBn group in 21ab could participate in the direct interaction with the TRPM8 channel, as the corresponding OMe analogue 20ab shows an important drop in activity. In the 3-methyl derivatives, a 3*R*,5*R* configuration (in 30ab) is preferred over the 3*S*,5*S* combination (in 26ab), while the 3*S*,5*R*-configured diastereoisomers (32ab) showed the lowest activity in this series. In this case, a 4-CH<sub>3</sub> group led to slightly less active derivatives (38ab, 40ab) compared to the corresponding 4-Bn analogues (15ab and 30ab, respectively), although the fall in activity due to this modification is less acute than in the  $\beta$ -lactam series.

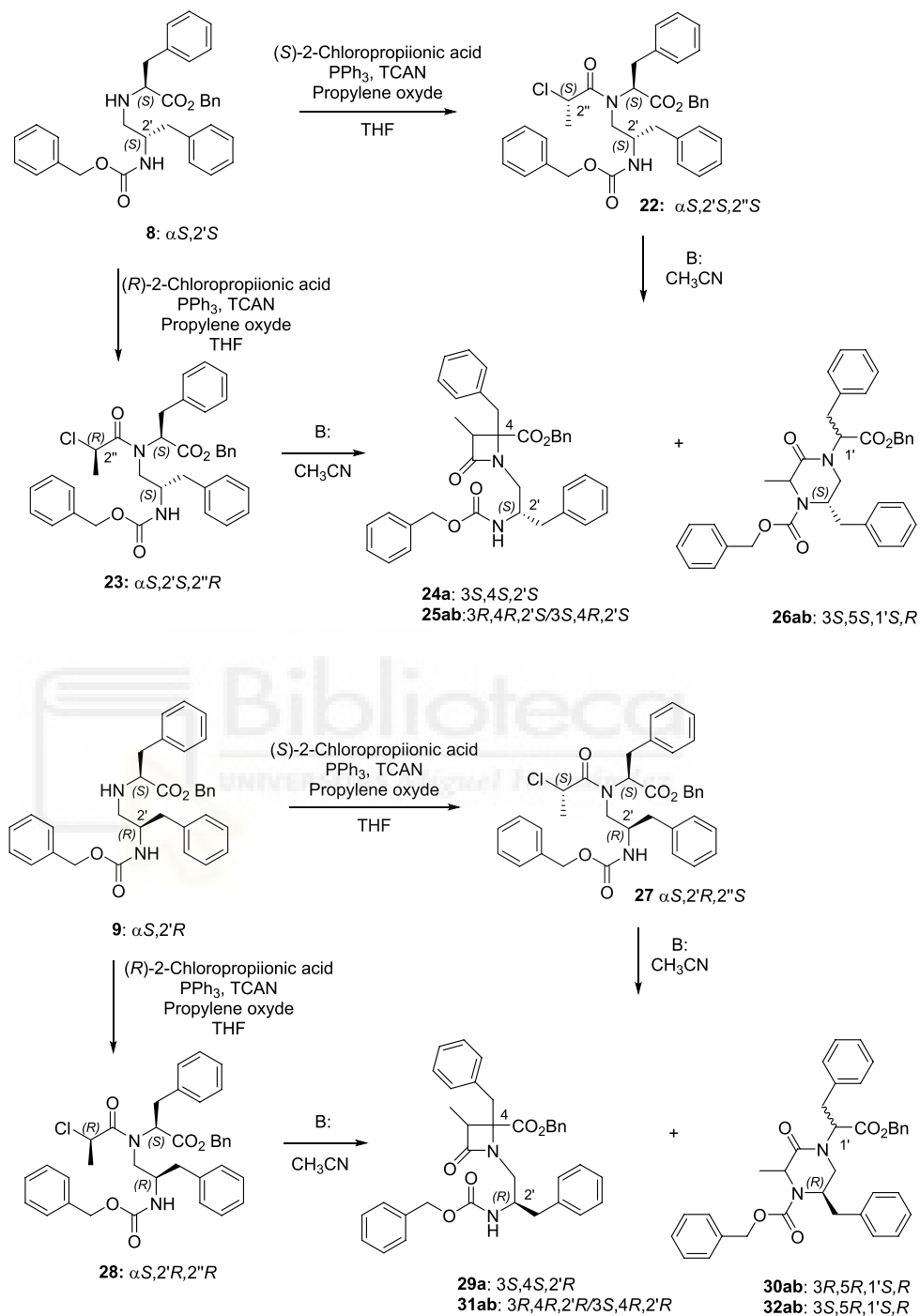
$\beta$ -Lactam and 2-ketopiperazine derivatives were also assayed for their activity in cell expressing hTRPV1 channels. No significant antagonist activity was measured for any derivatives within both chemotypes (Supplementary Tables S1, S2, and Fig. S3), indicating their selectivity for TRPM8 channels.

The TRPM8 antagonist activity of the enantiopure  $\beta$ -lactams 24a and 29a was further confirmed electrophysiologically by Patch-clamp experiments, using the whole cell configuration in HEK293 cells expressing TRPM8 channels.

As shown in Fig. 2, perfusion with 100  $\mu$ M menthol gives rise to a strongly outward rectifying ionic current characterized by the presence of negligible current at negative potential and the presence of a linear current increase (ohmic) at positive voltages  $\geq 40$  mV (1–50 mV/1 + 120 mV = 0.07). When 10  $\mu$ M of 24a was applied (Fig. 2A, blue), an important reduction on the menthol-mediated TRPM8 activity at depolarizing voltages (+120 mV) was observed. A similar behaviour was detected for diastereomeric  $\beta$ -lactam 29a (Fig. 2C, blue). The dose–response curve for both compounds was obtained at a holding potential of -60 mV (Supplementary Fig. S4). The IC<sub>50</sub> values were 1.4  $\pm$  1.1  $\mu$ M for 24a (Fig. 2B) and 0.8  $\pm$  1.1  $\mu$ M for 29a (Fig. 2D).

**Docking studies.** In order to investigate possible binding pockets within the TRPM8 channel for these families of KP and  $\beta$ -lactam TRPM8 antagonists, we performed computational studies with compounds 13a, 24a, and 29a. A model of the rat TRPM8 channel, created from the cryo-electron microscopy structure of the *Ficedula albicollis* (PDB code 6BPQ)<sup>24</sup>, was used, and docking simulations were performed with the software implemented in Yasara<sup>44–46</sup>

These docking studies predicted that the three compounds most likely (>80% solutions) interact with the TRPM8 by the pore zone, with two major solutions having the best binding energies (Supplementary Fig. S5, Table S3). Site 1 was identified in the middle of the transmembrane region, mainly involving TM5 (S5) and



**Scheme 2.** Preparation of 2-chloropropanoyl phenylalaninol-Phe conjugates and cyclization reactions.

Starting Compd	Base	Time (h)	$\beta$ -L/KP ratio (HPLC)	$\beta$ -Lactam# Yield (%)	Configuration (Isomer ratio)	KP # Yield (%)	Configuration (Isomer ratio)
22	BTPP	4	89:11	24a (65)	3S,4S,2'S	NI	–
	Cs <sub>2</sub> CO <sub>3</sub>	24	93:7	24a (70)	3S,4S,2'S	NI	–
23	BTPP	4	14:86	25ab (10)	3R,4R,2'R/3S,4R,2'S (85:15)	26ab (63)	3S,5S,1'S/3S,5S,1'R (81:19)
	Cs <sub>2</sub> CO <sub>3</sub>	336	11:89	NI	3R,4R,2'S/3S,4R,2'S (85:15)	NI	3S,5S,1'S/3S,5S,1'R (85:15)
27	BTPP	5	48:52	29a (39)	3S,4S,2'R	30ab (32)	3R,5R,1'S/3R,5R,1'R (82:18)
	Cs <sub>2</sub> CO <sub>3</sub>	168	48:52	NI	3S,4S,2'R/3R,4S,2'R (73:27)	NI	3R,5R,1'S/3R,5R,1'R (65:35)
28	BTPP	56	72:28	31ab (44)	3R,4R,2'R/3S,4R,2'R (77:23)	32ab (21)	3S,5R,1'S/3S,5R,1'R (85:15)
	Cs <sub>2</sub> CO <sub>3</sub>	336	82:18	31ab (59)	3R,4R,2'R/3S,4R,2'R (78:22)	NI	3S,5R,1'S/3S,5R,1'R (96:4)
37	BTPP	6	42:58	39a (30)	3S,4S,2'R	40ab (41)	3R,5R,1'S/3R,5R,1'R (58:42)

**Table 2.** Results of the cyclization reaction of 2-chloropropanoyl phenylalaninol conjugates. NI: not isolated.

Compd	Isomers	Isomers ratio	% Blockade 50 $\mu$ M	% Blockade 5 $\mu$ M	IC <sub>50</sub> ( $\mu$ M)
<b><math>\beta</math>-Lactams</b>					
12ab	4S,2'S/4R,2'S	83:17	100.0 $\pm$ 3.1	92.3 $\pm$ 6.2	1.5 $\pm$ 1.2
14ab	4S,2'R/4R,2'R	88:12	103 $\pm$ 2.7	91.0 $\pm$ 4.3	1.2 $\pm$ 1.0
24a	3S,4S,2'S	–	110.7 $\pm$ 11.7	65.4 $\pm$ 6.4	2.4 $\pm$ 1.2
25ab	3R,4R,2'S/3S,4R,2'S	85:15	89.2 $\pm$ 9.2	68.2 $\pm$ 5.6	3.9 $\pm$ 1.9
29a	3S,4S,2'R	–	100.0 $\pm$ 5.0	97.2 $\pm$ 4.8	0.4 $\pm$ 1.5
31ab	3R,4R,2'R/3S,4R,2'R	77:23	105.0 $\pm$ 5.5	91.0 $\pm$ 4.3	1.6 $\pm$ 1.3
39a	3S,4S,2'R	–	100.4 $\pm$ 3.5	46.6 $\pm$ 11.1	6.2 $\pm$ 1.1
<b>2-Ketopiperazines</b>					
13ab	5S,1'S/5S,1'R	80:20	102.1 $\pm$ 7.7	48.9 $\pm$ 6.2	17.9 $\pm$ 1.3
15ab	5R,1'S/5R,1'R	81:19	106 $\pm$ 5.06	101.4 $\pm$ 6.1	1.8 $\pm$ 1.9
20ab	5S,1'S/5S,1'R	4:96	61.0 $\pm$ 5.6	22.3 $\pm$ 5.5	18.8 $\pm$ 1.7
21ab	5S,1'S/5S,1'R	10:90	92.5 $\pm$ 4.3	70.0 $\pm$ 6.8	2.0 $\pm$ 1.5
26ab	3S,5S,1'S/3S,5S,1'R	81:19	102.4 $\pm$ 1.5	93.5 $\pm$ 3.4	2.4 $\pm$ 1.3
30ab	3R,5R,1'S/3R,5R,1'R	82:18	101.2 $\pm$ 11.4	101.7 $\pm$ 5.3	0.16 $\pm$ 1.6
32ab	3S,5R,1'S/3S,5R,1'R	96:4	115.1 $\pm$ 4.5	47.4 $\pm$ 6.8	17.4 $\pm$ 1.6
38ab	5R,1'S/5R,1'R	86:14	105.5 $\pm$ 3.2	66.0 $\pm$ 3.3	2.5 $\pm$ 1.3
40ab	3R,5R,1'S/3R,5R,1'R	58:42	107.9 $\pm$ 2.5	79.1 $\pm$ 3.3	0.8 $\pm$ 1.2
AMTB					7.3 $\pm$ 1.5

**Table 3.** Activity at TRPM8 of  $\beta$ -lactams derived from phenylalaninol conjugates.

TM6 (S6) of one monomer and segments of an adjacent subunit (S5 or S6 and/or the S5-S6 segment forming the pore). The second binding compartment, Site 2, correspond to the cytosolic mouth of the pore, involving the loops connecting TM6 and TRP domains of the 4 protein subunits forming the channel. As for the compounds, mainly hydrophobic interactions can be distinguished at both binding pockets, with some  $\pi$ - $\pi$  stacking and a few H-bonds identified.

Ketopiperazine **13a** binds TRPM8 channel at Site 1 through two  $\pi$ - $\pi$  stacking connections, a face-to-face stacked interaction between the phenyl group of the 1'-Bzl moiety and Y963 at subunit 1 (S6), and secondly a T-shaped (edge-to-face) contact encompassing the phenyl group of the  $\alpha$ -CO<sub>2</sub>Bzl moiety and F874 residue of TRPM8 subunit 3 (S5) (Supplementary Fig. S6). Among hydrophobic interactions, the Ph group of the Cbz moiety occupies a hydrophobic pocket delineated by residues located at subunit 3 (F870, L873, F874, I962, L965, and I969) and subunit 2 (I844). In addition, the 1'-Bn moiety is also involved in hydrophobic interactions through L871 and F874 (Subunit 3), while the phenyl group of the 5-Bn is in touch with I962 and Y963, also at subunit 3. At Site 2, a face-to-face  $\pi$ - $\pi$  stacking involves the Ph group of the Cbz and the aromatic ring of the Y981 residue (subunit 1). Moreover, the hydrophobic interactions comprise the four Ph rings of **13a** and residues from the four channel subunits (see Supplementary Fig. S7).

At Site 1,  $\beta$ -Lactams **24a** and **29a** occupy similar areas of the transmembrane region, involving two neighboring channel subunits, but their poses are clearly different, with the  $\beta$ -lactam ring pointing to the upper and

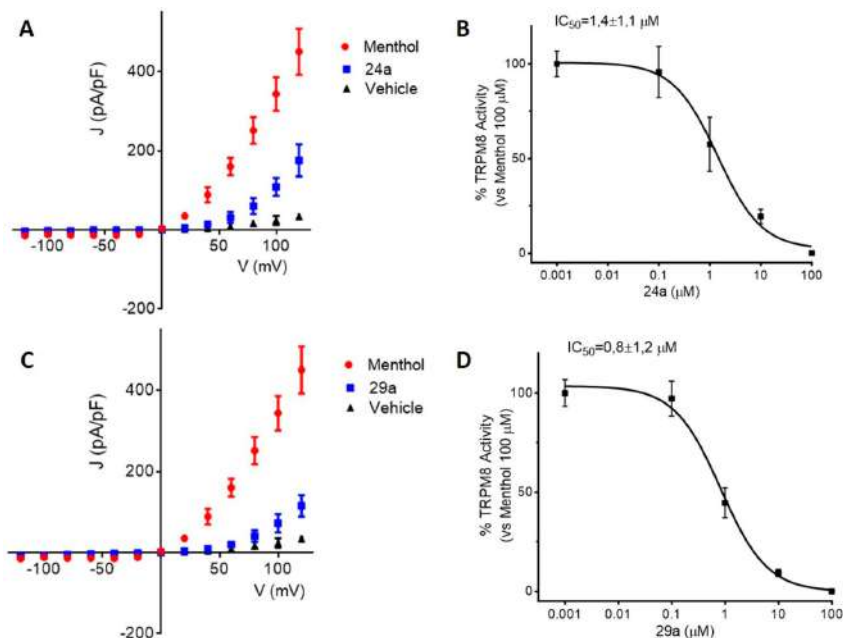


**Figure 2.** Compounds **24a** and **29a** block TRPM8-mediated responses evoked by menthol in rTRPM8-expressing HEK293 cells. (A, C). *I*-*V* curves obtained in HEK293 cells expressing TRPM8 and exposed to vehicle solution (Vehicle; black trace; A, C), 100  $\mu$ M menthol (red trace; A, C), 100  $\mu$ M menthol + 10  $\mu$ M **24a** (blue trace; A) or to 100  $\mu$ M menthol + 10  $\mu$ M compound **29a** (blue trace; C) (B, D). Concentration – response curves for TRPM8 current blockade by compound **24a** (B) or compound **29a** (D) at a holding voltage of -60 mV. Peak current data were expressed as pA/pF (to facilitate comparison among cells of different size) and expressed as a function of antagonist concentrations. The solid lines represent fits of the experimental data to the following binding isotherm:  $y = \max / (1 + x/EC_{50})^n$ , where  $x$  is the drug concentration and  $n$  the Hill coefficient. The fitted values for  $n$  were  $0.97 \pm 0.05$  or  $0.98 \pm 0.6$  for compound **24a** or **29a**, respectively. Each point is the mean  $\pm$  SD of 8 (for compound **24a**) or 9 (for compound **29a**) determinations, each obtained in different cells.

lower part of the binding pocket, respectively (Fig. 3 and Supplementary Figs. S8–S11). The 3*S*,4*S*,2'*S* isomer **24a** binds the channel through a H-bond involving its NH and the backbone CO of L959 (S5, subunit 3) (Fig. 4 and Supplementary Fig. S8). Additionally, three  $\pi$ - $\pi$  interactions contribute to the complex stabilization, two T-shaped contacts comprising the Ph group of the Cbz moiety and W877 and F881 side-chains (both at S5), and a face-to-face sandwich between the aromatic groups of 2'-Bn and Y963 residue (S6), all at subunit 3. This monomer contributes also to the complex with nine hydrophobic interactions among a series of residue side-chains of the channel and the four Ph groups of the antagonist, while subunit 2 (S5 and S5-S6 loop) add three additional hydrophobic contacts (specified in Supplementary Fig. S8). The diastereoisomeric 3*S*,4*S*,2'*R* compounds **29a** is fixed to the channel through a H-bond (NH  $\rightarrow$  CO of G913, S5-S6 segment, subunit 1) and a parallel displaced  $\pi$ - $\pi$  connection (OBn-Y963 of S6, subunit 1, Supplementary Fig. S10). Also, a number of residues at subunit 1 provide hydrophobic interactions with the four Ph groups of **29a**. As previously, the contiguous monomer (subunit 4) also supplies additional stabilizing interactions, in this case involving three residues at the pore-forming S5-S6 segment (Supplementary Fig. S10).

Main residues involved in the hydrophobic interactions of **24a** and **29a** at Site 2 are Y981 (from three out of four subunits), T982 of monomer 4, and R855 of two subunits. In addition, a H-bond between the CO group of Y981 (subunit 1, S6) and the NH group of **24a**, and a  $\pi$ - $\pi$  displaced stacking interaction involving the phenyl groups of the 2'-Bn moiety in **29a** and Y981 side-chain (Subunit 1, S6), contribute to the respective stabilization of the complexes at Site 2 (Fig. 4, and Supplementary Figs. S9 and S11). Interestingly, most residues of rTRPM8 suggested as important for the interaction with  $\beta$ -lactams and KPs at both sites 1 and 2 are highly conserved in hTRPM8 (Supplementary Fig. S12).

**Growth inhibitory activity in tumor cells.** A number of recent experimental evidences position TRPM channels as important players in cancer growth and progression<sup>47</sup>. Among these channels, the aberrant expression of the TRPM8 subtype has been described in different human malignant tumors, including those of prostate, pancreas, breast, colon, and skin, among others<sup>3</sup>. More importantly, sometimes the TRPM8 overexpression was associated to poor prognosis of cancer patients. In good agreement, several, structurally different TRPM8 antagonists demonstrated good antitumor activity in prostate<sup>32,48,49</sup>, and others human tumor cell lines<sup>50</sup>. A few

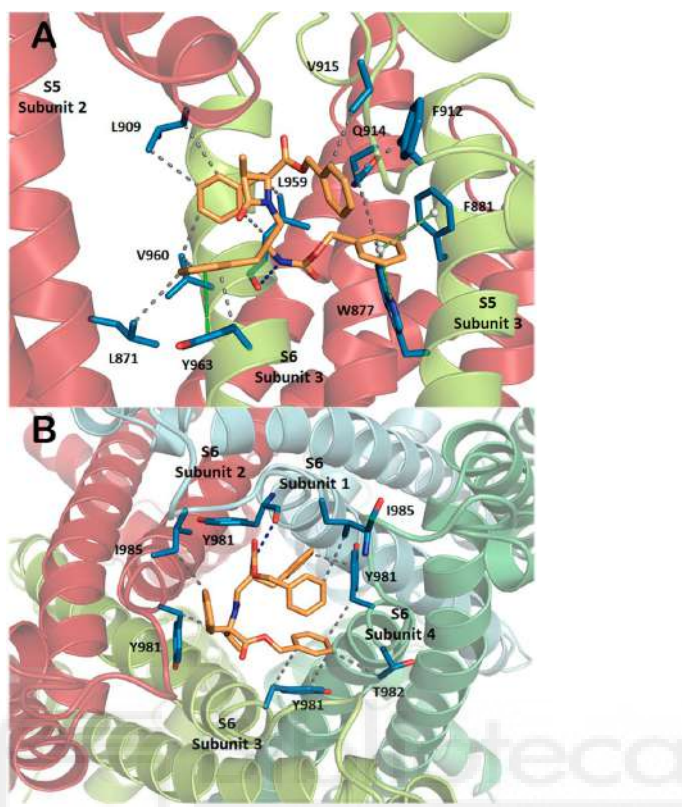


**Figure 3.** Low energy binding sites for  $\beta$ -lactam derivative **24a**, Site 1 (A), Site 2 (B). Compound **24a** is in pale orange, while side-chains of TRPM8 involved in the interaction are depicted in blue and labelled. Heteroatoms are indicated in red (O) and dark blue (N). H atoms have been removed.

years ago we have described that Phe-derived simpler  $\beta$ -lactams showed antitumor activity against three human cancer cell lines<sup>31</sup>. Based on these precedents, in this work we first aimed at evaluating the antitumor activity of enantiopure compounds **24a** and **29a**. Initially, we assessed the growth inhibition percentage by a 10  $\mu$ M concentration of these compounds on a 60 tumor cell screen at the National Cancer Institute (USA). In general, both  $\beta$ -lactam derivatives showed non-selective, modest cytotoxic effects in all cell assays, with the best data for leukemia (MOLT-4 cell line), melanoma (SK-MEL-5), lung (A549), colon (COLO-5), ovarian (OVCAR-4), renal (A498) and prostate (PC-3) cancer lines.

We then measured the in vitro cytotoxic activity of **24a** and **29a** in four human tumor cell lines, namely A459 (lung), HT29 (colon), MDA-MB-231 (breast) and PSN1 (pancreas). The results are recorded in Tables 4 and S4, and compared to those of the well-known chemotherapeutic agent doxorubicin. As shown in Table 4, compound **24a** displays in vitro cytotoxic activity in the micromolar range in three out of four assayed tumor cell lines, with no activity against the MDA-MB-231 breast cell line (at 10  $\mu$ M/mL). Compared to **24a**, slightly lower potencies were measured for  $\beta$ -lactam **29a** in lung, colon and pancreas tumor cell lines, but contrastingly it displays better, although moderate, in vitro cytotoxic activity in the breast cell line. Hence, no significant influence neither of the configuration of the  $\beta$ -lactam derivative nor of the TRPM8 antagonist potency was observed on the antiproliferative activity of these compounds. In general, these activities were one order of magnitude less potent than the control doxorubicin.

Three stereoisomeric 2-KP derivatives, having different TRPM8 antagonist capacity, were also assayed for their antitumoral activity (Table 4). In this case, compound **30ab**, showing submicromolar TRPM8 antagonist activity, is only moderately active in A549 and PSN1 cell lines, with no significant cytotoxicity in the colon and breast cell lines. Compound **15ab**, with micromolar potency as TRPM8 antagonist, is only cytotoxic in the pancreas cell line, while the less potent analogue **13ab** did not show any significant antiproliferative activity. It seems that for the 2-KP series the in vitro cytotoxicity follows the same order than TRPM8 antagonist potency. The lower antitumor potential, compared to  $\beta$ -lactams, could be due either to the evaluation of diastereoisomeric mixtures in 2-KPs versus enantiopure  $\beta$ -lactams, or to the fact that the cytotoxicity of  $\beta$ -lactam derivatives is independent of the TRPM8 activity or both.

Compd.	Family	TRPM8 IC <sub>50</sub> (μM)	Lung-NSCLC	Colon	Breast	Pancreas
			A549	HT29	MDA-MB-231	PSN1
24a	β-Lactam	2.4 ± 1.2	3.29	4.16	>17.3	5.55
29a	β-Lactam	0.4 ± 1.5	5.90	7.11	12.7	6.42
13ab	2-KP	17.9 ± 1.3	>17.8	>17.8	>17.8	>17.8
15ab	2-KP	1.8 ± 1.9	>17.8	>17.8	>17.8	6.4
30ab	2-KP	0.16 ± 1.6	12.7	>17.3	>17.3	8.3
Doxorubicin.HCl	–		0.24	0.19	0.17	0.17

**Table 4.** In vitro cytotoxicity (GI<sub>50</sub>, μM) of compounds **24a** and **29a** on four human cell cancer lines.

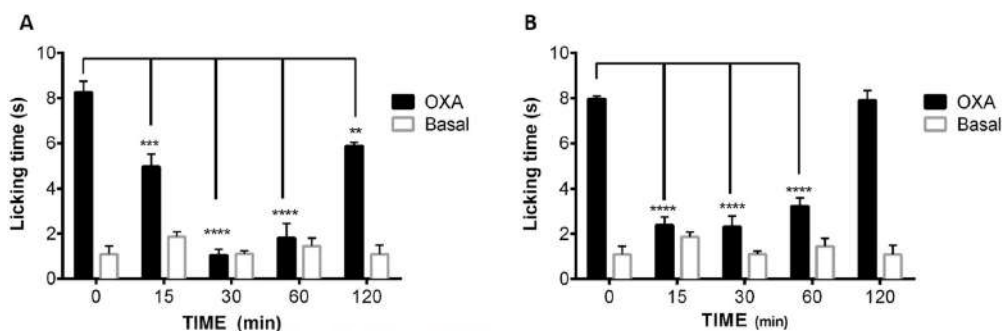


**Figure 4.** Effects of compound **24a** on the oxaliplatin-induced cold allodynia (acetone test). Male mice were treated with oxaliplatin (6 mg/Kg, ip) or vehicle on days 1, 3 and 5. Then, compound **24a** (1 μg/ipl, **A** or 3 μg/ipl, **B**) was administered to the oxaliplatin treated animals, and the time-course of cold allodynia was measured. Data are given ± SME (n = 5). \*\*P < 0.05; \*\*\*P < 0.001; \*\*\*\*P < 0.0001.

The expression of TRPM8 channels in different cancer cell lines has been scarcely studied<sup>52</sup>. To the best of our knowledge, there are no data on expression levels in A549, HT29 and PSN1 tumor cell lines, while for MDA-MB-231 the results described so far are contradictory. Thus, while the TRPM8 antagonist AMTB decreases viable cells in MDA-MB-231 breast cancer cells and TRPM8 levels are high in basal breast cancers, the TRPM8 expression does not seem very high in this and other breast cancer cell lines<sup>53</sup>. On the contrary, a work by Liu and coworkers identified high levels of channel expression in different breast cancer cell lines, including MDA-MB-231<sup>54</sup>. Because this lack of information and the controversial results, we cannot assure that the antitumor activity displayed by our compounds is partially due to a high expression of TRPM8 in the indicated cell lines or if it could be an effect totally independent of these channels.

No apparent, significant cytotoxic effects were observed for the β-lactam derivatives in HEK293 cells (up to 500 μM concentration, MTT assay).

**Antiallodynic effects in vivo.** Cold allodynia (painful sensation at cold temperatures that do not usually cause pain) and cold hyperalgesia (increased sensitivity to distressing cold temperatures) are associated to different peripheral neuropathies<sup>55</sup>. Several chemotherapeutic agents in first clinical line induce peripheral neuropathies (known as CIPN), affecting million patients worldwide and limiting the dose administered to them, as well as the quality of life of many survivors<sup>56</sup>. In oxaliplatin CIPN, the increased sensitivity to cold has been correlated to an augmented expression of TRPM8 channels, among others<sup>4–6,57</sup>. In good correlation, there are recent experimental evidences describing that TRPM8 antagonists are able to decrease oxaliplatin-induced allodynia and cold hypersensitivity<sup>34,58</sup>. According to these discoveries, we decided to explore the effects of β-lactam **24a** in an in vivo model of oxaliplatin CIPN, using acetone assay for monitoring cold allodynia. In male mice, the injection of oxaliplatin on days 1, 3 and 5 at a 6 mg/kg dose produces peripheral cold allodynia. As shown in Fig. 4, the intraplantar (i.pl.) administration of β-lactam derivative **24a** (1 μg), attenuates the cold-induced paw licking in a significant manner 15 min after administration, showing the maximum activity from 30 to 60 min. At a 3 μg dose, the antagonist activity is clearly increased at 15 min, and firmly maintained up to 60 min.

## Discussion

To search for new TRPM8 antagonist chemotypes, we explore the base-assisted cyclization of linear phenylalaninol-Phe conjugates, which afforded chiral β-lactam and/or 2-ketopiperazine (KP) heterocyclic derivatives. The regioselectivity (β-lactam versus KP) was dependent on the chloroalkyl substituent and the configuration of the linear precursor. While 2-chloroacetyl derivatives gave almost exclusively to the KP six-membered ring heterocycle, the cyclization of 2-chloropropanoyl analogues is governed by the configuration of both the

phenylalaninol-derived (2') and the 2-chloropropanoyl (2'') stereocenters. In short, 2'S,2''S and 2'R,2''R isomers provides  $\beta$ -lactams as the very major component of the reaction, while the KP heterocycle predominates after the cyclization of the 2'S,2''R diastereoisomer, and the 2'S,2''R linear precursor provides almost the same amount of the four- and six-membered heterocyclic systems. The epimerization at the C-3 stereocenter in 3-methyl- $\beta$ -lactam derivatives, not previously observed for related 2-azetidinones<sup>43</sup>, was low for 3S,4S-configured compounds and more important for 3R,4R-analogues.

Both, the phenylalaninol-Phe-derived  $\beta$ -lactams and KPs behave as new TRPM8 antagonist chemotypes, blocking the channel activation by menthol ( $\text{Ca}^{2+}$  entry assay) with micromolar or submicromolar potencies, and did not show activity at hTRPV1. Single isomer  $\beta$ -lactams **24a** and **29a** display  $\text{IC}_{50}$  values of 2.4 and 0.4  $\mu\text{M}$ , respectively, indicating that a 2'R-configuration of the phenylalaninol-derived substituent is preferred for TRPM8 antagonist activity. These antagonist activities were further confirmed using electrophysiology experiments, with Patch-clamp measurements sustaining that the 2'R diastereoisomer is slightly more potent than the corresponding 2'S isomer. In general, these phenylalaninol-Phe-derived  $\beta$ -lactams maintain significant TRPM8 blockade activity, although they showed somewhat decreased potency compared to the longer Asp-Phe analogues<sup>37</sup>. For KPs, a 1'R- and a 5R-configuration seem to favor the inhibition of TRPM8 channel activation.

Docking studies, using a homology model of rat TRPM8 channel, built on the cryo-electron microscopy structure of the TRPM8 from *Ficedula albicollis*<sup>24</sup>, propose two putative binding sites, by the pore zone, for the phenylalaninol-Phe-derived heterocyclic compounds described here. The first site involves transmembrane S5 and S6 of one channel subunit and the S5 or S6 and/or the S5-S6 segment forming the pore of one adjacent monomer, suggesting an allosteric modulation of the channel. The second most probable binding point is located at the bottom part of the pore, involving mainly hydrophobic interaction among the phenyl rings of the molecules and hydrophobic and aromatic residues of the four channel subunits, with the compound acting as a channel blocker. The sites predicted by these models of interaction differs from those proposed for tryptophan-derived antagonists<sup>33</sup>, and that from AMTB and TC-1/TRPM8 complexes solved by cryo-electron microscopy<sup>26</sup>, which adopt different poses within the channel, but all around the menthol-binding pocket (delineated by the lower half of the TM4-TM5 helices and the TRP domain)<sup>25</sup>. The larger volume of our molecules could be behind this different behaviour.

TRPM8 channels are overexpressed in a number of tumors, like prostate, melanoma, lung and colon adenocarcinomas, and some TRPM8 antagonists demonstrated good antitumor activity<sup>32,48,49</sup>. Interestingly, enantiopure  $\beta$ -lactams **24a** and **29a** exhibited non-selective antitumor activity in different tumor cell lines, showing micromolar potency in four of them, while 2-KP regioisomeric compounds displayed lower antitumor activity. No direct correlation between TRPM8 antagonist and antitumor activity could be established. Abnormalities in TRPM8 expression was also found in models of chemotherapy-induced peripheral neuropathy<sup>57</sup>. To evaluate the usefulness of this family of compounds in relieving persistent pain associated to antineoplastic agents, we evaluated  $\beta$ -lactam **24a** in a mice model of oxaliplatin-induced peripheral neuropathy. Compound **24a** demonstrated significant antiallodynic effects in vivo, with maximum activity from 30 to 60 min. Compared to literature reported results, the antiallodynic activity of compound **24a** seems superior or comparable to that of other described TRPM8 antagonists. Thus, its potency is higher than that of a described spirochromene derivative<sup>59</sup>, and seems to span longer than that of a Trp-OMe derivative, which showed more potent antagonist activity at the  $\text{Ca}^{2+}$  assay than **24a**<sup>34</sup>. At 1  $\mu\text{g}$  i.p.l.,  $\beta$ -lactam derivative **24a** showed slightly lower potency and similar duration of action than a biphenyl amide TRPM8 antagonist recently reported<sup>60</sup>.

In conclusion, the two phenylalaninol-Phe-derived heterocyclic systems, highly functionalized  $\beta$ -lactam and/or 2-ketopiperazine, allow the identification of new hits for TRPM8 modulation. Therefore, these two new chemotypes could constitute the starting point for further modifications on the road to improved compounds for future therapeutic applications in both pain and cancer.

## Experimental section

**Chemistry.** Preparation of synthetic intermediates, their characterization and that of most final compounds are detailed in Supplementary Information.

**Cyclization reactions.** BTTP (2.4 mmol, 0.75 mL), or BEMP (2.4 mmol, 0.69 mL) or  $\text{Cs}_2\text{CO}_3$  (3.2 mmol, 1.04 g) was added to a solution of the corresponding *N*-alkyl-*N*-chloroacetyl- or *N*-alkyl-*N*-chloropropanoyl-Xaa derivative (1.6 mmol) in dry  $\text{CH}_3\text{CN}$  (4 mL), under Ar atmosphere. The reaction mixture was stirred until consumption of the starting material. Then, the solvent was removed and the residue was extracted with EtOAc, and washed with 0.1 M HCl,  $\text{H}_2\text{O}$  and brine, successively. Finally, the organic phase was dried over  $\text{Na}_2\text{SO}_4$ , filtered, and concentrated. The resulting residue was purified by flash chromatography on silica gel, using the eluent indicated in each case.

**4S-Benzyl-4-benzyloxycarbonyl-3S-methyl-1-[(2'S-benzyloxycarbonylamino-3'-phenyl)prop-1'-yl]-2-oxoazetidine (24a).** Syrup. Yield: 65% (from 22, B: BTTP). Eluent: EtOAc:Hexane (1:2). HPLC:  $t_{\text{R}} = 16.20$  min (gradient of 30% to 95% of A, in 20 min).  $[\alpha]_{\text{D}} = -35.04$  (c 1,  $\text{CHCl}_3$ ). Isomer ratio M(3S,4S,2'S):m(3R,4S,2'S) = 97:3.  $^1\text{H}$  NMR (400 MHz,  $\text{CDCl}_3$ ):  $\delta$  7.35–6.96 (m, 20H, Ar), 5.75 (d, 1H,  $J = 7.4$  Hz, 2-NH), 5.24 (d, 1H,  $J = 12.0$  Hz,  $\text{OCH}_2$ ), 5.14 (d, 1H,  $J = 12.0$  Hz,  $\text{OCH}_2$ ), 5.05 (s, 2H,  $\text{OCH}_2$ ), 4.17 (m, 1H, 2'-H), 3.43 (d, 1H,  $J = 14.5$  Hz, 4- $\text{CH}_2$ ), 3.23 (dd, 1H,  $J = 14.5, 8.0$ , 1'-H), 3.11 (q, 1H,  $J = 7.6$  Hz, 3-H), 3.05 (d, 1H,  $J = 14.5$  Hz, 4- $\text{CH}_2$ ), 3.00 (dd, 1H,  $J = 14.5, 4.0$  Hz, 1'-H), 2.86 (dd, 1H,  $J = 14.0, 8.0$  Hz, 3'-H), 2.72 (dd, 1H,  $J = 14.0, 7.0$  Hz, 3'-H), 1.08 (d, 3H,  $J = 7.5$  Hz, 3- $\text{CH}_3$ ).  $^{13}\text{C}$  NMR (75 MHz,  $\text{CDCl}_3$ ):  $\delta$  171.0 (COO), 170.6 (C2), 156.0 (OCON), 137.8, 137.0, 134.9, 134.8, 129.7, 129.2, 128.9, 128.85, 128.8, 128.7, 128.5, 128.45, 127.9, 127.8, 127.5, 126.5 (Ar),

68.7 (C4), 67.7, 66.3 (OCH<sub>2</sub>), 53.8 (C3), 51.9 (C2'), 46.1 (C1'), 40.7 (4-CH<sub>2</sub>), 39.1 (C3'), 10.6 (3-CH<sub>3</sub>). MS (ES)<sup>+</sup>: 577.3 [M + H]<sup>+</sup>. Exact Mass calculated for C<sub>36</sub>H<sub>36</sub>N<sub>2</sub>O<sub>5</sub>: 576.26242; found: 576.26457.

**4S-Benzyl-4-benzoyloxycarbonyl-3S-methyl-1-[(2'R-benzoyloxycarbonylamino-3'-phenyl)prop-1'-yl]-2-oxoazetidine (29a).** Syrup. Yield: 39% (from 27, B: BTTP). Eluent: EtOAc:Hexane (1:3). HPLC: t<sub>R</sub> = 16.36 min (gradient of 30% to 95% of A, in 20 min). [α]<sub>D</sub><sup>20</sup> = -72.67 (c 1, CHCl<sub>3</sub>). Isomer ratio M(3S,4S,2'R):m(3R,4S,2'R) = 97:3. <sup>1</sup>H NMR (400 MHz, CDCl<sub>3</sub>): δ 7.37–6.99 (m, 20H, Ar), 5.83 (d, 1H, J = 8.1 Hz, 2-NH), 5.27 (d, 1H, J = 12.0 Hz, OCH<sub>2</sub>), 5.17 (d, 1H, J = 12.0 Hz, OCH<sub>2</sub>), 5.05 (s, 2H, OCH<sub>2</sub>), 4.07 (m, 1H, 2'-H), 3.56 (d, 1H, J = 14.5 Hz, 4-CH<sub>2</sub>), 3.43 (q, 1H, J = 7.6 Hz, 3-H), 3.03 (d, 1H, J = 14.5 Hz, 4-CH<sub>2</sub>), 2.99 (m, 2H, 1'-H), 2.71 (dd, 1H, J = 13.5, 7.4 Hz, 3'-H), 2.64 (dd, 1H, J = 13.4, 6.6 Hz, 3'-H), 1.08 (d, 3H, J = 7.5 Hz, 3-CH<sub>3</sub>). <sup>13</sup>C NMR (100 MHz, CDCl<sub>3</sub>): δ 171.3 (COO), 170.3 (C2), 156.3 (OCON), 137.5, 135.1, 134.8, 129.7, 129.5, 129.2, 129.0, 128.9, 128.8, 128.7, 128.5, 128.4, 127.9, 127.5, 126.5 (Ar), 69.0 (C4), 67.8, 66.3 (OCH<sub>2</sub>), 54.1 (C3), 51.6 (C2'), 47.0 (C1'), 41.2 (4-CH<sub>2</sub>), 39.3 (C3'), 10.6 (3-CH<sub>3</sub>). MS (ES)<sup>+</sup>: 577.25 [M + H]<sup>+</sup>. Exact Mass calculated for C<sub>36</sub>H<sub>36</sub>N<sub>2</sub>O<sub>5</sub>: 576.26242; found: 576.26248.

**Functional assays by calcium microfluorimetry.** Human embryonic kidney cell line (HEK) stably transfected with rTRPM8 or h-TRPV1 were used as previously described<sup>37</sup>. Briefly, cells were seeded in 96-well plates at a cell density of 30,000 cells 2 days before treatment. Buffer used was HBBS (in mM): 138 NaCl, 5.33 KCl, 1.26 CaCl<sub>2</sub>, 0.5 MgCl-6H<sub>2</sub>O, 0.4 MgSO<sub>4</sub>-7H<sub>2</sub>O, 4 NaHCO<sub>3</sub> 0.44 KH<sub>2</sub>PO<sub>4</sub>, 0.3 Na<sub>2</sub>HPO<sub>4</sub>, pH 7.4. The day of treatment the medium was replaced with 100 μL of the dye loading solution Fluo-4 NW supplemented with probenecid 2.5 mM. After incubation, plates were transferred to a fluorescence plate reader (Polastar BMG). In the experimental protocol, the baseline fluorescence was recorded (Em 485 nm/Ex 520 nm) for 3 cycles. After, vehicle, compound at different concentrations and the corresponding antagonist, 10 μM AMTB for TRPM8 or 10 μM Ruthenium Red for TRPV1 were added to the well. Fluorescence intensity was recorded during 7 cycles more. Finally, the agonist 100 μM menthol for TRPM8 or 1 μM capsaicin for TRPV1 was added and fluorescence intensity was recorded during 10 cycles more.

**Data analysis.** The degree of inhibition of TRPM8 channel gating was calculated by comparison to calcium increase signal elicited by test substances and menthol at 100 μM. Decrease of menthol signal was expressed as percentage of inhibition (%). All data are expressed as mean ± standard deviation (SD). Each condition was assessed by triplicate (n = 3) in 3 independent experiments (N = 3). Z-factor was calculated in each assay using the following equation: (3\*(SDmax + SDmin))/(Mean max-Mean min). In all the experiments Z-factor was ≥ 0.5. To calculate IC<sub>50</sub>, normalized responses (%) versus log [μM] were adjusted to a non-linear fit with variable slope, a four-parameter dose-response curve following curve  $Y = 100 / (1 + 10^{((\text{Log IC}_{50} - X) * \text{HillSlope}))}$  where X = % normalized response and Y = log [μM].

**Functional assays by Patch-clamp electrophysiology.** Electrophysiological recording was carried out 1–3 days after cells seeded. Membrane currents and voltages were recorded by patch clamp using the whole-cell configuration. For whole-cell recordings of HEK-rTRPM8 cells<sup>37</sup>, pipette solution contained (in mM) 150 NaCl, 5 EGTA, 3 MgCl<sub>2</sub> and 10 HEPES, adjusted to pH 7.2 with NaOH, and bath solution contained (in mM) 150 NaCl, 6 CsCl, 1.5 CaCl<sub>2</sub>, 1 MgCl<sub>2</sub>, 10 D-glucose and 10 HEPES, adjusted to pH 7.4 with NaOH. Data were sampled at 10 kHz (EPC10 amplifier with PatchMaster 2.53 software, HEKA Electronics, Lambrecht, Germany) and low-pass filtered at 3 kHz for analysis (PatchMaster 2.53 and GraphPad Prism 5, Graphpad Software, USA). The series resistance was < 10 MΩ and to minimize voltage errors was compensated to 60–80%. All measurements were performed at 24–25 °C. The TRPM8 response was quantified as the ratio P2/P1, being P2 the second menthol pulse in the presence of the vehicle or antagonist tested, and P1 refers to the first menthol pulse. This paradigm considers the extend of receptor desensitization as the P2/P1 obtained with the vehicle. Thus, the estimated IC50 values are corrected from receptor desensitization.

**Docking Studies.** The molecular model for rat TRPM8 was obtained using the structure of the TRPM8 from *Ficedula albicollis* determined by cryo-electron microscopy at 4.01 resolution<sup>24</sup>. First, the missing loops in the structure from *Ficedula albicollis* was completed by using Yasara<sup>44,61</sup>. Second, the rat TRPM8 sequence (Uniprot Q8R455) was modeled on completed *Ficedula a.* structure, although the N-term (44–719) and C-term (1,031–1,104) were removed for docking. The homology modelling was performed with the standard homology modelling protocol implemented in Yasara (version 19.9.17)<sup>44,45</sup>. Sequence alignment between rat and *Ficedula a.* TRPM8 was performed with ClustalO<sup>62</sup>, from the European Bioinformatic Institute (EBI, <https://www.ebi.ac.uk>). The visualization and edition of the molecules were also done with Yasara (<https://www.yasara.org>). Figures were drawn with open source Pymol (The PyMOL Molecular Graphics System, Version 1.8 Schrödinger, LLC) at <https://www.pymol.org>.

The global docking procedure was accomplished with AutoDock<sup>46</sup>, implemented in Yasara, in which a total of 800 flexible docking runs were set and clustered around the putative binding sites. The program then performed a simulated annealing optimization of the complexes, which moved the structure to a nearby stable energy minimum, by using the implemented Assisted Model Building with Energy Refinement (AMBER03) force field<sup>63</sup>. The Yasara pH command was set to 7.0, to ensure that molecules preserved their pH dependency of bond orders and protonation patterns. The best binding energy complex in each cluster was stored, analyzed, and used to select the best orientation of the interacting partners.

**Antitumor activity.** *Cell lines.* Human tumor cell lines used in this study were purchased from the ATCC. A-549 (CCL-185), lung carcinoma; HT-29 (HTB-38), colorectal adenocarcinoma; MDA-MB-231 (HTB-26), breast adenocarcinoma; PSN1, pancreas adenocarcinoma.

*Cell culture.* All cell lines were maintained in DMEM (Dulbecco's Modified Eagle's Medium) culture medium supplemented with 10% FBS (Fetal Bovine Serum), 100 Units/mL penicillin/streptomycin at 37 °C, 5% CO<sub>2</sub> and 95% humidity.

*Cytotoxicity Assay.* Triplicate cultures were incubated for 72 h in the presence or absence of test compounds in dose–response curves (10 concentrations, typically ranging from 10 to 0.0026 µg/mL). A colorimetric assay using sulforhodamine B (SRB) was adapted for quantitative measurement of cell growth and cytotoxicity<sup>27</sup>. A more detailed information on this assay is provided in the supplementary information. GI<sub>50</sub> is the compound concentration that produces 50% inhibition on cell growth as compared to control cells.

**In vivo anti-allodynic effects.** Male C57-mice (≈30 g) (Harlam, Holland) were used for the study. All experiments were approved by the Institutional Animal and Ethical Committee of the Universidad Miguel Hernandez where experiments were conducted and they were in accordance with the guidelines of the Economic European Community and the Committee for Research and Ethical Issues of the International Association for the Study of Pain. All parts of the study concerning animal care were performed under the control of veterinarians.

As previously described<sup>34</sup>, oxaliplatin (Tocris) was dissolved in water with gentle warming and was subcutaneously (s.c.) injected on days 1, 3 and 5 at a 6 mg/kg dose. The day 7 after administration, experiments were performed. Together with Oxaliplatin injection, saline and a 5% Mannitol solution were intraperitoneally injected to prevent kidney damage and dehydration. The compound 24a stock was prepared in DMSO (Sigma-Aldrich) and diluted in saline for injections. Compound at different doses (1 to 3 µg) was injected into the plantar surface (25 µL) of the right hind paw of mice. Cold chemical thermal sensitivity was assessed using acetone drop method. Mice were placed in a metal mesh cage and allowed to habituate for approximately 30 min in order to acclimatize them. Freshly dispensed acetone drop (10 µL) was applied gently on to the mid plantar surface of the hind paw. Cold chemical sensitive reaction with respect to paw licking was recorded as a positive response (nociceptive pain response). The responses were measured for 20-s with a digital stopwatch. For each measurement, the paw was sampled twice and the mean was calculated. The interval between each application of acetone was approximately 5 min.

### Data availability

The datasets generated during and/or analyzed during the current study are available from the corresponding author on reasonable request.

Received: 13 May 2020; Accepted: 3 August 2020

Published online: 25 August 2020

### References

- Almaraz, L., Manenschi, J.-A., de la Peña, E. & Viana, F. *Mammalian Transient Receptor Potential (TRP) Cation Channels* (Springer-Verlag, Berlin, 2014).
- Mizoguchi, S., Andoh, T., Yakura, T. & Kuraishi, Y. Involvement of c-Myc-mediated transient receptor potential melastatin 8 expression in oxaliplatin-induced cold allodynia in mice. *Pharmacol. Rep.* **68**, 645–648 (2016).
- Yee, N. S. Roles of TRPM8 Ion Channels in Cancer: Proliferation, Survival, and Invasion. *Cancers (Basel)*. **7**, 2134–2146 (2015).
- Gauchan, P., Andoh, T., Kato, A. & Kuraishi, Y. Involvement of increased expression of transient receptor potential melastatin 8 in oxaliplatin-induced cold allodynia in mice. *Neurosci. Lett.* **458**, 93–95 (2009).
- Ling, B. *et al.* Behavioral and immunohistological assessment of painful neuropathy induced by a single oxaliplatin injection in the rat. *Toxicology* **234**, 176–184 (2007).
- Ling, B., Authier, N., Balayssac, D., Eschalier, A. & Coudore, F. Behavioral and pharmacological description of oxaliplatin-induced painful neuropathy in rat. *Pain* **128**, 225–234 (2007).
- Weyer, A. & Lehto, S. Development of TRPM8 antagonists to treat chronic pain and migraine. *Pharmaceuticals*. **10**, E37. <https://doi.org/10.3390/ph10020037> (2017).
- Bigal, M. E. *et al.* Safety, tolerability, and efficacy of TEV-48125 for preventive treatment of high-frequency episodic migraine: a multicentre, randomised, double-blind, placebo-controlled, phase 2b study. *Lancet Neurol.* **14**, 1081–1090 (2015).
- Fu, X. *et al.* Association between PRDM16, MEF2D, TRPM8, LRP1 gene polymorphisms and migraine susceptibility in the She ethnic population in China. *Clin. Invest. Med.* **42**, E21–E30 (2019).
- Kaur, S., Ali, A., Ahmad, U., Pandey, A. K. & Singh, B. rs2651899 variant is associated with risk for migraine without aura from North Indian population. *Mol. Biol. Rep.* **46**, 1247–1255 (2019).
- Kayama, Y. *et al.* Functional interactions between transient receptor potential M8 and transient receptor potential V1 in the trigeminal system: Relevance to migraine pathophysiology. *Cephalalgia* **38**, 833–845 (2018).
- Noyer, L. *et al.* TRPM8 and prostate: a cold case?. *Pflugers Arch.* **470**, 1419–1429 (2018).
- Cucu, D. *et al.* Characterization of functional transient receptor potential melastatin 8 channels in human pancreatic ductal adenocarcinoma cells. *Pancreas (Philadelphia, PA, United States)* **43**, 795–800 (2014).
- Pan, Y. *et al.* Relevance of TRPA1 and TRPM8 channels as vascular sensors of cold in the cutaneous microvasculature. *Pflugers Arch. Eur. J. Physiol.* **470**, 779–786 (2018).
- Sabnis, A. S. Expression and characterization of the TRPM8 receptor in lung epithelial cells. **39**, 466–474 (2008).
- Yu, W., Hill, W. G., Apodaca, G. & Zeidel, M. L. Expression and distribution of transient receptor potential (TRP) channels in bladder epithelium. *Am. J. Physiol.* **300**, F49–F59 (2011).
- Prevarskaya, N., Zhang, L. & Barritt, G. TRP channels in cancer. *Biochim. Biophys. Acta* **1772**, 937–946 (2007).

18. Xiao, N. *et al.* Over-expression of TRPM8 is associated with poor prognosis in urothelial carcinoma of bladder. *Tumor Biol.* **35**, 11499–11504 (2014).
19. Yee, N. S. *et al.* Aberrantly over-expressed TRPM8 channels in pancreatic adenocarcinoma: correlation with tumor size/stage and requirement for cancer cells invasion. *Cells* **3**, 500–516 (2014).
20. Yee, N. S., Zhou, W. & Lee, M. Transient receptor potential channel TRPM8 is over-expressed and required for cellular proliferation in pancreatic adenocarcinoma. *Cancer Lett.* **297**, 49–55 (2010).
21. Bao, L. *et al.* Apoptosis-inducing effects of lentinan on the proliferation of human bladder cancer T24 cells. *Pak. J. Pharm. Sci.* **28**, 1595–1600 (2015).
22. Genova, T. *et al.* TRPM8 inhibits endothelial cell migration via a nonchannel function by trapping the small GTPase Rap1. *J. Cell Biol.* **216**, 2107–2130 (2017).
23. Ordas, P. *et al.* Expression of the cold thermoreceptor TRPM8 in rodent brain thermoregulatory circuits. *J. Comp. Neurol.* **1**, 23. <https://doi.org/10.1002/cne.24694> (2019).
24. Yin, Y. *et al.* Structure of the cold- and menthol-sensing ion channel TRPM8. *Science* **359**, 237–241 (2018).
25. Yin, Y. *et al.* Structural basis of cooling agent and lipid sensing by the cold-activated TRPM8 channel. *Science* **363**, eaav9334. <https://doi.org/10.1126/science.aav9334> (2019).
26. Diver, M. M., Cheng, Y. & Julius, D. Structural insights into TRPM8 inhibition and desensitization. *Science* **365**, 1434–1440 (2019).
27. Pérez De Vega, M. J., Gómez-Monterrey, I., Ferrer-Montiel, A. & González-Muñiz, R. Transient receptor potential melastatin 8 channel (TRPM8) modulation: cool entryway for treating pain and cancer. *J. Med. Chem.* **59**, 10006–10029 (2016).
28. Voets, T., Vriens, J. & Vennekens, R. Targeting TRP channels: valuable alternatives to combat pain, lower urinary tract disorders, and type 2 diabetes?. *Trends Pharmacol. Sci.* **40**, 669–683 (2019).
29. González-Muñiz, R., Bonache, M. A., Martín-Escura, C. & Gómez-Monterrey, I. Recent progress in TRPM8 modulation: an update. *Int. J. Mol. Sci.* **20**, E1628. <https://doi.org/10.3390/ijms20112618> (2019).
30. Arcas, J. M. *et al.* The Immunosuppressant macrolide tacrolimus activates cold-sensing TRPM8 channels. *J. Neurosci.* **39**, 949–969 (2019).
31. Legay, C. M. *et al.* Natural-product-derived transient receptor potential melastatin 8 (TRPM8) channel modulators. *Org. Lett.* **18**, 2746–2749 (2016).
32. De Petrocellis, L. *et al.* Tetrahydroisoquinoline-derived urea and 2,5-diketopiperazine derivatives as selective antagonists of the transient receptor potential melastatin 8 (TRPM8) channel receptor and antiprostata cancer agents. *J. Med. Chem.* **59**, 5661–5683 (2016).
33. Horne, D. B. *et al.* Discovery of TRPM8 Antagonist (S)-6-(((3-Fluoro-4-(trifluoromethoxy)phenyl)(3-fluoropyridin-2-yl)methyl) carbamoyl)nicotinic Acid (AMG 333), a Clinical Candidate for the Treatment of Migraine. *J. Med. Chem.* **61**, 8186–8201 (2018).
34. Bertamino, A. *et al.* Identification of a potent tryptophan-based TRPM8 antagonist with in vivo analgesic activity. *J. Med. Chem.* **61**, 6140–6152 (2018).
35. Beccari, A. R. *et al.* Novel selective, potent naphthyl TRPM8 antagonists identified through a combined ligand-and structure-based virtual screening approach. *Sci. Rep.* **7**, 10999. <https://doi.org/10.1038/s41598-017-11194-0> (2017).
36. Andrews, M. D. *et al.* Discovery of a selective TRPM8 antagonist with clinical efficacy in cold-related pain. *ACS Med. Chem. Lett.* **6**, 419–424 (2015).
37. de la Torre-Martínez, R. *et al.* Synthesis, high-throughput screening and pharmacological characterization of  $\beta$ -lactam derivatives as TRPM8 antagonists. *Sci. Rep.* **7**, 10766. <https://doi.org/10.1038/s41598-017-10913-x> (2017).
38. Cherney, R. J. & Wang, L. Efficient Mitsunobu Reactions with N-Phenylfluorenyl or N-Trityl Serine Esters. *J. Org. Chem.* **61**, 2544–2546 (1996).
39. Gerona-Navarro, G., Bonache, M. A., Herranz, R., García-López, M. T. & González-Muñiz, R. Entry to new conformationally constrained amino acids. First synthesis of 3-unsubstituted 4-alkyl-4-carboxy-2-azetidione derivatives via an intramolecular Na-Ca-cyclization strategy. *J. Org. Chem.* **66**, 3538–3547 (2001).
40. Fournie-Zaluski, M. C., Lucas-Soroca, E., Devin, J. & Roques, B. P. Proton NMR configurational correlation for retro-inverso dipeptides: application to the determination of the absolute configuration of 'enkephalinase' inhibitors. Relationships between stereochemistry and enzyme recognition. *J. Med. Chem.* **29**, 751–757 (1986).
41. Bonache, M. A. *et al.* Memory of chirality in the enantioselective synthesis of  $\beta$ -lactams derived from amino acids Influence of the reaction conditions. *Synlett* **7**, 1007–1011 (2003).
42. Bonache, M. A. *et al.* Memory of chirality in the stereoselective synthesis of  $\beta$ -lactams: importance of the starting amino acid derivative. *Tetrahedron Asymmetry* **14**, 2161–2169 (2003).
43. Perez-Faginas, P. *et al.* Exceptional stereoselectivity in the synthesis of 1,3,4-trisubstituted 4-Carboxy  $\beta$ -lactam derivatives from amino acids. *Org. Lett.* **9**, 1593–1596 (2007).
44. Krieger, E., Darden, T., Nabuurs, S. B., Finkelstein, A. & Vriend, G. Making optimal use of empirical energy functions: Force-field parameterization in crystal space. *Proteins Struct. Funct. Bioinforma.* **57**, 678–683 (2004).
45. Krieger, E., Koraimann, G. & Vriend, G. Increasing the precision of comparative models with yasara NOVA-a self-parameterizing force field. *Proteins Struct. Funct. Genet.* **47**, 393–402 (2002).
46. Morris, G. M. *et al.* AutoDock4 and AutoDockTools4: automated docking with selective receptor flexibility. *J. Comput. Chem.* **30**, 2785–2791 (2009).
47. Wong, K. K., Banham, A. H., Yaacob, N. S. & Nur Husna, S. M. The oncogenic roles of TRPM ion channels in cancer. *J. Cell. Physiol.* **234**, 14556–14573 (2019).
48. Liu, T. *et al.* Anti-tumor activity of the TRPM8 inhibitor BCTC in prostate cancer DU145 cells. *Oncol. Lett.* **11**, 182–188 (2016).
49. Borrelli, F. *et al.* Colon carcinogenesis is inhibited by the TRPM8 antagonist cannabigerol, a Cannabis derived non-psychoactive cannabinoid. *Carcinogenesis* **35**, 2787–2797 (2014).
50. Okamoto, Y., Ohkubo, T., Ikebe, T. & Yamazaki, J. Blockade of TRPM8 activity reduces the invasion potential of oral squamous carcinoma cell lines. *Int. J. Oncol.* **40**, 1431–1440 (2012).
51. Pérez-Faginas, P. *et al.* Optically active 1,3,4,4-tetrasubstituted  $\beta$ -lactams: Synthesis and evaluation as tumor cell growth inhibitors. *Eur. J. Med. Chem.* **46**, 5108–5119 (2011).
52. Hantute-Ghesquier, A., Haustrate, A., Prevarskaya, N. & Lehen'kyi, V. TRPM family channels in cancer. *Pharmaceuticals* **11**, 1–14 (2018).
53. Yapa, K. T. D. S. *et al.* Assessment of the TRPM8 inhibitor AMTB in breast cancer cells and its identification as an inhibitor of voltage gated sodium channels. *Life Sci.* **198**, 128–135 (2018).
54. Liu, J. *et al.* TRPM8 promotes aggressiveness of breast cancer cells by regulating EMT via activating AKT/GSK-3 pathway. *Tumor Biol.* **35**, 8969–8977 (2014).
55. Jensen, T. S. & Finnerup, N. B. Allodynia and hyperalgesia in neuropathic pain: clinical manifestations and mechanisms. *Lancet. Neurol.* **13**, 924–935 (2014).
56. Zajaczkowska, R. *et al.* Mechanisms of chemotherapy-induced peripheral neuropathy. *Int. J. Mol. Sci.* **20**, E1451. <https://doi.org/10.3390/ijms20061451> (2019).
57. Naziroglu, M. & Braidy, N. Thermo-sensitive TRP channels: novel targets for treating chemotherapy-induced peripheral pain. *Front. Physiol.* **8**, 1040. <https://doi.org/10.3389/fphys.2017.01040> (2017).

58. Cao, S. *et al.* Intrathecal TRPM8 blocking attenuates cold hyperalgesia via PKC and NF- $\kappa$ B signaling in the dorsal root ganglion of rats with neuropathic pain. *J. Pain Res.* **12**, 1287–1296 (2019).
59. Chaudhari, S. S. *et al.* Synthesis and pharmacological evaluation of novel N-aryl-3,4-dihydro-1'H-spiro[chromene-2,4'-piperidine]-1'-carboxamides as TRPM8 antagonists. *Bioorg. Med. Chem.* **21**, 6542–6553 (2013).
60. Journigan, V. B. *et al.* Structure-based design of novel biphenyl amide antagonists of human transient receptor potential cation channel subfamily m member 8 channels with potential implications in the treatment of sensory neuropathies. *ACS Chem. Neurosci.* **11**, 268–290 (2020).
61. Canutescu, A. A. & Dunbrack, R. L. J. Cyclic coordinate descent: A robotics algorithm for protein loop closure. *Protein Sci.* **12**, 963–972 (2003).
62. Sievers, F. *et al.* Fast, scalable generation of high-quality protein multiple sequence alignments using Clustal Omega. *Mol. Syst. Biol.* **7**, 539. <https://doi.org/10.1038/msb.2011.75> (2011).
63. Duan, Y. *et al.* A point-charge force field for molecular mechanics simulations of proteins based on condensed-phase quantum mechanical calculations. *J. Comput. Chem.* **24**, 1999–2012 (2003).

## Acknowledgements

This work was supported by the Spanish Ministerio de Ciencia y Universidades (MICYU-FEDER, RTI2018-097189-C2-1 and RTI2018-097189-C2-2), Comunidad de Madrid (IND2017/BMD7673) and the Spanish National Research Council (CSIC, 201980E030). We acknowledge the invaluable technical assistance of Jessy Medina (involved in the purification & characterization of some compounds).

## Author contributions

Idea: R.G.M.; Synthesis and characterization: M.A.B., C.M.E.; In vitro activity at TRPs: R.T.M., A.M., A.F.C.; Antitumor activity: C.C., A.F.; In vivo activity: S.G.R.; Modeling: R.T.M., G.F.B.; Supervision: A.M.R., A.F.M., A.F.C., R.G.M. This article has been written through the contribution of all authors, which have approved the final version.

## Competing interests

The authors declare no competing interests.

## Additional information

**Supplementary information** is available for this paper at <https://doi.org/10.1038/s41598-020-70691-x>.

**Correspondence** and requests for materials should be addressed to A.F.-C. or R.G.-M.

**Reprints and permissions information** is available at [www.nature.com/reprints](http://www.nature.com/reprints).

**Publisher's note** Springer Nature remains neutral with regard to jurisdictional claims in published maps and institutional affiliations.



**Open Access** This article is licensed under a Creative Commons Attribution 4.0 International License, which permits use, sharing, adaptation, distribution and reproduction in any medium or format, as long as you give appropriate credit to the original author(s) and the source, provide a link to the Creative Commons license, and indicate if changes were made. The images or other third party material in this article are included in the article's Creative Commons license, unless indicated otherwise in a credit line to the material. If material is not included in the article's Creative Commons license and your intended use is not permitted by statutory regulation or exceeds the permitted use, you will need to obtain permission directly from the copyright holder. To view a copy of this license, visit <http://creativecommons.org/licenses/by/4.0/>.

© The Author(s) 2020



**ANEXO II. Publicación 2 del capítulo 1*****Phenylalanine-Derived  $\beta$ -Lactam Trpm8 Modulators. Configuration Effect on the Antagonist Activity.***

María Ángeles Bonache<sup>1</sup>, Pedro Juan Llabrés<sup>1</sup>, Cristina Martín-Escura<sup>1,2</sup>, Roberto De la Torre-Martínez<sup>3</sup>, Alicia Medina-Peris<sup>3</sup>, Laura Butrón<sup>3</sup>, Isabel Gómez-Monterrey<sup>4</sup>, Ana María Roa<sup>2</sup>, Gregorio Fernández-Ballester<sup>3</sup>, Antonio Ferrer-Montiel<sup>3</sup>, Asia Fernández-Carvajal<sup>3</sup> y Rosario González-Muñiz<sup>1</sup>.

<sup>1</sup>Instituto de Química Médica (IQM-CSIC), Juan de la Cierva 3, 28006 Madrid, España.

<sup>2</sup>Alodia Farmacéutica SL, Santiago Grisolia 2, Tres Cantos, 28760 Madrid, España.

<sup>3</sup>IDI BE, Universidad Miguel Hernández, Avda. de la Universidad s/n, 03202 Elche, España.

<sup>4</sup>Departamento de Farmacia, Universidad Federico II de Napoles, 80131 Napoles, Italia.

International Journal of Molecular Sciences 2021, 22 (5), 1–22.

<https://doi.org/10.3390/ijms22052370>

(Q1; Factor de Impacto: 6.208)





Article

# Phenylalanine-Derived $\beta$ -Lactam TRPM8 Modulators. Configuration Effect on the Antagonist Activity

María Ángeles Bonache <sup>1</sup>, Pedro Juan Llabrés <sup>1</sup>, Cristina Martín-Escura <sup>1,2</sup>, Roberto De la Torre-Martínez <sup>3</sup>, Alicia Medina-Peris <sup>3</sup>, Laura Butrón <sup>3</sup>, Isabel Gómez-Monterrey <sup>4</sup>, Ana María Roa <sup>2</sup>, Gregorio Fernández-Ballester <sup>3</sup>, Antonio Ferrer-Montiel <sup>3</sup>, Asia Fernández-Carvajal <sup>3</sup> and Rosario González-Muñiz <sup>1,\*</sup>

<sup>1</sup> Instituto de Química Médica (IQM-CSIC), Juan de la Cierva 3, 28006 Madrid, Spain; angelesbonache@iqm.csic.es (M.Á.B.); pedrojuan637@gmail.com (P.J.L.); cristinamartinescura@gmail.com (C.M.-E.)

<sup>2</sup> Alodia Farmacéutica SL, Santiago Grisolia 2, 28760 Tres Cantos, Madrid, Spain; ana.maria.roa.arranz@gmail.com

<sup>3</sup> IDiBE, Universidad Miguel Hernández, Avda. de la Universidad s/n, 03202 Elche, Spain; rober.dltm@gmail.com (R.D.I.T.-M.); mepeas8@gmail.com (A.M.-P.); lbutron@umh.es (L.B.); gregorio@umh.es (G.F.-B.); aferrer@umh.es (A.F.-M.); asia.fernandez@umh.es (A.F.-C.)

<sup>4</sup> Department of Pharmacy, University Federico II of Naples, 80131 Naples, Italy; imgomez@unina.it

\* Correspondence: iqmg313@iqm.csic.es; Tel.: +34-912587434

**Citation:** Bonache, M.Á.; Llabrés, P.J.; Mart, C.; De la Torre-Mart, R.; Medina-Peris, A.; Butrón, L.; Gómez-Monterrey, I.; Mar, A.; Fern, G.; Ferrer-Montiel, A.; et al. Phenylalanine-Derived  $\beta$ -Lactam TRPM8 Modulators. Configuration Effect on the Antagonist Activity.

*Int. J. Mol. Sci.* **2021**, *22*, 2370.

<https://doi.org/10.3390/ijms22052370>

Academic Editor: Ludmilla A. Morozova-Roche

Received: 15 December 2020

Accepted: 23 February 2021

Published: 27 February 2021

**Publisher's Note:** MDPI stays neutral with regard to jurisdictional claims in published maps and institutional affiliations.



**Copyright:** © 2021 by the authors. Licensee MDPI, Basel, Switzerland. This article is an open access article distributed under the terms and conditions of the Creative Commons Attribution (CC BY) license (<http://creativecommons.org/licenses/by/4.0/>).

**Abstract:** Transient receptor potential cation channel subfamily M member 8 (TRPM8) is a Ca<sup>2+</sup> non-selective ion channel implicated in a variety of pathological conditions, including cancer, inflammatory and neuropathic pain. In previous works we identified a family of chiral, highly hydrophobic  $\beta$ -lactam derivatives, and began to intuit a possible effect of the stereogenic centers on the antagonist activity. To investigate the influence of configuration on the TRPM8 antagonist properties, here we prepare and characterize four possible diastereoisomeric derivatives of 4-benzyl-1-[(3'-phenyl-2'-dibenzylamino)prop-1'-yl]-4-benzoyloxycarbonyl-3-methyl-2-oxoazetidone. In microfluorography assays, all isomers were able to reduce the menthol-induced cell Ca<sup>2+</sup> entry to larger or lesser extent. Potency follows the order 3*R*,4*R*,2'*R* > 3*S*,4*S*,2'*R*  $\approx$  3*R*,4*R*,2'*S* > 3*S*,4*S*,2'*S*, with the most potent diastereoisomer showing a half inhibitory concentration (IC<sub>50</sub>) in the low nanomolar range, confirmed by Patch-Clamp electrophysiology experiments. All four compounds display high receptor selectivity against other members of the TRP family. Furthermore, in primary cultures of rat dorsal root ganglion (DRG) neurons, the most potent diastereoisomers do not produce any alteration in neuronal excitability, indicating their high specificity for TRPM8 channels. Docking studies positioned these  $\beta$ -lactams at different subsites by the pore zone, suggesting a different mechanism than the known *N*-(3-aminopropyl)-2-[(3-methylphenyl)methoxy]-*N*-(2-thienylmethyl)-benzamide (AMTB) antagonist.

**Keywords:** TRPM8; antagonists;  $\beta$ -lactams; absolute configuration; Ca<sup>2+</sup> microfluorimetry; Patch-Clamp

## 1. Introduction

Transient receptor potential cation channel subfamily M member 8 (TRPM8), is a calcium-permeable ion channel, activated by innocuous cooling to cold temperatures (below 28°C), membrane depolarization, changes in osmolarity and pH [1,2]. In addition, it is activated by chemical agents such as (-)-menthol and icilin, and by different endogenous molecules, such as the lipid PIP2 [3], testosterone [4], artemin [5] and Pirt (phosphoinositide interacting regulator of TRPs) [6]. TRPM8 is a cold-sensing multimodal nociceptor of the somatosensory nervous system and a major sensor of cold nociception in humans [7,8]. On one hand, they are highly expressed in primary sensory neurons (A $\delta$  and C-

fibers) of the dorsal root ganglia (DRG) and trigeminal ganglia (TG) [9], which participate in the sensory encoding of pain under both normal and pathological conditions. Accordingly, TRPM8 channels have been implicated in inflammatory pain, but also in migraine [10–12]. On the other hand, the cold allodynia associated to oxaliplatin-induced painful neuropathy has been correlated with TRPM8 expression and function [13,14], while other studies indicate that TRPM8 is implicated in cold allodynia after inflammation or nerve injury [15].

TRPM8 channels are also expressed on deep visceral afferents in bronchopulmonary tissue [16], bladder [17], prostate [18], brain [19], and other tissues such as in eyes [20], salivary glands [21] or the oropharyngeal system [22]. Recent experimental evidence seems to indicate that TRPM8 and its modulation by testosterone is behind the regulation of dimorphic sexual and social behaviors in mice [23]. Several tumor growth progression and invasion capacity initial phases of different cancers (prostate, pancreas, colon, breast, lung, and skin), have also been connected with aberrant expression of TRPM8 channels [24], and suggest a potential protective role for TRPM8 antagonists. Contrastingly, for advanced metastatic tumors, it seems that TRPM8 activation by agonists could have a protective function [25].

Among described TRPM8 agonists, we mainly found tertiary amides and diverse menthol derivatives [26–28], and some other natural products [29]. The family of TRPM8 antagonists is highly diverse, with either different acyclic (amide, sulfonamide, urea, glycine, tryptophan) or heterocyclic (thiazole, 2-azetidinone, benzothiofene, benzimidazole, isoquinoline) central scaffolds [27,28,30–34]. Despite the big number of TRPM8 modulators described to date, only a few have been extended to clinical studies, with the exception of menthol that has been profusely scrutinized as a topical antihyperalgesic agent. Among TRPM8 antagonists, only PF-05105679 and AMG 333 progressed into phase I clinical trials to explore pharmacokinetics safety and tolerability pharmacodynamics in healthy volunteers and migraneous patients, respectively [35,36]. Both compounds evidenced several adverse effects, including feeling hot, that preclude further progress into the clinic. Therefore, it is of great interest to push in the discovery of new, potent and selective TRPM8 antagonists, and to increase the knowledge about their specific binding sites on the target protein, to search for mechanistically different antagonists [37–39].

In a previous study, we described a library of highly substituted azetidin-2-ones, prepared from Phe and Asp/Glu amino acid conjugates, that potently and selectively block the activation of TRPM8 by voltage, menthol, and temperature [40]. The prototype  $\beta$ -lactams bear four hydrophobic substituents very important for activity, three benzyl groups and a *tert*-butoxycarbonyl (Boc) moiety, and a short *N*-alkyl chain (1-2 carbons). Very recently, we reported on the cyclization of a series of shorter phenylalaninol-Phe conjugated, affording 2-azetidinones and/or 2-ketopiperazine (KP) derivatives, depending on the *N*-chloroalkyl group and on the configuration of linear intermediates [41]. Cyclization of all *S*-configured linear choropropanoyl derivatives afforded the expected  $\beta$ -lactam **1** along with a small quantity of its regiomeric 2-ketopiperazine (KP), due to the cyclization through the 2'-NH group (indicated by a red arrow, Figure 1). Depending on the configuration of the starting chloropropanoyls, the 2-KP species can be the predominant cyclization product. In addition, for 2''-*R*-chloropropanoyl derivatives, the corresponding  $\beta$ -lactams were obtained as inseparable mixtures of diastereoisomers, thus precluding the study on the configuration influence. The prototype  $\beta$ -lactam (**1**, configuration 3*S*,4*S*,2'*S*) blocks the channel activation by menthol ( $\text{Ca}^{2+}$  entry assay) with micromolar values, significantly reduces the oxaliplatin-induced allodynia from 15 to up to 60 min in a mice model *in vivo*, and exhibits non-selective antitumor activity (micromolar potency in four tumor cell lines) [41]. More importantly, docking studies indicated that compound **1** localizes preferentially at two possible locations by the pore zone of the TRPM8 channel, suggesting either an allosteric or a pore blocking mechanism, different to that of other described antagonists.

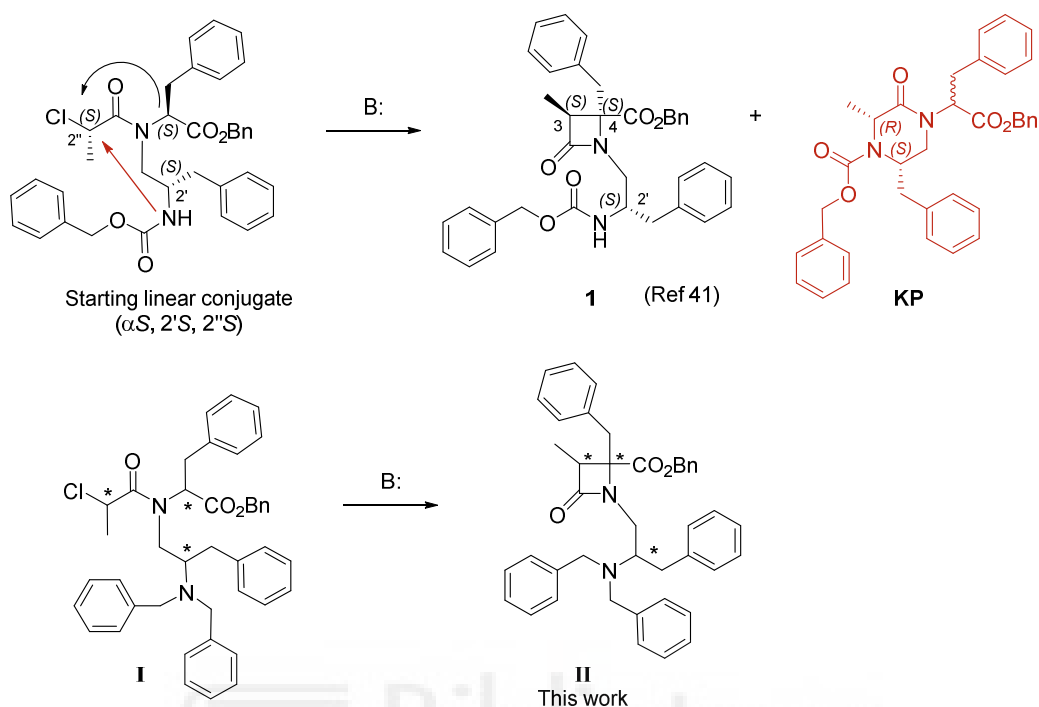


**Figure 1.** Previously described  $\beta$ -lactam (**1**) with transient receptor potential cation channel subfamily M member 8 (TRPM8) antagonist properties and analogues in this work (**II**), obtained from linear conjugates **I**. The black arrow denotes cyclization to  $\beta$ -lactam and red arrow to ketopiperazine (**KP**). \* Means the position of stereogenic centers.

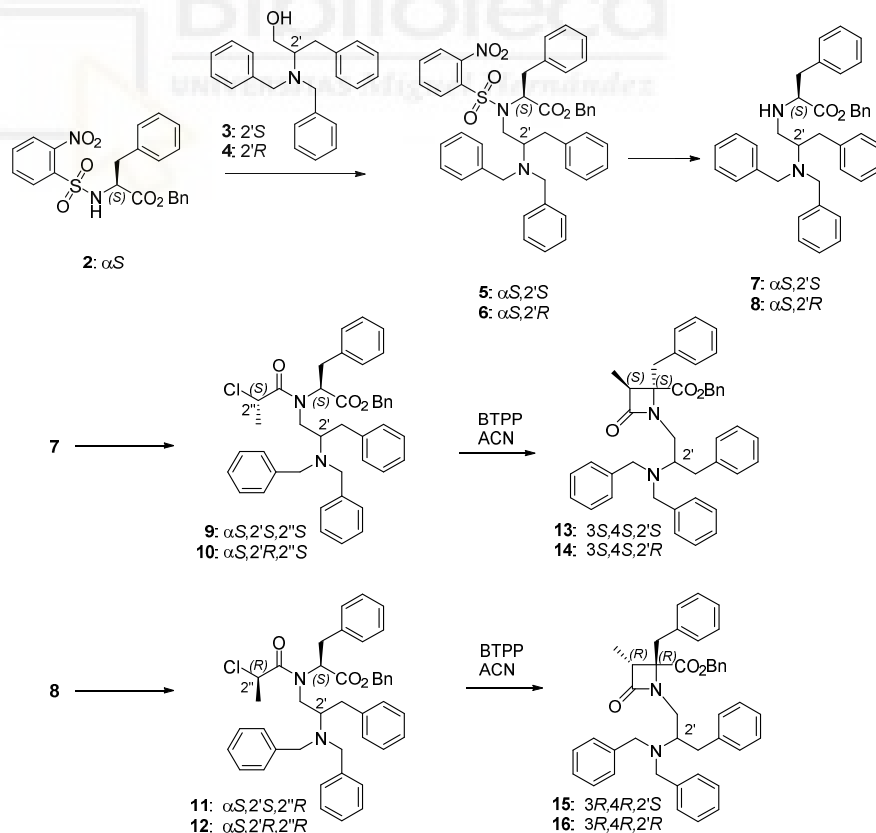
To avoid the regioisomeric formation of diastereomeric KPs, and thus making the synthetic approach to this type of  $\beta$ -lactams more efficient, here we propose the substitution of the Z-group in **1** by an  $\text{NBn}_2$  moiety (general formula **II**, Figure 1), lacking the reactive 2'-NH group in linear precursors **I**. The dibenzylamino moiety is present in other potent tryptamine- and tryptophan-derived TRPM8 antagonists [32,33], and some conformationally restricted tetrahydro- $\beta$ -carboline derivatives [42]. The 3*S*,4*S*,2'*R*-diastereoisomer of  $\beta$ -lactam **1** showed slightly better TRPM8 antagonist activity than the *N*-2'*S*-isomer (**1**), while the corresponding 3*R*,4*R*,2'*S*- and 3*R*,4*R*,2'*R*-isomers could not be obtained in diastereoisomeric pure form [41]. Given the intrinsic chirality of biological systems, the absolute configuration of drugs is normally an important issue. Therefore, to assess the influence of the configuration on the TRPM8 antagonist activity in this family of compounds, we first prepare enantiopure linear conjugates **I**, which were cyclized to four diastereoisomeric  $\beta$ -lactams of general structure **II**, those which are synthetically accessible in optical pure form linear precursors **I**. Then, these diastereomeric compounds were assayed for their potency as TRPM8 antagonists in a  $\text{Ca}^{2+}$  entry assay, the best antagonists were validated by Patch-Clamp experiments, and their selectivity over other TRPs was assessed. Finally, we have identified possible binding sites for these compounds in the TRPM8 channel through docking studies.

## 2. Results and Discussion

### 2.1. Chemistry

*N*-Dibenzylphenylalaninol 2-azetidinones **13–16** were prepared from commercial alcohols **3** and **4** in three steps (Scheme 1), following the previously described synthetic procedure [41].

The synthesis of enantiopure 2-chloropropanoyl derivatives **9**, **10**, **11** and **12** was started by a Mitsunobu reaction between Ns-L-Phe-OBn (**2**) and the corresponding commercial alcohol **3** and **4** to afford compounds **5** and **6** (Scheme 1). Then, the removal of the nosyl group gave NH derivatives **7** and **8**. Finally, compounds **7** and **8** were reacted with 2S- or 2R-chloropropanic acid in the presence of trichloroacetonitrile and triphenylphosphine. We have previously reported that in the cyclization of enantiopure 2-chloropropanoyl derivatives to  $\beta$ -lactams, the stereochemistry at the C3,C4 bond is exclusively governed by the configuration of the chloropropanoyl moiety, with 2''S- and 2''R-chloropropanoyl derivatives affording 3S,4S and 3R,4R  $\beta$ -lactams, respectively [43]. These configurational results were rationalized through quantum mechanics calculation, which indicated that the energy of the possible transition states leading to ring-closure is highly favorable for the formation of *cis*-3-methyl- $\beta$ -lactams, with >10 KJ/mol lower energy compared to the *trans*-diastereoisomers [44]. Therefore, the phosphazene base P1-*t*-Bu-tris(tetramethylene) (BTPP)-assisted cyclization of linear 2''S-conjugates **9** ( $\alpha$ S,2'S,2''S) and **10** ( $\alpha$ S,2'R,2''S) afforded *cis*-3-methyl 3S,4S- $\beta$ -lactams **13** (3S,4S,2'S) and **14** (3S,4S,2'R), respectively. In a similar manner, *cis*-3-methyl 3R,4R- $\beta$ -lactams **15** (3R,4R,2'S) and **16** (3R,4R,2'R) were obtained as single isomers after base-promoted cyclization of the corresponding 2''R-chloropropanoyl derivatives, **11** ( $\alpha$ S,2'S,2''R), and **12** ( $\alpha$ S,2'R,2''R). As expected, enantiomeric pairs (**13/16** and **14/15**) show similar values of optical rotation, but of opposite sign. As KPs are not possible in this case, the yield of  $\beta$ -lactams is in general higher than those obtained for the corresponding 2'-benzyloxycarbonyl derivatives [41], but some hydrolysis of the benzyl ester was observed during the cyclization step workup (higher for 2'R-diastereoisomers compared to 2'S-counterparts).



**Scheme 1.** Synthetic pathway for the preparation of the four diastereomeric  $\beta$ -lactam derivatives.

## 2.2. Biological Activity

### 2.2.1. Ca<sup>2+</sup> Intracellular Influx Assay

The four obtained diastereomeric compounds were evaluated for their ability to inhibit menthol-induced Ca<sup>2+</sup> intracellular influx into the cytosol on HEK293 cells heterologously expressing rat TRPM8. The well-known TRPM8 antagonist *N*-(3-aminopropyl)-2-[(3-methylphenyl)methoxy]-*N*-(2-thienylmethyl)-benzamide (AMTB) was used as control [45,46]. The results are depicted in Table 1. Some representative graphs for compound **14** and **16** at 10 μM on HEK-rTRPM8 cells are included in Figure A1.

In the Ca<sup>2+</sup> fluorometry assay, all diastereoisomeric compounds were able to antagonize the menthol-induced activation of TRPM8 channels, but with different potencies. Thus, β-lactam derivatives of 3*S*,4*S* configuration (**13** and **15**) display micromolar and sub-micromolar antagonist activity, respectively. Their IC<sub>50</sub> values are comparable to those found for stereoequivalent, enantiopure *N*-benzyloxycarbonyl derivatives previously described [41], thus indicating that the *Z*-group can be substituted by an *N*-dibenzyl moiety without significant changes in the TRPM8 activity. Comparing **13** to **15**, it is clear that the 2′*R*-stereogenic center in compound **15** results in one order of magnitude higher TRPM8 antagonist potency than the corresponding 2′*S*-isomer **13**. All *S*-configured compound **13** is equipotent to AMTB, while diastereoisomer **15** shows one order of magnitude higher IC<sub>50</sub> value than the model antagonist.

We could also prepare enantiopure 3*R*,4*R* β-lactam diastereoisomeric compounds, a configuration not explored already within this family of compounds. 3*R*,4*R*-Configured β-lactams **14** and **16** are the most potent TRPM8 antagonists in this series, showing IC<sub>50</sub> values of 0.3 and 0.02 μM. Once again, comparison between both configurations at 2′-position indicated that a 2′*R*-stereogenic center is preferred for high TRPM8 antagonist activity, with one order of magnitude higher potency for **16** versus **14**. Both compounds are more potent than the model antagonist AMTB, with isomer **16** showing two-orders of magnitude higher activity.

The dependence of the TRPM8 activity, activation or blocking, on the absolute configuration of the ligands has also been recorded in the literature for other families of TRPM8 agonists and antagonists [33][47][48]. Thus, a *N,N*-dibenzyl-*D*-Trp derivative showed highly reduced antagonist potency compared to the corresponding *L*-enantiomer [33]. Similarly, in a family of *N*-(thiophen-2-ylmethyl)-2-acetamide derivatives acting as TRPM8 agonists, the change of a unique chiral center provides either a nanomolar active or an inactive compound [47]. Approximately one order of magnitude reduced potency was also obtained for 4*S*(+)-4-hydroxy-3,4-dihydrospiro[chromene-2,4′-piperidine] derivatives compared to the corresponding 4*R*(-) analogues [48]. In symmetrical tetrahydroisoquinoline derivatives, only a *trans*-disposition between C-1 and C-1′-substituents led to compounds with significant TRPM8 antagonist activity [30]. Similarly, in a recently described family of *N*-acyl-*N*-indanyl-α-phenylglycinamides derivatives, α-*R* isomers are from one to three orders of magnitude more potent than the corresponding *S*-diastereoisomers [49].

Here, we discovered that for β-lactams of general structure **II**, the 3*R*,4*R*-arrangement is preferred over the 3*S*,4*S*-configuration, and the results recognize a predilection for a 2′*R* stereocenter at the phenylalaninol-derived moiety. Within phenylalanine-phenylalaninol-derived β-lactams, and until other diastereoisomers could be prepared in enantiopure form, the 3*R*,4*R*,2′*R* isomer can be considered the eutomer. In general, for the *SS* configured isomers at 3,4-positions of the β-lactam ring, the *N*-dibenzylphenylalaninol-Phe-derived β-lactams described here show similar potencies as *N*-*Z*-phenylalaninol previous analogues [41].

**Table 1.** Activity at TRPM8 channels of  $\beta$ -lactam derivatives ( $\text{Ca}^{2+}$  influx assay).

Compoundd	Configura-tion	% Blockade 50 $\mu\text{M}$	% Blockade 5 $\mu\text{M}$	$\text{IC}_{50}$ ( $\mu\text{M}$ )	95% Confidence Intervals
<b>13</b>	3 <i>S</i> ,4 <i>S</i> ,2' <i>S</i>	86.1 $\pm$ 5.0	57.7 $\pm$ 7.2	3.1 $\pm$ 1.1	2.574 to 3.997
<b>14</b>	3 <i>S</i> ,4 <i>S</i> ,2' <i>R</i>	87.7 $\pm$ 3.1	78.9 $\pm$ 1.7	0.3 $\pm$ 1.0	0.2162 to 0.2804
<b>15</b>	3 <i>R</i> ,4 <i>R</i> ,2' <i>S</i>	90.3 $\pm$ 2.8	71.1 $\pm$ 4.3	0.7 $\pm$ 1.1	0.6376 to 0.9071
<b>16</b>	3 <i>R</i> ,4 <i>R</i> ,2' <i>R</i>	98.5 $\pm$ 3.2	87.3 $\pm$ 8.1	0.02 $\pm$ 1.1	0.010 to 0.019
<b>1</b> <sup>a</sup>	3 <i>S</i> ,4 <i>S</i> ,2' <i>S</i>			2.4 $\pm$ 1.2	
AMTB <sup>a</sup>	—			7.3 $\pm$ 1.5	

<sup>a</sup> Values taken from reference [41].

Because some molecular cross-recognition may occur within thermoTRP members [50], we evaluated the effect of compounds **14** and **16** on recombinantly expressed hTRPV1 and hTRPA1 channels. Data shown in Table 2 indicate that these  $\beta$ -lactam derivatives marginally cross-reacted with these channels, thus substantiating that they are potent and selective inhibitors of TRPM8.

**Table 2.** Activity at TRPV1 and TRPA1 channels of  $\beta$ -lactam derivatives ( $\text{Ca}^{2+}$  influx assay).

Com-poundd	Configura-tion	% TRPV1 Blockade at 50 $\mu\text{M}$	% TRPA1 Blockade at 50 $\mu\text{M}$
<b>13</b>	3 <i>S</i> ,4 <i>S</i> ,2' <i>S</i>	7.9 $\pm$ 3.2	3.7 $\pm$ 4.1
<b>14</b>	3 <i>S</i> ,4 <i>S</i> ,2' <i>R</i>	2.8 $\pm$ 4.1	2.4 $\pm$ 1.4
<b>15</b>	3 <i>R</i> ,4 <i>R</i> ,2' <i>S</i>	5.3 $\pm$ 3.4	2.6 $\pm$ 1.9
<b>16</b>	3 <i>R</i> ,4 <i>R</i> ,2' <i>R</i>	4.2 $\pm$ 3.2	0.5 $\pm$ 4.1

### 2.2.2. Patch-Clamp Experiments

The TRPM8 antagonist activity of the most potent  $\beta$ -lactams in the previous  $\text{Ca}^{2+}$  intracellular influx test, **14** and **16**, was then confirmed by Patch-clamp experiments, using HEK293 cells expressing rat TRPM8 channels. In the electrophysiology assay, both compounds at 10  $\mu\text{M}$  concentration were able to block TRPM8-mediated responses induced by menthol (Figures 2 and A2, Table 3). As shown in Figure 2, perfusion with 100  $\mu\text{M}$  menthol produces a strongly outward rectifying ionic current, described by the absence of current at negative potentials and the presence of a linear current increase (ohmic) at positive voltages  $\geq 40$  mV. After 10  $\mu\text{M}$  of **14** was applied (Figure 2A, red), an important decrease on the menthol-induced TRPM8 activity at depolarizing voltages was observed. A similar behavior was detected after application of diastereomeric  $\beta$ -lactam **16** (Figure 2B). The dose–response curves for both compounds were obtained at a holding potential of  $-60$  mV (Figure 2). The measured  $\text{IC}_{50}$  values were  $0.9 \pm 1.0$   $\mu\text{M}$  for **14** (Figure 2C) and  $0.05 \pm 1.3$   $\mu\text{M}$  for **16** (Figure 2D).

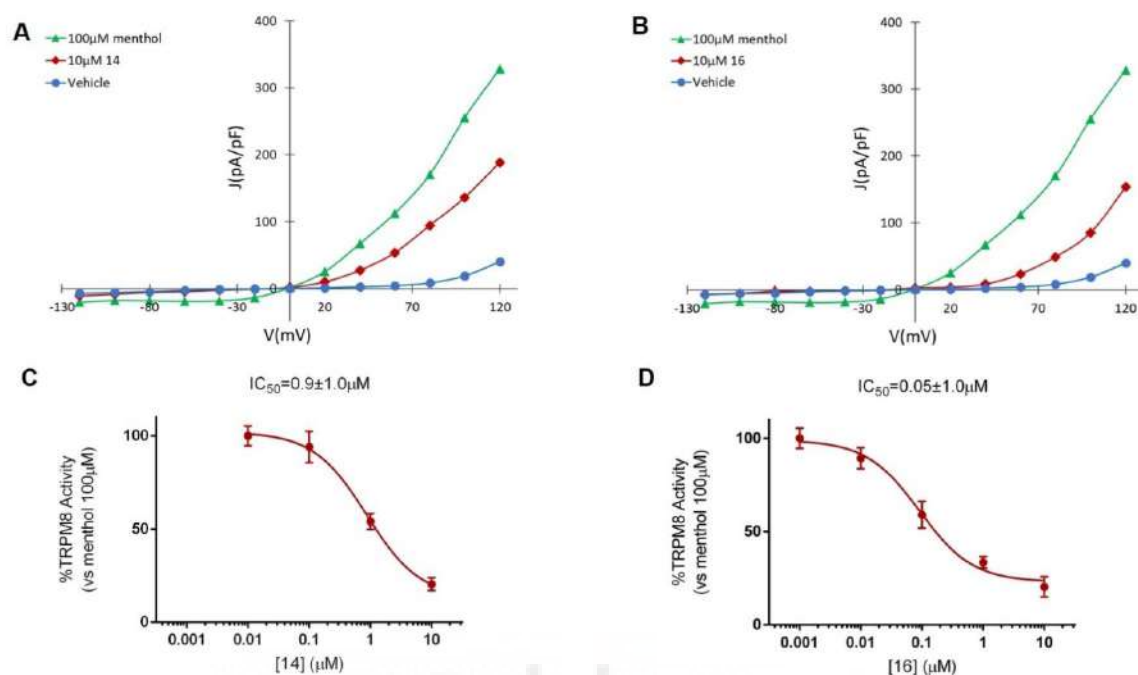


**Figure 2.** Compounds **14** and **16** block TRPM8-mediated responses evoked by menthol in rTRPM8-expressing HEK293 cells. (A,C). *I-V* curves obtained in HEK293 cells expressing TRPM8 and exposed to vehicle solution (vehicle; blue traces), 100  $\mu\text{M}$  menthol (green trace), 100  $\mu\text{M}$  menthol + 10  $\mu\text{M}$  **14** (red trace) or to 100  $\mu\text{M}$  menthol + 10  $\mu\text{M}$  compound **16** (red trace). Peak current data were expressed as pA/pF (to facilitate comparison among cells of different sizes) and expressed as a function of antagonist concentrations. (B,D), Concentration/response curves for TRPM8 current blockade by compound **14** (C) or compound **16** (D) at a holding voltage of  $-60$  mV. The solid lines represent fits of the experimental data to the following binding isotherm:  $y = \max/(1 + x/IC_{50})^n$ , where  $x$  is the drug concentration and  $n$  the Hill coefficient. The fitted values for  $IC_{50}$  were  $0.9 \pm 1.0$  and  $0.05 \pm 1.0$  for compound **14** and **16**, respectively. Each point is the mean  $\pm$  SEM of 15 determinations, each obtained in different cells.

**Table 3.** Patch-clamp experiments (whole cell configuration in HEK293 cells expressing TRPM8 channels).

Compound	Configuration	% Blockade at 10 $\mu\text{M}$	$IC_{50}$ ( $\mu\text{M}$ )
<b>14</b>	3 <i>S</i> ,4 <i>S</i> ,2' <i>R</i>	$77.2 \pm 2.7$	$0.9 \pm 1.0$
<b>16</b>	3 <i>R</i> ,4 <i>R</i> ,2' <i>R</i>	$79.3 \pm 2.7$	$0.05 \pm 1.0$
<b>1</b>	3 <i>S</i> ,4 <i>S</i> ,2' <i>S</i>		$1.4 \pm 1.1$

Electrophysiological results sustain that the 3*R*,4*R*-diastereoisomer **16** is more potent than the corresponding 3*S*,4*S*-isomer **14** blocking TRPM8 channel activity. Compound **16**, with an  $IC_{50}$  value of 50 nM is the most potent  $\beta$ -lactam derivative described to date within this family of TRPM8 antagonists. Its inhibitory activity of menthol-induced TRPM8 activation is comparable to many other structurally unrelated TRPM8 antagonists [28], although lower than that of *N*-dibenzyl-Trp-OMe [33].

Next, we investigated the effect of the membrane of rat DRG sensory neurons. Under current-clamp, small sensory neurons displayed a resting membrane potential of  $-50$  mV (Figure 3A, top trace, and 3B). Exposure of the neurons to 10  $\mu\text{M}$  of the  $\beta$ -lactam derivatives did not alter RMP of primary sensory neurons (Figure 3A, bottom traces and 3B). Sensory neurons were functional as evidenced by action potentials fired exposed to 100  $\mu\text{M}$  menthol (Figure 3A, top trace).

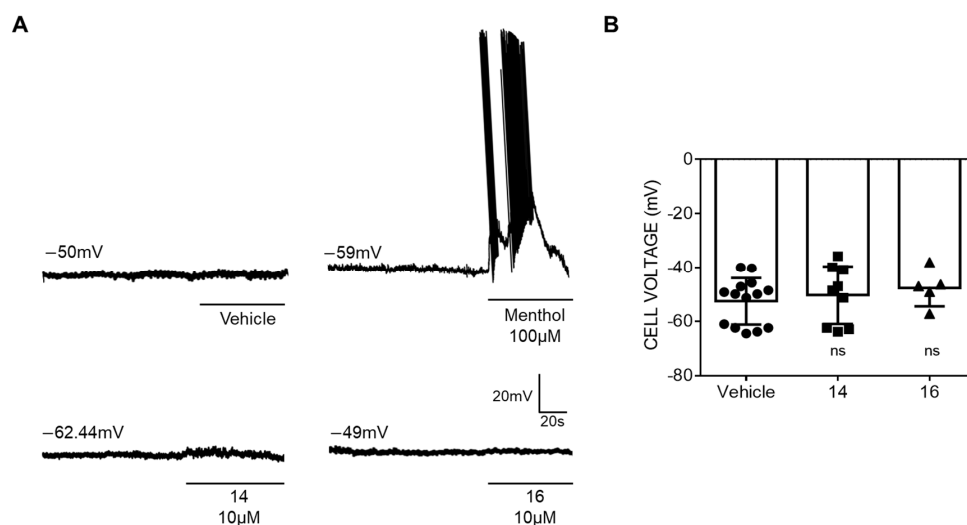


**Figure 3.** Compounds **14** and **16** do not affect the membrane resting potential of sensory neurons. **(A)** Representatives recordings of resting membrane potential measured under current-clamp configuration. The upper traces show the action potentials (APs) firings from the dorsal root ganglion (DRG) neuron elicited by 100  $\mu\text{M}$  menthol and the lower traces show the voltage membrane in the presence of the  $\beta$ -lactams derivatives. **(B)** Changes in  $V_m$  in the absence and in the presence of 10  $\mu\text{M}$  of compound **14** or **16** were analyzed by t-test, ns—no significance. Compounds were used at 10  $\mu\text{M}$ . Data are given as means  $\pm$  SEM;  $n \geq 10$  cells.

### 2.2.3. Microelectrode Array Experiments

To further interrogate  $\beta$ -lactam derivatives' action on the excitability of DRG neurons we next used microelectrode arrays (MEA). This technology records the electrogenic activity of neural populations that are located near to an electrode, but it cannot differentiate the number of neurons or other cells contributing to it. We used MEA chips with 60 electrodes and monitored the electrical activity at each electrode to measure if the potent inhibitory effect of  $\beta$ -lactam derivatives act on voltage-gated  $\text{Na}^+$  and  $\text{K}^+$  channels present in neurons and responsible for action potential propagation. Neurons isolated from neonatal rat dorsal root ganglions (DRG) were cultured on MEA chambers. The experimental paradigm consisted in applying a first 15-s pulse (P1) of 40 mM KCl, to evoke action potentials. After a recovery period of 10 min, a second pulse (P2) of  $\text{K}^+$  in absence (vehicle, V) or presence of 10  $\mu\text{M}$  compound **14** or compound **16** was applied to measure the effect of the compounds in  $\text{K}^+$ -induced electrical excitability of nociceptors. Figure 4 shows a typical MEA recording from one electrode (upper trace). It can be observed the KCl evoked bursts of neural action potential firing. The application of 10  $\mu\text{M}$   $\beta$ -lactam derivatives **14** and **16** did not affected the electrogenicity induced by  $\text{K}^+$  (Figure 4A, middle and lower traces). These results suggest that the  $\beta$ -lactam derivatives **14** and **16** did not affect  $\text{Kv}$  and  $\text{Nav}$  channels, discarding a potential anesthetic effect, and further strengthening the channel selectivity of the compounds.

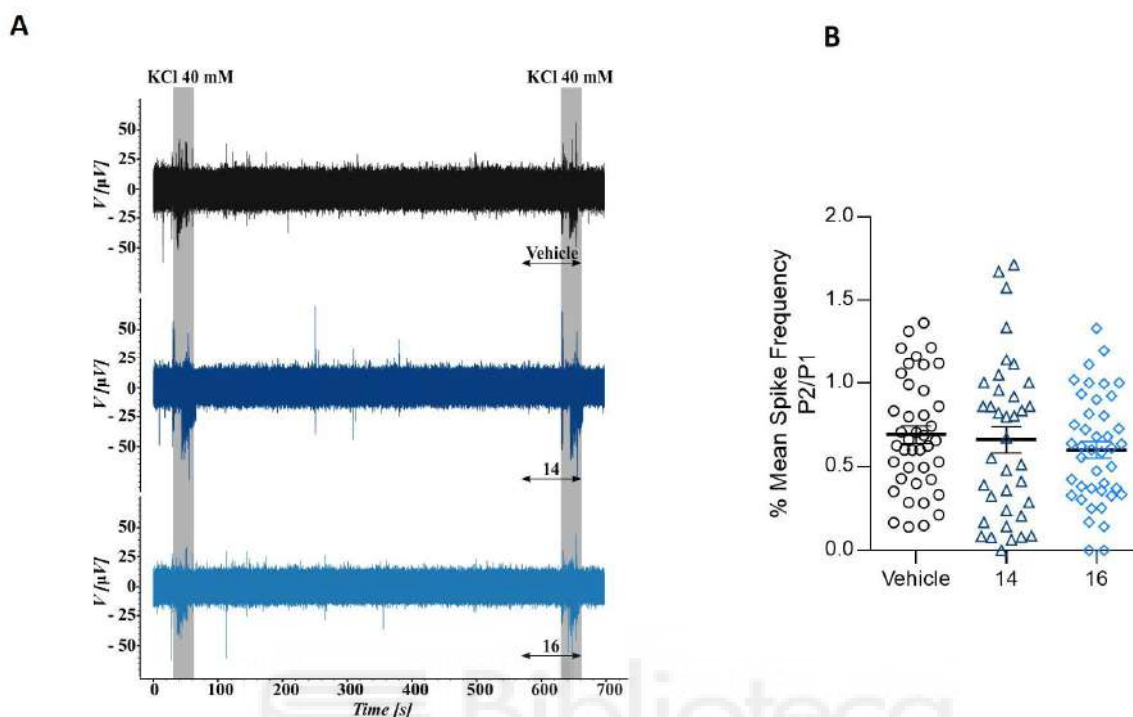


**Figure 4.** Compounds **14** and **16** do not alter potassium-evoked action potentials in primary cultures of rat sensory neurons. **(A)** Representative recordings of evoked action potentials in rat DRG neurons with 40 mM KCl (K) in the absence (top) and presence of 10  $\mu\text{M}$  compound **14** (medium trace) or 10  $\mu\text{M}$  compound **16** (bottom trace). **(B)** Mean spike frequency measured on the first pulse (P1) and second pulse (P2) of 40 mM KCl in absence or presence of 10  $\mu\text{M}$  compounds.

### 2.3. Molecular Modeling Studies

As for previous analogues [41], the fact that all isomers described here could antagonize TRPM8 receptors suggests that the binding of these diastereomeric compounds to the channel should occur in a pocket or area wide enough to accommodate different three-dimensional arrangements of the hydrophobic substituents. To identify possible binding pockets for these  $\beta$ -lactams in the TRPM8 channel, docking studies were performed with **13–16** diastereomeric compounds. Docking simulations were performed with Yasara software [51,52], in a model of a rat TRPM8 channel, generated from the cryo-electron microscopy (cryo-EM) structure of *Ficedula albicollis* TRPM8 (*fa*TRPM8, PDB code 6BPQ) [37]. Results from these studies indicated that all diastereoisomers preferentially or exclusively bind to the pore zone, occupying up to four different subsites (Table 4). As for *N*-benzyloxycarbonyl-described analogues [41], the most populated subsite 1 is situated at the middle of the transmembrane region and involves TM5 (S5) and TM6 (S6) of one protein monomer and S6 of a second monomer. Subsite 2 is located at the internal mouth of the pore and is formed by the loops connecting TM6 and TRP domains of the four monomers forming the channel. Subsite 3 is located upper in the pore region, and involves residues in the S3, S4 transmembranes of one protomer and S6 of an adjacent subunit. Finally, subsite 4 corresponds to the external part of the pore and is delineated by the loops connecting S5 and S6 of three contiguous protomers. In all cases, most connections between the channel and the isomeric  $\beta$ -lactams are Van de Waals interactions (VdW) and  $\pi$ - $\pi$  stacking.

**Table 4.** Main sites found for compounds **13–16**, and statistical distribution of the docking solutions.

Subsite	Location	% of Docking Solutions (Estimated Binding Energies, kcal/mol)			
		13	14	15	16
1	Inner pore, S5S6, S6	40% (10.64)	42% (10.53)	50% (10.58)	52% (10.26)
2	Internal mouth pore	34% (11.44)	18% (10.15)	22% (10.14)	20% (11.40)
3	Pore, high S3-S4, S6	12% (9.95)	24% (10.24)	10% (9.24)	12% (10.32)
4	Pore, external tower	4% (10.20)	16% (10.43)	18% (11.46)	16% (10.41)

At subsite 1, 3*R*,4*R*,2'*R*- $\beta$ -lactam **16** interconnects, on one hand, with a subunit of the channel through F874, W877 and F881, situated in one face of S5 helix, F912, E914 and V915, within the S5-S6 linker, and with T956, L959, V960, I962 and Y963 side-chains of TM S6 (Figure 5). On the other hand, the complex structure is stabilized by interaction with L909 and A910 of the S5-S6 connecting segment of an adjacent subunit. Among these interactions, those with W877 and F881 correspond to T-shaped  $\pi$ - $\pi$  stackings with the phenyl ring of one of the *N*-benzyl substituents. Quite similar interconnections were found for diastereoisomers **13–15** at subsite 1, showing repeated VdW intermolecular forces with F874, L909 and L959, and one or two  $\pi$ - $\pi$  stackings (Figure A3). The interplay between compound **16** and the TRPM8 channel at subsite 2 is mediated by VdW interactions with hydrophobic residues at the cytosolic area of the pore, namely M978 (one subunit), Y981 (all subunits), T982 (two subunits) and I985 (three subunits). Related attachments of compounds **13–15** to this subsite were observed, but compound **14** revealed three additional  $\pi$ - $\pi$  stackings with channel Y981 residues.

To exemplify the binding at subsite 3, the complex between compound **14** and the TRPM8 channel is shown in Figure A4. The main hydrophobic contacts are with S3 (Y808, A811, F815) and S4 (I831, L834) transmembrane segments of one protomer, and an S6 residue (W945) of a contiguous subunit. Y808, F951, and W954 aromatic side-chains in the receptor are involved in T-type  $\pi$ - $\pi$  interactions with the phenyl groups of 4-Bn and OBn moieties of the ligand. Subsite 4 is defined by the loops joining S5-S6, including the pore helix, of three contiguous protomers. In this subsite, compound **16** locates above the pore helix, and interacts with Y924 (from two subunits), D920 and D925 from subunits 1 and 2, and forms a salt bridge between the *N*-tertiary amine of the ligand and the D920 carboxylate of subunit 4. Very close interactions were observed for  $\beta$ -lactams **13–15** at subsites 3 and 4 (not shown).

The putative sites for our  $\beta$ -lactams at the TRPM8 are different to that described for the model TRPM8 antagonist AMTB. Cryo-electron microscopy has demonstrated that AMTB accommodates in a hole delimited by the lower half of S1-S4 transmembrane domain and the TRP domain [53]. This adaptable binding pocket also lodges the TC-I antagonist [53], although in a different pose than AMTB, a menthol-derived agonist [39], and was suggested by molecular modeling studies on tryptophan-derived antagonists [33]. The different behavior of our molecules could be due to their large size, and the interaction at the upper extracellular part of the channel (subsite 4) could initiate their ulterior distribution through the pore region (subsites 1–3).

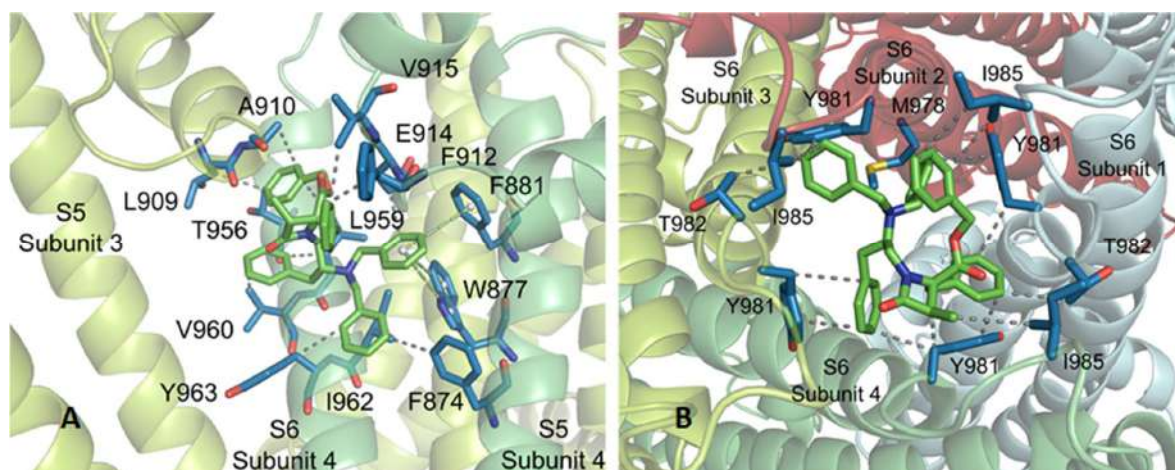


**Figure 5.** Subsites 1 (A) and 2 (B) found for  $\beta$ -lactam 16 (carbon atoms in green). WdV interactions are indicated by dotted gray lines, and  $\pi$ - $\pi$  stacking by centroids and non-continuous pale green lines. Channel residues involved in the interactions are shown in blue and labelled.

### 3. Materials and Methods

Details on the preparation of suitable synthetic intermediates in the road to the described  $\beta$ -lactams from commercially available Phe and phenylalaninol derivatives are given in Appendix A.

#### 3.1. $\beta$ -Lactam Formation

A solution of the corresponding *N*-alkyl-*N*-chloropropionyl-Phe-OBn derivative (1.6 mmol) in dry  $\text{CH}_3\text{CN}$  (4 mL), under Ar atmosphere, was treated with BTPP (2.4 mmol, 0.75 mL) and stirred at rt until consumption of the starting material. After removal of the solvent, the resulting residue was extracted with EtOAc, and successively washed with 0.1 M HCl,  $\text{H}_2\text{O}$  and brine. The organic layer was separated, dried over  $\text{Na}_2\text{SO}_4$ , filtered, and concentrated. The resulting residue was purified by flash chromatography on silica gel, using the indicated eluent system.

##### 3.1.1. 4*S*-Benzyl-1-[(2'*S*-dibenzylamino-3'-phenyl)prop-1'-yl]-4-benzyloxycarbonyl-3*S*-methyl-2-oxoazetidine (**13**)

Syrup. Yield: 63% (from **9**). Eluent: EtOAc:Hex (1:4). HPLC:  $t_R = 7.19$  min.  $[\alpha]_D = +49.16$  (c 1,  $\text{CHCl}_3$ ).  $^1\text{H NMR}$  (400 MHz,  $\text{CDCl}_3$ ):  $\delta$  7.40–6.89 (m, 25H, Ar), 5.23 (d, 1H,  $J = 11.9$  Hz,  $\text{OCH}_2$ ), 5.01 (d, 1H,  $J = 11.9$  Hz,  $\text{OCH}_2$ ), 3.64 (d, 2H,  $J = 13.9$  Hz,  $\text{NCH}_2$ ), 3.49 (m, 1H, 2'-H), 3.44 (d, 2H,  $J = 13.9$  Hz,  $\text{NCH}_2$ ), 3.41 (dd, 1H,  $J = 13.9, 4.0$  Hz, 1'-H), 3.22 (dd, 1H,  $J = 13.8, 9.8$  Hz, 1'-H), 3.10 (q, 1H,  $J = 7.5$  Hz, 3-H), 2.99 (d, 1H,  $J = 14.2$  Hz, 4- $\text{CH}_2$ ), 2.93 (d, 1H,  $J = 14.2$  Hz, 4- $\text{CH}_2$ ), 2.86 (dd, 1H,  $J = 14.4, 5.0$  Hz, 3'-H), 2.75 (dd, 1H,  $J = 14.4, 9.1$  Hz, 3'-H), 1.07 (d, 3H,  $J = 7.5$  Hz,  $\text{CH}_3$ ).  $^{13}\text{C NMR}$  (75 MHz,  $\text{CDCl}_3$ ):  $\delta$  170.8 (COO), 169.1 (C2), 140.4, 139.7, 135.2, 135.0, 130.0, 129.6, 129.2, 128.9, 128.8, 128.7, 128.6, 128.2, 128.1, 127.3, 126.9, 125.9 (Ar), 68.4 ( $\text{OCH}_2$ ), 67.2 (C4), 57.9 (C2'), 57.8 (C3), 53.3 ( $\text{NCH}_2$ ), 43.0 (C1'), 40.9 (4- $\text{CH}_2$ ), 36.2 (C3'), 10.6 ( $\text{CH}_3$ ). MS (ES) $^+$ : 623.01  $[\text{M}+\text{H}]^+$ . Exact Mass calculated for  $\text{C}_{42}\text{H}_{42}\text{N}_2\text{O}_3$ : 622.31954; found: 622.31993.

##### 3.1.2. 4*S*-Benzyl-1-[(2'*R*-dibenzylamino-3'-phenyl)prop-1'-yl]-4-benzyloxycarbonyl-3*S*-methyl-2-oxoazetidine (**14**)

Syrup. Yield: 49% (from **10**). Eluents: EtOAc:Hex (1:6). HPLC:  $t_R = 7.29$  min (gradient of 5% to 100% of A, in 20 min).  $[\alpha]_D = +122.29$  (c 0.24,  $\text{CHCl}_3$ ). HPLC:  $t_R = 7.29$  min (gradient of 5% to 100% of A, in 20 min).  $^1\text{H NMR}$  (400 MHz,  $\text{CDCl}_3$ ):  $\delta$  7.36–6.93 (m, 25H, Ar), 5.06 (d, 1H,  $J = 12.0$  Hz,  $\text{OCH}_2$ ), 4.84 (d, 1H,  $J = 12.0$  Hz,  $\text{OCH}_2$ ), 3.56 (d, 2H,  $J = 13.9$  Hz,  $\text{NCH}_2$ ),

3.47 (d, 2H,  $J = 13.9$  Hz, NCH<sub>2</sub>), 3.46 (m, 1H, 3-H), 3.37 (m, 1H, 2'-H), 3.14 (dd, 1H,  $J = 14.2$ , 8.1 Hz, 1'-H), 3.08 (m, 2H, 3'-H, 4-CH<sub>2</sub>), 2.81 (m, 3H, 4-CH<sub>2</sub>, 1'-H, 3'-H), 1.00 (d, 3H,  $J = 7.5$  Hz, CH<sub>3</sub>). <sup>13</sup>C NMR (75 MHz, CDCl<sub>3</sub>):  $\delta$  170.9 (COO), 169.9 (C2), 140.3, 140.0, 135.5, 135.1, 129.9, 129.8, 129.7, 129.1, 129.0, 128.8, 128.75, 128.7, 128.2, 127.4, 126.9, 126.0 (Ar), 68.6 (C4), 67.3 (OCH<sub>2</sub>), 58.7 (C2'), 54.4 (C3), 53.2 (NCH<sub>2</sub>), 42.1 (C1'), 40.6 (4-CH<sub>2</sub>), 35.9 (C3'), 10.5 (CH<sub>3</sub>). MS (ES)<sup>+</sup>: 623.52 [M+H]<sup>+</sup>. Exact Mass calculated for C<sub>42</sub>H<sub>42</sub>N<sub>2</sub>O<sub>3</sub>: 622.31954; found: 622.31861.

### 3.1.3. 4*R*-Benzyl-1-[(2'*S*-dibenzylamino-3'-phenyl)prop-1'-yl]-4-benzyloxycarbonyl-3*R*-methyl-2-oxoazetidine (**15**)

Syrup. Yield: 57% (from **11**). Eluent: EtOAc:Hex (1:4). HPLC:  $t_R = 7.29$  min.  $[\alpha]_D = -122.76$  (c 0.26, CHCl<sub>3</sub>). <sup>1</sup>H NMR (400 MHz, CDCl<sub>3</sub>) and <sup>13</sup>C NMR (75 MHz, CDCl<sub>3</sub>):  $\delta$  identical to its enantiomer **14**. MS (ES)<sup>+</sup>: 622.95 [M+H]<sup>+</sup>. Exact Mass calculated for C<sub>42</sub>H<sub>42</sub>N<sub>2</sub>O<sub>3</sub>: 622.31954; found: 622.32219.

### 3.1.4. 4*R*-Benzyl-1-[(2'*R*-dibenzylamino-3'-phenyl)prop-1'-yl]-4-benzyloxycarbonyl-3*R*-methyl-2-oxoazetidine (**16**)

Syrup. Yield: 38% (from **12**). Eluents: EtOAc:Hex (1:6). HPLC:  $t_R = 7.19$  min (gradient of 5% to 100% of A, in 20 min).  $[\alpha]_D = -49.09$  (c 0.23, CHCl<sub>3</sub>). <sup>1</sup>H NMR (400 MHz, CDCl<sub>3</sub>) and <sup>13</sup>C NMR (75 MHz, CDCl<sub>3</sub>):  $\delta$  identical to its enantiomer **13**. MS (ES)<sup>+</sup>: 623.52 [M+H]<sup>+</sup>. Exact Mass calculated for C<sub>42</sub>H<sub>42</sub>N<sub>2</sub>O<sub>3</sub>: 622.31954; found: 622.32026.

## 3.2. Functional Assays by Calcium Microfluorimetry

Compounds were evaluated for their activity against rTRPM8 using microfluorometry based calcium flux assays with Fluo-4 NW Ca<sup>2+</sup> dye and fluorescence were measured at excitation wavelength of 485 nm and emission wavelength of 520 nm using POLASTAR plate reader (BMG Labtech) [40]. Briefly human embryonic kidney cell line (HEK) stably transfected with rTRPM8 were seeded in 96-well plates at a cell density of 30,000 cells and 2 days before the medium was replaced with 100  $\mu$ L of the dye loading solution Fluo-4 NW supplemented with probenecid 2.5 mM. After 1 h incubation at 37 °C, plates were transferred to the plate reader and the baseline fluorescence was recorded for 3 cycles before the addition of vehicle, compound at different concentrations and the antagonist, 10  $\mu$ M AMTB for TRPM8. Fluorescence intensity was recorded during 7 more cycles and the agonist was added, 100  $\mu$ M menthol. Fluorescence intensity was recorded during 10 more cycles.

Data analysis: the fluorescence values obtained for each compound concentration were normalized to that prompted by the control agonist (100  $\mu$ M menthol). Decrease in menthol signal was expressed as percentage of inhibition (%). All data are expressed as the mean  $\pm$  standard deviation (SD). Each condition was assessed in triplicate ( $n = 3$ ) in 3 independent experiments ( $N = 3$ ). The Z-factor was calculated in each assay using the following equation:  $(3 \times (SD_{max} + SD_{min})) / (\text{Mean}_{max} - \text{Mean}_{min})$ . In all the experiments, the Z-factor was  $\geq 0.5$ . To calculate IC<sub>50</sub>, normalized responses (%) versus log ( $\mu$ M) were adjusted to a non-linear fit with variable slope, a four-parameter dose-response curve following curve  $Y = 100 / (1 + 10^{(\text{Log IC}_{50} - X) \times \text{HillSlope}})$  where  $X = \% \text{ normalized response}$  and  $Y = \log (\mu\text{M})$ .

## 3.3. Functional Assays by Patch-Clamp Electrophysiology

Whole-cell patch-clamp recordings from HEK-rTRPM8 cells were carried out 2 days after seeding on 12-mm  $\varnothing$  glass coverslips treated with poly-L-lysine solution (Sigma Aldrich, Spain) [40]; the intracellular pipette solution contained (in mM) 150 NaCl, 5 EGTA, 3 MgCl<sub>2</sub> and 10 HEPES, adjusted to pH 7.2 with NaOH, and the extracellular solution contained (in mM) 150 NaCl, 6 CsCl, 1.5 CaCl<sub>2</sub>, 1 MgCl<sub>2</sub>, 10 D-glucose and 10 HEPES, adjusted to pH 7.4 with NaOH. The TRPM8 activity was measured by the application of

two pulses of 100  $\mu\text{M}$  menthol in a time interval of 2 min and a 30-s perfusion of the different compound concentrations before the second menthol pulse.

Current-Clamp recordings from rat DRGs were carried out 24–48 h after seeding on 12-mm  $\emptyset$  glass coverslips treated with poly-L-lysine solution and Laminin (Sigma Aldrich). The intracellular pipette solution contained (in mM): 4 NaCl, 126 K gluconate, 0.02  $\text{CaCl}_2$ , 1  $\text{MgSO}_4$ , 5 HEPES, 15 glucose, 3 ATP, 0.1 GTP and 5 EGTA, pH 7.2 with KOH. The extracellular solution contained (in mM): 140 NaCl, 4 KCl, 2  $\text{CaCl}_2$ , 2  $\text{MgCl}_2$ , 10 HEPES, 5 glucose and 20 mannitol, pH 7.4 with NaOH. The membrane potential was measured in the absence and the presence of compounds 14 and 16 at 10  $\mu\text{M}$  in a time interval of 1 min.

Data were sampled at 10 kHz (EPC10 amplifier with PatchMaster 2.53 software, HEKA Electronics, Lambrecht, Germany) and low-pass filtered at 3 kHz for analysis (PatchMaster 2.53 and GraphPad Prism 5, Graphpad Software, USA). The series resistance was  $<10\text{ M}\Omega$  and to minimize voltage errors was compensated to 60–80%. All measurements were performed at 24–25  $^\circ\text{C}$ . Cell capacitance was measured and used to estimate the current density (J, pA/pF).

Data analysis: Results are expressed as the percentage of remaining activation of the TRPM8 channel. This is calculated by normalizing the ratio (p2/p1) of testing conditions to the ratio (p2/p1) of the control condition. Analysis of the data was performed by GraphPad 6.0, the Ordinary One-Way ANOVA analysis followed by the post hoc Bonferroni test established multiple comparisons and the ROUT method (Q = 10%) identified data outliers. A non-linear regression curve and  $\text{IC}_{50}$  were obtained by the representation of log (inhibitor) vs. response. All data are expressed as the mean  $\pm$  standard error of the mean (SEM) (n = 5–8).

### 3.4. Functional Assays by Microelectrode Arrays

Extracellular recordings were performed as described in Nikolaeva-Koleva et al. [54]. Briefly, measurement of neuronal firing activity was performed by applying two short 15-s applications (defined as P1 and P2, respectively) of the stimulus (KCl 40 mM) using a continuous perfusion system (2 mL/min). Between each stimulus, cells were washed with external solution for 10 min. Treated cells were perfused with  $\beta$ -lactam derivatives) 1 min before and together with 40 mM KCl. All measurements were performed at  $\sim 34.5\text{ }^\circ\text{C}$  (Multichannel Systems Temperature Controller).

Data analysis: Data were analyzed using an MC\_RACK spike sorter with a sample rate of 25 kHz and a Butterworth high-pass 2nd order filter applied with 200 Hz cutoff. An evoked spike was defined when the amplitude of the neuronal electrical activity was established by automatic threshold estimation at  $-5.0\text{ }\mu\text{V}$  Std. Dev. Spiking activity was measured in a temporal interval of 30 s, starting right after instillation of the activating stimuli. Electrodes not displaying electrical activity in the first KCl pulse were discarded. The recorded signals were then processed to extract mean spike frequency for each pulse (P1–P2). Then, the ratio P2/P1 of mean spike frequency was calculated and normalized to vehicle for comparing the different conditions used.

### 3.5. Docking Studies

These studies were performed as previously described [41]. Briefly, starting from the cryo-EM structure of *Ficedula albicollis* TRPM8 [37], the missing loops were added by using Yasara [51,55]. Then, the rat TRPM8 sequence (Uniprot Q8R455) was modeled on completed *Ficedula a.* structure. Sequence alignment between rat and *Ficedula a.* TRPM8 was performed with ClustalO [56], and homology modelling with the standard protocol implemented in Yasara (version 19.9.17) [51,52]. Global docking was accomplished with AutoDock [57] implemented in Yasara, and consisted in a total of 800 flexible docking runs that were then set and clustered around the putative binding sites, following by a simulated annealing optimization of each generated complex using an Assisted Model Building with Energy Refinement (AMBER03) force field [58]. The best binding energy complex

in each cluster was stored, analyzed, and used to select the best orientation of the interacting partners.

Visualization and edition of the molecules were also performed with Yasara (<http://www.yasara.org> accessed on: 12 December 2020). Finally, figures were drawn with the open source Pymol (The PyMOL Molecular Graphics System, Version 1.8 Schrödinger, LLC, New York, USA) obtained at <http://www.pymol.org> (accessed on: 12 December 2020).

#### 4. Conclusions

Since interactions of drugs with macromolecules (receptors, enzymes, channels, DNA) have long been recognized to occur in a stereoselective manner, it is important to know how the absolute configuration of a given compound correlates to its pharmacodynamic properties. To date, in our series of  $\beta$ -lactam TRPM8 antagonists we have mainly studied all *S* stereoisomers. Here, we evaluated and compared to each other, four synthetically accessible diastereoisomers of a  $\beta$ -lactam obtained from enantiopure *N*-dibenzylphenylalaninol-Phe conjugates. The *N*-dibenzylamino group can replace hydrophobic urethane moieties at 2'-position moieties without significant changes in the TRPM8 antagonist activity, but avoiding the formation of yield-lowering 2-ketopyperazine regioisomeric compounds [41]. The previously non-explored 3*R*,4*R*-configuration at the  $\beta$ -lactam ring, resulted in compounds that, at least, are one order of magnitude more potent than the corresponding 3*S*,4*S* enantiomeric analogues. At the phenylalaninol-derived moiety, the results described here corroborate the importance of an *R* configuration at the 2' position for potent TRPM8 antagonist activity, with 2'*R*-isomers clearly preferred over their 2'*S*-equivalents. While other enantiopure diastereoisomers could not be prepared, the 3*R*,4*R*,2'*R* isomer should be considered the eutomer of this family of phenylalanine-phenylalaninol-derived  $\beta$ -lactams. Docking studies with these diastereomeric compounds strongly suggest that they interact by the TRPM8 pore zone, with possible binding pockets different from that described for AMTB and other channel modulators. Our results open up new opportunities for isomerically pure TRPM8 antagonists, through the synthesis and biological study of innovative analogues within this family of  $\beta$ -lactams, which are currently being investigated in our labs and will be published in due course.

**Author Contributions:** Conceptualization, R.G.M., I.G.-M., A.F.-M. and A.F.-C.; synthetic methodology and characterization, M.Á.B., P.J.L. and C.M.-E.; biological methodology and validation, L.B. and A.M.-P.; docking studies: G.F.-B. and R.d.l.T.-M.; supervision, A.M.R., A.F.-C. and R.G.M.; writing—original draft preparation, M.Á.B., A.F.-C. and R.G.M.; writing—review and editing, A.M.R., I.G.-M., A.F.-C., A.F.-M. and R.G.M.; funding acquisition, A.F.-M., A.F.-C. and R.G.M. All authors have read and agreed to the published version of the manuscript.

**Funding:** This research was funded by the Spanish Ministerio de Ciencia y Universidades (MICYU-FEDER, RTI2018-097189-C2-1 to A.F.-M. and A.F.-C., and RTI2018-097189-C2-2 to R.G.M.), Comunidad de Madrid (IND2017/BMD7673 to R.G.M.) and the Spanish National Research Council (CSIC, 201980E030 to R.G.M.).

**Institutional Review Board Statement:** The study was conducted according to the guidelines of the Declaration of Helsinki, and approved by the Ethics Committee of Miguel Hernandez University (UMH.IBM.AFM.02.18- October 11<sup>th</sup>, 2018).

**Informed Consent Statement:** Not applicable.

**Data Availability Statement:** Not applicable.

**Acknowledgments:** We would like to thank our Economic Office manager, Pedro Pastur, for his tireless work and support, managing our projects and open access publications. We wish him all the best for his retirement.

**Conflicts of Interest:** The authors declare no conflict of interest.

#### Abbreviations

AMTB	<i>N</i> -(3-Aminopropyl)-2-[(3-methylphenyl)methoxy]- <i>N</i> -(2-thienylmethyl)benzamide
Bn	Benzyl
BTPP	Phosphazene base P <sub>1</sub> - <i>t</i> -Bu-tris(tetramethylene)
HEK	Human embryo kidney cells
HPLC	High-performance liquid chromatography
KP	2-Ketopiperazine
NMR	Nuclear magnetic resonance
Ns	Nosyl
Phe	Phenylalanine
PIP2	Phosphatidylinositol bisphosphate
SD	Standard deviation
TRP	Transient receptor potential channel
TRPM8	Transient receptor potential melastatin type 8 channel
Z	Benzoyloxycarbonyl

## Appendix A

### Appendix A.1. Chemistry, General Procedures

Reaction monitoring: TLC silica gel plates (Merck 60 F254, Spain) and analytic HPLC (Agilent Technologies 1120 Compact LC, Spain), Eclipse C18, 4.6 × 150 mm, 5 μm, reversed-phase column; mobile phase (A:B), CH<sub>3</sub>CN(A)/H<sub>2</sub>O(0.05% TFA)(B); flux, 1.5 mL/min; detection, UV, 254 nm). Chromatographic separations: flash column, silica gel Merck 60 (230–400). Optical rotations were measured in a Perkin Elmer 141 polarimeter. <sup>1</sup>H NMR spectra: Varian INOVA-300 (300 MHz), Bruker 300 (300 MHz), and Varian INOVA-400 (400 MHz), with TMS as internal standard. <sup>13</sup>C NMR spectra: INOVA-300 (75 MHz) and Bruker 300 (75 MHz). Chemical shifts are expressed in ppm, the coupling constants are expressed in Hz. Mass spectra; electrospray, positive mode, HPLC-MS Waters spectrometer. Exact mass: high resolution mass spectra (ESI-HRMS) were recorded on an Agilent 6520 Q-TOF instrument.

### Appendix A.2. Preparation of Synthetic Intermediates on the Road to *B*-Lactam Derivatives.

#### Appendix A.2.1. Synthesis of *N*-Ns-*N*-alkyl-Phe-OBn Derivatives

A solution of Ns-*L*-Phe-OBn (**2**, 3.8 mmol) in dry THF (33 mL) was treated with the corresponding alcohol derivative (**3** or **4**, 3.8 mmol) and PPh<sub>3</sub> (3.8 mmol, 1 g). Then, the reaction mixture was treated with diisopropyl azodicarboxylate (DIAD) (3.8 mmol, 0.75 mL), under Ar atmosphere. The reaction mixture was stirred overnight at rt. After removal of the solvent in vacuum, the resulting residue was purified by flash chromatography on silica gel, using the indicated eluent system.

#### *N*-[(2'*S*-Dibenzylamino-3-phenyl)prop-1'-yl]-Ns-*L*-Phe-OBn (**5**)

Syrup. Yield: 63% (from Ns-*L*-Phe-OBn (**2**) and **3**). Eluent: EtOAc:Hex (1:5). HPLC: t<sub>R</sub> = 18.40 min. <sup>1</sup>H NMR (400 MHz, CDCl<sub>3</sub>): δ 7.52–6.77 (m, 29H, Ar), 4.66 (s, 2H, OCH<sub>2</sub>), 4.54 (dd, 1H, *J* = 9.7, 5.5, α-Phe), 3.83 (dd, 1H, *J* = 14.8, 5.7, 1-H), 3.68 (d, 2H, *J* = 13.7, NCH<sub>2</sub>), 3.53 (d, 2H, *J* = 13.7, NCH<sub>2</sub>), 3.32 (dd, 1H, *J* = 14.8, 8.5, 1-H), 3.20 (m, 1H, 2-H), 2.81 (dd, 1H, *J* = 13.9, 8.5, 3-H), 2.67 (m, 3H, β-Phe and 3-H). <sup>13</sup>C NMR (75 MHz, CDCl<sub>3</sub>): δ 169.6 (COO), 147.8, 139.8, 139.7, 136.4, 135.0, 134.0, 133.3, 131.9, 131.9, 129.7, 129.6, 129.4, 129.2, 128.6, 128.55, 128.5, 128.45, 128.4, 128.3, 128.25, 127.0, 126.9, 126.8, 126.2, 124.4 (Ar), 67.1 (OCH<sub>2</sub>), 62.0 (α-Phe), 57.8 (2-C), 53.2 (NCH<sub>2</sub>), 47.1 (C1), 36.8 (C3), 34.6 (β-Phe). MS (ES)<sup>+</sup>: 754.35 [M+H]<sup>+</sup>.

#### *N*-[(2'*R*-Dibenzylamino-3-phenyl)prop-1'-yl]-Ns-*L*-Phe-OBn (**6**)

Syrup. Yield: 84% (from Ns-L-Phe-OBn (2) and 4). Eluents: EtOAc:Hex (1:5). HPLC:  $t_R = 18.36$  min (gradient of 5% to 100% of A, in 20 min).  $^1\text{H}$  NMR (400 MHz,  $\text{CDCl}_3$ ):  $\delta$  7.54–6.76 (m, 29H, Ar), 4.92 (d, 1H,  $J = 12.0$  Hz,  $\text{OCH}_2$ ), 4.78 (m, 1H,  $\alpha$ -Phe), 4.77 (d, 1H,  $J = 12.0$  Hz,  $\text{OCH}_2$ ), 3.85 (dd, 1H,  $J = 15.0$ , 10.9 Hz, 1-H), 3.68 (d, 2H,  $J = 14.0$  Hz,  $\text{NCH}_2$ ), 3.58 (dd, 1H,  $J = 15.0$ , 3.8 Hz, 1-H), 3.53 (d, 2H,  $J = 14.0$  Hz,  $\text{NCH}_2$ ), 3.21 (m, 1H, 2-H), 3.08 (dd, 1H,  $J = 13.8$ , 9.5 Hz, 3-H), 2.90 (dd, 1H,  $J = 15.1$ , 4.4 Hz,  $\beta$ -Phe), 2.86 (dd, 1H,  $J = 13.8$ , 5.1 Hz, 3-H), 2.74 (dd, 1H,  $J = 15.1$ , 11.0 Hz,  $\beta$ -Phe).  $^{13}\text{C}$  NMR (75 MHz,  $\text{CDCl}_3$ ):  $\delta$  169.3 (COO), 148.2, 140.7, 139.7, 136.6, 134.8, 133.6, 131.7, 131.5, 129.8, 129.3, 128.9, 128.8, 128.7, 128.6, 128.3, 128.0, 127.0, 126.9 (Ar), 67.4 ( $\text{OCH}_2$ ), 61.9 ( $\text{C}\alpha$ -Phe), 57.9 (C2), 53.1 ( $\text{NCH}_2$ ), 47.4 (C1), 37.8 (C3), 35.3 ( $\text{C}\beta$ -Phe). MS (ES) $^+$ : 754.42  $[\text{M}+\text{H}]^+$ .

#### Appendix A.2.2. Removal of the Ns Group

A solution of the corresponding N-Ns-N-alkyl-Phe-OBn derivative (1.1 mmol) in  $\text{CH}_3\text{CN}$  (20 mL) was treated with  $\text{K}_2\text{CO}_3$  (3.3 mmol, 0.455 g). Then, thiophenol (2.2 mmol, 0.22 mL) was added to the mixture and the reaction was stirred overnight at rt. The solvent was removed in a vacuum and the resulting residue was extracted with AcOEt and washed successively with  $\text{H}_2\text{O}$  and a saturated solution of NaCl. The organic phase was separated and dried over dry  $\text{Na}_2\text{SO}_4$ , filtered, and concentrated. The resulting residue was purified by flash chromatography on silica gel, using the indicated eluent system.

#### N-[(2'S-Dibenzylamino-3'-phenyl)prop-1'-yl]-L-Phe-OBn (7)

Syrup. Yield: 77% (from 5). Eluent: EtOAc:Hex (1:7). HPLC:  $t_R = 7.23$  min.  $^1\text{H}$  NMR (400 MHz,  $\text{CDCl}_3$ ):  $\delta$  7.28–6.87 (m, 25H, Ar), 4.96 (s, 2H,  $\text{OCH}_2$ ), 3.60 (d, 2H,  $J = 13.7$ ,  $\text{NCH}_2$ ), 3.43 (d, 2H,  $J = 13.7$ ,  $\text{NCH}_2$ ), 3.35 (dd, 1H,  $J = 7.8$ , 5.9,  $\alpha$ -Phe), 2.87 (m, 2H, 2'-H and 3'-H), 2.85 (dd, 1H,  $J = 13.5$ , 5.8,  $\beta$ -Phe), 2.73 (dd, 1H,  $J = 13.5$ , 7.8,  $\beta$ -Phe), 2.50 (m, 2H, 1-H, 1'-H), 2.38 (dd, 1H,  $J = 14.9$ , 10.1, 3'-H).  $^{13}\text{C}$  NMR (75 MHz,  $\text{CDCl}_3$ ):  $\delta$  174.0 (COO), 140.2, 139.9, 137.6, 135.8, 129.5, 129.45, 129.4, 128.9, 128.8, 128.75, 128.65, 128.6, 128.5, 128.4, 127.0, 126.9, 126.8, 125.9 (Ar), 66.3 ( $\text{OCH}_2$ ), 63.2 ( $\alpha$ -Phe), 59.8 (C2'), 53.7 ( $\text{NCH}_2$ ), 47.5 (C1'), 39.3 ( $\beta$ -Phe), 33.4 (C3'). MS (ES) $^+$ : 569.27  $[\text{M}+\text{H}]^+$ .

#### N-[(2'R-Dibenzylamino-3'-phenyl)prop-1'-yl]-L-Phe-OBn (8)

Syrup. Yield: 99% (from 6). Eluents: EtOAc:Hex (1:10). HPLC:  $t_R = 7.19$  min (gradient of 5% to 100% of A, in 20 min).  $^1\text{H}$  NMR (400 MHz,  $\text{CDCl}_3$ ):  $\delta$  7.31–7.00 (m, 25H, Ar), 5.30 (s, 1H, NH), 5.02 (d, 1H,  $J = 12.0$  Hz,  $\text{OCH}_2$ ), 4.98 (d, 1H,  $J = 12.0$  Hz,  $\text{OCH}_2$ ), 3.78 (d, 2H,  $J = 13.3$  Hz,  $\text{NCH}_2$ ), 3.46 (m, 1H,  $\alpha$ -Phe), 3.36 (d, 2H,  $J = 13.3$  Hz,  $\text{NCH}_2$ ), 3.10 (dd, 1H,  $J = 13.0$ , 3.7 Hz, 1'-H), 3.01 (m, 2H, 2'-H,  $\beta$ -Phe), 2.90 (dd, 1H,  $J = 13.4$ , 6.9 Hz, 1'-H), 2.69 (m, 1H  $\beta$ -Phe), 2.29 (m, 2H, 3'-H).  $^{13}\text{C}$  NMR (75 MHz,  $\text{CDCl}_3$ ):  $\delta$  174.3 (COO), 140.1, 139.9, 136.9, 135.8, 129.8, 129.3, 129.2, 128.8, 128.5, 128.4, 128.35, 128.3, 127.0, 126.8, 126.0 (Ar), 66.3 ( $\text{OCH}_2$ ), 62.2 ( $\text{C}\alpha$ -Phe), 59.8 (C2'), 53.1 ( $\text{NCH}_2$ ), 47.3 (C1'), 39.9 ( $\text{C}\beta$ -Phe), 32.5 (C3'). MS (ES) $^+$ : 569.55  $[\text{M}+\text{H}]^+$ .

#### Appendix A.2.3. Synthesis of N-Alkyl-N-Chloropropionyl-Xaa Derivatives

First, a solution of (R)- or (S)-2-chloropropionic acid (0.126 mL, 1.47 mmol) and  $\text{Cl}_3\text{CCN}$  (0.19 mL, 1.96 mmol) in THF (8 mL) was treated at  $0^\circ\text{C}$  with  $\text{PPh}_3$  (0.513 g, 1.96 mmol), and the reaction mixture was stirred for 30 min. Then, a solution of the corresponding secondary amine (0.98 mmol) and propylene oxide (1 mL, 14.7 mmol) in THF (2 mL) was added dropwise to the first reaction mixture. Stirring was continued for 48 h and the solvent was evaporated. The resulting residue was dissolved in  $\text{Et}_2\text{O}$ , filtered over celite and concentrated under a vacuum. The resulting residue was purified by flash chromatography on silica gel, using the indicated eluent system.

#### N-(2''S-Chloropropanoyl)-N-[2'S-dibenzylamino)-3'-phenyl)prop-1'-yl]-L-Phe-OBn (9)

Syrup. Yield: 25% (from 7). Eluent: EtOAc:Hex (1:6). Mixture of rotamers M,m = 2:1. HPLC:  $t_R$  = 7.93 min.  $^1\text{H}$  NMR (400 MHz,  $\text{CDCl}_3$ , major rotamer):  $\delta$  7.28–6.79 (m, 25H, Ar), 5.11 (d, 2H,  $J$  = 2.9,  $\text{OCH}_2$ ), 4.32 (q, 1H,  $J$  = 6.6, 1''-H), 3.62 (dd, 1H,  $J$  = 9.5, 5.7,  $\alpha$ -Phe), 3.55 (d, 2H,  $J$  = 13.9,  $\text{NCH}_2$ ), 3.47 (d, 2H,  $J$  = 13.8,  $\text{NCH}_2$ ), 3.31–3.10 (m, 3H, 1'-H,  $\beta$ -Phe), 3.07 (m, 1H, 2'-H), 2.90 (dd, 1H,  $J$  = 15.4, 8.4, 1'-H), 2.65 (m, 2H, 3'-H), 1.54 (d, 3H,  $J$  = 6.5, 2''-H).  $^{13}\text{C}$  NMR (75 MHz,  $\text{CDCl}_3$ ):  $\delta$  170.2 (COO), 169.5 (CON), 139.1, 137.9, 136.6, 129.9, 129.8, 129.4, 128.9, 128.8, 128.75, 128.7, 128.5, 128.45, 128.4, 127.3, 126.8, 126.5 (Ar), 67.4 ( $\text{OCH}_2$ ), 64.0 ( $\alpha$ -Phe), 59.1 ( $\text{C}2'$ ), 53.8 ( $\text{NCH}_2$ ), 52.1 ( $\text{C}1''$ ), 50.3 ( $\text{C}1'$ ), 36.3 ( $\beta$ -Phe), 34.8 ( $\text{C}3'$ ) 21.5 ( $\text{C}2''$ ). MS (ES) $^+$ : 659.35 [M+H] $^+$ .

*N*-(2''-S-Chloropropanoyl)-*N*-[2'*R*-dibenzylamino]-3'-phenylprop-1'-yl]-L-Phe-OBn (10)

Syrup. Yield: 20% (from 8). Eluents: EtOAc:Hex (1:7). Mixture of rotamers M/m = 2:1. HPLC:  $t_R$  = 7.88 min (gradient of 5% to 100% of A, in 20 min).  $^1\text{H}$  NMR (400 MHz,  $\text{CDCl}_3$ , Major rotamer):  $\delta$  7.27–6.91 (m, 25H, Ar), 5.10 (d, 1H,  $J$  = 12.2 Hz,  $\text{OCH}_2$ ), 5.03 (d, 1H,  $J$  = 12.2 Hz,  $\text{OCH}_2$ ), 4.44 (q, 1H,  $J$  = 7.0 Hz, 1'-H), 3.55 (d, 2H,  $J$  = 14.0 Hz,  $\text{NCH}_2$ ), 3.51 (d, 2H,  $J$  = 13.9 Hz,  $\text{NCH}_2$ ), 3.48 (m, 1H,  $\alpha$ -Phe), 3.34 (dd, 1H,  $J$  = 14.1, 5.9 Hz,  $\beta$ -Phe), 3.08 (m, 1H, 2'-H), 3.03 (m, 1H,  $\beta$ -Phe), 2.92 (m, 1H, 1'-H), 2.89 (dd, 1H,  $J$  = 14.0, 8.6 Hz, 1'-H), 2.76 (dd, 1H,  $J$  = 13.4, 7.5 Hz, 3'-H), 2.67 (dd, 1H,  $J$  = 13.4, 6.6 Hz, 3'-H), 1.72 (d, 3H,  $J$  = 6.5 Hz, 2''-H).  $^{13}\text{C}$  NMR (75 MHz,  $\text{CDCl}_3$ ):  $\delta$  169.6 (COO), 168.3 (CON), 139.0, 138.2, 135.8, 130.1, 129.6, 128.7, 128.6, 128.55, 128.5, 128.4, 127.3, 126.8, 126.5 (Ar), 67.2 ( $\text{OCH}_2$ ), 63.2 ( $\alpha$ -Phe), 59.2 ( $\text{C}2'$ ), 53.6 ( $\text{NCH}_2$ ), 50.9 ( $\text{C}1''$ ), 48.9 ( $\text{C}1'$ ), 34.6 ( $\text{C}3'$ ) 34.5 ( $\beta$ -Phe), 21.7 ( $\text{C}2''$ ). MS (ES) $^+$ : 659.56 [M+H] $^+$ .

*N*-(2''-R-Chloropropanoyl)-*N*-[2'*S*-dibenzylamino]-3'-phenylprop-1'-yl]-L-Phe-OBn (11)

Syrup. Yield: 52% (from 7). Eluent: EtOAc:Hex (1:6). Mixture of rotamers, M/m = 7:1. HPLC:  $t_R$  = 7.25 min.  $^1\text{H}$  NMR (400 MHz,  $\text{CDCl}_3$ , major rotamer):  $\delta$  7.26–6.76 (m, 25H, Ar), 4.93 (s, 2H,  $\text{OCH}_2$ ), 4.58 (q, 1H,  $J$  = 6.5, 1''-H), 3.53 (dd, 1H,  $J$  = 15.9, 4.7, 1'-H), 3.54 (d, 2H,  $J$  = 13.9,  $\text{NCH}_2$ ), 3.50 (d, 2H,  $J$  = 13.9,  $\text{NCH}_2$ ), 3.16 (dd, 1H,  $J$  = 13.8, 10.1,  $\beta$ -Phe), 3.10 (dd, 1H,  $J$  = 13.8, 4.7,  $\beta$ -Phe), 3.00 (m, 1H, 2'-H), 2.89 (dd, 1H,  $J$  = 10.1, 4.7,  $\alpha$ -Phe), 2.68 (dd, 1H,  $J$  = 13.2/6.6, 3'-H), 2.50 (dd, 1H,  $J$  = 13.1/8.4, 3'-H), 2.04 (dd, 1H,  $J$  = 15.9, 5.7, 1'-H), 1.34 (d, 3H,  $J$  = 6.4, 2''-H).  $^{13}\text{C}$  NMR (75 MHz,  $\text{CDCl}_3$ ):  $\delta$  169.3 (COO), 169.2 (CON), 139.1, 138.9, 137.8, 136.0, 129.9, 129.8, 128.8, 128.7, 128.6, 128.5, 128.4, 128.3, 127.4, 126.7, 126.6 (Ar), 67.1 ( $\text{OCH}_2$ ), 64.8 ( $\alpha$ -Phe), 62.4 ( $\text{C}2'$ ), 53.9 ( $\text{NCH}_2$ ), 52.5 ( $\text{C}1''$ ), 49.6 ( $\text{C}1'$ ), 34.5 ( $\beta$ -Phe), 34.4 ( $\text{C}3'$ ), 20.5 ( $\text{C}2''$ ). MS (ES) $^+$ : 659.35 [M+H] $^+$ .

*N*-(2''-R-Chloropropanoyl)-*N*-[2'*R*-dibenzylamino]-3'-phenylprop-1'-yl]-L-Phe-OBn (12)

Syrup. Yield: 43% (from 8). Eluents: EtOAc:Hex (1:8). Mixture of rotamers M/m = 3:1. HPLC:  $t_R$  = 7.84 min (gradient of 5% to 100% of A, in 20 min).  $^1\text{H}$  NMR (400 MHz,  $\text{CDCl}_3$ , Major rotamer):  $\delta$  7.32–6.92 (m, 25H, Ar), 5.21 (d, 1H,  $J$  = 12.2 Hz,  $\text{OCH}_2$ ), 4.91 (d, 1H,  $J$  = 12.2 Hz,  $\text{OCH}_2$ ), 4.45 (q, 1H,  $J$  = 7.0 Hz, 1''-H), 3.80 (dd, 1H,  $J$  = 10.1, 4.5 Hz,  $\alpha$ -Phe), 3.51 (d, 2H,  $J$  = 14.0 Hz,  $\text{NCH}_2$ ), 3.35 (m, 2H,  $\beta$ -Phe), 3.34 (d, 2H,  $J$  = 14.0 Hz,  $\text{NCH}_2$ ), 3.28 (dd, 1H,  $J$  = 15.2, 7.1 Hz, 1'-H), 3.12 (m, 1H, 2'-H), 2.68 (dd, 1H,  $J$  = 13.2, 8.3 Hz, 3'-H), 2.54 (dd, 1H,  $J$  = 13.2, 6.7 Hz, 3'-H), 2.45 (dd, 1H,  $J$  = 15.4, 4.0 Hz, 1'-H), 1.74 (d, 3H,  $J$  = 7.0 Hz, 2''-H).  $^{13}\text{C}$  NMR (75 MHz,  $\text{CDCl}_3$ ):  $\delta$  169.7 (COO), 168.3 (CON), 139.0, 138.2, 135.8, 130.0, 129.6, 128.75, 128.65, 128.6, 128.45, 128.4, 127.3, 126.9, 126.5 (Ar), 67.3 ( $\text{OCH}_2$ ), 63.2 ( $\alpha$ -Phe), 59.24 ( $\text{C}2'$ ), 53.2 ( $\text{NCH}_2$ ), 50.9 ( $\text{C}1''$ ), 48.9 ( $\text{C}1'$ ), 34.6 ( $\text{C}3'$ ), 34.5 ( $\beta$ -Phe), 21.6 ( $\text{C}2''$ ). MS (ES) $^+$ : 659.56 [M+H] $^+$ .

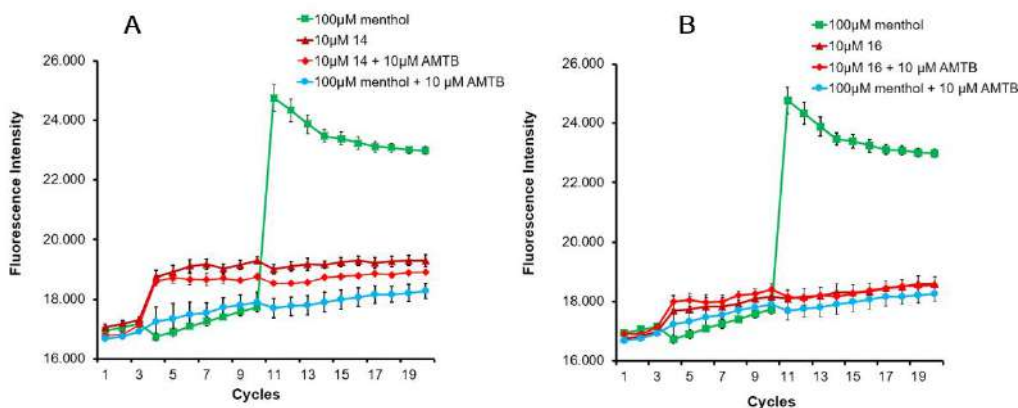


**Figure A1.** Effect of compounds on TRPM8 activity measured by fluorometric methods. Representative graph of compound 14 (A) and 16 (B) at 10  $\mu$ M on HEK-rTRPM8 cells. After 3 basal fluorescence measurements compounds 14 (A) and 16 (B) were applied (maroon trace) with hardly any effect. An amount of 10  $\mu$ M N-(3-aminopropyl)-2-[(3-methylphenyl)methoxy]-N-(2-thienylmethyl)-benzamide (AMTB) as a negative control was also applied in cycle 3 (blue trace). Subsequently after cycle 10, 100  $\mu$ M menthol was added being the fluorescent signal completely blocked. An amount of 100  $\mu$ M menthol was also applied in absence of blockers as a positive control (green trace). An amount of 10  $\mu$ M AMTB was added together with 14 and 16 (red trace) to ensure that the small increase in fluorescence after compounds' addition was not due to any agonist activity.

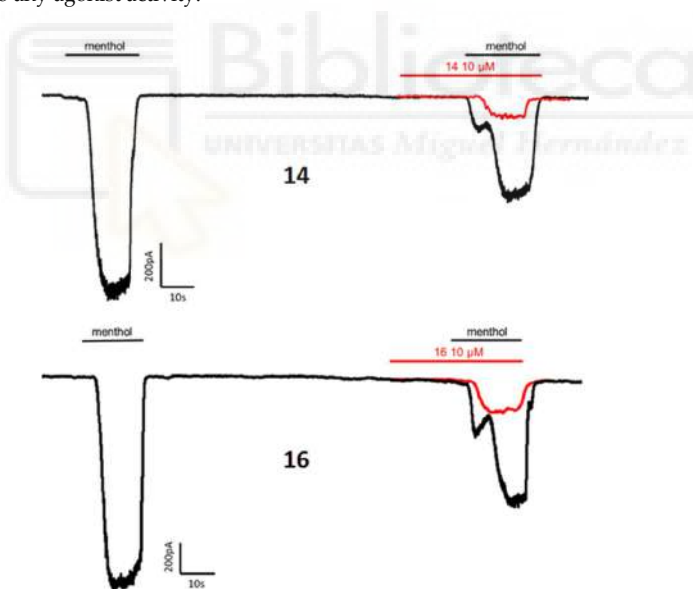


**Figure A2.** Compounds 14 and 16 inhibited TRPM8-mediated currents studied by whole cell Patch clamp. Representative menthol-evoked rTRPM8 current registered at a holding potential of -60 mV for control condition with two pulses of 100  $\mu$ M menthol (black traces) and test condition with 30s perfusion of 10  $\mu$ M 14 and 16 (red traces) before the second menthol pulse.

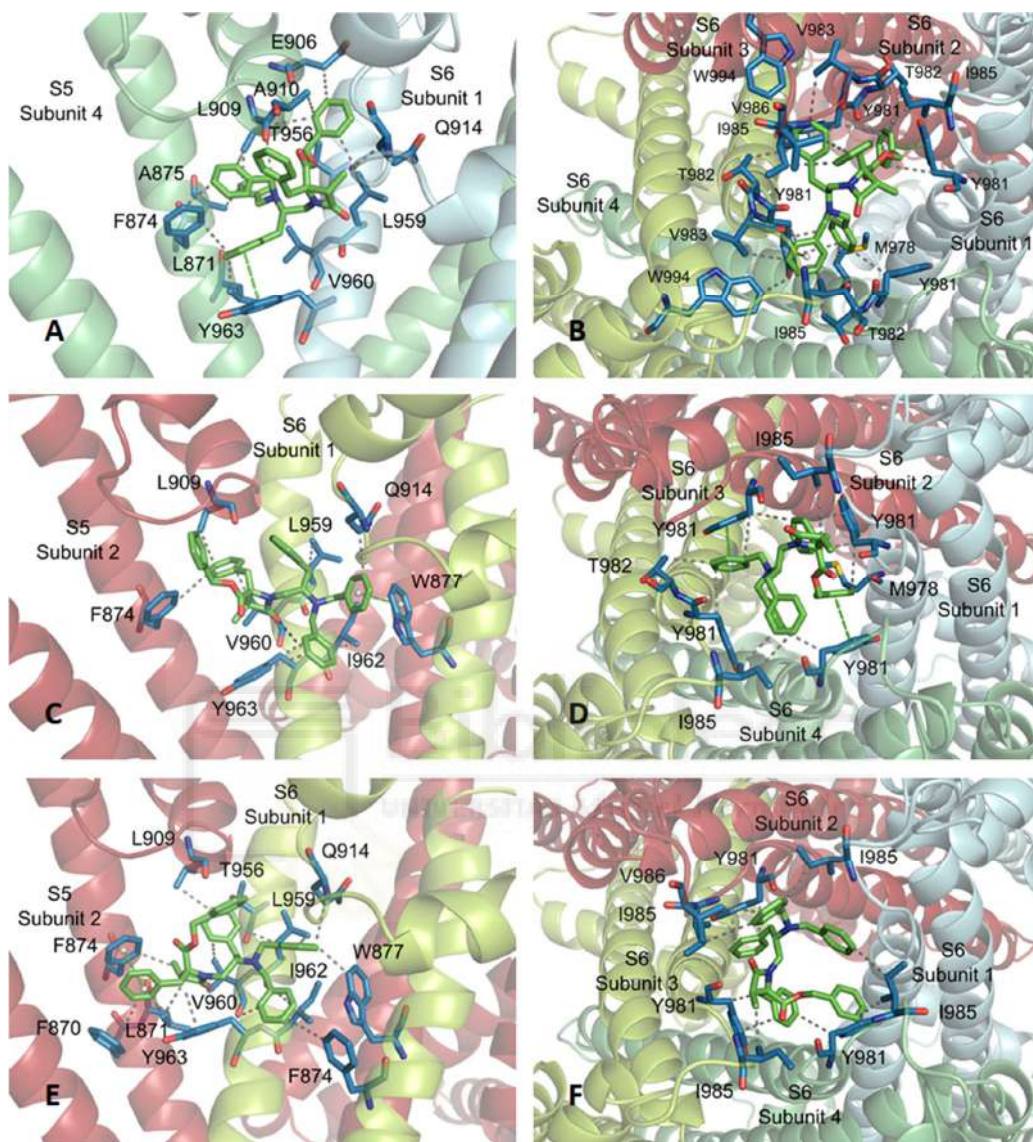


**Figure A3.** Subsite 1 (A) and 2 (B) found for  $\beta$ -lactam 13. Subsites 1 (C) and 2 (D) found for  $\beta$ -lactam 14. Subsite 1 (E) and 2 (F) found for  $\beta$ -lactam 15. WdV interactions are indicated by dotted gray lines, and  $\pi$ - $\pi$  stacking by centroids and non-continuous pale green lines. Channel residues involved in the interactions are shown in blue and labelled.

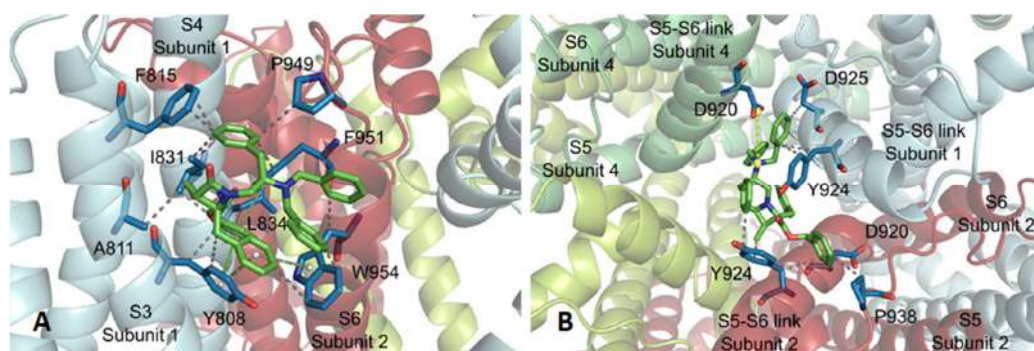


**Figure A4.** Subsite 3 (A) for  $\beta$ -lactam 14 and subsite 4 for  $\beta$ -lactam 16 (B). WdV interactions are indicated by dotted gray lines, and  $\pi$ - $\pi$  stacking by centroids and non-continuous pale green lines. Channel residues involved in the interactions are shown in blue and labelled.

## References

- Liu, Y.; Qin, N. TRPM8 in health and disease: Cold sensing and beyond. *Adv. Exp. Med. Biol.* **2011**, *704*, 185–208.
- Zakharian, E.; Cao, C.; Rohacs, T. Gating of transient receptor potential melastatin 8 (TRPM8) channels activated by cold and chemical agonists in planar lipid bilayers. *J. Neurosci.* **2010**, *30*, 12526–12534.
- Daniels, R.L.; Takashima, Y.; McKemy, D.D. Activity of the Neuronal Cold Sensor TRPM8 Is Regulated by Phospholipase C via the Phospholipid Phosphoinositol 4,5-Bisphosphate. *J. Biol. Chem.* **2009**, *284*, 1570–1582.
- Asuthkar, S.; Demirkhanyan, L.; Sun, X.; Velpula, K.K.; Zakharian, E.; Elustondo, P.A.; Krishnan, V.; Baskaran, P.; Thyagarajan, B.; Pavlov, E.V. The TRPM8 protein is a testosterone receptor: II. Functional evidence for an ionotropic effect of testosterone on TRPM8. *J. Biol. Chem.* **2015**, *290*, 2670–2688.
- Lippoldt, E.K.; Elmes, R.R.; McCoy, D.D.; Knowlton, W.M.; McKemy, D.D. Artemin, a glial cell line-derived neurotrophic factor family member, induces TRPM8-dependent cold pain. *J. Neurosci.* **2013**, *33*, 12543–12552.
- Tang, Z.; Kim, A.; Masuch, T.; Park, K.; Weng, H.; Wetzels, C.; Dong, X. Pirt functions as an endogenous regulator of TRPM8. *Nat. Commun.* **2013**, *4*, 1–9.
- Winchester, W.J.; Gore, K.; Glatt, S.; Petit, W.; Gardiner, J.C.; Conlon, K.; Postlethwaite, M.; Saintot, P.P.; Roberts, S.; Gosset, J.R.; et al. Inhibition of TRPM8 channels reduces pain in the cold pressor test in humans. *J. Pharmacol. Exp. Ther.* **2014**, *351*, 259–269.
- McKemy, D.D.; Neuhauser, W.M.; Julius, D. Identification of a cold receptor reveals a general role for TRP channels in thermosensation. *Nature* **2002**, *416*, 52–58.
- Kobayashi, K.; Fukuoka, T.; Obata, K.; Yamanaka, H.; Dai, Y.; Tokunaga, A.; Noguchi, K. Distinct expression of TRPM8, TRPA1, and TRPV1 mRNAs in rat primary afferent neurons with delta/c-fibers and colocalization with trk receptors. *J. Comp. Neurol.* **2005**, *493*, 596–606.
- Weyer, A.; Lehto, S. Development of TRPM8 Antagonists to Treat Chronic Pain and Migraine. *Pharmaceuticals* **2017**, *10*, 37.
- Rainero, I.; Rovetab, F.; Vaccac, A.; Noviellob, C.; Rubinoc, E. Migraine pathways and the identification of novel therapeutic targets Rubinoc. *Expert Opin. Ther. Target* **2020**, *3*, 245–253.
- Benemei, S.; Dussor, G. TRP Channels and Migraine: Recent Developments and New Therapeutic Opportunities. *Pharmaceuticals* **2019**, *12*, 54.
- Ling, B.; Coudore-Civiale, M.-A.; Balaýssac, D.; Eschalier, A.; Coudore, F.; Authier, N.; Ling, B.; Coudore-Civiale, M.-A.; Balaýssac, D.; Eschalier, A.; et al. Behavioral and Immunohistological Assessment of Painful Neuropathy Induced by a Single Oxaliplatin Injection in the Rat. *Toxicology* **2007**, *234*, 176–184.
- Ling, B.; Authier, N.; Balaýssac, D.; Eschalier, A.; Coudore, F. Behavioral and Pharmacological Description of Oxaliplatin-Induced Painful Neuropathy in Rat. *Pain* **2007**, *128*, 225–234.
- Mizoguchi, S.; Andoh, T.; Yakura, T.; Kuraishi, Y. Involvement of C-Myc-Mediated Transient Receptor Potential Melastatin 8 Expression in Oxaliplatin-Induced Cold Allodynia in Mice. *Pharmacol. Rep.* **2016**, *68*, 645–648.
- Sabnis, A.S. Expression and Characterization of the TRPM8 Receptor in Lung Epithelial Cells. *Cell Mol. Biol.* **2008**, *39*, 466–474.
- Yu, W.; Hill, W.G.; Apodaca, G.; Zeidel, M.L. Expression and Distribution of Transient Receptor Potential (TRP) Channels in Bladder Epithelium. *Am. J. Physiol.* **2011**, *300*, 49–59.
- Noyer, L.; Grolez, G.P.; Prevarskaya, N.; Gkika, D.; Noyer, L.; Grolez, G.P.; Prevarskaya, N.; Gkika, D.; Lemonnier, L. TRPM8 and Prostate: A Cold Case? *Pflugers Arch.* **2018**, *470*, 1419–1429.
- Ordas, P.; Hernandez-Ortego, P.; Vara, H.; Fernandez-Pena, C.; Morenilla-Palao, C.; Gomis, A.; Viana, F.; Reimundez, A.; Senaris, R.; Guadano-Ferraz, A.; et al. 2019. Expression of the cold thermoreceptor TRPM8 in rodent brain thermoregulatory circuits. *J. Comp. Neurol.* **2019**, *529*, 234–256.

20. Alcalde, I.; Íñigo-Portugués, A.; González-González, O.; Almaraz, L.; Artime, E.; Morenilla-Palao, C.; Gallar, J.; Viana, F.; Merayo-Llodes, J.; Belmonte, C. Morphological and functional changes in TRPM8-expressing corneal cold thermoreceptor neurons during aging and their impact on tearing in mice. *J. Comp. Neurol.* **2018**, *526*, 1859–1874.
21. Liu, X.; Ong, H.L.; Ambudkar, I. TRP Channel Involvement in Salivary Glands—Some Good, Some Bad. *Cells* **2018**, *7*, 74.
22. Alvarez-Berdugo, D.; Rofes, L.; Casamitjana, J.F.; Enrique, A.; Chamizo, J.; Vina, C.; Pollan, C.M.; Clave, P. TRPM8, ASIC1, and ASIC3 localization and expression in the human oropharynx. *Neurogastroenterol. Motil.* **2018**, *30*, e13398.
23. Mohandass, A.; Krishnan, V.; Gribkova, E.D.; Asuthkar, S.; Baskaran, P.; Nersesyan, Y.; Hussain, Z.; Wise, L.M.; George, R.E.; Stokes, N.; et al. TRPM8 as the rapid testosterone signaling receptor: Implications in the regulation of dimorphic sexual and social behaviors. *FASEB J.* **2020**, *34*, 10887–10906.
24. Lidao, B.; Yi, W.; Ruilian, M.; Xianhua, R.; Rui, C.; Agula, B. Apoptosis-inducing effects of lentinan on the proliferation of human bladder cancer T24 cells. *Pakistan Pharm. Sci.* **2015**, *8*, 1595–1600.
25. Genova, T.; Grolez, G.P.; Camillo, C.; Bernardini, M.; Bokhobza, A.; Richard, E.; Scianna, M.; Lemonnier, L.; Valdembri, D.; Munaron, L.; et al. TRPM8 Inhibits Endothelial Cell Migration via a Nonchannel Function by Trapping the Small GTPase Rap. *J. Cell Biol.* **2017**, *216*, 2107–2130.
26. Arcas, J.M.; Gonzalez, A.; Gers-Barlag, K.; Gonzalez-Gonzalez, O.; Bech, F.; Belmonte, C.; Gomis, A.; Viana, F.; Gonzalez-Gonzalez, O.; Bech, F.; et al. 2019 The Immunosuppressant Macrolide Tacrolimus Activates Cold-Sensing TRPM8 Channels. *J. Neurosci.* **2019**, *39*, 949–969.
27. Perez de Vega, M.J.; Gomez-Monterrey, I.; Ferrer-Montiel, A.; Gonzalez-Muniz, R. Transient Receptor Potential Melastatin 8 Channel (TRPM8) Modulation: Cool Entryway for Treating Pain and Cancer. *J. Med. Chem.* **2016**, *59*, 10006–10029.
28. Gonzalez-Muniz, R.; Bonache, M.A.; Martin-Escura, C.; Gomez-Monterrey, I. Recent Progress in TRPM8 Modulation: An Update. *Int. J. Mol. Sci.* **2019**, *20*, 1628.
29. Legay, C.M.; Gorobets, E.; Iftinca, M.; Ramachandran, R.; Altier, C.; Derksen, D.J. Natural-Product-Derived Transient Receptor Potential Melastatin 8 (TRPM8) Channel Modulators. *Org. Lett.* **2016**, *18*, 2746–2749.
30. De Petrocellis, L.; Arroyo, F.J.; Orlando, P.; Schiano Moriello, A.; Vitale, R.M.; Amodeo, P.; Sanchez, A.; Roncero, C.; Bianchini, G.; Martin, M.A.; et al. Tetrahydroisoquinoline-Derived Urea and 2,5-Diketopiperazine Derivatives as Selective Antagonists of the Transient Receptor Potential Melastatin 8 (TRPM8) Channel Receptor and Antiprstate Cancer Agents. *J. Med. Chem.* **2016**, *59*, 5661–5683.
31. Beccari, A.R.; Gemei, M.; Monte, M. Lo; Menegatti, N.; Fanton, M.; Pedretti, A.; Bovolenta, S.; Nucci, C.; Molteni, A.; Rossignoli, A. Novel Selective, Potent Naphthyl TRPM8 Antagonists Identified through a Combined Ligand-and Structure-Based Virtual Screening Approach. *Sci. Rep.* **2017**, *7*, 10999.
32. Bertamino, A.; Ostacolo, C.; Ambrosino, P.; Musella, S.; Di Sarno, V.; Ciaglia, T.; Soldovieri, M.V.; Iraci, N.; Fernandez Carvajal, A.; De La Torre-Martinez, R.; et al. Tryptamine-Based Derivatives as Transient Receptor Potential Melastatin Type 8 (TRPM8) Channel Modulators. *J. Med. Chem.* **2016**, *59*, 2179–2191.
33. Bertamino, A.; Iraci, N.; Ostacolo, C.; Ambrosino, P.; Musella, S.; Di Sarno, V.; Ciaglia, T.; Pepe, G.; Sala, M.; Soldovieri, M.V.; et al. Identification of a Potent Tryptophan-Based TRPM8 Antagonist with in Vivo Analgesic Activity. *J. Med. Chem.* **2018**, *61*, 6140–6152.
34. Journigan, V.B.; Feng, Z.; Rahman, S.; Wang, Y.; Amin, A.R.M.R.; Heffner, C.E.; Bachtel, N.; Wang, S.; Gonzalez-Rodriguez, S.; Fernández-Carvajal, A.; et al. Structure-Based Design of Novel Biphenyl Amide Antagonists of Human Transient Receptor Potential Cation Channel Subfamily M Member 8 Channels with Potential Implications in the Treatment of Sensory Neuropathies. *ACS Chem. Neurosci.* **2020**, *11*, 268–290.
35. Andrews, M.D.; Af Forselles, K.; Beaumont, K.; Galan, S.R.; Glossop, P.A.; Grenie, M.; Jessiman, A.; Kenyon, A.S.; Lunn, G.; Maw, G.; et al. Discovery of a Selective TRPM8 Antagonist with Clinical Efficacy in Cold-Related Pain. *ACS Med. Chem. Lett.* **2015**, *6*, 419–424.
36. Horne, D.B.; Biswas, K.; Brown, J.; Bartberger, M.D.; Clarine, J.; Davis, C.D.; Gore, V.K.; Harried, S.; Horner, M.; Kaller, M.R.; et al. 2018 Discovery of TRPM8 Antagonist (S)-6-(((3-Fluoro-4-(Trifluoromethoxy)Phenyl)(3-Fluoropyridin-2-Yl)methyl)Carbamoyl)Nicotinic Acid (AMG 333), a Clinical Candidate for the Treatment of Migraine. *J. Med. Chem.* **2018**, *61*, 8186–8201.
37. Yin, Y.; Wu, M.; Zubcevic, L.; Borschel, W.F.; Lander, G.C.; Lee, S.Y. Structure of the cold- and menthol-sensing ion channel TRPM8. *Science* **2018**, *359*, 237–241.
38. Yin, Y.; Lee, S.-Y. Current View of Ligand and Lipid Recognition by the Menthol Receptor TRPM8. *Trends Biochem. Sci.* **2020**, *45*, 806–819.
39. Yin, Y.; Le, S.C.; Hsu, A.L.; Borgnia, M.J.; Yang, H.; Lee, S.Y. Structural basis of cooling agent and lipid sensing by the coldactivated TRPM8 channel. *Science* **2019**, *363*, doi:10.1126/science.aav9334.
40. De la Torre-Martinez, R.; Bonache, M.A.; Llabres-Campaner, P.J.; Balsera, B.; Fernandez-Carvajal, A.; Fernandez-Ballester, G.; Ferrer-Montiel, A.; Perez de Vega, M.J.; Gonzalez-Muniz, R. Synthesis, high-throughput screening and pharmacological characterization of  $\beta$ -lactam derivatives as TRPM8 antagonists. *Sci. Rep.* **2017**, *7*, 1–13.
41. Bonache, M.A.; Martín-Escura, C.; de la Torre Martínez, R.; Medina, A.; Gonzalez-Rodriguez, S.; Francesch, A.; Cuevas, C.; Roa, A.M.; Fernandez-Ballester, G.; Ferrer-Montiel, A.; et al. Highly functionalized  $\beta$ -lactams and 2-ketopiperazines as TRPM8 antagonists with antiallodynic activity. *Sci. Rep.* **2020**, *10*, 14154.

42. Bertamino, A.; Ostacolo, C.; Medina, A.; Di Sarno, V.; Lauro, G.; Ciaglia, T.; Vestuto, V.; Pepe, G.; Basilicata, M.G.; Musella, S.; et al. Exploration of TRPM8 Binding Sites by  $\beta$ -Carboline-Based Antagonists and Their In Vitro Characterization and In Vivo Analgesic Activities. *J. Med. Chem.* **2020**, *63*, 9672–9694.
43. Perez-Faginas, P.; O'Reilly, F.; O'Byrne, A.; Garcia-Aparicio, C.; Martin-Martinez, M.; Perez de Vega, M.J.; Garcia-Lopez, M.T.; Gonzalez-Muniz, R. Exceptional Stereoselectivity in the Synthesis of 1,3,4-Trisubstituted 4-Carboxy  $\beta$ -Lactam Derivatives from Amino Acids. *Org. Lett.* **2007**, *9*, 1593–1596.
44. Perez-Faginas, P.; Alkorta, I.; Garcia-Lopez, M.T.; Gonzalez-Muniz, R. From theoretical calculations to the enantioselective synthesis of a 1,3,4-trisubstituted Gly-derived 2-azetidinone. *Tetrahedron Lett.* **2008**, *49*, 215–218.
45. Lampe, T.; Alonso-Alija, C.; Beck, H.; Rosentreter, U.; Sandner, P.; Stahl, E.; Stelte-Ludwig, B. Preparation of substituted 2-benzyloxy-benzoic acid amide derivatives as Cold Menthol Receptor 1 (CMR-1) modulators for treating and preventing urol. diseases or disorders. *PCT Int. Appl.* **2007**, WO 2007/017093.
46. Lashinger, E.S.R.; Steingang, M.S.; Hieble, J.P.; Leon, L.A.; Gardner, S.D.; Nagilla, R.; Davenport, E.A.; Hoffman, B.E.; Laping, N.J.; Su, X. AMTB, a TRPM8 channel blocker: Evidence in rats for activity in overactive bladder and painful bladder syndrome. *Am. J. Physiol. Renal Physiol.* **2008**, *295*, 803–810.
47. Noncovich, A.; Priest, C.; Ung, J.; Patron, A.P.; Servant, G.; Brust, P.; Servant, N.; Faber, N.; Liu, H.; Gonsalves, N.S.; et al. Discovery and development of a novel class of phenoxyacetyl amides as highly potent TRPM8 agonists for use as cooling agents. *Bioorg. Med. Chem. Lett.* **2017**, *27*, 3931–3938.
48. Chaudhari, S.S.; Kadam, A.B.; Khairatkar-Joshi, N.; Mukhopadhyay, I.; Karnik, P. V.; Raghuram, A.; Rao, S.S.; Vaiyapuri, T.S.; Wale, D.P.; Bhosale, V.M.; et al. Synthesis and pharmacological evaluation of novel N-aryl-3,4-dihydro-1'H-spiro[chromene-2,4'-piperidine]-1'-carboxamides as TRPM8 antagonists. *Bioorg. Med. Chem.* **2013**, *21*, 6542–6553.
49. Kobayashi, J.; Hirasawa, H.; Fujimori, Y.; Nakanishi, O.; Kamada, N.; Ikeda, T.; Yamamoto, A.; Kanbe, H. Identification of N-acyl-N-indanyl- $\alpha$ -phenylglycinamides as selective TRPM8 antagonists designed to mitigate the risk of adverse effects. *Bioorg. Med. Chem.* **2021**, *30*, 115903.
50. Kistner, K.; Siklosi, N.; Babes, A.; Khalil, M.; Selescu, T.; Zimmermann, K.; Wirtz, S.; Becker, C.; Neurath, M.F.; Reeh, P.W.; et al. Systemic desensitization through TRPA1 channels by capsazepine and mustard oil—A novel strategy against inflammation and pain. *Sci. Rep.* **2016**, *6*, 28621.
51. Krieger, E.; Darden, T.; Nabuurs, S.B.; Finkelstein, A.; Vriend, G. Making optimal use of empirical energy functions: Force-field parameterization in crystal space. *Proteins Struct. Funct. Bioinform.* **2004**, *57*, 678–683.
52. Krieger, E.; Koraimann, G.; Vriend, G. Increasing the precision of comparative models with yasara NOVA—a self-parameterizing force field. *Proteins Struct. Funct. Genet.* **2002**, *47*, 393–402.
53. Diver, M.M.; Cheng, Y.; Julius, D. Structural insights into TRPM8 inhibition and desensitization. *Science* **2019**, *365*, 1434–1440.
54. Nikolaeva-Koleva, M.; Butron, L.; Gonzalez-Rodriguez, S.; Devesa, I.; Valente, P.; Serafini, M.; Genazzani, A.A.; Pirali, T.; Ballester, G.F.; Fernandez-Carvajal, A.; et al. A capsaicinoid-based soft drug, AG1529, for attenuating TRPV1-mediated histaminergic and inflammatory sensory neuron excitability. *Sci. Rep.* **2021**, *11*, 246.
55. Canutescu, A.A.; Dunbrack, R.L.J. Cyclic coordinate descent: A robotics algorithm for protein loop closure. *Protein Sci.* **2003**, *12*, 963–972.
56. Sievers, F.; Wilm, A.; Dineen, D.; Gibson, T.J.; Karplus, K.; Li, W.; Lopez, R.; McWilliam, H.; Remmert, M.; Soding, J.; et al. Fast, scalable generation of high-quality protein multiple sequence alignments using Clustal Omega. *Mol. Syst. Biol.* **2011**, *7*, 539.
57. Morris, G.M.; Huey, R.; Lindstrom, W.; Sanner, M.F.; Belew, R.K.; Goodsell, D.S.; Olson, A.J. AutoDock4 and AutoDockTools4: Automated docking with selective receptor flexibility. *J. Comput. Chem.* **2009**, *30*, 2785–2791.
58. Duan, Y.; Wu, C.; Chowdhury, S.; Lee, M.C.; Xiong, G.; Zhang, W.; Yang, R.; Cieplak, P.; Luo, R.; Lee, T.; et al. A point-charge force field for molecular mechanics simulations of proteins based on condensed-phase quantum mechanical calculations. *J. Comput. Chem.* **2003**, *24*, 1999–2012.

**ANEXO III. Publicación 3 del capítulo 1*****β-Lactam TRPM8 Antagonist RGM8-51 Displays Antinociceptive Activity in Different Animal Models.***

Cristina Martín-Escura<sup>1,2,†</sup>, Alicia Medina-Peris<sup>3,†</sup>, Luke A. Spear<sup>1</sup>, Roberto de la Torre Martínez<sup>3</sup>, Luis A. Olivos-Oré<sup>4,5</sup>, María Victoria Barahona<sup>4,5</sup>, Sara González-Rodríguez<sup>3</sup>, Gregorio Fernández-Ballester<sup>3</sup>, Asia Fernández-Carvajal<sup>3</sup>, Antonio R. Artalejo<sup>4,5</sup>, Antonio Ferrer-Montiel<sup>3</sup> y Rosario González-Muñiz<sup>1</sup>.

<sup>1</sup>Instituto de Química Médica (IQM-CSIC), Juan de la Cierva 3, 28006 Madrid, España.

<sup>2</sup>Alodia Farmacéutica SL, 28108 Alcobendas, España.

<sup>3</sup>IDiBE, Universidad Miguel Hernández, Avda. de la Universidad s/n, 03202 Elche, España.

<sup>4</sup>Departamento de Farmacología y Toxicología, Facultad de Veterinaria, Universidad Complutense de Madrid, 28040 Madrid, España.

<sup>5</sup>Instituto Universitario de Investigación en Neuroquímica, Universidad Complutense de Madrid, 28040 Madrid, España.

<sup>†</sup>Estos autores contribuyeron por igual en este trabajo.

International Journal of Molecular Sciences 2022, 23 (5), 2692.

<https://doi.org/10.3390/ijms23052692>

(Q1; Factor de Impacto: 6.208)





Article

# $\beta$ -Lactam TRPM8 Antagonist RGM8-51 Displays Antinociceptive Activity in Different Animal Models

Cristina Martín-Escura <sup>1,2,†</sup>, Alicia Medina-Peris <sup>3,†</sup>, Luke A. Spear <sup>1</sup>, Roberto de la Torre Martínez <sup>3</sup>, Luis A. Olivos-Oré <sup>4,5</sup>, María Victoria Barahona <sup>4,5</sup>, Sara González-Rodríguez <sup>3,†</sup>, Gregorio Fernández-Ballester <sup>3</sup>, Asia Fernández-Carvajal <sup>3,\*</sup>, Antonio R. Artalejo <sup>4,5</sup>, Antonio Ferrer-Montiel <sup>3</sup> and Rosario González-Muñiz <sup>1,\*</sup>

<sup>1</sup> Instituto de Química Médica (IQM-CSIC), 28006 Madrid, Spain; cristinamartinescura@gmail.com (C.M.-E.); lukeanthonyspear@gmail.com (L.A.S.)

<sup>2</sup> Alodia Farmacéutica SL, 28108 Alcobendas, Spain

<sup>3</sup> IDiBE, Universidad Miguel Hernández, 03202 Elche, Spain; mepeas8@gmail.com (A.M.-P.); rober.dltm@gmail.com (R.d.l.T.M.); saragonzalezrodriguez@gmail.com (S.G.-R.); gregorio@umh.es (G.F.-B.); aferrer@umh.es (A.F.-M.)

<sup>4</sup> Departamento de Farmacología y Toxicología, Facultad de Veterinaria, Universidad Complutense de Madrid, 28040 Madrid, Spain; olivos@ucm.es (L.A.O.-O.); vbg@ucm.es (M.V.B.); antonio.artalejo@vet.ucm.es (A.R.A.)

<sup>5</sup> Instituto Universitario de Investigación en Neuroquímica, Universidad Complutense de Madrid, 28040 Madrid, Spain

\* Correspondence: asia.fernandez@umh.es (A.F.-C.); iqmg313@iqm.csic.es (R.G.-M.); Tel.: +00-34-258-74-34 (R.G.-M.)

† These authors contributed equally to the work.

‡ Present address: Facultad de Medicina, Instituto Universitario de Oncología del Principado de Asturias (IUOPA), Universidad de Oviedo, Julián Clavería 6, 33006 Oviedo, Spain.



**Citation:** Martín-Escura, C.; Medina-Peris, A.; Spear, L.A.; de la Torre Martínez, R.; Olivos-Oré, L.A.; Barahona, M.V.; González-Rodríguez, S.; Fernández-Ballester, G.; Fernández-Carvajal, A.; Artalejo, A.R.; et al.  $\beta$ -Lactam TRPM8 Antagonist RGM8-51 Displays Antinociceptive Activity in Different Animal Models. *Int. J. Mol. Sci.* **2022**, *23*, 2692. <https://doi.org/10.3390/ijms23052692>

Academic Editor: Irmgard Tegeder

Received: 25 January 2022

Accepted: 22 February 2022

Published: 28 February 2022

**Publisher's Note:** MDPI stays neutral with regard to jurisdictional claims in published maps and institutional affiliations.



**Copyright:** © 2022 by the authors. Licensee MDPI, Basel, Switzerland. This article is an open access article distributed under the terms and conditions of the Creative Commons Attribution (CC BY) license (<https://creativecommons.org/licenses/by/4.0/>).

**Abstract:** Transient receptor potential melastatin subtype 8 (TRPM8) is a cation channel extensively expressed in sensory neurons and implicated in different painful states. However, the effectiveness of TRPM8 modulators for pain relief is still a matter of discussion, since structurally diverse modulators lead to different results, depending on the animal pain model. In this work, we described the antinociceptive activity of a  $\beta$ -lactam derivative, RGM8-51, showing good TRPM8 antagonist activity, and selectivity against related thermoTRP channels and other pain-mediating receptors. In primary cultures of rat dorsal root ganglion (DRG) neurons, RGM8-51 potently reduced menthol-evoked neuronal firing without affecting the major ion conductances responsible for action potential generation. This compound has in vivo antinociceptive activity in response to cold, in a mouse model of oxaliplatin-induced peripheral neuropathy. In addition, it reduces cold, mechanical and heat hypersensitivity in a rat model of neuropathic pain arising after chronic constriction of the sciatic nerve. Furthermore, RGM8-51 exhibits mechanical hypersensitivity-relieving activity, in a mouse model of NTG-induced hyperesthesia. Taken together, these preclinical results substantiate that this TRPM8 antagonist is a promising pharmacological tool to study TRPM8-related diseases.

**Keywords:** TRPM8 channels; antagonist;  $\beta$ -lactam; oxaliplatin-induced peripheral neuropathy; CCI chronic neuropathic; nociception; NTG-induced hyperesthesia

## 1. Introduction

The cold-temperature thermosensor TRPM8 is a non-selective cation channel, widely expressed in peripheral sensory neurons having their soma in the dorsal root (DRG) and trigeminal (TG) ganglia, but also in different organs and tumor malignancies [1]. The important role of TRPM8 channels in the pathophysiology of diverse biological processes fosters the development of agonist/antagonist modulators, to enlarge the arsenal of pharmacological tools to study TRPM8-related diseases, including inflammatory and neuropathic

disorders, as well as tumor growth and dissemination [1]. In fact, a number of agonists and antagonists, belonging to different chemical families, have already been described [2,3].

The high expression of TRPM8 channels both in sensory neurons and organs, in addition to their activation by cold, point to these channels as mediators of cold-induced nociception and cold-hypersensitivity developed in certain peripheral neuropathies [4]. Nevertheless, some discrepancies have been found in the literature, and the exact role of TRPM8 in different pain types, and the usefulness of TRPM8 modulators to relieve them, is still a matter of profuse research.

The chronic constriction injury of the sciatic nerve (CCI) is a model of neuropathic pain that courses with hypersensitivity to cold, heat and mechanical stimuli [5]. Initial investigations on the expression of TRPM8 and TRPA1 channels after CCI injury, identified a low expression level of both channels in DRG neurons, and discard their involvement in cold hypersensitivity [6]. However, other experimental evidence indicates that sensitivity to cold after CCI is aggravated by TRPM8 activation and the increased expression of these channels in DRG neurons, whereas their downregulation or pharmacological blockade ameliorates CCI-induced cold hypersensitivity [7–9]. In good agreement, it has been described that the intrathecal administration of the TRPM8-selective antagonist AMTB reduces cold hypersensitivity in rats, but it exacerbates thermal nociception and has no apparent influence on mechanical hypersensitivity in the CCI model [10]. Likewise, the TRPM8 antagonist AMG2850, displaying a potent nanomolar profile *in vitro*, was able to reduce the number of wet-dog-like shakes induced by icilin, a TRPM8 agonist, but was ineffective on mechanical hypersensitivity in the complete Freund's adjuvant (CFA) model of inflammatory pain and the spinal nerve ligation model of neuropathic pain [11]. The authors suggest that TRPM8 channels could not have a relevant role in nociception in this model, but this is in contrast with recent results found for the novel TRPM antagonists DFL23693 and DFL23448 (imidazo[1',5':1,6]pyrido[3,4-*b*]indole-1,3(2H)-dione derivatives), which indicate that they effectively relieve thermal and mechanical hypersensitivity in CCI rats [12,13].

Thermal and mechanical hypersensitivity are also prominent symptoms in the peripheral neuropathy developed after chemotherapeutic treatments for cancer (i.e., platinum-derived drugs, vinca alkaloids and taxanes) [14] or viral infections (HIV, HCV, HSV, HZV) [15,16]. Some channels of the TRP family expressed in nociceptors, like TRPV1, TRPV4, TRPA1 and TRPM8 seem to contribute to this painful, exacerbated sensitivity [17]. For instance, oxaliplatin (OXA) causes acute and chronic peripheral pain, characterized by cold hypersensitivity, and seems to be related to increased activity of the TRPM8 channels, linked to the activation of phospholipase C and reduction in phosphatidylinositol 4,5-bisphosphate production [18]. In primary sensory neurons, the overexpression of TRPM8 mRNA and protein in oxaliplatin-induced peripheral neuropathy seems also to be mediated through the c-Myc regulatory gene [19]. Moreover, in both short- and long-term oxaliplatin-induced neuropathy animal models, both TRPA1 (HC033031) and TRPM8 (AMTB) antagonists attenuated the initially observed vasodilation after cold exposure [20]. Similarly, a recent study describes that oxaliplatin causes excitability of IB4 neurons, which can be attenuated by antagonists of TRPA1 (A-967079) and TRPM8 (TC-I), but not by capsazepine, a TRPV1 blocker, suggesting the contribution of cold channels in neuronal sensitization [21]. However, only the pretreatment with TC-I prevented cold and mechanical hypersensitivity induced by oxaliplatin, denoting key importance of the TRPM8 channel in the initial phase of sensitization. The involvement of L-type voltage-gated Ca<sup>2+</sup> channels in the over-expression of TRPM8 receptors leading to oxaliplatin-associated peripheral neuropathy has also been reported [22].

Cold hypersensitivity is also referred to as an important, undesirable secondary effect by patients receiving chronic treatment with opioids [23]. The hypersensitivity after sustained morphine administration was linked to TRPM8 upregulation, and can be blocked by TRPM8 antagonists, while TRPM8 knockout mice are not able to develop it [24].

Migraine, a neurovascular disorder affecting more than 14% of the adult population and more frequent in women than in men, is one of the most disabling conditions in the world. Some experimental evidence indicated that TRPM8 channels are overexpressed in a rat model of migraine, and that these channels could be implicated in the migraine mechanism, possibly through activation of NMDA receptors [25]. In addition, among other genetic factors, TRPM8 single-nucleotide polymorphisms (SNPs), such as rs10166942 and rs11562975, have been associated with chronic migraine and connected to allodynic symptoms [26–28]. Similarly, the SNP rs2651899 was described as a possible genetic marker for migraine susceptibility [27]. Concerning described TRPM8 antagonists, AMG 333 reached phase 1 clinical trials for the treatment of migraines [29]. However, the important side effects reported by volunteers, consisting of paresthesia, dysesthesia, dysgeusia and intolerable hot feeling, led to the compound's withdrawal, preventing its further progress to later clinical studies.

A few years ago, we described a new series of  $\beta$ -lactams acting as potent and selective TRPM8 antagonists (i.e., compounds 1, 2, Figure 1) [30,31], with compound 2 displaying significant activity for relieving oxaliplatin-induced cold hypersensitivity [31]. To advance in the characterization of our  $\beta$ -lactam derivatives, we selected a prototype in the series, RGM8-51 (3) for parallel evaluation in different animal models of pain occurring with upregulation of TRPM8 channels. Here, we describe the *in vitro* properties of RGM8-51 as a blocker of the TRPM8 activation and its selectivity over other TRP channels and receptors related to pain. In addition, we report the results of its *in vivo* activity in a mouse model of oxaliplatin-induced peripheral neuropathy, in the CCI model of neuropathic pain, and in NTG-induced hyperesthesia.

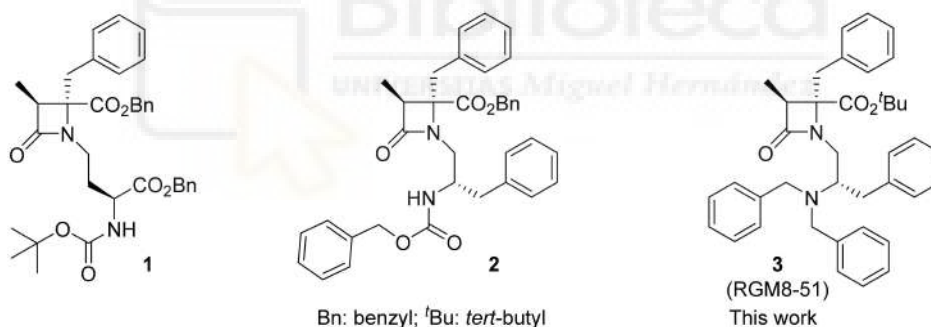
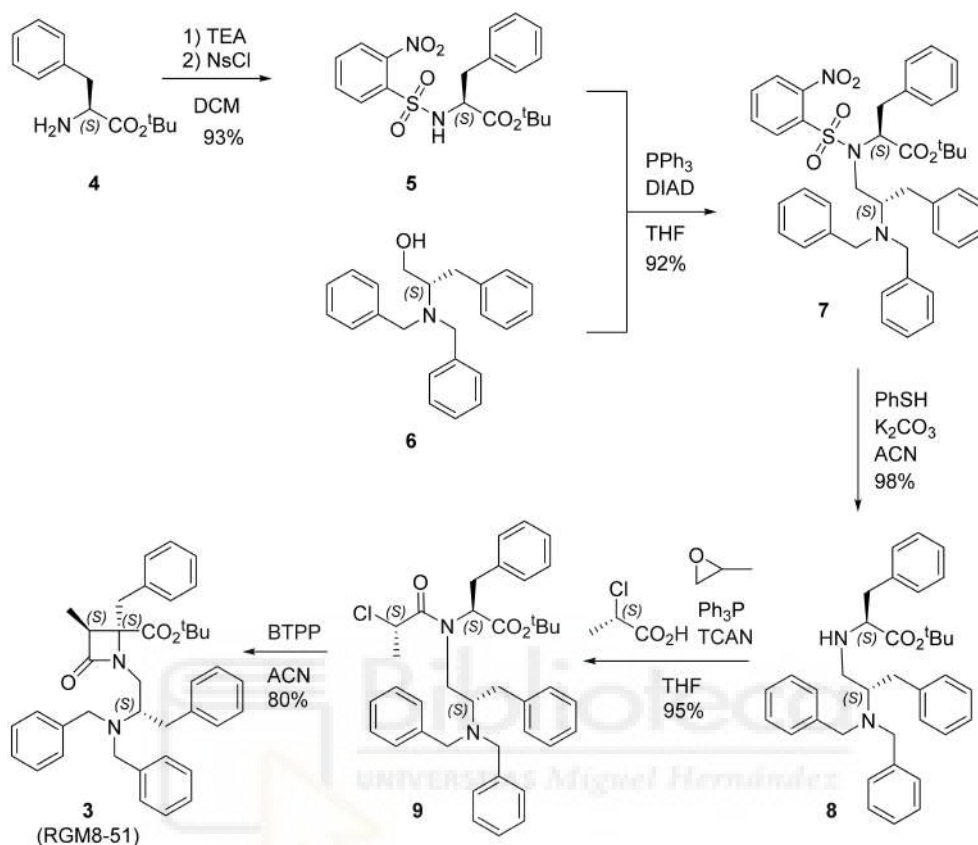


**Figure 1.**  $\beta$ -lactam TRPM8 antagonists: Compounds 1 and 2 came from previous works [30,31]; Compound 3 (RGM8-51), described in this work.

## 2. Results and Discussion

### 2.1. Synthesis

The synthetic multistep procedure to prepare  $\beta$ -lactam 3 (RGM8-51) is depicted in Scheme 1. Briefly, the commercial amino acid derivative HCl·H-L-Phe-O<sup>t</sup>Bu (4) is reacted with nosyl chloride to afford *N*-Ns-L-Phe-O<sup>t</sup>Bu (5) in very good yield. Under Mitsunobu conditions, using triphenylphosphine and diisopropylazido dicarboxylate (DIAD), amino acid derivative 5 reacts with 2*S*-(dibenzylamino-3-phenyl)propanol (6) to give the Phe-phenylalaninol conjugate 7 in excellent yield. Subsequently, the removal of the nosyl group, carried out with PhSH in a basic medium, led to the secondary amine 8, almost quantitatively. Then, an acylation reaction with 2*S*-chloropropanoyl chloride, prepared *in situ* from 2*S*-chloropropanoic acid, trichloroacetonitrile and triphenyl phosphine, allowed the formation of the enantiopure chloropropanoyl derivative 9. Finally, the BTTP-assisted cyclization of intermediate 9 gave rise to the desired  $\beta$ -lactam 3, with an overall yield of 64%. A 3*S*,4*S*,2'*S* configuration was assigned to compound 3, since the configuration of the 2-chloropropanoic acid used, 2*S*, directs the exclusive formation of the 3*S*,4*S*  $\beta$ -lactam ring, as previously demonstrated [32].



**Scheme 1.** Synthetic procedure for the preparation of  $\beta$ -lactam 3 (RGM8-51) from H-L-Phe-O<sup>t</sup>Bu (4). Compounds 5–9 are the synthetic intermediates in the process.

## 2.2. In Vitro TRPM8 Antagonist Activity

### 2.2.1. Experiments in Cell Lines

Calcium (Ca<sup>2+</sup>) micro-fluorography assays were performed on HEK293 cells that heterologously express both rat (*r*) or human (*h*) TRPM8 channel isoforms, using menthol as activation stimulus [30].  $\beta$ -lactam RGM8-51 (3) did not have any ability to activate TRPM8 channels, but produced a concentration-dependent inhibition of menthol activation. As indicated in Table 1, compound RGM8-51 displays antagonist activity at both isoforms of the TRPM8 channel. The IC<sub>50</sub> values are in the micromolar range, 1.06 ± 1.21 and 1.74 ± 1.19  $\mu$ M, respectively, slightly higher for *h*TRPM8. This represents a similar activity as  $\beta$ -lactam 2 and a somewhat higher potency than the model TRPM8 antagonists AMTB.

To confirm the antagonistic activity, electrophysiology (patch-clamp) studies were performed on HEK293 cells expressing the *r*TRPM8 channel. As shown in Figure 2, perfusion with 100  $\mu$ M menthol (blue line) produces a strong outward rectifying ionic current, characterized by a negligible current at negative potential and a linear increase (ohmic behavior) at positive voltages. This current is clearly reduced by addition of  $\beta$ -lactam RGM8-51 (10  $\mu$ M, red line). Then, using a holding voltage of −60 mV, different concentrations of RGM8-51 were used to establish the concentration/response curve for *r*TRPM8 current blockade. The obtained IC<sub>50</sub> value, 0.97 ± 1.56  $\mu$ M (Table 1), confirms a micromolar antagonist potency.

**Table 1.** Antagonist activity of RGM8-51 at *r*TRPM8 and *h*TRPM8 channels (Ca<sup>2+</sup> microfluorography and patch-clamp assays).

Compd.	Ca <sup>2+</sup> Microfluorography Assays			Patch-Clamp Assay	
	<i>r</i> TRPM8 IC <sub>50</sub> (μM)	Intervals	<i>h</i> TRPM8 IC <sub>50</sub> (μM)	Intervals	<i>r</i> TRPM8 IC <sub>50</sub> (μM)
RGM8-51 (3)	1.06 ± 1.21	0.72 to 1.55	1.74 ± 1.19	1.23 ± 2.45	0.97 ± 1.56
2	3.1 ± 1.1	2.57 to 3.99	–	–	0.9 ± 1.0
AMTB	7.3 ± 1.5 *	–	6.23 ± 0.02 **	–	–

*r*TRPM8: transient receptor potential melastatin, type 8 channel, rat isoform. *h*TRPM8: transient receptor potential melastatin, type 8 channel, human isoform. Three different experiments, performed in triplicate. \* Reference [31]. \*\* Versus icilin (Reference [33]).

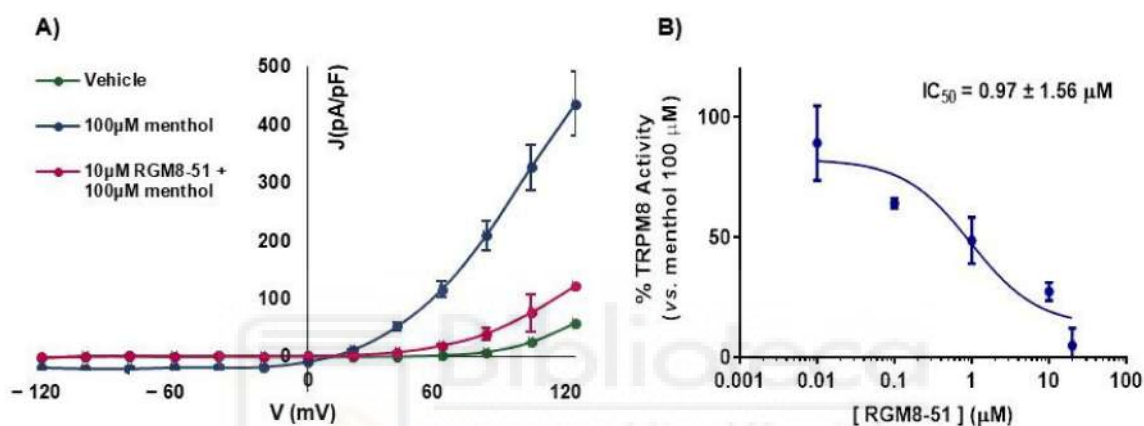


**Figure 2.** Compound 3 (RGM8-51) blocks TRPM8-mediated responses evoked by menthol in *r*TRPM8-expressing HEK293 cells. (A) IV curves obtained after exposure to vehicle solution (green trace), 100 μM menthol (blue trace), and 100 μM menthol + 10 μM RGM8-51 (red trace). Peak current data were expressed as pA/pF (to allow comparison among different size cells). Each point is the mean ± SEM of  $n = 15$ . (B) Concentration/response curves for *r*TRPM8 current blockade by RGM8-51, at a holding voltage of  $-60$  mV. The solid line represents fits of the experimental data to the following binding isotherm:  $y = \max / (1 + x / IC_{50})^n$ , where  $x$  is the drug concentration and  $n$  the Hill coefficient. The fitted value for  $IC_{50}$  was  $0.97 \pm 1.56$ . Each point is the mean ± SEM of  $n = 15$ .

To uncover the selectivity of RGM8-51 for the TRPM8 channel, its activity was measured on different ion channels and receptors involved in pain-related processes. Firstly, *h*TRPV1, *h*TRPV3 and *h*TRPA1 ion channels were selected, since they are expressed in primary afferent neurons, and involved in the integration of temperature and nociception [34,35]. The *h*ASIC3 channel was also included in the selectivity study because it is widely distributed in the peripheral nervous system, and its activation augments excitability of primary sensory neurons [36].

In all cases, the compound was evaluated at 10 μM, a concentration that is ~10 and >5 times higher than the  $IC_{50}$  value for *r*TRPM8 and *h*TRPM8, respectively. As indicated in Table 2, compound RGM8-51 shows some ability to activate the *h*TRPV1 channel (~30%), while its activity as an antagonist at this heat receptor is lower than 20%. β-lactam RGM8-51 did not display any agonist or antagonist profile in cool-activated TRPA1 channels and has negligible activity as TRPV3 and ASIC3 channel antagonists. In general, this β-lactam is selective for cold-activated TRPM8 channels, although TRPV1 channels could be activated to some extent at high concentrations.

**Table 2.** Functional activity of RGM8-51 (10  $\mu\text{M}$ ) in  $\text{Ca}^{2+}$  microfluorography assays of TRPV1, TRPV3, TRPA1 and ASIC3 channels, and percentage of inhibition of specific binding at CGRPR, CB2 and M3 receptors.

Compd.	<i>h</i> TRPV1 ago. (%)	<i>h</i> TRPV1 antago. (%)	<i>h</i> TRPV3 antago. (%)	<i>h</i> TRPA1 ago. (%)	<i>h</i> TRPA1 Antago. (%)	ASIC3 Antago. (%)	Binding <i>h</i> CGRPR (%)	Binding <i>h</i> CB <sub>2</sub> (%)	Binding <i>h</i> M <sub>3</sub> (%)
RGM8-51	31.3 $\pm$ 3.6	19.4 $\pm$ 1.7	−6.3 $\pm$ 5.9	0.4 $\pm$ 0.3	4.3 $\pm$ 1.1	6.0 $\pm$ 0.9	−1.0 $\pm$ 4.3	7.3 $\pm$ 0.3	−4.1 $\pm$ 3.1

*h*TRPV1: transient receptor potential vanilloid, type 1. *h*TRPV3: transient receptor potential vanilloid, type 3. *h*TRPA1: transient receptor potential ankirin, type 1. ASIC3: acid sensing ion channel, subunit 3. *h*CGRPR: human calcitonin gene-related peptide receptor. *h*CB<sub>2</sub>: human cannabinoid receptor, subtype 2. *h*M<sub>3</sub>: human muscarinic receptor, subtype 3. In all cases, data is from two experiments in duplicate. Ago.: assay for agonist activity. Antago.: assay for antagonist activity (see methods). Agonists used for activation: TRPV1 (Capsaicin, 30 nM), TRPV3 (2-Aminoethoxydiphenyl borate, 2-APB, 30  $\mu\text{M}$ ), TRPA1 (Allylisothiocyanate, 10  $\mu\text{M}$ ), ASIC3 (Buffer, pH 5.5). Reference antagonists: TRPV1 (Capsazepin,  $\text{CI}_{50}$  1.3·10<sup>−7</sup>), TRPV3 (Ruthenium red,  $\text{CI}_{50}$  2.5·10<sup>−7</sup> M), TRPA1 (Ruthenium red, 10  $\mu\text{M}$ ), ASIC3 (Amiloride, 1 mM). Radioligand for *h*CGRPR: [<sup>125</sup>I]hGCRP $\alpha$ , agonist *h*CGRP $\alpha$  (1  $\mu\text{M}$ ). Radioligand for *h*CB<sub>2</sub>: [<sup>3</sup>H]WIN 55212-2, agonist WIN 55212-2 (5  $\mu\text{M}$ ). Radioligand for *h*M<sub>3</sub>: [<sup>3</sup>H]4-DMAP, agonist 4-DMAP (1  $\mu\text{M}$ ).

Next, the assessment of activity at other peripheral receptors related to pain, inflammation or migraine was considered. Calcitonin gene related peptide (CGRP) receptors are expressed in numerous tissues and in primary sensory neurons of TGG, where they are involved in pain transmission and inflammatory processes [37]. CGRP levels have also been shown to increase in cranial circulation of patients with migraine symptoms [38]. Cannabinoid receptor CB2 is highly expressed in the peripheral nervous system, where it is rapidly regulated in peripheral neurons after injury and inflammation to dampen neuronal excitability and has been associated with paclitaxel-induced peripheral neuropathy [39–41]. Muscarinic acetylcholine receptors (mAChRs) are mainly located at the dorsal horn of the spinal cord and also seem to contribute to nociceptive regulation [42]. Among mAChRs, the M3 subtype is also expressed in different types of skin cells, such as keratinocytes and melanocytes [43,44].

To define whether  $\beta$ -lactam derivative RGM8-51 could bind to CGRPR, CB2 and M3 receptors, in vitro binding assays were performed, using CHO cell lines transfected with these receptors. The degree of binding was determined by using specific radioligands for each receptor (Table 2, footnote). As shown in Table 2, RGM8-51 at a 10  $\mu\text{M}$  concentration did not show significant affinity for the mentioned receptors, thus reinforcing its selectivity for TRPM8 channels.

### 2.2.2. Experiments in DRG Neurons

We also investigated the effect of RGM8-51 on native TRPM8 channels from rat DRG neurons. Whole-cell patch-clamp recordings from small size DRG neurons evidenced menthol (100  $\mu\text{M}$ )-activated inward currents at a holding voltage of −80 mV (Figure 3A). As expected from results obtained in *r*TRPM8-expressing HEK293 cells, RGM8-51 (1  $\mu\text{M}$ ) inhibited menthol-activated currents. Mean peak current inhibition amounted to 65.01  $\pm$  4.67% (from 1.50  $\pm$  0.19 to 0.51  $\pm$  0.09 pA/pF; n = 8 cells) (Figure 3A). Interestingly, RGM8-51 did not modify on its own the baseline current at -80 mV and had no effect on voltage-activated Na<sup>+</sup> and K<sup>+</sup> currents evoked by a depolarization pulse to +10 mV (Figure 3B). Besides extending results obtained with RGM8-51 in heterologously expressed TRPM8 channels to native TRPM8 channels, these data rule out a direct effect of this compound on major ion conductances responsible for action potential generation in primary nociceptive neurons.

In order to test if compound RGM8-51 could affect the membrane resting potential (MRP) of DRG sensory neurons, we also measured MRP of sensory neurons in the current-clamp mode of patch-clamp. In this condition, small sensory neurons displayed a MRP of ~−50 mV (Figure 4A, top trace, and Figure 4B). Exposure of the neurons to 10  $\mu\text{M}$  of RGM8-51 did not alter the MRP of these neurons (Figure 4A, middle trace, and Figure 4B). As control to ensure that neurons were able to exhibit action potential firing they were exposed to 0.5  $\mu\text{M}$  capsaicin (Figure 4A, bottom trace, and Figure 4B).

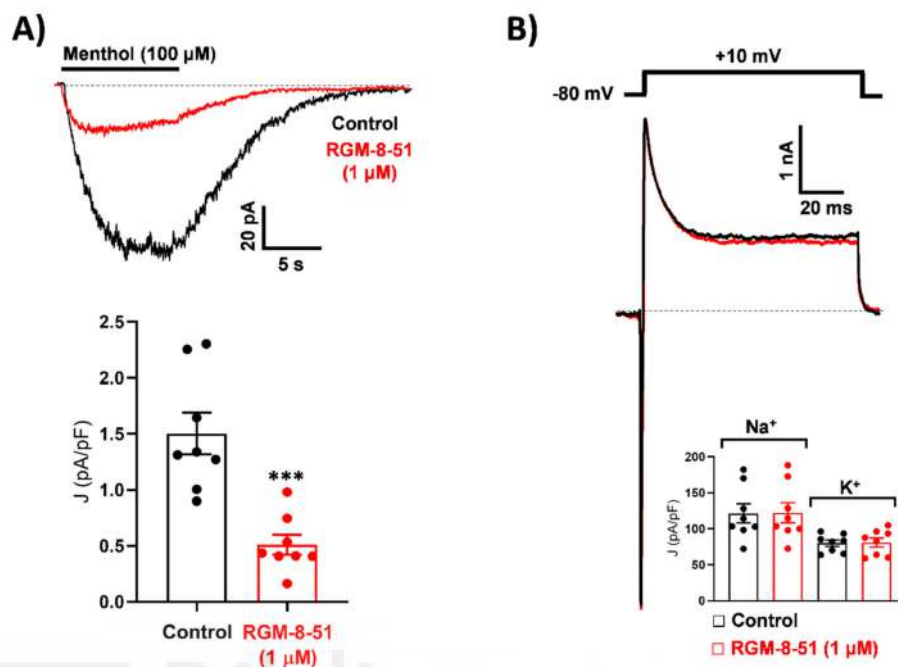


**Figure 3.** Effect of RGM8-51 on TRPM8-mediated and voltage-activated Na<sup>+</sup> and K<sup>+</sup> currents in rat DRG neurons. Currents were evoked by menthol (100 μM) (A) or a voltage depolarization to +10 mV (B). The horizontal bar on top of the recordings in A indicates the time period of menthol application. Holding voltage was −80 mV. Bar/scatter plot graphs in the lower part of the panels show peak-current densities (J; pA/pF) before and after RGM8-51 (1 μM). Data are mean ± S.E.M (n = 8 cells from 5 cultures). Statistical analysis was performed by using the paired *t*-test. \*\*\* < 0.001.

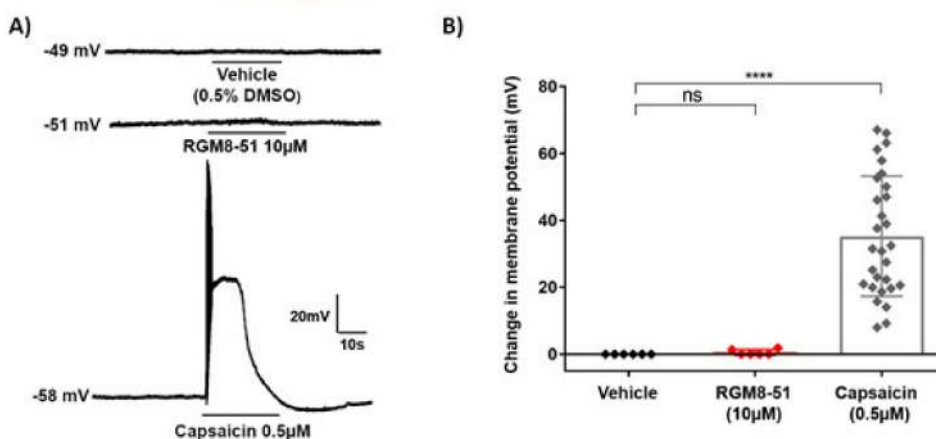


**Figure 4.** Compound RGM8-51 does not affect the membrane resting potential of sensory neurons. (A) Representative recordings of resting membrane potential measured under current-clamp conditions. The upper trace shows how the resting membrane potential remains constant after the addition of vehicle, and 10 μM of compound RGM8-51 (middle trace). The bottom trace shows action potentials firing in a DRG neuron exposed to 0.5 μM capsaicin. (B) Changes in membrane potential in the absence and the presence of 10 μM of compound RGM8-51, and in the presence of capsaicin (Cap) 0.5 μM. Data were analyzed by one-way ANOVA followed by Bonferroni post hoc test for multiple comparisons (ns = no significance, \*\*\*\* = 0.0001) and given as mean ± SEM; n ≥ 6 cells from 2 cultures.

### 2.2.3. In Vitro Preliminary Pharmacokinetic Studies

RGM8-51 displayed quite good solubility (198  $\mu\text{M}$ ) in simulated gastric conditions (pH < 5.5). This compound has a logD of 5.7 and was not able to permeate CACO-2 cell monolayers, indicating that oral administration cannot be selected for in vivo experiments (Table S1). RGM8-51 shows high binding to serum proteins (99–100%). As expected by the high number of phenyl rings, the ester moiety and the N-benzyl groups, neither the stability in human hepatic microsome cultures is high ( $t_{1/2} = 11$  min) nor the intrinsic clearance is very good ( $\text{Cl}_{\text{int}} = 614$   $\mu\text{L}/\text{min}/\text{mg}$ ), although the value is better than that of terfenadine, used as one of the reference controls. As indicated later, despite not optimal PK properties, RGM8-51 displayed significant activity in in vivo experiments after intraplantar (i.pl.) and intraperitoneal administration (i.p.).

### 2.3. Molecular Modeling Studies

The identification of putative binding pockets for RGM8-51 within the TRPM8 tetrameric channel was performed by docking studies simulations, using Yasara software [45,46], in a 3D model of the *r*TRPM8 channel. This model was constructed from the cryo-electron microscopy (cryo-EM) structure of the bird *Ficedula albicollis* TRPM8 (*fa*TRPM8, PDB code 6BPQ) [47].

Four main solutions were found for the accommodation of RGM8-51 in the TRPM8 channel, most of them located by the pore zone (Table 3). The most populated subsite 1 is a cavity formed by residues at S5-S6 transmembrane helices, located at the upper part of a protein subunit, and the S5 and the S5-to-S6 pore loop of a contiguous subunit (Figure 5, left). As for the concrete interconnections, three incidences of  $\pi$ - $\pi$  stacking were identified. Two of them involve the aromatic ring of the 4-Bn group of RGM8-51 and Trp877 and Phe881 of the channel, and are T-shape interactions, while the third one is a face-to-face  $\pi$ - $\pi$  stacking between the small molecule N-Bn group and the Phe 963 of the protein. In addition, a high number of Van der Waals interactions contribute to the stabilization of the complex, including the *tert*-butyl group on the  $\beta$ -actam and Tyr963, the  $\text{CH}_2$  of the 4-Bn and the  $\text{CH}_2$  of Tyr963, the 2'-Bn group and Phe874 and Ile963, and the N-Bn<sub>2</sub> and Leu871, Phe 874, Leu909, Thr956 and Val960.

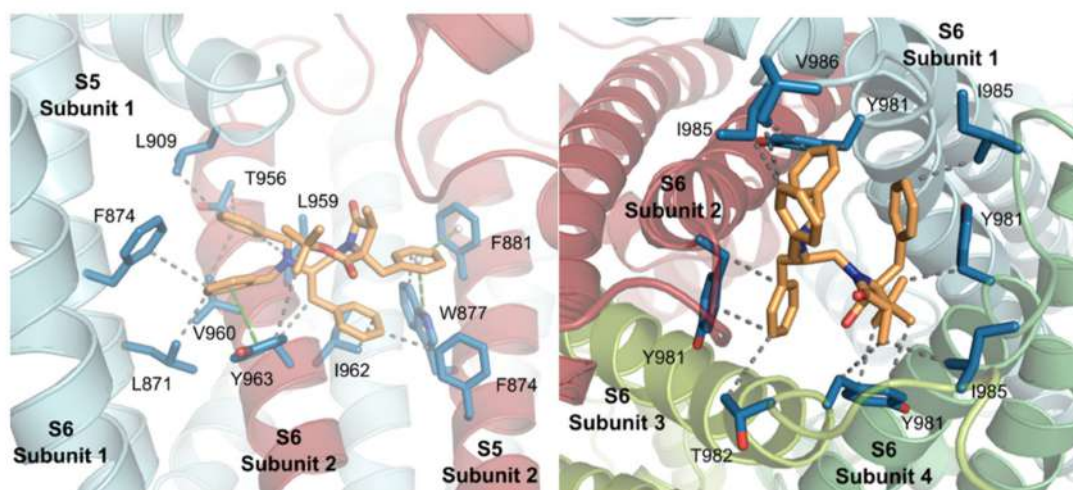


**Figure 5.** Interaction of  $\beta$ -lactam RGM8-51 (carbon atoms in wheat color) at subsite 1 (left) and subsite 2 (right). Channel residues involved in the interactions are shown in blue. WdV interactions are indicated by dotted gray lines, and  $\pi$ - $\pi$  stacking by centroids and non-continuous pale green lines.

**Table 3.** Main sites found for compound RGM8-51 and statistical distribution of docking solutions.

Subsite	Location	% of Docking Solutions (Estimated Binding Energies, kcal/mol)
1	Inner pore, S5S6, S5	58% (8.39)
2	Internal mouth pore	12% (8.44)
3	External pore, S3S4, S6	16% (6.63)
4	External loops	8% (6.65)

The second subsite locates the small molecule at the very bottom part of the pore, interacting with the loops joining S6 and TRP domain of the four channel subunits (Figure 5, right). In this case, the interplay is mediated by a network of Van der Waals (VdW) hydrophobic interactions, involving all substituents on the  $\beta$ -lactam. Thus, the *tert*-butyl group interacts with both the CH<sub>2</sub> of Tyr981 in subunit 1 and the aromatic ring of Tyr981 in subunit 2. This latter Tyr residue also interacts with the 3-Me group, as does Leu985 of the same subunit. The 2'-Bn moiety connects to Thr982 in protein monomer 2 and Tyr981 of subunit 3. Finally, the tertiary N-Bn<sub>2</sub> moiety establishes contacts with Tyr981, Ile985 and Val986, all in monomer 4.

In addition, there are two other possible binding sites. The third subsite where the molecule interacts with the channel is a cavity formed by S3 and S4 from a subunit and S6 from the adjacent subunit, at the top part of this one. The fourth pocket is located between the two small alpha helices that join S5 and S6 of the same subunit, at the top of the ion channel. Although they are also possible binding sites, they were less populated in the modeling studies and yielded lower binding energies than subsites 1 and 2 (Table 3).

The structure of TRPM8/AMTB and TRPM8/TC-I2014 complexes reveals interconnection of these small molecules by the menthol binding site, revealed as a highly adaptable pocket [48]. Our modeling studies, once again, point to a different mode of interaction of our  $\beta$ -lactam derivatives with respect to other described TRPM8 antagonists, making them a unique class within described modulators.

#### 2.4. In Vivo Antinociceptive Activity

RGM8-51 was further used as a chemical tool to explore the role of TRPM8 in different animal models of pain in vivo, including CIPN, CCI model of neuropathic pain, and NTG-induced mechanical hypersensitivity.

##### 2.4.1. Mouse Chemotherapy-Induced Peripheral Neuropathy

It is known that the painful peripheral neuropathy associated with the use of the chemotherapeutic drug oxaliplatin (OXA) is intensified by cold [49], and that TRPM8 channels play an important role in this debilitating condition [18,21]. In fact, the OXA-induced peripheral neuropathy mice model is being increasingly used to characterize TRPM8 antagonists. For instance, an imidazo[1',5':1,6]pyrido[3,4-*b*]indole-1,3(2*H*)-dione derivative, acting as a potent nanomolar TRPM8 antagonist, inhibited OXA-induced cold hypersensitivity after intraplantar (i.pl.) administration of 10 and 30  $\mu$ g of compound, with remarkable effect after 15 min and up to 30 min [12]. Of special interest is a biphenylamide *N*-spiro[4.5]decan-8-yl derivative that showed nanomolar potency on human TRPM8, and attenuated cold allodynia from 15-60 min at 0.1  $\mu$ g (i.pl.) dose, maintaining a significant effect up to 60 min after administration of a 1  $\mu$ g dose [50].

For the OXA-induced peripheral neuropathy assay, OXA was subcutaneously (s.c.) injected on days 1, 3 and 5 to male mice, at a 6 mg/kg dose, to induce hypersensitivity to cold, as monitored by the acetone drop test (Figure 6).

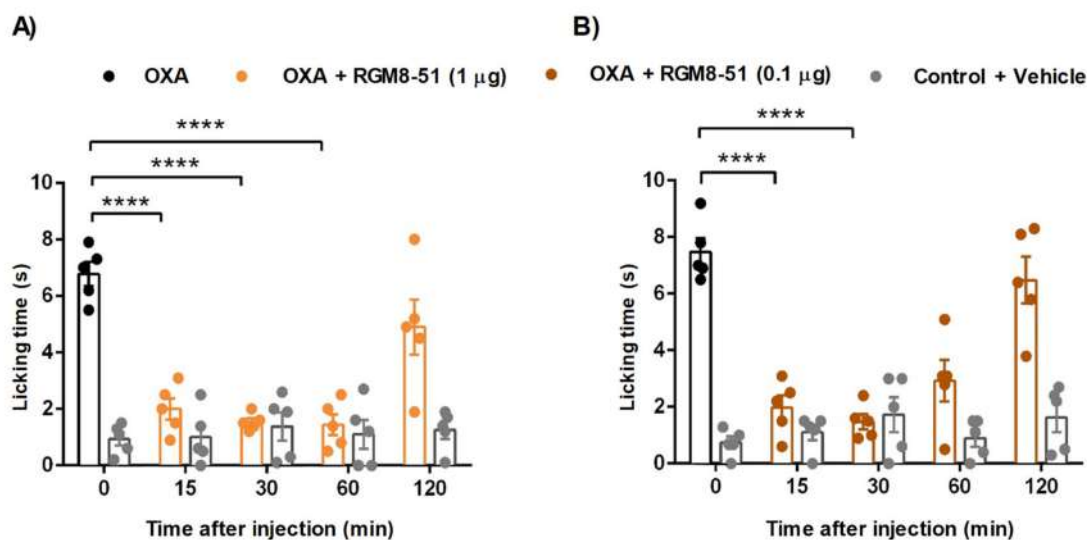


**Figure 6.** Effects of compound RGM8-51 on the oxaliplatin (OXA)-induced cold hypersensitivity (drop acetone test). Peripheral neuropathy was induced in male mice by injecting OXA (6 mg/kg, s.c.) on days 1, 3 and 5. Control animals were treated with vehicle. Compound RGM8-51 (1 µg/i.p., (A) or 0.1 µg/i.p., (B)) was administered to the OXA-treated animals, and the time-course of cold hypersensitivity was measured. Data are given  $\pm$  SEM (n = 5). Statistical analysis, comparing with oxaliplatin-treated mice, was performed by two-way ANOVA followed by post hoc Bonferroni test by multiple comparisons: \*\*\*\*  $p < 0.0001$ .

Compound RGM8-51 was administered intraplantarly (i.p., 1 and 0.1 µg), to evaluate its potential to reduce the OXA-induced cold hypersensitivity. As shown in Figure 6A, RGM8-51 (1 µg) attenuates the cold-induced paw licking in a significant manner 15 min after administration, showing the peak effect from 30 to 60 min. The compound is still highly active at a 0.1 µg dose, again with a sustained activity from 15 to 30 min. Compared to compound 2 [31],  $\beta$ -lactam analogue RGM8-51 needs lower doses (more potent) to reduce cold hypersensitivity in a significant manner. The potency is also higher than that described for imidazo[1',5':1,6]pyrido[3,4-*b*]indole-1,3(2H)-dione derivatives [12], and similar to the best biphenylamide-spiro derivative [50]. The period of time in which RGM8-51 effectively decreases cold allodynia is higher than that described for an imidazo[1',5':1,6]pyrido[3,4-*b*]indole-1,3(2H)-dione heterotricyclic TRPM8 antagonist [12], despite the *in vitro* potency being lower in our case.

#### 2.4.2. Chronic Constriction Injury (CCI) of the Sciatic Nerve

The CCI model of neuropathic pain allowed the evaluation of the effect RGM8-51 on cold, heat and mechanical sensitivity [5], as assayed by the acetone test, the Hargreaves test, and the automatized von Frey test, respectively. RGM8-51 was applied either locally (i.p.; 10 µg) in the affected paw or systemically (intraperitoneally, i.p., 10 and 30 mg/kg) and the effect evaluated before (Baseline) and after CCI surgery. The nocifensive response after administration of RGM8-51 was compared with that of vehicle, while non-operated animals and the uninjured (contralateral) hind paw in CCI animals were used as controls. As expected from previous results on the role of TRPM channels and the effect of TRPM8 antagonists (DFL23448, DFL23693, IGM-18) in cold hypersensitivity in CCI animals [12,13], RGM8-51 reduced cold hypersensitivity following i.p. application, and inhibited it dose-dependently after i.p. administration (Figure 7A). Interestingly, no effect was observed in either non-operated animals (baseline in Figure 7A) or the contralateral uninjured paw (data not shown).

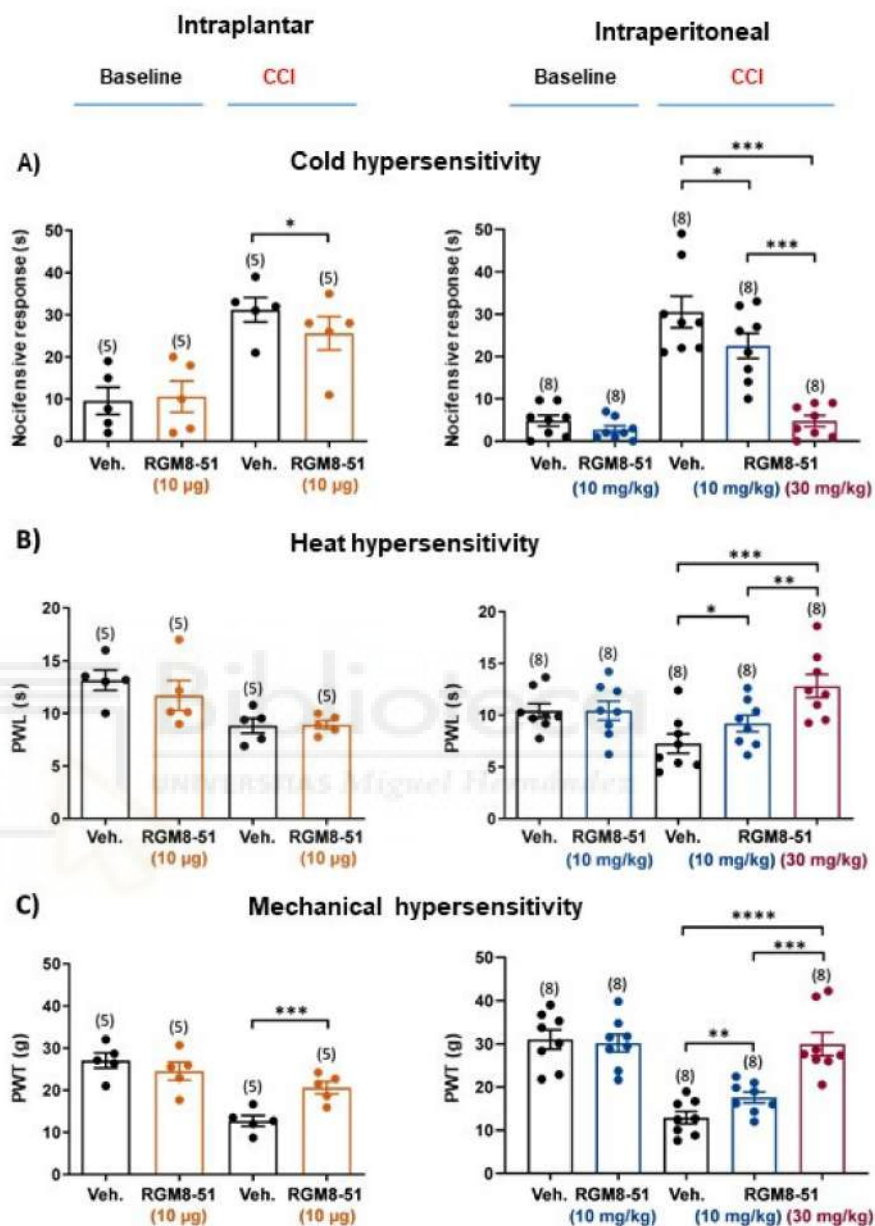


**Figure 7.** Effects of compound RGM8-51 on cold, heat and mechanical hypersensitivity in the CCI model in the rat. RGM8-51 was administered before (baseline) and after CCI surgery (CCI) by both the intraplantar (10 µg, left panels) and the intraperitoneal (10 and 30 mg/kg, right panels) routes. Note that vehicle administration after CCI surgery was associated to an increase in the nocifensive response duration to acetone application, and to reductions in the paw withdrawal latency (PWL) to heat radiation and the paw withdrawal threshold (PWT) to tactile stimulation of the injured hind paw, indicative of cold (A), heat (B) and mechanical (C) hypersensitivity, respectively. Data are mean ± SEM of the number of animals specified between parentheses. Statistical analysis was performed by using the paired *t*-test. \* < 0.05; \*\* < 0.01; \*\*\* < 0.001; \*\*\*\* < 0.0001 with regard to vehicle (Veh.) or between the two i.p. doses.

Compound RGM8-51 was also effective in decreasing hypersensitivity to heat following i.p. administration and it did it dose-dependently (Figure 7B). This result is in line with those obtained with  $\beta$ -carboline-based TRPM antagonists in CCI mice by using the thermal ring assay, which measures thermal preference behavior [11]. Curiously, i.pl. application of RGM8-51 did not influence the animal response to heat, which points towards the possibility that the effect of RGM8-51 could be related to body temperature regulation rather than heat sensing. In fact, TRPM8 antagonists are known to decrease the body temperature, a phenomenon that is abrogated in TRPM<sup>-/-</sup> mice [9,13,51,52]. As it was the case for cold stimulation, RGM8-51 had no effect on heat perception in non-operated animals (baseline in Figure 7B) or in the uninjured hind paw (data not shown).

Last, we tested the effect of RGM8-51 on mechanical sensitivity. Again, this compound dose-dependently reverted paw withdrawal thresholds after i.p. administration, this effect also being produced after local (i.pl.) delivery, whereas it could not be observed in the absence of neuropathy (Figure 7C).

Altogether, the results obtained with RGM8-51 in the CCI model point to a multi-sensory modality (cold, heat, and tactile) antinociceptive effect, without affecting normal sensory perception. Likewise, the fact that the effects on cold and mechanical sensitivity were observed after i.pl. application suggests the involvement of a peripheral site of action, most likely the skin terminals of the small sized (C-type) DRG neurons, which are specialized in nociceptive transduction. This possibly provides an explanation for the seemingly contrasting results obtained when TRPM8 receptors are downregulated or blocked by intrathecal administration of TRPM8 antisense oligonucleotides or antagonists (AMTB), where no effect could be observed on mechanical allodynia in CCI rats [6,9].

Notably, a writhing behavior was observed in a small number of animals following i.p. injection of 30 mg/kg RGM8-51. This behavior lasted 3-5 min and could possibly be related to the TRPV1 agonist activity of compound RGM8-51.

#### 2.4.3. NTG-Induced Mechanical Hypersensitivity

Recently, it has been shown that both CGRP receptors and different TRP ion channels (TRPM8, among them) are associated to the development of migraines [53]. In addition, treatment with TRPM8 agonists has been claimed to alleviate topically the symptoms of this pathology [54], whereas the clinical development of the oral antagonist, AMG333, was stopped due to serious side effects, mainly related to body temperature dysregulation [29]. To the best of our knowledge, apart from AMG333, no other TRPM8 antagonists have been evaluated in vivo for migraine. Since  $\beta$ -lactam RGM8-51 possesses analgesic activity in other animal models, we considered also its evaluation in a mouse model of chronic migraine characterized by mechanical hypersensitivity and induced by administration of nitroglycerin (NTG), a known vasodilator used in the treatment of angina pectoris [55]. This model has been used to evaluate the effects of known acute and preventive migraine therapies and to demonstrate the role of miR155-5p upregulation in the pathological mechanism of chronic migraine [56,57].

Administration of NTG intermittently produces a baseline hypersensitivity to mechanical stimulation, which can be measured by the von Frey test. The mechanical stimulus was applied at different times to obtain the time course of the effects produced after compound administration, and both male and female mice were used to investigate a possible sex dimorphism.

Figure 8A graphically compiles the results obtained in male mice. Thus, it can be observed that the administration of NTG decreases the mechanical stimulation that the animals are capable of bearing, compared to controls without NTG. This NTG-induced hypersensitivity can only be significantly blocked by RGM8-51 at a 30 mg/kg i.p. dose, 60 min post-administration. Figure 8B shows the results of the same test carried out in female mice. In this case, compound RGM8-51 significantly reduces the hypersensitivity threshold induced by NTG at both 10 and 30 mg/kg i.p. doses. In addition, the observed positive effect takes place faster, with significant antinociceptive activity at 30 min, and

is of longer duration (even after 120 min post-administration). This differential behavior could be explained by the fact that TRPM8 acts as a fast integrator of the testosterone hormone, an agonist of the channel [58,59]. As testosterone is mainly found in males, the activation of the TRPM8 receptor by this hormone could counteract the effect of the  $\beta$ -lactam. Actually, previous results with TRPM8<sup>-/-</sup> male and female mice demonstrated that TRPM8 is involved in the regulation of dimorphic sexual and social behaviors [60].

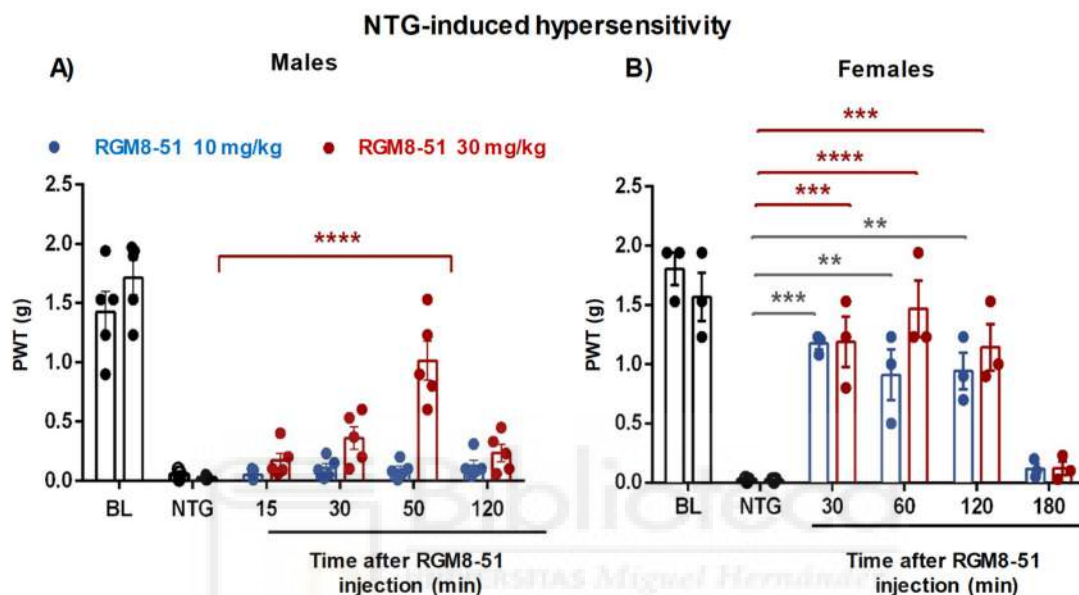


**Figure 8.**  $\beta$ -lactam RGM8-51 reduces NTG-induced hypersensitivity in a sex-dependent manner. (A) Paw withdrawal threshold (PWT) increased dose-dependently in C57 male mice 2 h after injection of 30 mg/kg of NTG. (B) NTG-induced mechanical hypersensitivity was fully blocked in female mice by the systemic injection of RGM8-51 compound in a dose dependent manner. Compound RGM8-51 was intraperitoneally injected 2 h after NTG injection and 30 min before von Frey measurements. Data are given  $\pm$  SEM ( $n = 3-5$ ). Statistical analysis was two-way ANOVA followed by post hoc Bonferroni test by multiple comparison \*\*  $p < 0.05$ ; \*\*\*  $p < 0.001$ ; \*\*\*\*  $p < 0.0001$ .

### 3. Conclusions

TRPM8 channels in sensory neurons have been involved in different pain processes. However, the dissimilar results found with different TRPM8 antagonists demand new studies to establish the future dimension of TRPM8 channel inhibition for pain relief. To shed light on the participation of TRPM8 channels in different animal models of pain, we selected a prototype from our family of  $\beta$ -lactams, RGM8-51. In *in vitro* experiments, we demonstrated that this compound has good TRPM8 antagonist activity (rat and human isoforms), and appreciable selectivity versus other thermoTRP channels and pain-mediating receptors. Additionally, in DRG neurons, RGM8-51 inhibited menthol-activated currents, while it did not have a direct effect on major ion conductances involved in action potential generation. *In vivo* experiments evidenced that compound RGM8-51 was highly effective in different TRPM8-mediated types of pain. The inhibition of cold hypersensitivity in oxaliplatin-induced peripheral neuropathy anticipates the potential utility of this type of compound in the disabling condition associated to chemotherapeutic cancer treatments. Additionally, in the CCI model of neuropathic pain, this  $\beta$ -lactam was shown to attenuate cold and mechanical hypersensitivity and had some effect on heat stimulation. Lastly, RGM8-51 mitigates, in a sex-dependent manner, the NTG-induced mechanical hypersensitivity. Despite non-optimal pharmacokinetic properties, RGM8-51 was revealed as a helpful

chemical tool for studying TRPM8-mediated pharmacology after i.p. and i.p. administration. These results also ratify the 1,3,4,4-tetrasubstituted  $\beta$ -lactam ring as a valuable central scaffold in the search for new TRPM8 modulators. Further research on this family of TRPM8 antagonists is ongoing in our labs.

## 4. Methods

### 4.1. Synthesis

*General procedures:* Reactions were monitored either by TLC and/or analytic HPLC (UV, detection, 220 nm). Flash columns, filled with silica gel Merck 60 (230–400) were used for chromatographic separations. A reversed-phase column, Sunfire C18 (4.6  $\times$  50 mm, 3.5  $\mu$ m), a flux of 1 mL/min, and mixtures of CH<sub>3</sub>CN, phase A, and H<sub>2</sub>O, phase B, both containing 0.01% formic acid, were used for analytical HPLCs. Mass spectra, in electrospray, positive mode, were obtained on a Waters Micromass ZQ spectrometer. High resolution mass spectrum (ESI-HRMS) was recorded on an Agilent 6520 Q-TOF instrument. Optical rotation for final compound RGM8-51 was measured in a polarimeter Perkin Elmer 141 apparatus. NMR spectra were recorded in a Varian INOVA-400 (400 MHz) spectrometer, operating at 400 and 100 MHz for <sup>1</sup>H and <sup>13</sup>C experiments, respectively (with chemical shifts expressed in ppm and coupling constants in Hz).

#### 4.1.1. Ns-L-Phe-O<sup>t</sup>Bu (5)

To a solution of H-L-Phe-O<sup>t</sup>Bu.HCl (11.64 mmol, 3.00 g) in dry DMF (70 mL), triethylamine (TEA) (11.64 mmol, 1.61 mL) was added, and the reaction stirred 20 min at rt. Then, the reaction mixture was cooled to 0 °C, a second portion of TEA (12.22 mmol, 1.69 mL) and *o*-nosylchloride (12.22 mmol, 2.71 g) were added, and stirred overnight at rt. The solvent was evaporated, and the reaction mixture was dissolved in EtOAc, and successively washed with citric acid (10%), NaHCO<sub>3</sub> (10%) and brine. The organic layer was dried over Na<sub>2</sub>SO<sub>4</sub>, filtered and evaporated to dryness. The final product was precipitated in cold Et<sub>2</sub>O, and the precipitate filtered. Product still remaining in mother liquids was purified on a silica gel column, using 11% EtOAc in hexane as eluent. A total of 4.37 g (93%) of compound 5 was obtained as a white solid. Mp: 90 °C (AcOEt:hexano). Published: 92–93 °C [61]. HPLC: t<sub>R</sub> = 8.73 min (gradient from 30% to 95% of A, in 10 min). <sup>1</sup>H-NMR (300 MHz, CDCl<sub>3</sub>):  $\delta$  8.02 (m, 1H, Ar), 7.87 (m, 1H, Ar), 7.68 (m, 2H, Ar), 7.30–7.13 (m, 5H, Ar), 6.02 (d, 1H, *J* = 9.1 Hz,  $\alpha$ NH), 4.35 (m, 1H,  $\alpha$ -Phe), 3.09 (m, 2H,  $\beta$ -Phe), 1.19 (s, 9H, <sup>t</sup>Bu). MS (ES)<sup>+</sup>: 351.10 [M-<sup>t</sup>Bu]<sup>+</sup>.

#### 4.1.2. N-[(2S-Dibenzylamino-3-phenyl)prop-1-yl]-Ns-L-Phe-O<sup>t</sup>Bu (7)

To a solution of 2S-dibenzylamino-3-phenyl-1-propanol (6) (7.49 mmol, 2.48 g), Ns-L-Phe-O<sup>t</sup>Bu (5) (8.24 mmol, 3.35 g) and triphenylphosphine (8.24 mmol, 2.16 g) in dry THF (60 mL), under Ar atmosphere at 0 °C, diisopropyl azodicarboxylate (8.24 mmol, 1.62 mL) was added. Then, the reaction was stirred at rt overnight. The solvent was removed under vacuum, and the resulting residue was purified on a silica gel column, using a gradient from 66 to 80% DCM in hexane. Compound 7 (4.94 g, 92%) was obtained as a syrup. HPLC: t<sub>R</sub> = 5.00 min (gradient from 80% to 95% of A, in 10 min). <sup>1</sup>H-NMR (300 MHz, CDCl<sub>3</sub>):  $\delta$  7.59 (m, 2H, Ar), 7.37 (m, 1H, Ar), 7.27–7.16 (m, 18H, Ar), 7.08 (m, 2H, Ar), 6.86 (m, 1H, Ar), 4.51 (t, 1H, *J* = 7.7 Hz,  $\alpha$ -Phe), 4.01 (dd, 1H, *J* = 15.0, 5.6 Hz, H<sub>1</sub>), 3.81 (d, 2H, *J* = 13.7 Hz, NCH<sub>2</sub>), 3.63 (d, 2H, *J* = 13.8 Hz, NCH<sub>2</sub>), 3.45 (dd, 1H, *J* = 15.0, 8.8 Hz, H<sub>1</sub>), 3.29 (ddd, 1H, *J* = 8.6, 5.8, 2.8 Hz, H<sub>2</sub>), 2.83 (m, 2H, H<sub>3</sub>), 2.75 (m, 2H,  $\beta$ -Phe), 1.11 (s, 9H, CH<sub>3</sub>, <sup>t</sup>Bu). <sup>13</sup>C-NMR (75 MHz, CDCl<sub>3</sub>):  $\delta$  169.0 (COO), 148.2, 140.1, 139.9, 136.8, 134.6, 133.3, 132.0, 129.7, 129.5, 128.4, 121.3, 128.2, 127.0, 126.9, 126.1, 124.4 (Ar), 82.0 (C, <sup>t</sup>Bu), 62.6 ( $\alpha$ -Phe), 57.9 (C<sub>2</sub>), 53.3 (NCH<sub>2</sub>), 47.0 (C<sub>1</sub>), 37.1 ( $\beta$ -Phe), 34.7 (C<sub>3</sub>), 27.7 (CH<sub>3</sub>, <sup>t</sup>Bu). MS (ES)<sup>+</sup>: 721.38 [M + H]<sup>+</sup>.

#### 4.1.3. N-[(2S-Dibenzylamino-3-phenyl)prop-1-yl]-L-Phe-O<sup>t</sup>Bu (8)

To a solution of the *N*-nosyl-*N*-alkyl derivative 7 (6.77 mmol, 4.87 g) in dry ACN (125 mL) K<sub>2</sub>CO<sub>3</sub> (20.30 mmol, 2.80 g) and phenylthiol (13.53 mmol, 1.38 mL) were added

slowly and stirred at rt overnight. After evaporation of the solvent in vacuum, the resulting residue was dissolved in EtOAc:H<sub>2</sub>O (1:1) and the phases were separated. The organic layer was dried over Na<sub>2</sub>SO<sub>4</sub>, filtered and evaporated to dryness. The resulting mixture was purified on a silica gel column, using a gradient from 9 to 33% of EtOAc in hexane. Compound **8** (3.56 g 98%) was obtained as a syrup. HPLC: t<sub>R</sub> = 4.50 min (gradient from 15% to 95% of A in 5 min). <sup>1</sup>H-NMR (300 MHz, CDCl<sub>3</sub>): δ 7.37–7.17 (m, 18H, Ar), 7.02 (m, 2H, Ar), 3.77 (d, 2H, J = 13.7 Hz, NCH<sub>2</sub>), 3.59 (d, 2H, J = 13.7 Hz, NCH<sub>2</sub>), 3.32 (dd, 1H, J = 7.9, 5.8 Hz, α-Phe), 3.02 (m, 2H, H<sub>2</sub>, H<sub>3</sub>), 2.92 (dd, 1H, J = 13.6, 5.9 Hz, β-Phe), 2.82 (dd, 1H, J = 13.4, 7.8 Hz, β-Phe), 2.70–2.45 (m, 3H, H<sub>1</sub>, H<sub>3</sub>), 1.78 (NH), 1.33 (s, 9H, CH<sub>3</sub>, <sup>t</sup>Bu). <sup>13</sup>C-NMR (75 MHz, CDCl<sub>3</sub>): δ 173.5 (COO), 140.4, 140.0, 138.0, 129.6, 129.4, 128.9, 128.5, 128.4, 128.4, 126.9, 126.7, 125.9 (Ar), 81.0 (C, <sup>t</sup>Bu), 64.0 (α-Phe), 60.3 (C<sub>2</sub>), 53.9 (NCH<sub>2</sub>), 47.5 (C<sub>1</sub>), 39.4 (β-Phe), 34.1 (C<sub>3</sub>), 28.1 (CH<sub>3</sub>, <sup>t</sup>Bu). MS (ES)<sup>+</sup>: 536.16 [M + H]<sup>+</sup>.

#### 4.1.4. N-[(2S-Dibenzylamino-3-phenyl)prop-1-yl]-N-(2'S-chloropropanoyl)-L-Phe-O<sup>t</sup>Bu (**9**)

A solution of 2(S)-chloropropionic acid (11.47 mmol, 1.067 mL) and trichloroacetonitrile (12.62 mmol, 1.265 mL), in anhydrous THF (35 mL), was cooled to 0 °C and triphenylphosphine (12.61 mmol, 3.31 g) was slowly added. Then, the reaction mixture was stirred at rt for 1h. This solution was slowly added, at 0 °C, to a second solution containing the secondary amine derivative **8** (5.73 mmol, 3.06 g) and propylene oxide (114.69 mmol, 2.666 mL) in anhydrous THF (10 mL). The evolution of the reaction was controlled by analytical HPLC. Once completed, the solvent was evaporated, the resulting residue was dissolved in EtOAc, and washed with citric acid (10%), NaHCO<sub>3</sub> (10%) and brine. The organic layer was dried over Na<sub>2</sub>SO<sub>4</sub>, filtered and evaporated in vacuum. Purification was performed on silica gel column, using as eluent a gradient from 6 to 9% of EtOAc in hexane. Compound **9** (3.40 g, 95%) was obtained as a syrup. HPLC: t<sub>R</sub> = 5.61 min (gradient from 60% to 95% of A in 10 min). <sup>1</sup>H-NMR (400 MHz, DMSO-d<sub>6</sub>, rotamers ratio M:m, 12:1): δ major rotamer 7.30–7.10 (m, 12H, Ar), 6.90 (m, 8H, Ar), 4.09 (q, 1H, J = 6.5 Hz, H<sub>1'</sub>), 3.64 (dd, 1H, J = 9.5, 5.6 Hz, α-Phe), 3.56 (d, 2H, J = 13.8 Hz, NCH<sub>2</sub>), 3.45 (d, 2H, J = 13.8 Hz, NCH<sub>2</sub>), 3.25 (dd, 1H, J = 14.2, 4.8 Hz, H<sub>1</sub>), 3.19 (dd, 1H, J = 14.2, 9.6 Hz, H<sub>1</sub>), 3.04 (m, 3H, β-Phe, H<sub>2</sub>), 2.82 (dd, 1H, J = 13.6, 4.9 Hz, H<sub>3</sub>), 2.65 (dd, 1H, J = 13.6, 9.3 Hz, H<sub>3</sub>), 1.54 (d, 3H, J = 6.5 Hz, H<sub>2'</sub>), 1.44 (s, 9H, CH<sub>3</sub>, <sup>t</sup>Bu). <sup>13</sup>C-NMR (75 MHz, DMSO-d<sub>6</sub>): δ major rotamer 169.9 (COO), 168.8 (CON), 139.3, 139.2, 139.1, 138.6, 129.8, 129.4, 128.8, 128.7, 128.3, 127.3, 126.7, 126.4 (Ar), 82.0 (C, <sup>t</sup>Bu), 64.9 (α-Phe), 58.3 (C<sub>2</sub>), 53.7 (NCH<sub>2</sub>), 52.3 (C<sub>1</sub>), 49.9 (C<sub>1'</sub>), 35.5 (β-Phe), 34.8 (C<sub>3</sub>), 28.1 (CH<sub>3</sub>, <sup>t</sup>Bu), 21.3 (C<sub>2'</sub>). MS (ES)<sup>+</sup>: 625.43 [M + H]<sup>+</sup>.

#### 4.1.5. 4(S)-Benzyl-3S-methyl-4-(tert-butoxy)carbonyl-1-[(2'S-dibenzylamino-3'-phenyl)prop-1'-yl]-2-oxoazetidine (RGM8-51, **3**)

A solution of compound **9** (5.15 mmol, 3.22 g) in dry ACN (20 mL), was treated, under Ar atmosphere, with BTTP (7.73 mmol, 2.360 mL) and stirred at rt until the chloropropanoyl derivative disappeared. Then, the solvent was evaporated and the residue dissolved in EtOAc and washed with 0.1 M HCl and brine. The organic layer was dried over Na<sub>2</sub>SO<sub>4</sub>, filtered and evaporated in vacuum. Purification was performed on silica gel column, using as eluent a gradient from 9 to 50% EtOAc in hexane. Compound **3** (2.43 g, 80%) was obtained as a syrup. HPLC: t<sub>R</sub> = 2.33 min (gradient from 50 to 95% of A in 5 min). [α]<sub>D</sub> = −1.64 (c 1, CH<sub>3</sub>Cl). <sup>1</sup>H-NMR (400 MHz, CDCl<sub>3</sub>): δ 7.31–7.04 (m, 20H, Ar), 3.76 (d, 2H, J = 13.9 Hz, NCH<sub>2</sub>), 3.56 (d, 2H, J = 13.8 Hz, NCH<sub>2</sub>), 3.57 (m, 2H, H<sub>1'</sub>, H<sub>2'</sub>), 3.42 (m, 1H, H<sub>1'</sub>), 3.14 (q, 1H, J = 7.5 Hz, H<sub>3</sub>), 2.95 (m, 3H, H<sub>3'</sub>, 4-CH<sub>2</sub>), 2.92 (d, 1H, J = 14.3 Hz, 4-CH<sub>2</sub>), 1.46 (s, 9H, CH<sub>3</sub>, <sup>t</sup>Bu), 1.19 (d, 3H, J = 7.6 Hz, 3-CH<sub>3</sub>). <sup>13</sup>C-NMR (75 MHz, CDCl<sub>3</sub>): δ 170.2 (COO), 169.7 (C<sub>2</sub>), 140.2, 139.6, 135.6, 129.8, 129.5, 128.6, 128.3, 128.1, 127.9, 127.0, 126.8, 125.7 (Ar), 82.8 (C <sup>t</sup>Bu), 68.3 (C<sub>4</sub>), 58.0 (C<sub>2'</sub>), 53.3 (NCH<sub>2</sub>), 53.1 (C<sub>3</sub>), 42.7 (C<sub>1'</sub>), 41.3 (4-CH<sub>2</sub>), 36.4 (C<sub>3'</sub>), 28.0 (CH<sub>3</sub>, <sup>t</sup>Bu), 10.7 (3-CH<sub>3</sub>). MS (ES)<sup>+</sup>: 589.47 [M + H]<sup>+</sup>. Exact mass calculated for C<sub>39</sub>H<sub>44</sub>N<sub>2</sub>O<sub>3</sub>: 588.33519, found 588.33556. Before biological assays, compound **9** was transformed into its hydrochloride salt by treatment with 0.1 M HCl (1 equiv) in a mixture of ACH/H<sub>2</sub>O (1:1), followed by lyophilization. <sup>1</sup>H-NMR (400 MHz, Methanol-d<sub>4</sub>) δ 7.79

(m, 1H, Ar), 7.60 (m, 3H, Ar), 7.43 (m, 3H, Ar), 7.33 (m, 3H, Ar), 7.24 (m, 7H, Ar, NH), 7.12 (m, 2H, Ar), 6.99 (m, 2H, Ar), 5.10 (d,  $J = 12.9$  Hz, 1H, NCH<sub>2</sub>), 4.53 (d,  $J = 13.6$  Hz, 1H, 4-CH<sub>2</sub>), 4.45 (d,  $J = 13.6$  Hz, 1H, 4-CH<sub>2</sub>), 4.30 (d,  $J = 12.9$  Hz, 1H, NCH<sub>2</sub>), 4.16 (m, 1H, H<sub>1'</sub>), 4.02 (dd,  $J = 16.6, 10.6$  Hz, 1H, H<sub>1'</sub>), 3.56 (m, 1H, H<sub>2'</sub>), 3.49 (d,  $J = 14.6$  Hz, 1H, NCH<sub>2</sub>), 3.22 (q,  $J = 7.6$  Hz, 1H, H<sub>3</sub>), 2.96 (d,  $J = 14.3$  Hz, 1H, NCH<sub>2</sub>), 2.72 (t,  $J = 12.9$  Hz, 1H, H<sub>3'</sub>), 2.51 (d,  $J = 15.8$  Hz, 1H, H<sub>3'</sub>), 1.23 (s, 9H, CH<sub>3</sub>, <sup>t</sup>Bu), 0.88 (d,  $J = 7.6$  Hz, 3H, 3-CH<sub>3</sub>).

#### 4.2. Molecular Modeling Studies

Molecular modeling studies started from the TRPM8 cryo-EM structure of *Ficedula albicollis* (PDB code: 6BPQ [45]), as previously described [30]. The homology modeling of rat TRPM8 was performed on completed TRPM8 sequence (Uniprot code Q8R455), using the *Ficedula albicollis* structure as template, and adding the missing loops with the standard protocol implemented in the program Yasara [43,44,59] (version 20.12.24). The sequence alignment between *Ficedula a.* and rat TRPM8 was performed with ClustalO [60], a service located in the European Bioinformatics Institute EMBL-EBI (<https://www.ebi.ac.uk/> accessed on 2 December 2020). Docking studies were accomplished with AutoDock [61] implemented in Yasara and consisted in a total of 800 flexible global docking runs that were set and clustered around the putative binding sites, following by a simulated annealing optimization of each generated complex, using the force field AMBER03 (Assisted Model Building with Energy Refinement) [62]. The best binding energy complex in each cluster was analyzed, stored, and selected as the best orientation of the interacting partners. Edition, modeling and visualization of the molecules were performed with Yasara (<http://www.yasara.org> accessed on 2 December 2020). Figures were drawn with Pymol, the open source version of the PyMOL Molecular Graphics System, version 2.4.1 (Schrödinger, LLC, New York, NY, USA) obtained at <http://www.pymol.org> accessed on 2 December 2020.

#### 4.3. Functional Assays by Calcium Microfluorimetry

To measure the effect of the compounds against TRPM8 activity we used microfluorometry-based calcium flux assays with Fluo-4 NW Ca<sup>2+</sup> dye and fluorescence as described in [30]. Briefly, human embryonic kidney cell line (HEK293) cells stably transfected with rTRPM8 or hTRPM8 were seeded in 96-well plates at a cell density of 30,000 cells. After 2 days the medium was replaced with 100  $\mu$ L of the dye, Fluo-4 NW, loading solution supplemented with probenecid 2.5 mM and incubated 1 h at 37 °C. The TRPM8 activity was measured using POLASTAR plate reader (BMG Labtech) setting the excitation wavelength at 485 nm and the emission wavelength at 520 nm. The baseline fluorescence was recorded for 3 cycles before the addition of vehicle compound at different concentrations and the antagonist, 10  $\mu$ M AMTB. Fluorescence intensity was recorded during 7 more cycles and 100  $\mu$ M menthol was added. Fluorescence intensity was recorded during 10 more cycles.

Data analysis: The Z-factor was calculated in each assay using the following equation:  $(3 \times (SD_{max} + SD_{min})) / (Mean_{max} - Mean_{min})$ . In all the experiments, the Z-factor was  $\geq 0.5$ . The effect of the compounds against TRPM8 activity was determined by normalizing their effect on the maximum fluorescence observed after application of 100  $\mu$ M menthol. Decrease in menthol signal was expressed as percentage of inhibition (%). All data are expressed as the mean  $\pm$  standard deviation (SD). Data are expressed as the concentration exerting a half-maximal inhibition of agonist-induced [Ca<sup>2+</sup>]<sub>i</sub> elevation (IC<sub>50</sub>), which was calculated again using GraphPad Prism® software. All determinations were performed in triplicate (n = 3) in 3 independent experiments (N = 3).

#### 4.4. Isolation of Rat DRG Neurons

Voltage-activated Na<sup>+</sup> and K<sup>+</sup> currents and TRPM8-mediated currents were recorded in DRG neurons isolated from 6-8 weeks old Sprague-Dawley rats, as previously described [62]. Rats were sacrificed by cervical dislocation followed by decapitation and lumbar segments of the spinal column were removed and placed in a cold Ca<sup>2+</sup>, Mg<sup>2+</sup>-free Hank's solution (Sigma-Aldrich, Madrid, Spain). The bone surrounding the spinal cord was

removed and the right L4, L5 and L6 DRG were exposed and pulled out. After removing the roots, DRG were chopped in half and incubated for 30 min at 37°C in Dulbecco's modified Eagle's Medium-low glucose (DMEM; Sigma-Aldrich) containing 5 mg/mL collagenase XI (Sigma-Aldrich, Madrid, Spain), 100 U/mL penicillin (Sigma-Aldrich), and 0.1 mg/mL streptomycin (Sigma-Aldrich). Then, the cell suspension was washed with DMEM by centrifugation (300 G, 5 min at 4 °C), filtered through a 100 µm mesh to eliminate cell clumps and washed again by centrifugation. The cell pellet was resuspended in DMEM and 40 µL were dropped onto 10 mm diameter glass coverslips treated with poly-L-lysine (1 mg/mL, 30 min; Sigma-Aldrich) placed in 35 mm diameter Petri dishes. Finally, plated cells were flooded with 2.5 mL of DMEM supplemented with 10% fetal calf serum (Sigma-Aldrich, Madrid, Spain), 100 U/mL penicillin and 0.1 mg/mL streptomycin, and stored in an incubator (Hera Cell, Heraeus, Hanau, Germany) with a 5% CO<sub>2</sub>/95% air atmosphere at 37 °C. This protocol yields spherical cell bodies without neurites, from which only small to medium DRG neurons (diameter < 30 µm) were chosen for electrophysiological recording within 12–24 h of plating.

Changes in membrane potential were studied in neonatal DRGs isolated from 3–5 days-old Wistar rats. After isolation, DRGs were digested first using collagenase type IA (0.25% *w/v*) in DMEM GlutaMax with penicillin/streptomycin (P/S) solution (1% *v/v*) for 1 h (37 °C, 5% CO<sub>2</sub>, ThermoScientific incubator) and secondly by mechanical dissociation. Single cell suspension was passed through a 100 µm cell strainer and washed with DMEM GlutaMax with FBS (10%*v/v*) and P/S solution (1% *v/v*). Cells were seeded in a drop on 24-well plates containing 12 mm Ø glass coverslips pretreated with poly-L-lysine (8.3 µg/mL) and laminin (5 µg/mL). After 1 h, medium was replaced with DMEM GlutaMax with FBS (10%*v/v*) and P/S solution (1% *v/v*), supplemented with mouse 2.5S NGF (50 ng/mL) and cytosine arabinoside (1.25 µg/mL). All cell culture procedures were performed in a laminar flow cabinet (Model Telstar AV-100, Institut Català de Nanociència i Nanotecnologia, Bellaterra, Spain). Experiments were performed 24–48 h after cell seeding [63].

#### 4.5. Functional Assays by Patch-Clamp Electrophysiology

Whole-cell patch-clamp recordings from HEK293-rTRPM8 cells were carried out 2 days after seeding on 12 mm Ø glass coverslips treated with poly-L-lysine solution (Sigma Aldrich, Spain) [30]; the intracellular pipette solution contained (in mM) 150 NaCl, 5 EGTA, 3 MgCl<sub>2</sub> and 10 HEPES, adjusted to pH 7.2 with NaOH, and the extracellular solution contained (in mM) 150 NaCl, 6 CsCl, 1.5 CaCl<sub>2</sub>, 1 MgCl<sub>2</sub>, 10 D-glucose and 10 HEPES, adjusted to pH 7.4 with NaOH. The TRPM8 activity was measured by the application of two pulses of 100 µM menthol in a time interval of 2 min and a 30 s perfusion of the different compound concentrations before the second menthol pulse.

The extracellular solution used in whole-cell voltage-clamp recordings from rat DRG neurons contained (mM) 145 NaCl, 2.8 KCl, 3 CaCl<sub>2</sub>, 1 MgCl<sub>2</sub>, 10 4-(2-Hydroxyethyl)piperazine-1-ethanesulfonic acid, N-(2-Hydroxyethyl) piperazine-N'-(2-ethanesulfonic acid) (HEPES), and 12 glucose (pH 7.35 adjusted with NaOH; ≈320 mOsm); the internal solution contained (mM) 145 KCl, 2 MgCl<sub>2</sub>, 0.3 EGTA, 0.3 GTP.Li<sub>3</sub>, 2 ATP.Na<sub>2</sub>, 10 HEPES (pH 7.2 adjusted with KOH; ≈310 mOsm). Menthol (100 µM) or RGM8-51 (1 µM; 2–4 min superfusion) were applied directly onto the cell under investigation by means of a multibarrel concentration-clamp device coupled to electronically driven miniature solenoid valves under the control of PatchMaster software (HEKA Electronics, Lambrecht, Germany). Voltage-activated currents were elicited by a step depolarization to +10 mV, 100 ms long, associated to a P/4 protocol for on-line leak and capacitive current subtraction.

For current-clamp recordings from rat DRG neurons the intracellular pipette solution contained (in mM): 4 NaCl, 126 K gluconate, 0.02 CaCl<sub>2</sub>, 1 MgSO<sub>4</sub>, 5 HEPES, 15 glucose, 3 ATP, 0.1 GTP and 5 EGTA, pH 7.2 with KOH and the extracellular solution contained (in mM): 140 NaCl, 4 KCl, 2 CaCl<sub>2</sub>, 2 MgCl<sub>2</sub>, 10 HEPES, 5 glucose and 20 mannitol, pH 7.4 with NaOH. The membrane potential was measured in the absence and the presence of compound RGM8-51 at 10 µM in a time interval of 1 min.

Data were sampled at 10 kHz (EPC10 amplifier with PatchMaster 2.53 software, HEKA Electronics, Lambrecht, Germany) and low-pass filtered at 3 kHz for analysis (PatchMaster 2.53 and GraphPad Prism 6.0, Graphpad Software, San Diego, CA, USA). The series resistance was  $<10\text{ M}\Omega$  and to minimize voltage errors was compensated by 60–80%. All measurements were performed at 24–25 °C. Cell capacitance was measured and used to estimate the current density (J, pA/pF).

Data analysis: For the whole-cell patch-clamp experiments, results are expressed as the percentage of remaining activation of the TRPM8 channel. This is calculated by normalizing the ratio (p2/p1) of testing conditions to the ratio (p2/p1) of the control condition. Analysis of the data was performed by GraphPad 6.0, the Ordinary One-Way ANOVA analysis followed by the post hoc Bonferroni test for multiple comparisons and the ROUT method (Q = 10%) identified data outliers. A non-linear regression curve and  $IC_{50}$  were obtained by the representation of log (inhibitor) vs. response. Paired or unpaired Student's *t*-tests were also used for data comparison between two groups. All data are expressed as the mean  $\pm$  standard error of the mean (SEM) (n = 5–8). In the current-clamp experiments, the change in membrane potential is expressed as the difference between the resting membrane potential and the membrane potential after the addition of a stimuli. Data were analyzed as previously described (GraphPad 6.0, one-way ANOVA followed by Bonferroni multiple comparisons test, and ROUT method, Q = 10%).

#### 4.6. Selectivity and Preliminary PK Properties

These studies were subcontracted to Eurofins-CEREP or Eurofins-PANLABS. Briefly, agonists and antagonist assays were performed in cell cultures overexpressing the corresponding channel (CHO: TRPV1 and TRPA1; HEK293: TRPV3 and ASIC3). In vitro pharmacology, cellular channel functional assays: the compound was prepared in assay buffer to the final concentration, 10  $\mu\text{M}$ . The compound wells, reference agonist and background vehicle controls were prepared in DMSO at 0.3%. The reference agonist for each Ion Channel assayed was prepared in a similar manner to serve as the assay control. The reference agonist for each Ion Channel was included at  $E_{max}$  (the concentration where the reference agonist elicited a maximal response). The agonist assay was conducted on fluorimeter instruments where the test compound, vehicle controls, and reference agonist were added to the assay plate after a fluorescence baseline was established. The agonist assay was used to assess each compound's ability to activate each Ion Channel assayed. For the antagonist assay, the compound was pre-incubated for five minutes at room temperature, and then challenged with the  $EC_{80}$  concentration of the reference agonist after establishment of a fluorescence baseline. Vehicle controls and  $EC_{80}$  concentration of reference agonist were added to appropriate wells. The antagonist assay was used to assess each compound's ability to inhibit activation by the corresponding Ion Channel agonist. ASIC3 ionflux antagonist assay: all recordings were obtained from a holding potential of -60 mV. The compound addition sequence was as follows: one addition of pH5.5 buffer was added to establish the baseline response, the test concentration of compound was applied for 30 s, followed by the addition of pH5.5 of compound for 2 s. Binding assays were performed in CHO cell cultures overexpressing human CGRPR, CB2 and M2 receptors. RGM8-51 (10  $\mu\text{M}$ ) was tested, and reference compounds used as control agonists and antagonists are detailed in Table 2, footnote. Binding assay results are expressed as a percent of control specific binding. Preliminary PK analysis, namely solubility, log D, in vitro Caco-2 permeability, human binding to plasma protein and in vitro metabolism (human liver microsomes) was performed at Eurofins-CEREP, using established methods. Aqueous solubility ( $\mu\text{M}$ ) was determined by comparing the peak area of the principal peak in a calibration standard (200  $\mu\text{M}$ ) containing organic solvent (methanol/water, 60/40, v/v) with the peak area of the corresponding peak in a buffer sample. Partition coefficient: the total amount of compound was determined as the peak area of the principal peak in a calibration standard (100  $\mu\text{M}$ ) containing organic solvent (methanol/water, 60/40, v/v). The amount of compound in buffer was determined as the combined, volume-corrected, and weighted areas of the

corresponding peaks in the aqueous phases of three organic-aqueous samples of different composition. An automated weighting system was used to ensure the preferred use of raw data from those samples with well quantifiable peak signals. The amount of compound in organic phase was calculated by subtraction. Subsequently, Log D was calculated as the Log<sub>10</sub> of the amount of compound in the organic phase divided by the amount of compound in the aqueous phase. Protein binding: percentage of compound bound to serum proteins. Permeability was measured in CACO-2 monolayers. Percentage of compounds in the receptors wells was measured using HPLC. Lucifer yellow was used to assess cell monolayer integrity. In vitro metabolism was measured in human liver microsomes. The half-life ( $t_{1/2}$ ) was estimated from the slope of the initial linear range of the logarithmic curve of compound remaining (%) vs. time, assuming the first-order kinetics. The apparent intrinsic clearance (CL<sub>int</sub>, in  $\mu\text{L}/\text{min}/\text{mg}$ ) was calculated from the half-life time.

#### 4.7. Mouse Model of Oxaliplatin-Induced Peripheral Neuropathy

For the experiments, 6–8 weeks C57 male mice ( $\approx 30\text{g}$ ) (Harlan, Holland) were used. All experiments were approved by the Institutional Animal and Ethical Committee of the Universidad Miguel Hernandez and Comunidad Valencian ethical committees (2021/VSC/PEA/0089) where experiments were conducted and they were in accordance with the guidelines of the Economic European Community and the Committee for Research and Ethical Issues of the International Association for the Study of Pain. All parts of the study concerning animal care were performed under the control of veterinarians. Experiments were performed blinded for NTG and compound treatment.

Oxaliplatin (OXA, Tocris, Bristol, UK) was used to induce peripheral neuropathy and was dissolved in water with gentle warming as formerly described [34]. OXA was intraperitoneally injected on days 1, 3 and 5 at a 6 mg/kg dose. On day 7, experiments were carried out. Additionally, and in order to prevent kidney damage or dehydration, animals were also i.p. injected with saline solution and a 5% mannitol solution. The compound RGM8-51 stock was prepared in DMSO (Sigma-Aldrich) and freshly diluted in saline just before injections. RGM8-51 compound was injected i.pl. at different doses (0.1–1  $\mu\text{g}$ ) in a volume of 25  $\mu\text{L}$  in the right hind paw of mice. Cold chemical sensitivity was assessed using the acetone drop test. Briefly, animals were kept in a metal mesh cage and allowed to habituate for approximately 30 min in order to acclimatize them. An acetone drop (10  $\mu\text{L}$ ) was applied on the plantar surface of one of the hind paws. Positive nociceptive responses (licking time in seconds) were recorded with a digital stopwatch during 20 s (cut-off). Acetone was applied twice in an interval of 5 min between each application and the mean was calculated.

#### 4.8. Rat Chronic Constriction Injury (CCI) Model

Adult male Sprague-Dawley rats (weighing 200–220 g/6–8 weeks old) were used in these experiments. All experimental procedures were conducted according to the animal welfare guidelines of the European Community (European Directive 2010/63/UE) to minimize animal suffering and were approved by Universidad Complutense de Madrid and Comunidad de Madrid ethical committees on animal experimentation (PROEX 207.8/21).

CCI was performed according to Bennett and Xie (1988) [5]. Briefly, rats were anesthetized with i.p. ketamine (100 mg/kg; Merial Labs, Barcelona, Spain) and medetomidine (100  $\mu\text{g}/\text{kg}$ ; Esteve Labs, Barcelona, Spain). Under sterile conditions, approximately 7 mm of the right nerve was freed proximal to the sciatic trifurcation, and four barely constricting ligatures (1 mm apart) using 4/0 chromic catgut were applied. The incision was closed in layers with silk thread 6/0. Animals were then allowed to recover from surgery for 7 days before being used in additional procedures.

For behavioral testing, rats were placed in individual methacrylate boxes with a wire mesh floor, and after a period of 15 min acclimatization, the cold, heat and mechanical sensitivity of the ipsilateral and contralateral paws was determined. Cold sensitivity was assessed with the acetone test. In total, 100  $\mu\text{L}$  acetone were locally applied to the plantar

surface of the hind paw and the duration of the subsequent nocifensive response (licking, brushing, and flinching of the paw) was determined during 60 s. Acetone application and assessment were repeated 2 times with a 5 min interval and the sum of the two values was recorded. Heat sensitivity was determined with the Hargreaves test, which uses infrared light as a heat source, with a Hargreaves apparatus (Serie 8, Model 336, IITC Life Science, Woodland Hills, CA USA). The light beam was directed to the plantar surface of the hind paw and the time from the beginning of irradiation to the appearance of first paw withdrawal movement was measured (paw withdrawal latency). A cut-off of 20 s was set to prevent tissue injury. Two measurements were taken separated by a 1 min interval, and the mean value was calculated. Mechanical sensitivity was evaluated with a dynamic plantar aesthesiometer (Ugo Basile, Gemonio, Italy) by means of a 0.5 mm filament exerting increasing force (up to 50 g over 20 s) onto the plantar surface of the hind paw until the animal lifted its paw, the actual force at that time was automatically registered (paw withdrawal threshold). Measurements were repeated 3 times at 5 min intervals, and the mean value was reported. Behavioral tests were carried out before surgery (mean of 3 measurements on alternate days the week preceding surgery, collectively designated as baseline) and on days 7–21 post-surgery.

Rats were allocated into 2 groups to receive RGM8-51 and vehicle (DMSO 2% i.pl., or 150  $\mu$ L/kg i.p.) by either the i.pl. (10  $\mu$ g in 20  $\mu$ L; n = 5 animals) or i.p. (10 or 30 mg/kg in 150  $\mu$ L/kg; n = 8 animals) route. Responses to cold/heat/mechanical stimulation were assessed 30 min before and 30 min after RGM8-51 or vehicle injection. Behavioral testing prior to drug administration served to ascertain baseline conditions and the stability of cold, heat and mechanical hypersensitivity after surgery. RGM-8-51 stock was prepared in DMSO (Sigma-Aldrich) and diluted in saline for injections. Data are given as the mean  $\pm$  standard error of the mean (SEM) of the corresponding number of behavioral measurements/ animals used. Statistical analysis was performed by using the paired *t*-test (GraphPad 8; San Diego, CA, USA).

#### 4.9. Mouse Model of NTG-Induced Mechanical Hypersensitivity

C57BL6 mice (males and females,  $\approx$ 25 g) (Envigo, Blackthorn, UK) were used for the study. All experiments were approved by the Institutional Animal and Ethical Committee of the Universidad Miguel Hernandez where experiments were conducted and they were in accordance with the guidelines of the Economic European Community and the Committee for Research and Ethical Issues of the International Association for the Study of Pain. All parts of the study concerning animal care were performed under the control of veterinarians. Commercially available nitroglycerin (NTG) formulation (Nitro Pohl, 10 mg/kg) was administered i.p. 2h before measurements. The NTG stock solution was diluted in saline up to a final dose of 10 mg/kg, which was injected to the animals. RGM-8-51 stock was prepared in DMSO (Sigma-Aldrich) and diluted in saline for injections. Compound was i.p. administered. The first von Frey measurement was performed 30 min after RGM8-51 injection, and subsequently at the indicated times (60, 120, and 180 in females). Mechanical threshold values were obtained by performing the von Frey test as previously reported [1]. Mice were placed on a wire mesh platform and, after a 20 min habituation period, von Frey filaments (Stoelting, Wood Dale, IL, USA) were applied to the plantar side of the paws. von Frey filaments 2.44, 2.83, 3.22, 3.61, 4.08 and 4.56 were used and, starting with the 3.61 filament, 6 measurements were taken in each animal randomly starting by the left or right paw. Based on the "up and down" method [2], the observation of a positive response (lifting, shaking or licking of the paw) was followed by the application of the immediate thinner filament or the immediate thicker one if the response was negative. The 50% response threshold was calculated using the following formula:

$$50\% \text{ (g) threshold} = (10^{(X_f + kd)})/10,000$$

where  $Xf$  is the value of the last von Frey filament applied;  $k$  is a correction factor based on pattern of responses (from the Dixon's calibration table);  $d$  is the mean distance in log units between stimuli (here, 0.4).

Von Frey threshold for each animal was calculated, according to the formula, and data analysis was performed by using GraphPad 6.0. Ordinary two-way ANOVA analysis followed by the post hoc *Bonferroni* test for multiple comparisons.

**Supplementary Materials:** The following supporting information can be downloaded at: <https://www.mdpi.com/article/10.3390/ijms23052692/s1>.

**Author Contributions:** Conceptualization, R.G.-M.; synthetic methodology and characterization, C.M.-E. and L.A.S.; in vitro experiments, R.d.I.T.M., A.M.-P., L.A.O.-O. and M.V.B.; docking studies: R.d.I.T.M.; in vivo experiments: S.G.-R., L.A.O.-O. and M.V.B.; supervision, G.F.-B., A.F.-C., A.R.A., A.F.-M. and R.G.-M.; writing—original draft preparation, G.F.-B., A.F.-C., A.R.A. and R.G.-M.; writing—review and editing, A.F.-C., A.R.A., L.A.O.-O., A.F.-M. and R.G.-M.; funding acquisition, A.F.-M., A.F.-C., A.R.A. and R.G.-M. All authors have read and agreed to the published version of the manuscript.

**Funding:** This research was funded by the Spanish Ministerio de Ciencia y Universidades (MICYU-FEDER, RTI2018-097189-C2-1 to A.F.-M. and A.F.-C., and RTI2018-097189-C2-2 to R.G.-M.), Comunidad de Madrid (IND2017/BMD7673 to R.G.-M.) and the Spanish National Research Council (CSIC, 201980E030 to R.G.-M.), and Universidad Complutense de Madrid (PR75/18-21593, FEI20/35 and PID2019-109155RB-I00 to A.R.A.).

**Institutional Review Board Statement:** The study was conducted according to the guidelines of the Declaration of Helsinki and approved by the Ethics Committee of Miguel Hernández University (UMH.IBM.AFM.02.18—11 October 2018), and Universidad Complutense de Madrid (PROEX 207.8/21, 29 June 2021).

**Acknowledgments:** We would like to thank Jessy Medina for purifications and Aída García for her support in the economic management of the projects.

**Conflicts of Interest:** The authors declare no conflict of interest.

## References

1. Liu, Y.; Mikrani, R.; He, Y.; Faran Ashraf Baig, M.M.; Abbas, M.; Naveed, M.; Tang, M.; Zhang, Q.; Li, C.; Zhou, X. TRPM8 channels: A review of distribution and clinical role. *Eur. J. Pharmacol.* **2020**, *882*, 173312. [CrossRef]
2. Pérez De Vega, M.J.; Gómez-Monterrey, I.; Ferrer-Montiel, A.; González-Muñiz, R. Transient Receptor Potential Melastatin 8 Channel (TRPM8) Modulation: Cool Entryway for Treating Pain and Cancer. *J. Med. Chem.* **2016**, *59*, 10006–10029. [CrossRef] [PubMed]
3. Gonzalez-Muñiz, R.; Bonache, M.A.; Martin-Escura, C.; Gomez-Monterrey, I. Recent Progress in TRPM8 Modulation: An Update. *Int. J. Mol. Sci.* **2019**, *20*, 2618. [CrossRef] [PubMed]
4. Lolignier, S.; Gkika, D.; Andersson, D.; Leipold, E.; Vetter, I.; Viana, F.; Noel, J.; Busserolles, J. New insight in cold pain: Role of ion channels, modulation, and clinical perspectives. *J. Neurosci.* **2016**, *36*, 11435–11439. [CrossRef]
5. Bennett, G.J.; Xie, Y.-K. A peripheral mononeuropathy in rat that produces disorders of pain sensation like those seen in man. *Pain* **1988**, *33*, 87–107. [CrossRef]
6. Caspani, O.; Zurborg, S.; Labuz, D.; Heppenstall, P.A. The contribution of TRPM8 and TRPA1 channels to cold allodynia and neuropathic pain. *PLoS ONE* **2009**, *4*, e7383. [CrossRef]
7. Su, L.; Shu, R.; Song, C.; Yu, Y.; Wang, G.; Li, Y.; Liu, C. Downregulations of TRPM8 expression and membrane trafficking in dorsal root ganglion mediate the attenuation of cold hyperalgesia in CCI rats induced by GFR $\alpha$ 3 knockdown. *Brain Res. Bull.* **2017**, *135*, 8–24. [CrossRef]
8. Su, L.; Wang, C.; Yu, Y.-H.; Ren, Y.-Y.; Xie, K.-L.; Wang, G.-L. Role of TRPM8 in dorsal root ganglion in nerve injury-induced chronic pain. *BMC Neurosci.* **2011**, *12*, 120. [CrossRef] [PubMed]
9. De Caro, C.; Cristiano, C.; Avagliano, C.; Bertamino, A.; Ostacolo, C.; Campiglia, P.; Gomez-Monterrey, I.; La Rana, G.; Gualillo, O.; Calignano, A.; et al. Characterization of new TRPM8 modulators in pain perception. *Int. J. Mol. Sci.* **2019**, *20*, 5544. [CrossRef] [PubMed]
10. Cao, S.; Hou, J.; Li, Z.; Cao, X.; Qin, B.; Cao, S.; Li, Q.; Liu, X. Intrathecal TRPM8 blocking attenuates cold hyperalgesia via PKC and NF- $\kappa$ B signaling in the dorsal root ganglion of rats with neuropathic pain. *J. Pain Res.* **2019**, *12*, 1287–1296. [CrossRef]

11. Lehto, S.G.; Weyer, A.D.; Zhang, M.; Youngblood, B.D.; Wang, J.; Wang, W.; Kerstein, P.C.; Davis, C.; Wild, K.D.; Stucky, C.L.; et al. AMG2850, a potent and selective TRPM8 antagonist, is not effective in rat models of inflammatory mechanical hypersensitivity and neuropathic tactile allodynia. *Naunyn-Schmiedeberg's Arch. Pharmacol.* **2015**, *388*, 465–476. [[CrossRef](#)] [[PubMed](#)]
12. Bertamino, A.; Ostacolo, C.; Medina, A.; Di Sarno, V.; Lauro, G.; Ciaglia, T.; Vestuto, V.; Pepe, G.; Basilicata, M.G.; Musella, S.; et al. Exploration of TRPM8 Binding Sites by  $\beta$ -Carboline-Based Antagonists and Their In Vitro Characterization and In Vivo Analgesic Activities. *J. Med. Chem.* **2020**, *63*, 9672–9694. [[CrossRef](#)]
13. De Caro, C.; Russo, R.; Avagliano, C.; Cristiano, C.; Calignano, A.; Aramini, A.; Bianchini, G.; Allegretti, M.; Brandolini, L. Antinociceptive effect of two novel transient receptor potential melastatin 8 antagonists in acute and chronic pain models in rat. *Br. J. Pharmacol.* **2018**, *175*, 1691–1706. [[CrossRef](#)] [[PubMed](#)]
14. Park, S.B.; Goldstein, D.; Krishnan, A.V.; Lin, C.S.Y.; Friedlander, M.L.; Cassidy, J.; Koltzenburg, M.; Kiernan, M.C. Chemotherapy-Induced Peripheral Neurotoxicity: A Critical Analysis. *CA Cancer J. Clin.* **2013**, *63*, 419–437. [[CrossRef](#)] [[PubMed](#)]
15. Zanone, M.M.; Marinucci, C.; Ciancio, A.; Cocito, D.; Zardo, F.; Spagone, E.; Ferrero, B.; Cerruti, C.; Charrier, L.; Cavallo, F.; et al. Peripheral neuropathy after viral eradication with direct-acting antivirals in chronic HCV hepatitis: A prospective study. *Liver Int.* **2021**, *41*, 2611–2621. [[CrossRef](#)]
16. Egan, K.E.; Caldwell, G.M.; Eckmann, M.S. HIV Neuropathy—a Review of Mechanisms, Diagnosis, and Treatment of Pain. *Curr. Pain Headache Rep.* **2021**, *25*, 55. [[CrossRef](#)] [[PubMed](#)]
17. Nassini, R.; Benemei, S.; Fusi, C.; Trevisan, G.; Materazzi, S. Transient receptor potential channels in chemotherapy-induced neuropathy. *Open Pain J.* **2013**, *6*, 127–136. [[CrossRef](#)]
18. Rimola, V.; Osthues, T.; Koenigs, V.; Geisslinger, G.; Sisignano, M. Oxaliplatin causes transient changes in TRPM8 channel activity. *Int. J. Mol. Sci.* **2021**, *22*, 4962. [[CrossRef](#)]
19. Mizoguchi, S.; Andoh, T.; Yakura, T.; Kuraishi, Y. Involvement of c-Myc-mediated transient receptor potential melastatin 8 expression in oxaliplatin-induced cold allodynia in mice. *Pharmacol. Rep.* **2016**, *68*, 645–648. [[CrossRef](#)] [[PubMed](#)]
20. Pan, Y.; Chen, F.; Huang, S.; Cai, Z.; Lan, H.; Tong, Y.; Yu, X.; Zhao, G. TRPA1 and TRPM8 Receptors May Promote Local Vasodilation that Aggravates Oxaliplatin-Induced Peripheral Neuropathy Amenable to 17 $\beta$ -Estradiol Treatment. *Curr. Neurovasc. Res.* **2016**, *13*, 309–317. [[CrossRef](#)]
21. Wu, B.; Su, X.; Zhang, W.; Zhang, Y.-H.; Feng, X.; Ji, Y.-H.; Tan, Z.-Y. Oxaliplatin depolarizes the IB4- dorsal root ganglion neurons to drive the development of neuropathic pain through TRPM8 in mice. *Front. Mol. Neurosci.* **2021**, *14*, 690858. [[CrossRef](#)]
22. Kawashiri, T.; Egashira, N.; Kurobe, K.; Tsutsumi, K.; Yamashita, Y.; Ushio, S.; Yano, T.; Oishi, R. L type Ca<sup>2+</sup> channel blockers prevent oxaliplatin-induced cold hyperalgesia and TRPM8 overexpression in rats. *Mol. Pain* **2012**, *8*, 7. [[CrossRef](#)]
23. Hogan, D.; Baker, A.L.; Moron, J.A.; Carlton, S.M. Systemic morphine treatment induces changes in firing patterns and responses of nociceptive afferent fibers in mouse glabrous skin. *Pain* **2013**, *154*, 2297–2309. [[CrossRef](#)] [[PubMed](#)]
24. Gong, K.; Jasmin, L. Sustained Morphine Administration Induces TRPM8-Dependent Cold Hyperalgesia. *J. Pain* **2017**, *18*, 212–221. [[CrossRef](#)] [[PubMed](#)]
25. Qin, D.; Zou, Z.; Zhou, C.; Mu, F. Role of transient receptor potential melastatin 8 channels in migraine mechanism in rats. *Zhongguo Dangdai Erke Zazhi* **2015**, *17*, 515–519. [[PubMed](#)]
26. Ling, Y.H.; Chen, S.P.; Fann, C.S.J.; Wang, S.J.; Wang, Y.F. TRPM8 genetic variant is associated with chronic migraine and allodynia. *J. Headache Pain* **2019**, *20*, 115. [[CrossRef](#)]
27. Kaur, S.; Ali, A.; Ahmad, U.; Pandey, A.K.; Singh, B. rs2651899 variant is associated with risk for migraine without aura from North Indian population. *Mol. Biol. Rep.* **2019**, *46*, 1247–1255. [[CrossRef](#)]
28. Kozyreva, T.V.; Tkachenko, E.Y.; Potapova, T.A.; Romashchenko, A.G.; Voevoda, M.I. Single-nucleotide polymorphism rs11562975 of the thermosensitive ion channel TRPM8 gene and human sensitivity to cold and menthol. *Hum. Physiol.* **2011**, *37*, 188–192. [[CrossRef](#)]
29. Horne, D.B.; Biswas, K.; Brown, J.; Bartberger, M.D.; Clarine, J.; Davis, C.D.; Gore, V.K.; Harried, S.; Horner, M.; Kaller, M.R.; et al. Discovery of TRPM8 Antagonist (S)-6-(((3-Fluoro-4-(trifluoromethoxy)phenyl)(3-fluoropyridin-2-yl)methyl)carbamoyl)nicotinic Acid (AMG 333), a Clinical Candidate for the Treatment of Migraine. *J. Med. Chem.* **2018**, *61*, 8186–8201. [[CrossRef](#)]
30. De la Torre-Martinez, R.; Bonache, M.A.; Llabres-Campaner, P.J.; Balsera, B.; Fernandez-Carvajal, A.; Fernandez-Ballester, G.; Ferrer-Montiel, A.; Perez de Vega, M.J.; Gonzalez-Muniz, R. Synthesis, high-throughput screening and pharmacological characterization of  $\beta$ -lactam derivatives as TRPM8 antagonists. *Sci. Rep.* **2017**, *7*, 10766.
31. Bonache, M.A.; Martin-Escura, C.; de la Torre Martinez, R.; Medina, A.; Gonzalez-Rodriguez, S.; Francesch, A.; Cuevas, C.; Roa, A.M.; Fernandez-Ballester, G.; Ferrer-Montiel, A.; et al. Highly functionalized  $\beta$ -lactams and 2-ketopiperazines as TRPM8 antagonists with antiallodynic activity. *Sci. Rep.* **2020**, *10*, 14154. [[CrossRef](#)]
32. Perez-Faginas, P.; O'Reilly, F.; O'Byrne, A.; Garcia-Aparicio, C.; Martin-Martinez, M.; Perez de Vega, M.J.; Garcia-Lopez, M.T.; Gonzalez-Muniz, R. Exceptional Stereoselectivity in the Synthesis of 1,3,4-Trisubstituted 4-Carboxy  $\beta$ -Lactam Derivatives from Amino Acids. *Org. Lett.* **2007**, *9*, 1593–1596. [[CrossRef](#)] [[PubMed](#)]
33. Lashinger, E.S.R.; Steingina, M.S.; Hieble, J.P.; Leon, L.A.; Gardner, S.D.; Nagilla, R.; Davenport, E.A.; Hoffman, B.E.; Laping, N.J.; Su, X. AMTB, a TRPM8 channel blocker: Evidence in rats for activity in overactive bladder and painful bladder syndrome. *Am. J. Physiol. Ren. Physiol.* **2008**, *295*, F803–F810. [[CrossRef](#)]
34. Hung, C.-Y.; Tan, C.-H.; Tan, C.-H. TRP Channels in Nociception and Pathological Pain. *Adv. Exp. Med. Biol.* **2018**, *1099*, 13–27.

35. Ferrer-Montiel, A.; Fernández-Carvajal, A.; Planells-Cases, R.; Fernández-Ballester, G.; González-Ros, J.M.; Messeguer, À.; González-Muñiz, R. Advances in modulating thermosensory TRP channels. *Expert Opin. Ther. Pat.* **2012**, *22*, 999–1017. [[CrossRef](#)]
36. Li, W.-G.; Xu, T.-L. ASIC3 Channels in Multimodal Sensory Perception. *ACS Chem. Neurosci.* **2011**, *2*, 26–37. [[CrossRef](#)]
37. Schou, W.S.; Ashina, S.; Amin, F.M.; Goadsby, P.J.; Ashina, M. Calcitonin gene-related peptide and pain: A systematic review. *J. Headache Pain* **2017**, *18*, 34. [[CrossRef](#)]
38. Benemei, S.; Nicoletti, P.; Capone, J.G.; Geppetti, P. CGRP receptors in the control of pain and inflammation. *Curr. Opin. Pharmacol.* **2009**, *9*, 9–14. [[CrossRef](#)]
39. Xu, J.J.; Diaz, P.; Bie, B.; Astruc-Diaz, F.; Wu, J.; Yang, H.; Brown, D.L.; Naguib, M. Spinal gene expression profiling and pathways analysis of a CB2 agonist (MDA7)-targeted prevention of paclitaxel-induced neuropathy. *Neuroscience* **2014**, *260*, 185–194. [[CrossRef](#)] [[PubMed](#)]
40. Clapper, J.R.; Moreno-Sanz, G.; Russo, R.; Guijarro, A.; Vacondio, F.; Duranti, A.; Tontini, A.; Sanchini, S.; Sciolino, N.R.; Spradley, J.M.; et al. Anandamide suppresses pain initiation through a peripheral endocannabinoid mechanism. *Nat. Neurosci.* **2010**, *13*, 1265–1270. [[CrossRef](#)] [[PubMed](#)]
41. Anand, U.; Otto, W.R.; Sanchez-Herrera, D.; Facer, P.; Yiangou, Y.; Korchev, Y.; Birch, R.; Benham, C.; Bountra, C.; Chessell, I.P.; et al. Cannabinoid receptor CB2 localisation and agonist-mediated inhibition of capsaicin responses in human sensory neurons. *Pain* **2008**, *138*, 667–680. [[CrossRef](#)] [[PubMed](#)]
42. Bernardini, N.; Levey, A.I.; Augusti-Tocco, G. Rat dorsal root ganglia express m1-m4 muscarinic receptor proteins. *J. Peripher. Nerv. Syst.* **1999**, *4*, 222–232. [[PubMed](#)]
43. Buchli, R.; Ndoye, A.; Arredondo, J.; Webber, R.J.; Grando, S.A. Identification and characterization of muscarinic acetylcholine receptor subtypes expressed in human skin melanocytes. *Mol. Cell. Biochem.* **2001**, *228*, 57–72. [[CrossRef](#)]
44. Metzger, M.; Just, L.; Drews, U. Identification and Functional Characterization of the Muscarinic Receptor M3 in the Human Keratinocyte Cell Line HaCaT. *Cells Tissues Organs* **2005**, *180*, 96–105. [[CrossRef](#)]
45. Krieger, E.; Darden, T.; Nabuurs, S.B.; Finkelstein, A.; Vriend, G. Making optimal use of empirical energy functions: Force-field parameterization in crystal space. *Proteins Struct. Funct. Bioinform.* **2004**, *57*, 678–683. [[CrossRef](#)]
46. Krieger, E.; Koraimann, G.; Vriend, G. Increasing the precision of comparative models with yasara NOVA—a self-parameterizing force field. *Proteins Struct. Funct. Genet.* **2002**, *47*, 393–402. [[CrossRef](#)] [[PubMed](#)]
47. Yin, Y.; Wu, M.; Zubcevic, L.; Borschel, W.F.; Lander, G.C.; Lee, S.Y. Structure of the cold- and menthol-sensing ion channel TRPM8. *Science* **2018**, *359*, 237–241. [[CrossRef](#)] [[PubMed](#)]
48. Diver, M.M.; Cheng, Y.; Julius, D. Structural insights into TRPM8 inhibition and desensitization. *Science* **2019**, *365*, 1434–1440. [[CrossRef](#)]
49. Ewertz, M.; Qvortrup, C.; Eckhoff, L. Chemotherapy-induced peripheral neuropathy in patients treated with taxanes and platinum derivatives. *Acta Oncol.* **2015**, *54*, 587–591. [[CrossRef](#)]
50. Journigan, V.B.; Feng, Z.; Rahman, S.; Wang, Y.; Amin, A.R.M.R.; Heffner, C.E.; Bachtel, N.; Wang, S.; Gonzalez-Rodriguez, S.; Fernandez-Carvajal, A.; et al. Structure-Based Design of Novel Biphenyl Amide Antagonists of Human Transient Receptor Potential Cation Channel Subfamily M Member 8 Channels with Potential Implications in the Treatment of Sensory Neuropathies. *ACS Chem. Neurosci.* **2020**, *11*, 268–290.
51. Gavva, N.R.; Sandrock, R.; Arnold, G.E.; Davis, M.; Lamas, E.; Lindvay, C.; Li, C.-M.; Smith, B.; Gabriel, K.; Vargas, G.; et al. Reduced TRPM8 expression underpins reduced migraine risk and attenuated cold pain sensation in humans. *Sci. Rep.* **2019**, *9*, 19655. [[CrossRef](#)] [[PubMed](#)]
52. Knowlton, W.M.; Daniels, R.L.; Palkar, R.; McCoy, D.D.; McKemy, D.D. Pharmacological blockade of TRPM8 ion channels alters cold and cold pain responses in mice. *PLoS ONE* **2011**, *6*, e25894. [[CrossRef](#)] [[PubMed](#)]
53. Benemei, S.; Dussor, G. TRP Channels and Migraine: Recent Developments and New Therapeutic Opportunities. *Pharmaceuticals* **2019**, *12*, 54. [[CrossRef](#)] [[PubMed](#)]
54. Haghighi, A.B.; Motazedian, S.; Rezaii, R.; Mohammadi, F.; Salarian, L.; Pourmokhtari, M.; Khodaei, S.; Vossoughi, M.; Miri, R. Cutaneous application of menthol 10% solution as an abortive treatment of migraine without aura: A randomised, double-blind, placebo-controlled, crossed-over study. *Int. J. Clin. Pract.* **2010**, *64*, 451–456. [[CrossRef](#)]
55. Moye, L.S.; Pradhan, A.A.A. Animal Model of Chronic Migraine-Associated Pain. *Curr. Protoc. Neurosci.* **2017**, *80*, 9.60.1–9.60.9. [[CrossRef](#)]
56. Tipton, A.F.; Pradhan, A.A.; Tarash, I.; McGuire, B.; Charles, A. The effects of acute and preventive migraine therapies in a mouse model of chronic migraine. *Cephalalgia* **2016**, *36*, 1048–1056. [[CrossRef](#)]
57. Wen, Q.; Zhang, D.; Qin, G.; Chen, L.; Wang, Y.; Pan, Q.; Tian, R.; Zhou, J.; Wang, Y. MicroRNA-155-5p promotes neuroinflammation and central sensitization via inhibiting SIRT1 in a nitroglycerin-induced chronic migraine mouse model. *J. Neuroinflamm.* **2021**, *18*, 287. [[CrossRef](#)]
58. Asuthkar, S.; Elustondo, P.A.; Demirkhanyan, L.; Sun, X.; Baskaran, P.; Velpula, K.K.; Thyagarajan, B.; Pavlov, E.V.; Zakharian, E. The TRPM8 protein is a testosterone receptor: I. Biochemical evidence for direct TRPM8-testosterone interactions. *J. Biol. Chem.* **2015**, *290*, 2659–2669. [[CrossRef](#)]
59. Asuthkar, S.; Demirkhanyan, L.; Sun, X.; Elustondo, P.A.; Krishnan, V.; Baskaran, P.; Velpula, K.K.; Thyagarajan, B.; Pavlov, E.V.; Zakharian, E. The TRPM8 Protein Is a Testosterone Receptor. II. Functional Evidence for an Ionotropic Effect of Testosterone on TRPM8. *J. Biol. Chem.* **2015**, *290*, 2670–2688. [[CrossRef](#)]

60. Mohandass, A.; Krishnan, V.; Gribkova, E.D.; Asuthkar, S.; Baskaran, P.; Nersesyan, Y.; Hussain, Z.; Wise, L.M.; George, R.E.; Stokes, N.; et al. TRPM8 as the rapid testosterone signaling receptor: Implications in the regulation of dimorphic sexual and social behaviors. *FASEB J.* **2020**, *34*, 10887–10906. [[CrossRef](#)]
61. Huo, C.; Wang, C.; Zhao, M.; Peng, S. Stereoselective synthesis of natural N-(1-deoxy-D- $\beta$ -fructos-1-yl)-L- amino acids and their effect on lead decorporation. *Chem. Res. Toxicol.* **2004**, *17*, 1112–1120. [[CrossRef](#)] [[PubMed](#)]
62. Arribas-Blazquez, M.; Olivos-Ore, L.A.; Barahona, M.V.; Sanchez de la Muela, M.; Solar, V.; Jimenez, E.; Gualix, J.; McIntosh, J.M.; Ferrer-Montiel, A.; Miras-Portugal, M.T.; et al. Overexpression of P2X3 and P2X7 receptors and TRPV1 channels in adrenomedullary chromaffin cells in a rat model of neuropathic pain. *Int. J. Mol. Sci.* **2019**, *20*, 155. [[CrossRef](#)] [[PubMed](#)]
63. Nikolaeva-Koleva, M.; Butron, L.; Gonzalez-Rodriguez, S.; Devesa, I.; Valente, P.; Serafini, M.; Genazzani, A.A.; Pirali, T.; Ballester, G.F.; Fernandez-Carvajal, A.; et al. A capsaicinoid-based soft drug, AG1529, for attenuating TRPV1-mediated histaminergic and inflammatory sensory neuron excitability. *Sci. Rep.* **2021**, *11*, 246. [[CrossRef](#)] [[PubMed](#)]



**ANEXO IV. Publicación 1 del capítulo 2*****In Vitro and In Vivo Pharmacological Characterization of a Novel TRPM8 Inhibitor Chemotype Identified by Small-Scale Preclinical Screening.***

Nunzio Iraci<sup>1,†</sup>, Carmine Ostacolo<sup>2,†</sup>, Alicia Medina-Peris<sup>3,†</sup>, Tania Ciaglia<sup>4</sup>, Anton M. Novoselov<sup>5</sup>, Andrea Altieri<sup>5,6</sup>, David Cabañero<sup>3</sup>, Asia Fernandez-Carvajal<sup>3</sup>, Pietro Campiglia<sup>4</sup>, Isabel Gomez-Monterrey<sup>2</sup>, Alessia Bertamino<sup>4</sup> y Alexander V. Kurkin<sup>5</sup>.

<sup>1</sup>Departamento de Ciencias Químicas, biológicas, farmacéuticas y medioambientales. Universidad de Messina, Viale Ferdinando Stagno d'Alcontres 31, 98166 Mesina, Italia.

<sup>2</sup>Departamento de Farmacia, Universidad Federico II de Napoles, Via D. Montesano 49, 80131 Napoles, Italia.

<sup>3</sup>Instituto de Investigación, Desarrollo e Innovación en Biotecnología Sanitaria de Elche (IDiBE), Universidad Miguel Hernández de Elche, Avenida de la Universidad, 03202 Elche, España.

<sup>4</sup>Departamento de Farmacia, Universidad de Salerno, Via G. Paolo II, 84084 Fisciano, Italia.

<sup>5</sup>Departamento de Química, Lomonosov Moscow State University, 1/3 Leninsky Gory, 119991 Moscú, Rusia.

†Estos autores contribuyeron por igual en este trabajo.

International Journal of Molecular Sciences 2022, Vol. 23, Page 2070 2022, 23 (4), 2070.

<https://doi.org/10.3390/ijms23042070>

(Q1; Factor de Impacto: 6.208)





Article

# In Vitro and In Vivo Pharmacological Characterization of a Novel TRPM8 Inhibitor Chemotype Identified by Small-Scale Preclinical Screening

Nunzio Iraci <sup>1,†</sup>, Carmine Ostacolo <sup>2,†</sup>, Alicia Medina-Peris <sup>3,†</sup>, Tania Ciaglia <sup>4</sup>, Anton M. Novoselov <sup>5</sup>, Andrea Altieri <sup>5,6</sup>, David Cabañero <sup>3</sup>, Asia Fernandez-Carvajal <sup>3</sup>, Pietro Campiglia <sup>4</sup>, Isabel Gomez-Monterrey <sup>2</sup>, Alessia Bertamino <sup>4,\*</sup> and Alexander V. Kurkin <sup>5,\*</sup>

<sup>1</sup> Department of Chemical, Biological, Pharmaceutical and Environmental Sciences, University of Messina, Viale Ferdinando Stagno d'Alcontres 31, 98166 Messina, Italy; nunzio.iraci@unime.it

<sup>2</sup> Department of Pharmacy, University of Naples Federico II, Via D. Montesano 49, 80131 Naples, Italy; ostacolo@unina.it (C.O.); imgomez@unina.it (I.G.-M.)

<sup>3</sup> Instituto de Investigación, Desarrollo e Innovación en Biotecnología Sanitaria de Elche (IDiBE), Universidad Miguel Hernández de Elche, Avenida de la Universidad, 03202 Elche, Spain; alicia.medinap@umh.es (A.M.-P.); dcabanero@umh.es (D.C.); asia.fernandez@umh.es (A.F.-C.)

<sup>4</sup> Department of Pharmacy, University of Salerno, Via G. Paolo II, 84084 Fisciano, Italy; tciaglia@unisa.it (T.C.); pcampiglia@unisa.it (P.C.)

<sup>5</sup> Department of Chemistry, Lomonosov Moscow State University, 1/3 Leninsky Gory, 119991 Moscow, Russia; antonnovoselov@yandex.ru (A.M.N.); aaltieri@edasascientific.com (A.A.)

<sup>6</sup> EDASA Scientific srls, Via Stingi 37, 66050 San Salvo, Italy

\* Correspondence: abertamino@unisa.it (A.B.); kurkin@direction.chem.msu.ru (A.V.K.)

† These authors contributed equally to this work.



**Citation:** Iraci, N.; Ostacolo, C.; Medina-Peris, A.; Ciaglia, T.; Novoselov, A.M.; Altieri, A.; Cabañero, D.; Fernandez-Carvajal, A.; Campiglia, P.; Gomez-Monterrey, I.; et al. In Vitro and In Vivo Pharmacological Characterization of a Novel TRPM8 Inhibitor Chemotype Identified by Small-Scale Preclinical Screening. *Int. J. Mol. Sci.* **2022**, *23*, 2070. <https://doi.org/10.3390/ijms23042070>

Academic Editors: Martin Hohenegger and Jose Javier Lopez

Received: 31 December 2021

Accepted: 11 February 2022

Published: 13 February 2022

**Publisher's Note:** MDPI stays neutral with regard to jurisdictional claims in published maps and institutional affiliations.



**Copyright:** © 2022 by the authors. Licensee MDPI, Basel, Switzerland. This article is an open access article distributed under the terms and conditions of the Creative Commons Attribution (CC BY) license (<https://creativecommons.org/licenses/by/4.0/>).

**Abstract:** Transient receptor potential melastatin type 8 (TRPM8) is a target for the treatment of different physio-pathological processes. While TRPM8 antagonists are reported as potential drugs for pain, cancer, and inflammation, to date only a limited number of chemotypes have been investigated and thus a limited number of compounds have reached clinical trials. Hence there is high value in searching for new TRPM8 antagonistic to broaden clues to structure-activity relationships, improve pharmacological properties and explore underlying molecular mechanisms. To address this, the EDASA Scientific in-house molecular library has been screened in silico, leading to identifying twenty-one potentially antagonist compounds of TRPM8. Calcium fluorometric assays were used to validate the in-silico hypothesis and assess compound selectivity. Four compounds were identified as selective TRPM8 antagonists, of which two were dual-acting TRPM8/TRPV1 modulators. The most potent TRPM8 antagonists (**BB 0322703** and **BB 0322720**) underwent molecular modelling studies to highlight key structural features responsible for drug-protein interaction. The two compounds were also investigated by patch-clamp assays, confirming low micromolar potencies. The most potent compound (**BB 0322703**,  $IC_{50}$   $1.25 \pm 0.26$   $\mu$ M) was then profiled in vivo in a cold allodynia model, showing pharmacological efficacy at 30  $\mu$ M dose. The new chemotypes identified showed remarkable pharmacological properties paving the way to further investigations for drug discovery and pharmacological purposes.

**Keywords:** TRPM8 antagonist; virtual screening; calcium fluorimetry; in silico studies; patch-clamp electrophysiology; oxaliplatin-induced allodynia model

## 1. Introduction

Transient receptor potential melastatin type 8 (TRPM8) is emerging as a potential target for the treatment of a variety of disorders, given its key role in many physio-pathological processes [1]. It is a non-selective  $Ca^{2+}$  permeable channel that shows a highly complicated

gating behaviour regulated by multiple factors [2,3] including temperature, endogenous and exogenous modulators or mechanisms, and depolarizing voltages [4,5].

TRPM8 is expressed mainly in a subpopulation of primary afferent neurons present in dorsal root and trigeminal ganglia, and in the nodose and geniculate ganglia of the peripheral nervous system. In these neurons, TRPM8 participates in the amplification of pain sensation after injury [6], suggesting that TRPM8 channel blockers could be effective for the treatment of chronic pain and migraine [7,8]. Furthermore, TRPM8 modulators have been investigated as therapeutics for the symptomatology of bladder pain syndromes, given their increased expression in patients suffering from these disorders [9]. Moreover, the channel overexpression in different kinds of tumors, such as prostate tumor [10], melanoma [11], breast cancer [12], and human pancreatic adenocarcinoma [13], together with the evidence of its implication in cellular proliferation, survival, and invasion, makes it an attractive target for cancer modulation [14]. The critical role of this receptor in humans and all living beings [15–17] has also been witnessed by the 2021 Nobel prize in Physiology and Medicine [18].

Despite the high interest in this area, to date, the number of known TRPM8 modulators is limited to a few natural agonists, such as menthol, or synthetic derivatives, like icilin [19,20] and a few synthetic and natural antagonists, including BCTC, CTPC, and capsaizepine [21]. Of note, the antifungal drug clotrimazole has strong TRPM8 antagonistic activity [22], while SKF96365, a non-specific blocker of several types of calcium channels, also inhibits TRPM8 in vitro [23]. Finally, a cyclic peptide specifically targeting the outer pore of the channels has been described as a potent antagonist endowed with anti-allodynic effects [24]. Nevertheless, none of the described TRPM8 antagonists has reached the clinical stage, so far [25]. Thus, the discovery of new chemotypes acting as TRPM8 antagonists appears important in order to improve the knowledge about their structure-activity relationships, to reduce some of the reported side effects [26], and to further investigate the molecular mechanisms underlying TRPM8 antagonism. Our research group has been deeply involved in the design and synthesis of new TRPM8 modulators. In particular, we have identified several chemotypes, showing a very remarkable inhibitory effect against TRPM8 channels and selectivity over other TRPs [27–29]. Some of these derivatives exhibited in vivo analgesic activity [30], while other compounds were characterized for their inhibitory effect over androgen-dependent prostate cancer cell proliferation, migration, and invasiveness [31]. On the other hand, structure-based virtual screening represents an outstanding alternative tool for putative hit compounds discovery, allowing the investigation of large chemical libraries through computational methods by applying knowledge about the protein target [32]. This approach has been profitably used for the identification of several chemotypes as TRPM8 antagonists [25,33].

In this work, starting from the recently released cryo-EM structure of the antagonist-bound *Parus major* TRPM8 [2], we have built a homology model of the human TRPM8 binding site. Then, a virtual screening (VS) protocol was applied to a commercially available molecular library (<http://zinc12.docking.org/catalogs/edasa/targets/clustered>, lastly accessed on 31 December 2021), leading to the identification of two novel chemotypes as potent and selective inhibitors of menthol-evoked TRPM8 currents, as assessed by  $Ca^{2+}$ -microfluorometric imaging and patch-clamp assays. The effect of one of these compounds was also studied in an in vivo model of cold allodynia, revealing its efficacy and suitability for further development.

## 2. Results

### 2.1. Virtual Screening

In order to maximize the chances to identify active inhibitors by testing just a small number of molecules, the library was submitted to a docking-based virtual screening (VS) workflow using a two targets ensemble. In particular, we used two homology models of human TRPM8 (hTRPM8) domains S1 to TRP (residues 723–1013) in homotetrameric assembly. The models were built by homology modelling using as templates the Cryo-EM

structures of Parus major TRPM8 in complex with AMTB (PDB ID: 6O6R) and TC-I 2014 (PDB ID: 6O72) [2]. The whole library was docked into the two target structures using a stepwise protocol consisting of two docking stages. Compounds were initially flexibly docked using Glide SP, and the best scoring ones were advanced to the following step that refined and rescored the docking poses using Glide XP (see materials and methods), finally giving a list of compounds ranked according to their XP GlideScore values, that ranged from  $-11.982$  to  $-8.903$ . Twenty-one compounds were selected (Table 1) from the list of top-scoring 100 compounds (Table S1) for the following experimental screening, on the basis of their stock availability and quality control results.

**Table 1.** Compounds selected for experimental screening.

Compound	XP GlideScore	VS Rank <sup>a</sup>
1 (BB 0220221)	-9.315	57
2 (BB 0301246)	-9.556	34
3 (BB 0301259)	-9.621	29
4 (BB 0301261)	-9.382	49
5 (BB 0304240)	-9.019	85
6 (BB 0304398)	-9.432	39
7 (BB 0304425)	-9.245	64
8 (BB 0305409)	-9.786	22
9 (BB 0305411)	-9.004	87
10 (BB 0305430)	-9.528	35
11 (BB 0310197)	-9.400	43
12 (BB 0310217)	-9.349	51
13 (BB 0310244)	-9.589	31
14 (BB 0322703)	-9.242	66
15 (BB 0322720)	-9.063	81
16 (BB 0323219)	-9.092	79
17 (BB 0323225)	-9.106	77
18 (BB 0301235)	-10.104	14
19 (BB 0310198)	-10.235	10
20 (BB 0310207)	-10.694	6
21 (BB 0237332)	-8.964	90

<sup>a</sup> Compounds ranking by XP GlideScore. Full ranking of top scoring 100 compounds, together with their structures and XP GlideScore values, is given in supporting information.

## 2.2. Screening by $Ca^{2+}$ -Microfluorometric Assay

The inhibitory activity of the 21 selected compounds over TRPM8 was challenged by  $Ca^{2+}$  fluorometric assays using HEK293 cells stably expressing the rat isoform of TRPM8 channels. Menthol and AMTB were used as reference agonist and antagonist, respectively. The compounds were initially tested at three different concentrations (50  $\mu$ M, 5  $\mu$ M, and 0.5  $\mu$ M) to assess their ability in blocking 100  $\mu$ M menthol evoked currents. As shown in Figure 1, six out of twenty-one compounds (1, 5, 13–15, and 19) showed a remarkable antagonist activity.

Calculation of the  $IC_{50}$ s for these compounds led to the identification of TRPM8 inhibitors with a potency that was comparable or higher than the canonical TRPM8 antagonist AMTB [27], in the 11.1–0.22  $\mu$ M range (Table 2). Moreover, two compounds, namely 14 (BB 0322703) and 15 (BB 0322720), together with the lowest  $IC_{50}$  among this set of derivatives (0.25 and 0.22  $\mu$ M respectively), showed 100% of efficacy in TRPM8 blocking.

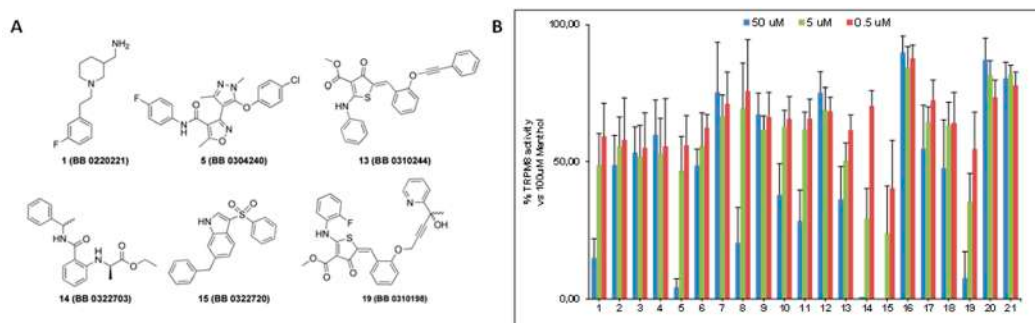


**Figure 1.** (A) Molecular structures of the most active compounds as TRPM8 blockers in Calcium fluorometric assays. In brackets are the original library codes (B) Bar-graph reporting the blocking activity of the 21 compounds arising from the virtual screening protocol against TRPM8 menthol-evoked currents.

**Table 2.** IC<sub>50</sub>s and efficacy for the selected compounds. Results are given as mean ± SD of at least three independent measurements.

Compound	IC <sub>50</sub> (µM)	Efficacy <sup>a</sup>
1 (BB 0220221)	10.21 ± 1.31	85
5 (BB 0304240)	11.10 ± 1.32	95
13 (BB 0310244)	1.01 ± 0.51	90
14 (BB 0322703)	0.25 ± 0.15	100
15 (BB 0322720)	0.22 ± 0.10	100
19 (BB 0310198)	5.52 ± 1.45	90
AMTB	7.15 ± 1.24	100

<sup>a</sup> Expressed as a percentage of inhibition of menthol evoked currents at the maximum concentration used (50 µM).

Results obtained for the prototypical TRPM8 blocker AMTB are in accordance with the literature [27]. Among the selected compounds **1**, **5**, and **19** showed comparable potencies to AMTB. On the other hand, compound **13** showed a 7-fold decrease in potency, maintaining 90% of efficacy. Compounds **14** and **15** were the most promising compounds of the series. They both showed 100% efficacy in blocking the menthol-evoked currents, with IC<sub>50</sub>s about 30-folds lower than the reference compound AMTB, comparable with the calcium fluorometric results obtained for the most potent in vitro TRPM8 inhibitor described so far [25–27].

### 2.3. Molecular Modeling

The VS docking poses of compounds **14** (BB 0322703) and **15** (BB 0322720) (Figure 2) were submitted to molecular dynamics (MD) simulations in explicit solvent and membrane to get insight into the ligand/hTRPM8 interactions.

The two inhibitors dock into the VSLD (voltage-sensor-like domain) assuming similar bound conformations, surrounded by S1–S4 and TRP residues, with both of them lacking interactions with the “roof” of the binding site, that is instead exploited by AMTB and TC-I 2014 (Figure 2).

The compound **14** (BB 0322703) docks into the VSLD, where it stably interacts with residues V742, Y745, I846, Y1005, and F1013. (Figure 3A,B). The terminal phenyl moiety π-π stacks with Y1005, while another tyrosine residue, i.e., 745, interacts with the ligand ester oxygen through a hydrogen bond. Tyrosine 745 interacts, although to a lesser extent, by π-π stacking with the ligand core phenyl ring.

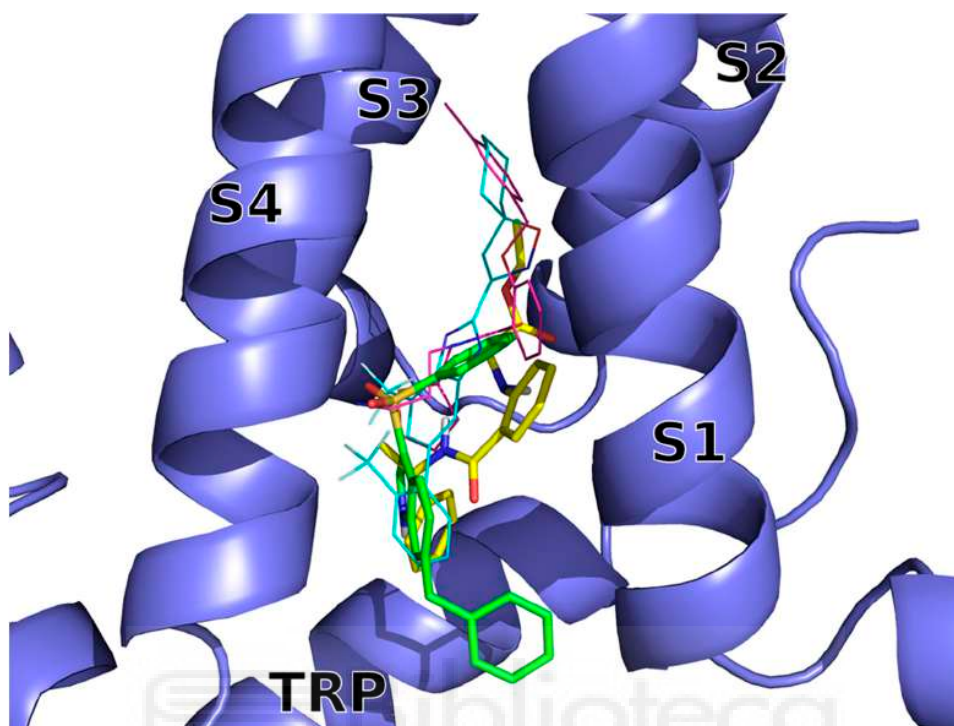


**Figure 2.** Docking-predicted bound conformations of **14** (BB 0322703) and **15** (BB 0322720) into hTRPM8<sub>723–1013</sub>. hTRPM8 is represented in blue cartoons. **14** (BB 0322703) and **15** (BB 0322720) in their hTRPM8-bound conformations are represented in yellow and green thick sticks, respectively. TC-I 2014 (PDB ID: 6O72) and AMTB (PDB ID: 6O6R) experimental bound conformations are shown in cyan and magenta thin sticks, respectively, for reference.

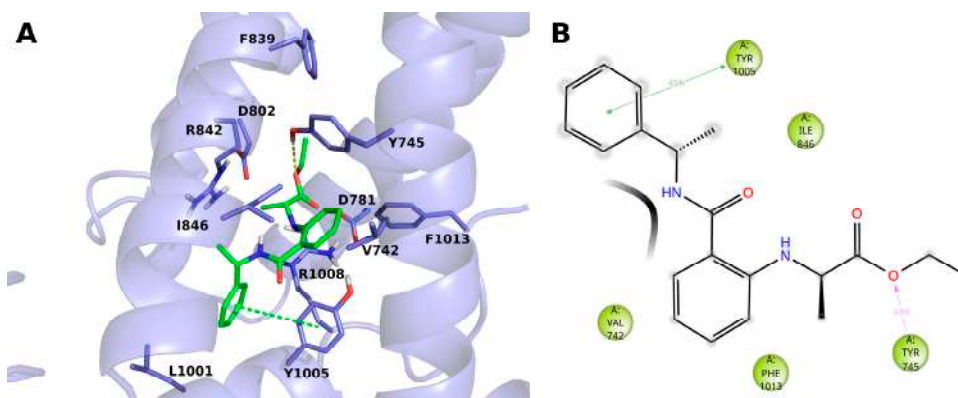


**Figure 3.** (A) Docking-predicted pose of **14** (BB 0322703) into hTRPM8<sub>723–1013</sub>. hTRPM8 is represented in cartoons, and its residues interacting with the ligand are represented in sticks. **14** (BB 0322703) in its hTRPM8-bound conformation is represented in solid green sticks. H-bonds are highlighted by yellow dashed lines,  $\pi$ - $\pi$  interaction by green dashed lines. (B) Ligand interaction diagram of **14** (BB 0322703) in complex with hTRPM8. Only residues interacting with the ligand for at least 40 ns out 120 ns of MD simulation are shown. Hydrophobic residues are colored green. Grey halos highlight solvent exposure. H-bonds are represented by magenta arrows (dashed when side-chain atoms are involved); green solid lines represent  $\pi$ - $\pi$  interactions.

The compound **15** (**BB 0322720**) docks in the lower part of the VSLD, on top of the TRP box, where it stably interacts with several residues. (Figure 4A,B) In particular, the benzyl moiety sticks out of VSLD, in a region surrounded by hydrophobic residues P734, V1002, Y1005, and F735. The latter phenylalanine residue stably makes  $\pi$ - $\pi$  interaction with the aromatic group. The indole ring, surrounded by residues V849, L853, L1001, V1002, E1004, Y1005, F735, and F738, makes an H-bond with the backbone of L1001 by its nitrogen atom, and  $\pi$ - $\pi$  interacts with F738. The benzenesulfonyl moiety is surrounded by residues I846, Y1005, F738, R1008, and R842, and its sulfonyl oxygens make both direct and water-mediated H-bonds with H845 and R842. It is worth noting that, in our model, the phenyl group does not make any specific and stable interaction during the MD simulation time but offers a handle to grow the molecule toward the VSLD roof, where additional interaction with residues such as Y745, L778, L806, F839, D802, Q782, D781 might be established, as in the case of AMTB, TC-I-2014, and many other TRPM8 modulators.

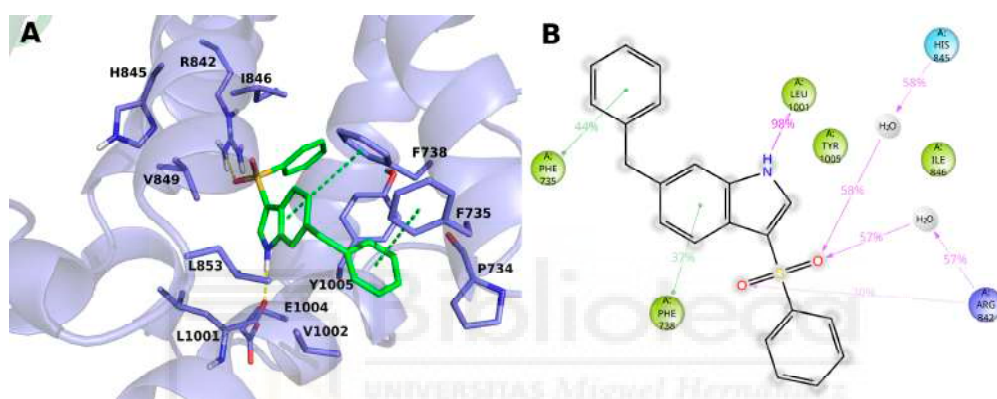


**Figure 4.** (A) Docking-predicted pose of **15** (**BB 0322720**) into hTRPM8<sub>723–1013</sub>. hTRPM8 is represented in cartoons, and its residues interacting with the ligand are represented in sticks. **15** (**BB 0322720**) in its hTRPM8-bound conformation is represented in solid green sticks. H-bonds are highlighted by yellow dashed lines,  $\pi$ - $\pi$  interaction by green dashed lines. (B) Ligand interaction diagram of **15** (**BB 0322720**) in complex with hTRPM8. Only residues interacting with the ligand for at least 40ns out 120ns of MD simulation are shown. Residues are coloured according to the following scheme: cyan—polar; blue—charged (positive); green—hydrophobic; gray—water molecule. Grey halos highlight solvent exposure. H-bonds are represented by magenta arrows (dashed when side-chain atoms are involved); green solid lines represent  $\pi$ - $\pi$  interactions.

#### 2.4. Selectivity Studies

The lack of selectivity of TRPM8 modulators over other members of the TRP channel family is widely reported in literature [25–27]. Cross modulation of TRPV1 by prototypical TRPM8 agonists and antagonists, such as menthol [34] and BCTC [35] is reported and reciprocal modulation of these two channels has been proposed as suitable strategy to attain synergistic pharmacological effects [36–38]. Therefore, we decided to screen the library members showing TRPM8 inhibition over TRPV1 using calcium-fluorometric experiments. None of the compounds proved modulatory ability over TRPV1 either as activators or inhibitors (data not shown), with the exceptions of compounds **13** (**BB 0310244**) and **19** (**BB 0310198**) showing low micromolar potencies as TRPV1 agonists, with  $1.34 < EC_{50s} < 1.68 \mu\text{M}$  (Figure 5).

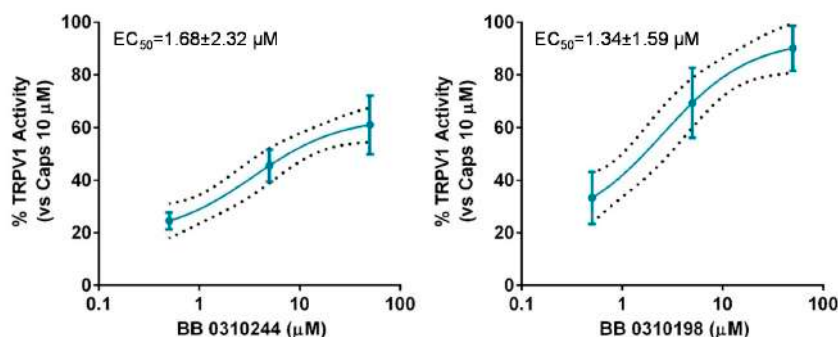


**Figure 5.** Dose-response curve for **13** (BB 0310244) (left panel) and **19** (BB 0310198) (right panel) for TRPV1 activation. Response is expressed as percentage of TRPV1 activation normalized to the effect of the prototypical agonist capsaicine at 10  $\mu\text{M}$ , considered as 100% of activation. The discontinuous line shows the 95% confidence intervals. The solid line represents fits of the experimental data to the following equation:  $Y = \text{Bottom} + (\text{Top} - \text{Bottom}) / (1 + 10^{((\text{LogEC}_{50} - X) \times \text{HillSlope}))}$ , with the restriction of the minimum (Bottom = 0).  $\text{EC}_{50} = 1.69$  (0.26–10.73)  $\mu\text{M}$  with  $r^2 = 0.82$  and Hill Slope = 0.53 for **13** (BB 0310244) and  $\text{EC}_{50} = 1.34$  (0.49–3.62)  $\mu\text{M}$  with  $r^2 = 0.85$  and Hill Slope = 0.67 for **19** (BB 0310198).

### 2.5. Patch-Clamp Electrophysiology Assays

Considering the potency, efficacy, and selectivity shown, further investigation about TRPM8 antagonistic activity of compounds **14** and **15** (BB 0322703 and BB 0322720) were performed by patch-clamp protocols. This study confirmed the efficacy of the two compounds, administered at 10  $\mu\text{M}$ , in abolishing the TRPM8 menthol-evoked currents, reducing the current density at a lower level than the vehicle (Figure 6A). Dose-response curves were then recorded to evaluate the compound relative potencies. As shown in Figure 6B,C, both compounds showed low micromolar inhibitory potencies, with compound **14** (BB 0322703) slightly more potent. For this reason, the compound was selected for the following in vivo studies.

### 2.6. In Vivo Assays

TRPM8 antagonism is deeply related to analgesic in vivo effects and has been proposed as a suitable pharmacological strategy for the treatment of chronic pain, migraine, and painful syndromes [39–41]. TRPM8 antagonists are particularly known to counteract the chemotherapy-induced neuropathic pain evoked by oxaliplatin [24,27–29]. For these reasons we challenged compound **14** (BB 0322703) in vivo using the oxaliplatin-induced cold hypersensitivity assay. As shown in Figure 7, repeated oxaliplatin administration induced, as expected, cold hypersensitivity in the acetone drop test, reflected in longer duration of the response to acetone application to the hind paw ( $p < 0.05$  vs. Baseline). Interestingly, mice receiving an intraplantar dose of 30  $\mu\text{g}$  **14** (BB 0322703) showed significant inhibition of this cold hypersensitivity for at least 1 h ( $p < 0.05$  vs. Oxaliplatin), whereas mice receiving 10  $\mu\text{g}$  **14** (BB 0322703) or vehicle did not show significant modification of their nociceptive sensitivity at these time points. These results are in good accordance with previous reports concerning the use of TRPM8 antagonists as anti-allodynic agents in the oxaliplatin-induced allodynia model [28,29]. In particular, a correspondence between the in vitro potency and the effective in vivo dose is typical for TRPM8 modulators in the oxaliplatin-induced neuropathic pain model. Extremely in-vitro potent compounds are effective also at lower doses (10 mg) [28]. When in vitro potency is reduced [29], as also in the present case, in vivo efficacy decreases correspondingly. It is also worthy of note that non metabolically stable TRPM8 antagonists exhibit a short-acting effect (30 min, [28]) while metabolically stable analogs prolong the antiallodynic effect up to 1 h [29]. This is also the case of compound **14**, which for these reasons could be considered a promis-

ing hit-compound for the development of new chemotypes as TRPM8 antagonists and a pharmacological tool for the treatment of neuropathic pain.

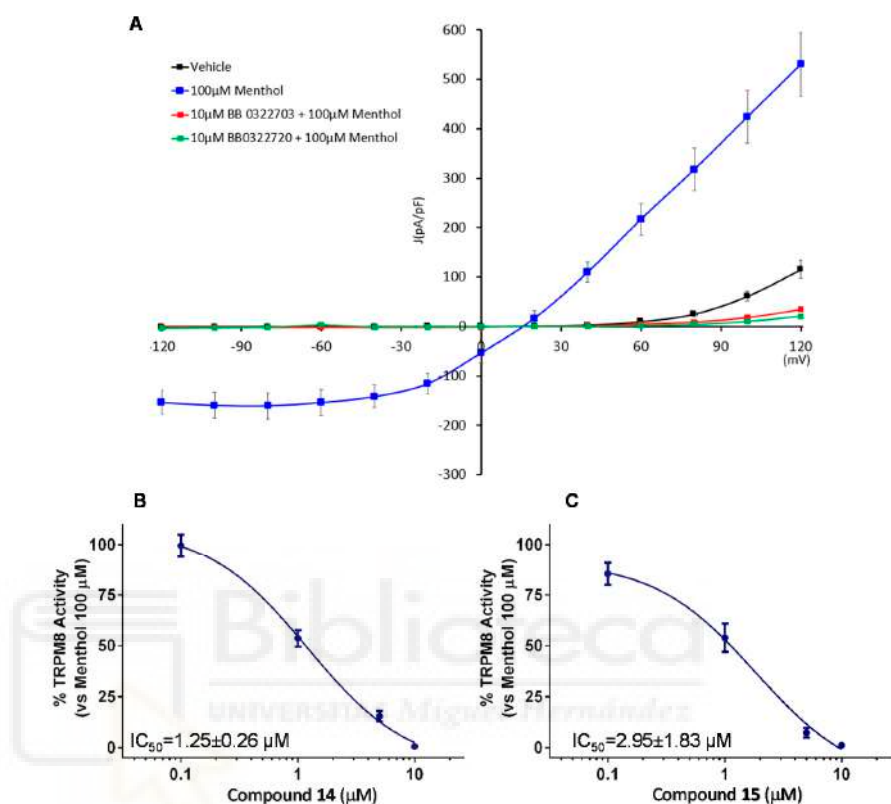


**Figure 6.** Compounds 14 and 15 (BB 0322703 and BB 0322720, respectively) blocks TRPM8-mediated responses evoked by menthol in rTRPM8-expressing HEK293 cells (A) Curves obtained after: exposure to vehicle solution (black trace) 100  $\mu$ M menthol (blue trace), 100  $\mu$ M menthol + 10  $\mu$ M 14 (BB 0322703) (red trace), and 100  $\mu$ M menthol + 10  $\mu$ M 15 (BB 0322720) (green trace). Peak current data were expressed as pA/pF (to allow comparison among different size cells). Each point is the mean  $\pm$  SEM of  $n = 15$ . (B) Dose-response curve for the inhibitory effect over the currents evoked by 100  $\mu$ M menthol in HEK293 cells expressing TRPM8 by compound 15 (BB 0322720). (C) Dose-response curve for the inhibitory effect over the currents evoked by 100  $\mu$ M menthol in HEK293 cells expressing TRPM8 by compound 14 (BB 0322703). The solid line represents fits of the experimental data to the following equation:  $Y = Bottom + (Top - Bottom) / (1 + 10^{((LogEC50-X) \times HillSlope)})$ , with the restriction of the minimum (Top = 100)  $IC_{50} = 1.25$  (1.00–1.56)  $\mu$ M with  $r^2 = 0.99$  and Hill slope =  $-1.23$  for 14 (BB 0322703) and  $IC_{50} = 2.95$  (0.82–10.61)  $\mu$ M with  $r^2 = 0.97$  and Hill slope =  $-0.71$  for 15 (BB 0322720) Each point is the mean  $\pm$  SEM of  $n = 15$ .

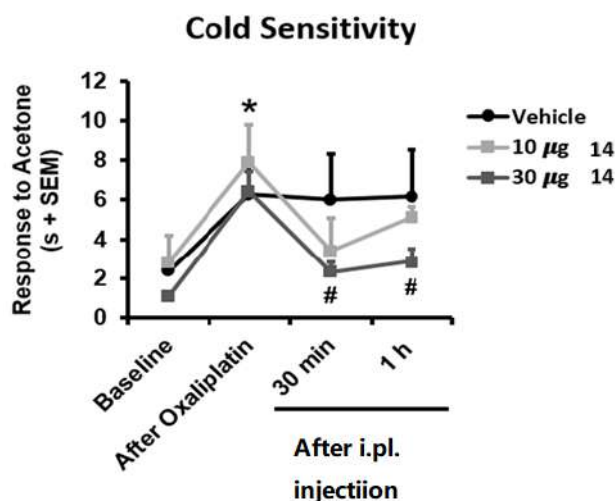


**Figure 7.** Reduced oxaliplatin (OXP)-induced cold allodynia by TRPM8 blocker **14** (BB 0322703). Mice were treated with three i.p. injections of OXP (6 mg/kg) or the vehicle (VH) on alternate days and on day 7 the cold allodynia behaviour was evaluated by the acetone test, before (baseline) and after OXP treatment. Time course effect of the TRPM8 blocker at 10 or 30 µg. Data are given as mean ± SEM ( $n = 6$ ), one-way ANOVA with Tukey post hoc test. \*  $p < 0.05$  OXA vs. baseline. #  $p < 0.05$  OXP vs. 30 µg **14** (BB 0322703).

### 3. Discussion

The stepwise application of virtual and experimental screening to the selected molecular library allowed the identification of different compounds characterized by efficacy and potency in TRPM8 inhibition, confirming the robustness and the yield of this approach. In particular, two of these compounds showed low micromolar potencies when challenged in patch-clamp measurements, with compound **14** (BB 0322703) also exhibiting *in vivo* efficacy in a model of oxaliplatin-induced cold allodynia. It should be considered that this compound has been administered as a diastereoisomeric mixture of (R)-ethyl 2-((2-(((S)-1-phenylethyl)carbamoyl)phenyl)amino)propanoate and (R)-ethyl 2-((2-(((R)-1-phenylethyl)carbamoyl)phenyl)amino)propanoate. Molecular modelling studies suggest that the configuration S at the phenylethyl moiety represents the eutomer, since the other enantiomer was not retrieved among the top scoring compounds. This prompts for further investigation about this chemotype, biological characterization of both the enantiomers would indeed help the discovery of more potent and promising derivatives.

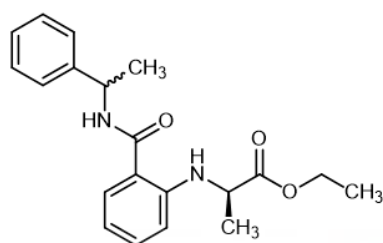
On the other hand, **15** (BB 0322720), with its sulphonamide moiety, represents another interesting chemotype to be further investigated for hit-to-lead development of a new potent TRPM8 antagonist in consideration of its biological profile, chemical versatility, and metabolic stability. Moreover, selectivity studies of the reported compounds led to the identification of two dual-acting compounds, able to inhibit TRPM8 while activating TRPV1. Further studies involving these chemotypes would help in improving the knowledge about the structural discriminants for selectivity among these two channel subtypes. Additionally, considering the recent evidence about the analgesic and anticancer activity of both TRPV1 and TRPM8 modulators, it would be interesting to further explore the potential pharmacological activity of the dual-acting compounds **13** and **19** (BB 0310244 and BB 0310198, respectively), in the search for more potent and effective pain-reliever and anticancer drug candidates. Nevertheless, further experiments have to be addressed in order to determine more accurate  $EC_{50}$  values for these two compounds.

## 4. Materials and Methods

### 4.1. Chemistry

NMR spectra were acquired on Bruker Avance 400 spectrometer (Bruker corporation, Billerica, MA, USA) at room temperature; the chemical shifts  $\delta$  were measured in ppm with respect to solvent ( $^1\text{H}$ :  $\text{CDCl}_3$ ,  $\delta = 7.28$  ppm;  $\text{DMSO}-d_6$ :  $\delta = 2.50$  ppm;  $^{13}\text{C}$ :  $\text{CDCl}_3$ ,  $\delta = 77.2$  ppm;  $\text{DMSO}-d_6$ :  $\delta = 39.5$  ppm). Splitting patterns are designated as s, singlet; d, doublet; t, triplet; q, quadruplet; quint, quintet; m, multiplet; dd, double doublet, br., broad. Coupling constants ( $J$ ) are given in Hertz. The structures of synthesized compounds were elucidated with the aid of  $^1\text{H}$ ,  $^{13}\text{C}$  spectroscopy. Low-resolution mass spectra were on Finnigan MAT mass spectrometer using electron ionization (direct inlet) and an ITD-700 detector with the ionizing electron energy being 70 eV and the mass range being  $m/z$  35–400. The melting points (m.p.) were measured in open capillaries and presented without correction.

#### Ethyl (R)-N-[2-[(1-Phenylethyl)amino]carbonyl]phenyl]-2-aminopropionic acid (14)



**14** (BB 0322703)

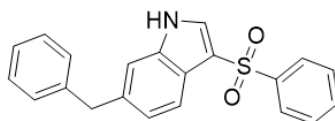
A mixture of *a*-methylbenzylamine (2.25 g, 2.1 mmol) in DMF (4 mL) and (R)-Ethyl-2-(2,4-dioxo-2H-3,1-benzoxazin-1(4H)-yl)propanoate [42] (3.26 g, 2.0 mmol) in DMF (10 mL) was stirred at 45–50 °C for 3 h. The reaction mixture was cooled to rt, diluted with cold water (100 mL), and then basified with 50% KOH to pH of 9. The resulting mixture was extracted with  $\text{CH}_2\text{Cl}_2$ , washed with water until the pH was ~7, and dried over anhydrous  $\text{Na}_2\text{SO}_4$ . The solvent was evaporated under reduced pressure. The crude product was purified by column chromatography on silica gel (eluent: ethyl acetate/petroleum ether = 1/10) to afford 14 (80%) as a yellowish oil (mixture of diastereomers  $D_{\#1}:D_{\#2} = 1:1$ ).

$^1\text{H}$  NMR (400 MHz,  $\text{CDCl}_3$ , 25 °C),  $\delta$ : 7.88–7.84 (m, 1H, NH), 7.41–7.34 (m, 5H,  $5 \times \text{CH}_{\text{Ar}}$ ), 7.30–7.23 (m, 2H,  $2 \times \text{CH}_{\text{Ar}}$ ), 6.64–6.60 (m, 2H,  $2 \times \text{CH}_{\text{Ar}}$ ), 6.58–6.55 (m, 1H,  $\text{CH}_{\text{Ar}}$ ), 6.33–6.30 (m, 1H, NH), 5.33–5.25 (m, 1H,  $\text{CHCH}_3$ ), 4.29–4.08 (m, 4H,  $\text{PhCHCH}_3$ ,  $\text{CH}_2\text{CH}_3$ ), 1.60 (d,  $J = 6.9$ , 3H,  $\text{CHCH}_3$ ), 1.52 (dd,  $J_1 = 7.0$  Hz,  $J_2 = 2.1$  Hz, 3H,  $\text{PhCHCH}_3$ ), 1.25, 1.22 (both t,  $J_{D\#1} = 7.1$ ,  $J_{D\#2} = 7.1$ , sum 3H,  $\text{CH}_2\text{CH}_3$ ) ppm.

rt (D#1) = 1.376 min. LC-MS:  $m/z$   $[\text{M} + \text{H}]^+ = 341$  Da.

rt (D#2) = 1.390 min. LC-MS:  $m/z$   $[\text{M} + \text{H}]^+ = 341$  Da.

#### 3-(Benzenesulfonyl)-6-benzyl-1H-indole (15)



**15** (BB 0322720)

To a suspension of 540 mg (22.5 mmol) of sodium hydride in anhydrous dimethylformamide (40 mL), portions of 1.76 g (15.0 mmol) of 6-benzyl-1H-indole [43] were added, and the mixture was stirred at a temperature until the evolution of hydrogen completely ceases. Then diphenyl disulfide 3.6 g (16.5 mmol) was added portion wise and a mixture was stirred at room temperature for 18 h. The mixture is diluted with water (300 mL) and extracted with ether ( $3 \times 45$  mL). The extracts were combined and washed several times

with water and dried over anhydrous  $\text{Na}_2\text{SO}_4$ . The solvent was evaporated. The crude was recrystallized from a mixture of toluene-hexane. Yield of 6-benzyl-3-(phenylthio)-1H-indole 2.95 g (95%).

6-Benzyl-3-(phenylthio)-1H-indole 2.90 g (9.2 mmol, 1 equiv) was dissolved in  $\text{CH}_2\text{Cl}_2$  (250 mL) and to this solution m-chloroperbenzoic acid 5.55 g (32.2 mmol, 3.5 equiv) was added portion wise. The mixture was stirred at room temperature for 18 h. The reaction mixture was then poured into water (350 mL) and extracted with  $\text{CH}_2\text{Cl}_2$  ( $3 \times 50$  mL). The extracts were combined and washed with water, an aqueous solution of sodium metabisulfate, sodium bicarbonate, and dried over  $\text{Na}_2\text{SO}_4$ . The crude was recrystallized from  $\text{CH}_2\text{Cl}_2$ . Yield 2.50 g (78%). M.p. 247–248 °C.

$^1\text{H}$  NMR (400 MHz,  $\text{CDCl}_3$ ),  $\delta$ : 12.29 (1H, c, NH), 8.00 (s, 1H), 7.57 (d,  $J = 8.1$  Hz, 1H), 7.32–7.26 (m, 6H), 7.25–7.18 (m, 4H), 7.15 (dd,  $J = 8.4, 6.0$  Hz, 1H), 6.55–6.47 (m, 1H), 4.11 (s, 2H) ppm.

rt = 1.420 min. Purity = 100%. LC-MS:  $m/z$   $[\text{M} + \text{H}]^+ = 348$  Da.

## 4.2. In Vitro Biological Assays

### 4.2.1. Cell Cultures

Cells, HEK-293 cells stably expressing rTRPM8 or hTRPV1, were cultured in a monolayer in Earle's minimum essential medium with Earle's salts supplemented with 10% fetal calf serum, 1% nonessential amino acids, 2 mM L-glutamine, 100  $\mu\text{g}$  streptomycin/mL, 100 U penicillin/mL, and 0.4  $\mu\text{g}$ /mL puromycin (referred to as Puro-EMEM) and kept at 37 °C in a humidified atmosphere of 5%  $\text{CO}_2$  in a suitable incubator (STERI-CyCLE  $\text{CO}_2$  Incubator Hepa Class 100, Thermo Electrón Corporation, Waltham, MA, USA). Cells were stored under liquid nitrogen and used for 15 generations from unfreezing.

For fluorometric experiments, HEK-293 cells stably expressing rTRPM8 or hTRPV1 were detached by means of Trypsin/EDTA solution, resuspended in DMEM-10%FCS and seeded at a concentration of  $2 \times 10^4$  cells/mL.

### 4.2.2. Fluorometric Assays

To measure the effectiveness of the compounds against TRPM8 activity we have used microfluorometry-based calcium flux assays with Fluo-4 NW  $\text{Ca}^{2+}$  dye and fluorescence as described previously [44]. Briefly human embryonic kidney cell line (HEK) stably transfected with rTRPM8 or hTRPV1 were seeded in 96-well plates at a cell density of 30,000 cells. After 2 days the medium was replaced with 100  $\mu\text{L}$  of the dye loading solution Fluo-4 NW supplemented with probenecid 2.5 mM and incubated 1 h at 37 °C. The TRP ion channel activity was measured using POLASTAR plate reader (BMG Labtech, Ortenberg, Germany) setting the excitation wavelength at 485 nm and emission wavelength at 520 nm. The baseline fluorescence was recorded for 3 cycles before the addition of the vehicle, compound at different concentrations, and the antagonist, 10  $\mu\text{M}$  AMTB for TRPM8 and Ruthenium red for TRPV1. Fluorescence intensity was recorded during 7 more cycles and agonist 100  $\mu\text{M}$  menthol for TRPM8 or 10  $\mu\text{M}$  capsaicin for TRPV1 was added. Fluorescence intensity was recorded during 10 more cycles.

Data analysis: The Z-factor was calculated in each assay using the following equation:  $(3 \times (\text{SD}_{\text{max}} + \text{SD}_{\text{min}})) / (\text{Mean}_{\text{max}} - \text{Mean}_{\text{min}})$ . In all the experiments, the Z-factor was  $\geq 0.5$ . The effect of the compounds against TRPM8 activity was determined by normalizing their effect to the maximum fluorescence observed with the application of 100  $\mu\text{M}$  menthol. A decrease in menthol signal was expressed as a percentage of inhibition (%). All data are expressed as the mean  $\pm$  standard deviation (SD). Data are expressed as the concentration exerting a half-maximal inhibition of agonist-induced ( $\text{Ca}^{2+}$ )<sup>i</sup> elevation ( $\text{IC}_{50}$ ), which was calculated again using GraphPad Prism<sup>®</sup> software (GraphPad Prism 5, Graphpad Software, San Diego, CA, USA). The equation used was  $Y = \text{Bottom} + (\text{Top} - \text{Bottom}) / (1 + 10^{(\text{LogEC}_{50-X}) \times \text{HillSlope}})$ , with the restriction of the minimum (Bottom = 0). All determinations were performed in triplicate ( $n = 3$ ) in 3 independent experiments ( $n = 3$ ).

#### 4.2.3. Patch-Clamp Experiments

Whole-cell patch-clamp recordings from HEK-rTRPM8 cells were carried out 2 days after seeding on 12-mm Ø glass coverslips treated with poly-L-lysine solution (Sigma Aldrich, Madrid, Spain) [30]; the intracellular pipette solution contained (in mM) 150 NaCl, 5 EGTA, 3 MgCl<sub>2</sub>, and 10 HEPES, adjusted to pH 7.2 with NaOH, and the extracellular solution contained (in mM) 150 NaCl, 6 CsCl, 1.5 CaCl<sub>2</sub>, 1 MgCl<sub>2</sub>, 10 D-glucose and 10 HEPES, adjusted to pH 7.4 with NaOH. The TRPM8 activity was measured by the application of two pulses of 100 µM menthol in a time interval of 2 min and 30-s perfusion of the different compound concentrations before the second menthol pulse.

Menthol (100 µM) or compounds (0.1–10 µM; 2 min perfusion) were applied directly onto the cell under investigation by means of a multibarrel concentration-clamp device coupled to an electronically driven miniature solenoid valves under the control of PatchMaster software (HEKA Electronics, Lambrecht, Germany).

Data were sampled at 10 kHz (EPC10 amplifier with PatchMaster 2.53 software, HEKA Electronics, Lambrecht, Germany) and low-pass filtered at 3 kHz for analysis (PatchMaster 2.53 and GraphPad Prism 5). The series resistance was <10 MΩ and to minimize voltage errors was compensated to 60–80%. All measurements were performed at 24–25 °C. Cell capacitance was measured and used to estimate the current density (J, pA/pF).

For the whole-cell patch-clamp experiments, results are expressed as the percentage of the remaining activation of the TRPM8 channel. This is calculated by normalizing the ratio (p<sub>2</sub>/p<sub>1</sub>) of testing conditions to the ratio (p<sub>2</sub>/p<sub>1</sub>) of the control condition. The analysis of the data was performed by GraphPad 6.0, the ordinary one-way ANOVA analysis followed by the post hoc Bonferroni test established multiple comparisons, and the ROUT method (Q = 10%) identified data outliers. A non-linear regression curve and IC<sub>50</sub> were obtained by the representation of log (inhibitor) vs. response. The equation used was  $Y = \text{Bottom} + (\text{Top} - \text{Bottom}) / (1 + 10^{(\text{LogEC}_{50-X}) \times \text{HillSlope}})$ , with the restriction of the maximum (Top = 100). Paired or unpaired Student's *t*-tests were also used for data comparison between two groups. All data are expressed as the mean ± standard error of the mean (SEM) (*n* = 12–15).

#### 4.3. In Vivo Studies

##### 4.3.1. Animals

C57BL/6J RccHSd female mice (10–15 week-old, ~20 g) (Harlan, The Netherlands) were used for the oxaliplatin-induced neuropathic pain study. Care was taken to minimize the number of animals used and the pain and stress they experienced. All experimental procedures were approved by the Animal Care and Use Committees of Universidad Miguel Hernández and the regional government and were conducted according to the ethical principles of the International Association for the Study of Pain (IASP) for the evaluation of pain in conscious animals [45], the European Parliament and the Council Directive (2010/63/EU) and the Spanish law (RD 53/2013). Housing conditions were maintained at 21 ± 1 °C and 55 ± 15% relative humidity in a controlled light/dark cycle (light on between 8:00 a.m. and 8:00 p.m.). Animals had free access to food and water except during the habituation or the evaluation of nociceptive sensitivity. All parts of the study concerning animal care were performed under veterinary control.

##### 4.3.2. Drugs

Compound **14** (**BB 0322703**) was dissolved in 2.5% dimethyl sulfoxide (Merck, Darmstadt, Germany) and 2.5% cremophor EL (Merck) diluted in saline. Compound **14** (**BB 0322703**) was prepared at 1.2 or 0.4 mg/mL and intraplantar injected in a 25 µL volume. Oxaliplatin was obtained from Tocris (ref#2623, Tocris, Bristol, UK).

##### 4.3.3. Oxaliplatin-Induced Neuropathic Pain

Oxaliplatin-induced neuropathic pain was induced by repeated oxaliplatin administration (Cat. No. 2623, Tocris, Bristol, UK). Oxaliplatin was freshly prepared every day of

administration. It was dissolved in water with 5% dextrose after gentle warming, and it was intraperitoneally injected every other day for 5 days at a 6 mg/kg dose. Nociceptive sensitivity was assessed before oxaliplatin treatment and 3 days after the last oxaliplatin administration.

#### 4.3.4. Cold Sensitivity

Cold chemical thermal sensitivity was assessed using the acetone drop method as previously described. Briefly, mice were first handled and habituated to the experimenter before the experiments. To measure acetone sensitivity, mice were placed over a metal grid and allowed to habituate for approximately 1 h. Freshly dispensed acetone drops (20  $\mu$ L) were applied gently onto the mid-plantar surface of the right hind paw. Paw licking, attending, dragging, or lifting were considered nociceptive-like responses. The responses were measured for 1 min with a digital stopwatch. For each measurement, the paw was sampled three times and the mean was calculated. The interval between each application of acetone was at least 3 min.

#### 4.3.5. Statistical Analysis

Behavioral data were analyzed with a repeated-measures ANOVA followed by a post-hoc Tukey test (GraphPad Prism 7.04, GraphPad Software Inc.). *p*-values lower than 0.05 were considered statistically significant.

### 4.4. In Silico-Studies

#### 4.4.1. Models Building

The hTRPM8 protein sequence Q7Z2W7 was downloaded from the Universal Protein Resource (UniProt) [46] and template Cryo-EM structures of TRPM8 cold receptor in complex with AMTB (PDB ID: 6O6R) and TC-I 2014 (PDB ID: 6O72) were downloaded from the Protein Data Bank [2]. The region of our interest that comprised domains S1 to TRP (residues 723–1013) was aligned using ClustalW [47] to *Parus major* TRPM8 and modelled by homology with the two experimentally solved template structures. It is worth noting that *Parus major* and *human* TRPM8 share a high degree of similarity (Identity: 82%; Similarity: 92%; Conservation: 91%), analogously to *Ficedula albicollis* [25], *Mus musculus* and *Rattus norvegicus* [26].

The energy-based method of Prime [48,49] was used to build two models of hTRPM8<sub>723–1013</sub> tetramer: in complex with AMTB (A\_hTRPM8<sub>723–1013</sub>—template 6O6R) and in complex with TC-I 2014 (T\_hTRPM8<sub>723–1013</sub>—template 6O72). Rotamers of conserved residues were retained and all side chains were optimized. The two models and the library to screen were then prepared, as previously reported [50], for the subsequent studies, using the Schrödinger Protein Preparation Wizard [51] and the ligprep utility [52]. Docking calculations were carried on by means of Glide [53–55] using a target ensemble composed of the two previously prepared protein structures, i.e., AMTB/hTRPM8<sub>723–1013</sub> and TC-I/hTRPM8<sub>723–1013</sub>.

The docking space was defined as a (35 Å)<sup>3</sup> cube centered on the bound pose of AMTB for A\_hTRPM8<sub>723–1013</sub> and of TC-I 2014 for T\_hTRPM8<sub>723–1013</sub>; the ligands diameter midpoints were required to dock into a smaller, nested (20 Å)<sup>3</sup> cube. No constraint was applied during docking calculations, nonpolar ligand atoms (partial charge < 0.25) were scaled by a 0.80 factor, and protein hydroxyl and thiol groups were allowed to rotate. Molecular docking simulations were performed in a stepwise manner using Glide SP and Glide XP. The library to screen (2543 compounds; 4721 after ligand preparation) was submitted to Glide SP docking and all docking poses scoring worse than −4 were ruled out, while those scoring better than −4 were advanced to the subsequent step where their docking poses were refined, minimized and re-scored using Glide XP. For each ligand, the best scoring pose only was finally retrieved, regardless of the target it was retrieved by, as in previously reported studies [56,57].

#### 4.4.2. Molecular Dynamics Simulations of 14 (BB 0322703) and 15 (BB 0322720) in Complex with hTRPM8<sub>723–1013</sub>

Predicted bound conformations of 14 (BB 0322703) and 15 (BB 0322720) in complex with T\_hTRPM8<sub>723–1013</sub> were submitted to molecular dynamics MD simulations in order to investigate the most important inhibitor/ligand interactions. The simulations were set up and run using Desmond [58]. The simulated environments were inserted into a POPC bilayer, based on the coordinates (ID: 6O72) downloaded from the OPM database [59].

OPLS-2005 [60] was used as a force field and solvation was treated explicitly by the TIP3P water model [61]. The system was neutralized by Na<sup>+</sup> and Cl<sup>−</sup> ions that were added to the final concentration of 0.15 M. Protein/membrane systems were submitted to the standard equilibration protocol for membrane proteins distributed with Desmond. Systems were finally submitted to 120 ns long MD simulations at a temperature of 300 K in the isothermal–isobaric ensemble using a Nose–Hoover chain thermostat and a Martyna–Tobias–Klein barostat. Backbone atoms were constrained during the simulation (1 kcal/mol). Trajectory analyses were performed using the Desmond simulation event analysis and the simulation interaction diagram tools.

**Supplementary Materials:** The following supporting information can be downloaded at: <https://www.mdpi.com/article/10.3390/ijms23042070/s1>.

**Author Contributions:** Conceptualization, A.B., A.V.K., A.A., C.O., N.I.; data curation, I.G.-M., P.C., A.F.-C.; formal analysis, I.G.-M., P.C., A.F.-C.; investigation, N.I., A.M.-P., T.C., A.M.N., D.C.; methodology, C.O., N.I., A.B., A.A., A.V.K.; supervision, A.B., A.V.K., P.C., I.G.-M., A.F.-C.; validation, I.G.-M., A.B., A.V.K.; writing—original draft, C.O., N.I., A.A., A.M.-P.; writing—review and editing, A.B., A.V.K., A.F.-C. All authors have read and agreed to the published version of the manuscript.

**Funding:** This research was funded by a grant from Regione Campania–PON Campania FESR 2014–2020 “Combattere la resistenza tumorale: piattaforma integrate multidisciplinare per un approccio tecnologico innovativo alle oncoterapie–Campania Oncoterapie (Project N. B61G18000470007) to researchers from Universities of Naples and Salerno and by a grant from the Spanish Ministry of Science, Innovation and Universities RTI2018-097189-B-C21 to A.F.-C.

**Institutional Review Board Statement:** All experimental procedures were approved by the Animal Care and Use Committees of Universidad Miguel Hernández (Authorization number 2021/VSC/PEA/0089) and the Regional Government, and were conducted according to the ethical principles of the International Association for the Study of Pain (IASP) for the evaluation of pain in conscious animals, the European Parliament and the Council Directive (2010/63/EU) and the Spanish law (RD 53/2013).

**Informed Consent Statement:** Not applicable.

**Data Availability Statement:** The data presented in this study are available in the supplementary information file. Any other raw data can be requested to the corresponding authors.

**Acknowledgments:** The authors gratefully acknowledge the support of NVIDIA Corporation with the donation of the Tesla K40 GPU used for this research.

**Conflicts of Interest:** The authors declare no conflict of interest.

## References

1. Izquierdo, C.; Martín-Martínez, M.; Gómez-Monterrey, I.; González-Muñiz, R. TRPM8 Channels: Advances in Structural Studies and Pharmacological Modulation. *Int. J. Mol. Sci.* **2021**, *22*, 8502. [CrossRef] [PubMed]
2. Diver, M.M.; Cheng, Y.; Julius, D. Structural insights into TRPM8 inhibition and desensitization. *Science* **2019**, *365*, 1434–1440. [CrossRef] [PubMed]
3. Nilius, B.; Owsianik, G. The transient receptor potential family of ion channels. *Genome Biol.* **2011**, *12*, 218. [CrossRef]
4. Brauchi, S.; Orio, P.; Latorre, R. Clues to understanding cold sensation: Thermodynamics and electrophysiological analysis of the cold receptor TRPM8. *Proc. Natl. Acad. Sci. USA* **2004**, *101*, 15494–15499. [CrossRef] [PubMed]
5. Voets, T.; Droogmans, G.; Wissenbach, U.; Janssens, A.; Flockerzi, V.; Nilius, B. The principle of temperature-dependent gating in cold- and heat-sensitive TRP channels. *Nature* **2004**, *430*, 748–754. [CrossRef]
6. Su, L.; Wang, C.; Yu, Y.-H.; Ren, Y.-Y.; Xie, K.-L.; Wang, G.-L. Role of TRPM8 in dorsal root ganglion in nerve injury-induced chronic pain. *BMC Neurosci.* **2011**, *12*, 120. [CrossRef]

7. Alarcón-Alarcón, D.; Cabañero, D.; de Andrés-López, J.; Fernández-Ballester, G.; Fernández-Carvajal, A.; Ferrer-Montiel, A. Androgenic TRPM8 activity drives sexual dimorphism in a murine model of chronic migraine. *Res. Sq.* **2021**. [CrossRef]
8. Proudfoot, C.J.; Garry, E.M.; Cottrell, D.F.; Rosie, R.; Anderson, H.; Robertson, D.C.; Fleetwood-Walker, S.M.; Mitchell, R. Analgesia mediated by the TRPM8 cold receptor in chronic neuropathic pain. *Curr. Biol.* **2006**, *16*, 1591–1605. [CrossRef]
9. Andersson, K.-E.; Gratzke, C.; Hedlund, P. The role of the transient receptor potential (TRP) superfamily of cation-selective channels in the management of the overactive bladder. *BJU Int.* **2010**, *106*, 1114–1127. [CrossRef]
10. Grolez, G.P.; Gkika, D. TRPM8 Puts the Chill on Prostate Cancer. *Pharmaceuticals* **2016**, *9*, 44. [CrossRef]
11. Guo, H.; Carlson, J.A.; Slominski, A. Role of TRPM in melanocytes and melanoma. *Exp. Dermatol.* **2012**, *21*, 650–654. [CrossRef] [PubMed]
12. Liu, J.; Chen, Y.; Shuai, S.; Ding, D.; Li, R.; Luo, R. TRPM8 promotes aggressiveness of breast cancer cells by regulating EMT via activating AKT/GSK-3 $\beta$  pathway. *Tumor Biol.* **2014**, *35*, 8969–8977. [CrossRef] [PubMed]
13. Yee, N.S.; Brown, R.D.; Lee, M.S.; Zhou, W.; Jensen, C.; Gerke, H.; Yee, R.K. TRPM8 ion channel is aberrantly expressed and required for preventing replicative senescence in pancreatic adenocarcinoma. *Cancer Biol. Ther.* **2014**, *13*, 592–599. [CrossRef] [PubMed]
14. Liu, Z.; Wu, H.; Wei, Z.; Wang, X.; Shen, P.; Wang, S.; Wang, A.; Chen, W.; Lu, Y. TRPM8: A potential target for cancer treatment. *J. Cancer Res. Clin. Oncol.* **2016**, *142*, 1871–1881. [CrossRef] [PubMed]
15. Peabody, N.C.; Pohl, J.B.; Diao, F.; Vreede, A.P.; Sandstrom, D.J.; Wang, H.; Zelensky, P.K.; White, B.H. Characterization of the Decision Network for Wing Expansion in *Drosophila* Using Targeted Expression of the TRPM8 Channel. *J. Neurosci.* **2009**, *29*, 3343–3353. [CrossRef]
16. Pertusa, M.; Rivera, B.; González, A.; Ugarte, G.; Madrid, R. Critical role of the pore domain in the cold response of TRPM8 channels identified by ortholog functional comparison. *J. Biol. Chem.* **2018**, *293*, 12454–12471. [CrossRef]
17. Yang, S.; Lu, X.; Wang, Y.; Xu, L.; Chen, X.; Yang, F.; Lai, R. A paradigm of thermal adaptation in penguins and elephants by tuning cold activation in TRPM8. *Proc. Natl. Acad. Sci. USA* **2020**, *117*, 8633–8638. [CrossRef]
18. Press Release: The Nobel Prize in Physiology or Medicine 2021. Available online: <https://www.nobelprize.org/prizes/medicine/2021/summary/> (accessed on 30 December 2021).
19. Xu, L.; Han, Y.; Chen, X.; Aierken, A.; Wen, H.; Zheng, W.; Wang, H.; Lu, X.; Zhao, Z.; Ma, C.; et al. Molecular mechanisms underlying menthol binding and activation of TRPM8 ion channel. *Nat. Commun.* **2020**, *11*, 3790. [CrossRef]
20. Andersson, D.A.; Chase, H.W.N.; Bevan, S.J. TRPM8 Activation by Menthol, Icilin, and Cold Is Differentially Modulated by Intracellular pH. *J. Neurosci.* **2004**, *24*, 5364–5369. [CrossRef]
21. Weil, A.; Moore, S.E.; Waite, N.J.; Randall, A.; Gunthorpe, M.J. Conservation of Functional and Pharmacological Properties in the Distantly Related Temperature Sensors TRPV1 and TRPM8. *Mol. Pharmacol.* **2005**, *68*, 518–527. [CrossRef]
22. Meseguer, V.; Karashima, Y.; Talavera, K.; D’Hoedt, D.; Donovan-Rodríguez, T.; Viana, F.; Nilius, B.; Voets, T. Transient Receptor Potential Channels in Sensory Neurons Are Targets of the Antimycotic Agent Clotrimazole. *J. Neurosci.* **2008**, *28*, 576–586. [CrossRef] [PubMed]
23. Schwarz, G.; Droogmans, G.; Nilius, B. Multiple effects of SK&F 96365 on ionic currents and intracellular calcium in human endothelial cells. *Cell Calcium.* **1994**, *15*, 45–54. [PubMed]
24. Aierken, A.; Xie, Y.; Dong, W.; Apaer, A.; Lin, J.; Zhao, Z.; Yang, S.; Xu, Z.; Yang, F. Rational Design of a Modality-Specific Inhibitor of TRPM8 Channel against Oxaliplatin-Induced Cold Allodynia. *Adv. Sci.* **2021**, *8*, 2101717. [CrossRef]
25. Beccari, A.R.; Gemei, M.; Monte, M.L.; Menegatti, N.; Fanton, M.; Pedretti, A.; Bovolenta, S.; Nucci, C.; Molteni, A.; Rossignoli, A.; et al. Novel selective, potent naphthyl TRPM8 antagonists identified through a combined ligand- and structure-based virtual screening approach. *Sci. Rep.* **2017**, *7*, 10999. [CrossRef]
26. Knowlton, W.M.; Daniels, R.; Palkar, R.; McCoy, D.D.; McKemy, D.D. Pharmacological Blockade of TRPM8 Ion Channels Alters Cold and Cold Pain Responses in Mice. *PLoS ONE* **2011**, *6*, e25894. [CrossRef] [PubMed]
27. Bertamino, A.; Ostacolo, C.; Ambrosino, P.; Musella, S.; Di Sarno, V.; Ciaglia, T.; Soldovieri, M.V.; Iraci, N.; Carvajal, A.F.; de la Torre-Martinez, R.; et al. Tryptamine-Based Derivatives as Transient Receptor Potential Melastatin Type 8 (TRPM8) Channel Modulators. *J. Med. Chem.* **2016**, *59*, 2179–2191. [CrossRef]
28. Bertamino, A.; Iraci, N.; Ostacolo, C.; Ambrosino, P.; Musella, S.; Di Sarno, V.; Ciaglia, T.; Pepe, G.; Sala, M.; Soldovieri, M.V.; et al. Identification of a Potent Tryptophan-Based TRPM8 Antagonist With in Vivo Analgesic Activity. *J. Med. Chem.* **2018**, *61*, 6140–6152. [CrossRef]
29. Bertamino, A.; Ostacolo, C.; Medina, A.; Di Sarno, V.; Lauro, G.; Ciaglia, T.; Vestuto, V.; Pepe, G.; Basilicata, M.G.; Musella, S.; et al. Exploration of TRPM8 Binding Sites by  $\beta$ -Carboline-Based Antagonists and Their In Vitro Characterization and In Vivo Analgesic Activities. *J. Med. Chem.* **2020**, *63*, 9672–9694. [CrossRef]
30. De Caro, C.; Cristiano, C.; Avagliano, C.; Bertamino, A.; Ostacolo, C.; Campiglia, P.; Gomez-Monterrey, I.; La Rana, G.; Gualillo, O.; Calignano, A.; et al. Characterization of New TRPM8 Modulators in Pain Perception. *Int. J. Mol. Sci.* **2019**, *20*, 5544. [CrossRef]
31. Di Donato, M.; Ostacolo, C.; Giovannelli, P.; Di Sarno, V.; Monterrey, I.M.G.; Campiglia, P.; Migliaccio, A.; Bertamino, A.; Castoria, G. Therapeutic potential of TRPM8 antagonists in prostate cancer. *Sci. Rep.* **2021**, *11*, 23232. [CrossRef]
32. Bechelane-Maia, E.H.; Assis, L.C.; Alves de Oliveira, T.; Marques da Silva, A.; Gutterres Taranto, A. Structure-Based Virtual Screening: From Classical to Artificial Intelligence. *Front. Chem.* **2020**, *8*, 343. [CrossRef] [PubMed]

33. Talarico, C.; Gervasoni, S.; Manelfi, C.; Pedretti, A.; Vistoli, G.; Beccari, A.R. Combining Molecular Dynamics and Docking Simulations to Develop Targeted Protocols for Performing Optimized Virtual Screening Campaigns on the hTRPM8 Channel. *Int. J. Mol. Sci.* **2020**, *21*, 2265. [[CrossRef](#)] [[PubMed](#)]
34. Zhang, Z.; Wu, X.; Zhang, L.; Mao, A.; Ma, X.; He, D. Menthol relieves acid reflux inflammation by regulating TRPV1 in esophageal epithelial cells. *Biochem. Biophys. Res. Commun.* **2020**, *525*, 113–120. [[CrossRef](#)] [[PubMed](#)]
35. Valenzano, K.J.; Grant, E.R.; Wu, G.; Hachicha, M.; Schmid, L.; Tafesse, L.; Sun, Q.; Rotshteyn, Y.; Francis, J.; Limberis, J.; et al. N-(4-Tertiarybutylphenyl)-4-(3chloropyridin-2-yl)tetrahydropyrazine-1(2H)-carbox-amide (BCTC), a novel, orally effective vanilloid receptor 1 antagonist with analgesic properties: I. In Vitro characterization and pharmacokinetic properties. *J. Pharmacol. Exp. Ther.* **2003**, *306*, 377–386. [[CrossRef](#)] [[PubMed](#)]
36. Hossain, M.Z.; Ando, H.; Unno, S.; Masuda, Y.; Kitagawa, J. Activation of TRPV1 and TRPM8 Channels in the Larynx and Associated Laryngopharyngeal Regions Facilitates the Swallowing Reflex. *Int. J. Mol. Sci.* **2018**, *19*, 4113. [[CrossRef](#)] [[PubMed](#)]
37. Bereiter, D.A.; Rahman, M.; Thompson, R.; Stephenson, P.; Saito, H. TRPV1 and TRPM8 Channels and Nocifensive Behavior in a Rat Model for Dry Eye. *Investig. Ophthalmol. Vis. Sci.* **2018**, *59*, 3739–3746. [[CrossRef](#)] [[PubMed](#)]
38. Pérez-Faginas, P.; Aranda, M.T.; de la Torre-Martínez, R.; Quirce, S.; Fernández-Carvajal, A.; Ferrer-Montiel, R.; González-Muñiz, R. New transient receptor potential TRPV1, TRPM8 and TRPA1 channel antagonists from a single linear  $\beta,\gamma$ -diamino ester scaffold. *RCS Adv.* **2016**, *6*, 6868–6877.
39. Weyer, A.D.; Lehto, S.G. Development of TRPM8 Antagonists to Treat Chronic Pain and Migraine. *Pharmaceuticals* **2017**, *10*, 37. [[CrossRef](#)]
40. González-Muñiz, R.; Bonache, M.A.; Martín-Escura, C.; Gómez-Monterrey, I. Recent Progress in TRPM8 Modulation: An Update. *Int. J. Mol. Sci.* **2019**, *20*, 2618. [[CrossRef](#)]
41. Winchester, W.; Gore, K.; Glatt, S.; Petit, W.; Gardiner, J.C.; Conlon, K.; Postlethwaite, M.; Saintot, P.-P.; Roberts, S.; Gosset, J.R.; et al. Inhibition of TRPM8 channels reduces pain in the cold pressor test in human. *J. Pharmacol. Exp. Ther.* **2022**, *380*, jpet.114.216010. [[CrossRef](#)]
42. Kurkin, A.V.; Bernovskaya, A.A.; Yurovskaya, M.A. Synthesis of N-alkylanthranilamides with a chiral substituent at the nitrogen atom. *Tetrahedron Asymmetry* **2010**, *21*, 2100–2107. [[CrossRef](#)]
43. Jiang, H.; Sha, S.-C.; Jeong, S.A.; Manor, B.C.; Walsh, P.J. Ni(NIXANTPHOS)-Catalyzed Mono-Arylation of Toluenes with Aryl Chlorides and Bromides. *Org. Lett.* **2019**, *21*, 1735–1739. [[CrossRef](#)]
44. Cordero-Sánchez, C.; Mudarra-Fraguas, I.; Fernández-Carvajal, A. Fluorescence-Based Functional Assays for Ca<sup>2+</sup>-Permeable ThermoTRP Channels. *Methods Mol. Biol.* **2019**, *1987*, 99–110. [[PubMed](#)]
45. Zimmermann, M. Ethical considerations in relation to pain in animal experimentation. *Acta Physiol. Scand. Suppl.* **1986**, *554*, 221–233. [[PubMed](#)]
46. UniProt Consortium. UniProt: The universal protein knowledgebase in 2021. *Nucleic Acids Res.* **2021**, *49*, D480–D489. [[CrossRef](#)] [[PubMed](#)]
47. Thompson, J.D.; Higgins, D.G.; Gibson, T.J. CLUSTAL W: Improving the sensitivity of progressive multiple sequence alignment through sequence weighting, position-specific gap penalties and weight matrix choice. *Nucleic Acids Res.* **1994**, *22*, 4673–4680. [[CrossRef](#)] [[PubMed](#)]
48. Jacobson, M.P.; Pincus, D.L.; Rapp, C.S.; Day, T.J.; Honig, B.; Shaw, D.E.; Friesner, R.A. A hierarchical approach to all-atom protein loop prediction. *Proteins* **2004**, *55*, 351–367. [[CrossRef](#)]
49. Jacobson, M.P.; Friesner, R.A.; Xiang, Z.; Honig, B. On the Role of the Crystal Environment in Determining Protein Side-chain Conformations. *J. Mol. Biol.* **2002**, *320*, 597–608. [[CrossRef](#)]
50. Sancineto, L.; Iraci, N.; Massari, S.; Attanasio, V.; Corazza, G.; Barreca, M.L.; Sabatini, S.; Manfroni, G.; Avanzi, N.R.; Cecchetti, V.; et al. Computer-Aided Design, Synthesis and Validation of 2-Phenylquinazolinone Fragments as CDK9 Inhibitors with Anti-HIV-1 Tat-Mediated Transcription Activity. *ChemMedChem* **2013**, *8*, 1941–1953. [[CrossRef](#)]
51. Sastry, G.M.; Adzhigirey, M.; Day, T.; Annabhimoju, R.; Sherman, W. Protein and ligand preparation: Parameters, protocols, and influence on virtual screening enrichments. *J. Comput. Aided. Mol. Des.* **2013**, *27*, 221–234. [[CrossRef](#)]
52. Schrödinger LLC. *Schrödinger Release 2019-1: LigPrep*; Schrödinger LLC: New York, NY, USA, 2019.
53. Friesner, R.A.; Murphy, R.B.; Repasky, M.P.; Frye, L.L.; Greenwood, J.R.; Halgren, T.A.; Sanschagrin, P.C.; Mainz, D.T. Extra precision glide: Docking and scoring incorporating a model of hydrophobic enclosure for protein-ligand complexes. *J. Med. Chem.* **2006**, *49*, 6177–6196. [[CrossRef](#)] [[PubMed](#)]
54. Friesner, R.A.; Banks, J.L.; Murphy, R.B.; Halgren, T.A.; Klicic, J.J.; Mainz, D.T.; Repasky, M.P.; Knoll, E.H.; Shelley, M.; Perry, J.K.; et al. Glide: A New Approach for Rapid, Accurate Docking and Scoring. 1. Method and Assessment of Docking Accuracy. *J. Med. Chem.* **2004**, *47*, 1739–1749. [[CrossRef](#)]
55. Halgren, T.A.; Murphy, R.B.; Friesner, R.A.; Beard, H.S.; Frye, L.L.; Pollard, W.T.; Banks, J.L. Glide: A New Approach for Rapid, Accurate Docking and Scoring. 2. Enrichment Factors in Database Screening. *J. Med. Chem.* **2004**, *47*, 1750–1759. [[CrossRef](#)] [[PubMed](#)]
56. Astolfi, A.; Iraci, N.; Sabatini, S.; Barreca, M.; Cecchetti, V. p38 $\alpha$  MAPK and Type I Inhibitors: Binding Site Analysis and Use of Target Ensembles in Virtual Screening. *Molecules* **2015**, *20*, 15842–15861. [[CrossRef](#)] [[PubMed](#)]

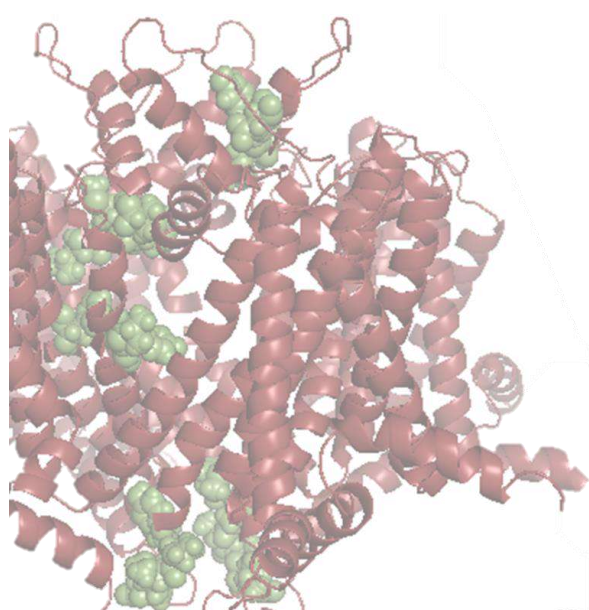
57. Barreca, M.L.; Iraci, N.; Manfroni, G.; Gaetani, R.; Guercini, C.; Sabatini, S.; Tabarrini, O.; Cecchetti, V. Accounting for Target Flexibility and Water Molecules by Docking to Ensembles of Target Structures: The HCV NS5B Palm Site I Inhibitors Case Study. *J. Chem. Inf. Model.* **2013**, *54*, 481–497. [[CrossRef](#)]
58. Bowers, K.J.; Chow, D.E.; Xu, H.; Dror, R.O.; Eastwood, M.P.; Gregersen, B.A.; Klepeis, J.L.; Kolossvary, I.; Moraes, M.A.; Sacerdoti, F.D.; et al. Scalable Algorithms for Molecular Dynamics Simulations on Commodity Clusters, In Proceedings of the SC'06: 2006 ACM/IEEE Conference on Supercomputing, Tampa, FL, USA, 11–17 November 2006.
59. Lomize, M.A.; Lomize, A.L.; Pogozheva, I.D.; Mosberg, H.I. OPM: Orientations of Proteins in Membranes database. *Bioinformatics* **2006**, *22*, 623–625. [[CrossRef](#)]
60. Jorgensen, W.L.; Maxwell, D.S.; Tirado-Rives, J. Development and Testing of the OPLS All-Atom Force Field on Conformational Energetics and Properties of Organic Liquids. *J. Am. Chem. Soc.* **1996**, *118*, 11225–11236. [[CrossRef](#)]
61. Jorgensen, W.L.; Chandrasekhar, J.; Madura, J.D.; Impey, R.W.; Klein, M.L. Comparison of simple potential functions for simulating liquid water. *J. Chem. Phys.* **1983**, *79*, 926–935. [[CrossRef](#)]







## **AGRADECIMIENTOS**





## AGRADECIMIENTOS

Hace menos de un año ni siquiera sabía por dónde empezar a escribir este trabajo.. y ahora, por fin me encuentro escribiendo las últimas líneas. He tenido algo de tiempo para mirar atrás, siendo verdaderamente consciente de lo afortunada que he sido, todo lo que he aprendido y lo bien acompañada que he estado durante esta etapa.

En primer lugar, agradecer a mi directora de tesis, la Dra. Asia Fernández Carvajal, darme la oportunidad de unirme a este equipo increíble, tanto personal como profesionalmente. Por darme su confianza y por su accesibilidad, paciencia y ayuda. Porque sin ti, esto no hubiera tenido ni un principio.

Agradecer también al Dr. Antonio Ferrer Montiel y al Dr. Gregorio Fernández Ballester por haber compartido sus conocimientos conmigo y por sus buenos consejos.

Gracias Dra. Rosario González Muñiz y Dra. Isabel Gómez Monterrey por haberme hecho partícipe de vuestros proyectos y confiar en mí. Agradecer también a la Dra. Catarina Rosado y la Dra. Patricia Rijo haberme permitido realizar una estancia en sus laboratorios y por hacer que fuera un éxito.

Cómo empezar compañer@s, si gran parte de lo que sé me lo habéis enseñado vosotros.. Laura, ha sido más que un placer compartir contigo ese despachito y todo lo que ha llevado. Nuestros momentos de grandeza científica, y los de bajeza. Pero sobre todo risas y últimamente fenómenos patológicos (jajaja). Agradecerte la escucha, los apoyos y las conversaciones. Y a ti Simona, por saber siempre qué decirme y hacerme sentir mejor. Nuestras miniconversaciones durante los tres primeros ciclos del PolarStar para mí no tienen precio. ¡Gracias a las dos por hacer mi día a día más fácil ¡Mucho ánimo, queda nada!

Jose, desde que entraste al laboratorio nuestra vida es más sencilla y es que hay una parte de ti en todos nuestros experimentos. David A., gracias por haber estado siempre disponible y por tu manera de explicar. También por todas las risas y momentitos cuando aún íbamos de cañas. David C., gracias por tu paciencia, comprensión y ayuda especialmente con los *little angels*. También nos hemos reído eh.. Angela, qué pena coincidir tan breve periodo, espero que te conviertas en una *Patch warrior* y poderlo ver. Jorge, tú también has estado ahí, te deseo lo mejor en tus experimentos. Y a ti Eva, mucha suerte en este tramo final.

Y como no, continuar con los agradecimientos a mis dos doctoras preferidas. Dra. Maggie, qué voy a decir si desde que llegué sigo tus pasos. Me costó.. pero las sonrisas fueron creciendo, como el vínculo. Gracias por ser nuestro *troublesholver*. Te hemos

## Agradecimientos

echado de menos este último año, pero seguro que nos quedan muchos más momentitos. Y Cristina, hermana, compartimos bautismo en trabalenguas y varias técnicas *in vitro*. Para mí, a tu lado empezó todo. Y aunque solo haya sido afortunada de tenerte pocos meses al año, han sido suficientes para llevarme a una gran amiga. Ojalá nos volviéramos a cruzar. Y en Madrid, Carol, ya sabes.. “you can count on me like 1, 2, 3, I’ll be there...” No ha sido poquito lo vivido. Gracias por endulzarnos sobre todo en esta última etapa.

Y.. nunca podré olvidar este último congreso en familia. Gracias por vuestro apoyo, escucha (repetida) y confianza. Pero.. ¡Me debéis una fiesta!

Además de los nombrados, no puedo dejar de agradecer a toda la gente que ha estado a mi lado durante estos años: Irene, porque contigo también empezó todo; Gema, esa felicidad y facilidad siempre; Vero, por tus buenos consejos en todos los ámbitos, sobre todo en este último empujón; Cloti, por saber de todo y alegrarnos la vista; Sara, Silvia, Ángeles, todo el laboratorio de Portugal y todos los estudiantes que me habéis sacado una sonrisa. ¡Espero haberos servido de algo!

¡He tenido a los mejores compañeros del mundo! ¡Os deseo mucha suerte en todo! Espero que el futuro siga cruzando nuestros caminos ya sea en ciencia o fuera de ella. Y no hace falta decir que.. ¡AQUÍ ESTOY!

Aunque mis agradecimientos no acaban aquí, fuera del ámbito científico también tengo mucho que agradecer. A Jumano, que desde que apareció siempre ha estado ahí, intentando hacer mi vida más fácil. Gracias a él he obtenido un C2 en preparación, embotellado y cata de cerveza, música canaria y portugués. Y a mis incondicionales: Reyes, Caterina, Cristina, Andrea, Alexandra, Nuria y Casandra. Porque nuestras conversaciones y risas curan cualquier pena.

Y por último, eternamente agradecida a mi familia, especialmente a mi madre y a mi tía. A ti mamá, por ser una mujer todoterreno, luchadora y perseverante. Eres mi inspiración, no existen agradecimientos suficientes en el mundo. Y a ti tía, porque a pesar de las adversidades siempre ves el lado positivo. Eres luz e iluminas.

Ahora sí, llegó el momento de despedirme, eternamente agradecida a tod@s vosotr@s, a sobrevivir a un doctorado, a una pandemia mundial y a haber conseguido escribir esta tesis. Fuera de bromas, con constancia, empeño y buena compañía se consiguen muchos “imposibles”.

**“Las buenas personas están hechas de acero **inolvidable**”.**



